MODELING OF STANDING COLUMN WELLS IN GROUND SOURCE HEAT PUMP SYSTEMS

By

ZHENG DENG

Bachelor of Science
Shenyang Architectural and Civil Engineering Institute
Shenyang, P. R. China
1996

Master of Science
Tongji University
Shanghai, P. R. China
2000

Submitted to the Faculty of the
Graduate College of the
Oklahoma State University
in partial fulfillment of
the requirements for
the degree of
DOCTOR OF PHILOSOPHY
December, 2004

MODELING OF STANDING COLUMN WELLS IN GROUND SOURCE HEAT PUMP SYSTEMS

Thesis Approved:

Dr. Jeffrey Spitler

Thesis Adviser

Dr. Daniel Fisher

Dr. David Lilley

Dr. James Bose

Dr. Gordon Emslie

Dean of the Graduate College

ACKNOWLEDGEMENTS

I owe a lot to my advisor, Dr. Jeffrey Spitler, who first introduced me to the fascinating areas of geothermal technology and building energy simulation, which I have enjoyed greatly ever since. Dr. Spitler taught me how to do research: how to understand a problem from a fundamental level, how to spell out the core idea of a solution, and how to strike a good balance between being intuitive and being rigorous. An excellent speaker himself, he also taught me how to give good talks, which I found extremely useful. I thank him for his constructive guidance, constant support, patience, direction, and inspiration throughout my graduate study. Without his timely encouragement and support, this work would not have been done.

I would like to extend my sincere gratitude and appreciation to Dr. Simon Rees who served as co-advisor along the course of the research before he returned to the U.K. His expertise in computational methods was quite valuable in helping me to achieve the project goals.

My appreciation also extends to the members of my doctoral committee, Dr. Daniel Fisher, Dr. David Lilley, and Dr. Jim Bose for their committed service and support, ideas, and suggestions that helped improve my work significantly.

I wish to deliver special credit to Mr. Carl Orio of the Water and Energy System Corporation for advice on standing column well design and operation and to Mr. Hugh Henderson of the CDH Energy Corporation for his generous assistance in providing experimental data used in validation of the standing column well system model.

I would also like to thank my colleagues at the Building and Environmental Thermal Systems Research Group in Oklahoma State University, both present and former, namely, Andrew Chiasson, Xiaobing Liu, Dongyi Xiao, Weixiu Kong, Tracy Xiao, Xiaowei Xu, Haider Khan, and Bereket Nigusse for their ideas and precious help in a direct or indirect way.

I am indebted to my parents, twin sister, and my brother who constantly support my every pursuit. Whatever I am today is because of their love, understanding, encouragement, and sacrifices. My infinite thanks go to Rob, absolutely for everything.

This work was partially supported by the ASHRAE RP-1119, and partially supported by an ASHRAE Grant-in-Aid scholarship. ASHRAE's support is gratefully acknowledged.

TABLE OF CONTENTS

LIST OF TABLES

TABLE……...PAGE

TABLE……...PAGE

LIST OF FIGURES

FIGURE……...PAGE

FIGURE……...PAGE

FIGURE……...PAGE

FIGURE……...PAGE

FIGURE……...PAGE

FIGURE……...PAGE

NOMENCLATURE

a	the radius of pipe(m [ft])
$bleedrate$	the normalized bleed rate in the system (%)
B	the integration variable
C	the summation of the series $\sum_{N=1}^{\infty} \frac{(-1)^{N+1} y^N}{N \cdot (N!)}$
C_p	the specific heat of the ground(J/kg-K [Btu/lbm-ºF])
C_{pw}	the specific heat of water (J/kg-K [Btu/lbm-ºF])
D	the distance in feet to the recharge well (m [ft])
$D_{borehole}$	the hydraulic diameter of borehole (m [ft])
f	the Moody friction factor
Fo	the Fourier number defined as: $Fo = \alpha t / r_0^2$
g	the acceleration due to the gravity (m/s^2 [ft/s^2])
G_f	the groundwater factor (+ denotes flow into the well; - denotes flow out of the well)
h	the hydraulic head (m [ft])
$h_{borehole}$	the heat transfer coefficient at the borehole wall (W/m^2-K [Btu/hr-ft^2-ºF])
H	the total dynamic head for the water pump (Pa)
J_i	the Bessel function of order i

k_s	the thermal conductivity of the ground (W/m-K [Btu/hr-ft-ºF])
k_{water}	the thermal conductivity of water (W/m-K [Btu/hr-ft-ºF])
k_{eff}	the effective thermal conductivity (W/m-K [Btu/hr-ft-ºF])
$\bar{\bar{k}}$	the intrinsic permeability (m^2 or Darcy [ft^2])
K	the hydraulic conductivity of ground (m/s [gpd/ft^2])
K_{eff}	the effective hydraulic conductivity (m/s [ft/s])
L	the borehole depth (m [ft])
$\dot{m}_w$	the mass flow rate of water through heat pump system (kg/s [lbm/sec])
m	the mass of water in the standing column well (kg [lbm])
n	the porosity of rock
Nu	the local Nusselt number
p	the pressure (N/m^2 [lbf/ft^2])
Pr	the Prandtl number
q	the specific discharge (m/s [ft/s])
q''	the heat flux (W/m^2 [Btu/hr-ft^2])
$\vec{q}$	the specific discharge (volume flow rate per unit of cross-sectional area) (m/s [gpd/ft^2])
q_{sc}	the short-circuiting heat transfer rate (W/m [Btu/ft-hr])
R_∞	the far field radius
r_b	the borehole radius (m [ft])
R_b	the thermal resistance of the borehole (K/(W/m) [hr-ft-ºF/Btu])

R_{sc} the short circuiting thermal resistance (K/(W/m) [hr-ft-ºF/Btu])

$\mathrm{Re}_{\varepsilon}$ the roughness Reynolds number $\mathrm{Re}_{\varepsilon} = \dfrac{\mathrm{Re}\sqrt{f/2}}{D/\varepsilon}$

S_1 the thermal capacity of the cylinder of perfect conductor (J/m^3-K [Btu/ft^3-ºF])

t the heat pump run time (hr)

T_b the borehole wall temperature (ºC [ºF])

T_{f1} the temperature of water in the annulus (ºC [ºF])

T_{f2} the temperature of water in the dip tube (ºC [ºF])

T_f the average fluid temperature (ºC [ºF])

T_{fo} the water temperature leaving the well (ºC [ºF])

T_{fi} the water temperature returning to the well (ºC [ºF])

T_{f_old} the representative water temperature at the previous time step (ºC [ºF])

$T_f^q(t)$ the average fluid temperature at time t (ºC [ºF])

T_{gw} the temperature of groundwater entering into the well (ºC [ºF])

$T_{r\infty}$ the far field temperature (ºC [ºF])

T_u the undisturbed temperature of the ground (ºC [ºF])

T_w the borehole wall temperature (ºC [ºF])

T_{freeze} the fluid temperature at freezing point (^{o}C [ºF])]

T_{ExFT} the exiting fluid temperature from the heat pump (i.e., the fluid temperature entering the ground heat exchanger) (^{o}C [ºF])]

T_{EFT}	the entering fluid temperature to the heat pump (i.e., the fluid temperature leaving the ground heat exchanger) (^{o}C [ºF)])
u	the integration variable
v	the mean velocity in the given pipe(m/s [ft/s])
V_r	the average linear groundwater velocity vector (m/s [ft/s])
w	the power consumption of the circulating water pump (W)
Y_i	the modified Bessel function of order i
z	the vertical coordinate (m [ft])
α	the thermal diffusivity of the ground (m^2/s [ft^2/hr])
β	the under-relaxation factor
λ	the integration variable
γ	the Euler's constant, 0.5772157…
ρ	the density of the ground (kg/m^3[lbm/ft^3])
ρ_w	the density of the groundwater (kg/m^3 [lbm/ft^3])
ρc	the volumetric heat capacity (J/m^3-K [Btu/ft^3-ºF])
$\frac{\rho v^2}{2}$	the velocity pressure (Pa)
$\rho g z$	the elevation pressure (Pa)
ν	the kinematic fluid viscosity (m^2/s [ft^2/sec])
ε	the height of the surface roughness (m [ft])
μ	the dynamic viscosity of water (N-s/m^2 [lbf-s/ft])
η	the efficiency of the circulating water pump
ΔT	the fluid temperature change across the heat pump (^{o}C [ºF)])

Δt	the time increment(sec [sec])
Δp	the total pressure loss (fitting +friction) (Pa)
ΔT_{sc}	the temperature difference caused by the short circuiting (ºC [ºF])

1. INTRODUCTION

In recent years, ground heat source heat pump systems have become increasingly popular for use in residential and commercial buildings. These systems include several different variations, all of which reject heat and/or extract heat from ground:

(1) ground-coupled heat pump (GCHP) systems;

(2) surface water heat pump (SWHP) systems;

(3) ground-water heat pump (GWHP) systems:

   a. Standing column well (SCW) systems;

   b. Open loop groundwater systems.

The schematics of these different systems are shown in Figure 1-1. Considerable research effort has been spent on ground heat source heat pump systems, especially on the single U-tube ground heat exchanger, in recent decades. Existing engineering design manuals, such as IGSHPA (1988), ASHRAE (1995), Kavanaugh and Rafferty (1997), cover the first two system types and open loop groundwater systems. However, relatively few design tools and simulation models are available for SCW systems. SCW systems are the focus of this research. SCW systems are also referred to in the literature as “turbulent wells”, “energy wells”, “concentric wells”, “recirculating wells”, “geo-wells”, “thermal wells”, and “closed-loop, open-pipe systems”.

Rawlings and Sykulski (1999) stated that the first documented suggestion of using the ground as a heat source was in 1912 in Switzerland, and the first ground source heat

pump in North America was installed in a house in Indianapolis in 1945. However, commercial use of the ground as a heat source/sink didn't begin until the first oil crisis in 1973. By the mid 1980's, advances in heat pump efficiencies and operating ranges, combined with better materials for ground loops, allowed this technology to enter the market. At the same time, commercial type applications started to gain popularity. Geothermal systems have the potential to reduce primary energy consumption and thus significantly reduce the emission of greenhouse gases and other pollutants.

The use of SCW was first suggested by local Maine well drillers and hydrogeologists (Orio 1994). In fact, the concept of standing column well systems is about as old as the ground water heat pump systems, but is recently receiving much more attention because of their lower installation cost, lower operating cost, and improved overall performance in the regions with suitable geological conditions. In the mid-1970's, Dr. Bose from Oklahoma State University began to do field tests on standing column well systems. Later, Dr. Braud from Louisiana State University further evaluated this technology.

Compared with other ground heat source heat pump systems, shorter boreholes and more stable water temperatures make the SCW system an attractive commercial and industrial design approach. Now, there are approximately 1000 SCW installations in the United States. Most of them are located in the Northeast and Pacific Northwest in addition to parts of Canada in heating-dominated residential and light commercial applications (ASHRAE 1119-TRP). These regions have lower mean ground temperature and higher heating loads than other areas, so now most SCW design is focused on heat extraction.

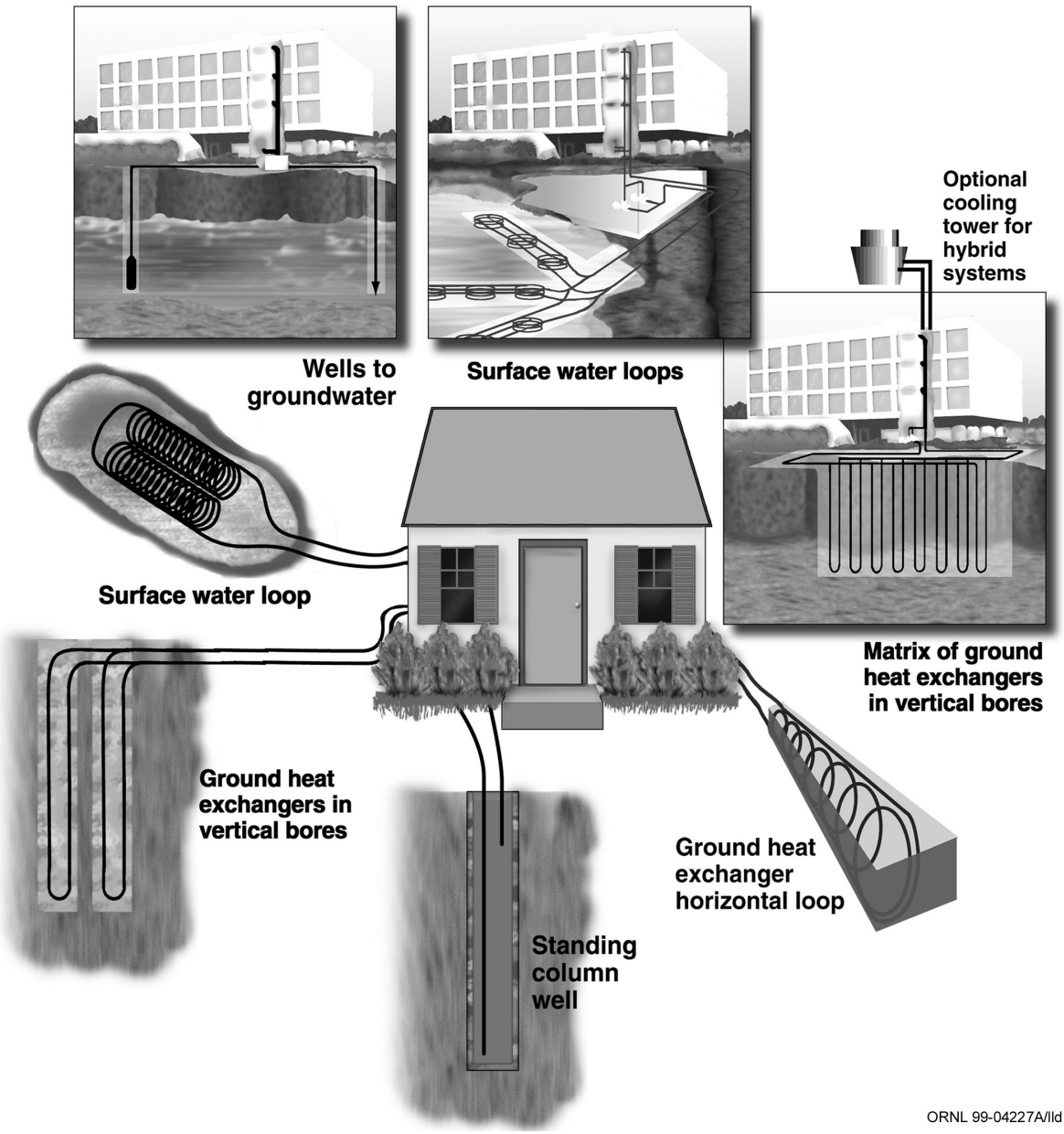

Figure 1-1 Schematics of different ground source heat pump systems

(Reprinted by permission from Oak Ridge National Laboratory)

(http://www.eren.doe.gov/femp)

1.1. Operation

The SCW system can be thought of as a cross between closed-loop earth-coupled system and open-loop ground-water source system. During much of the year, they operate by recirculating water between the well and the heat pump. However, during peak temperature periods, they can " bleed" some water from the system to induce groundwater flow. Usually, only one well is required; larger projects may have several wells in parallel.

In SCW systems, water is re-circulated between the well and the building (heat pump). Deep bores are drilled in hard rock, creating a standing column of water from the static water level down to the bottom of the bore. Water is re-circulated from one end of the column to the heat pump, and back to the other end of the column (Figure 1-2).

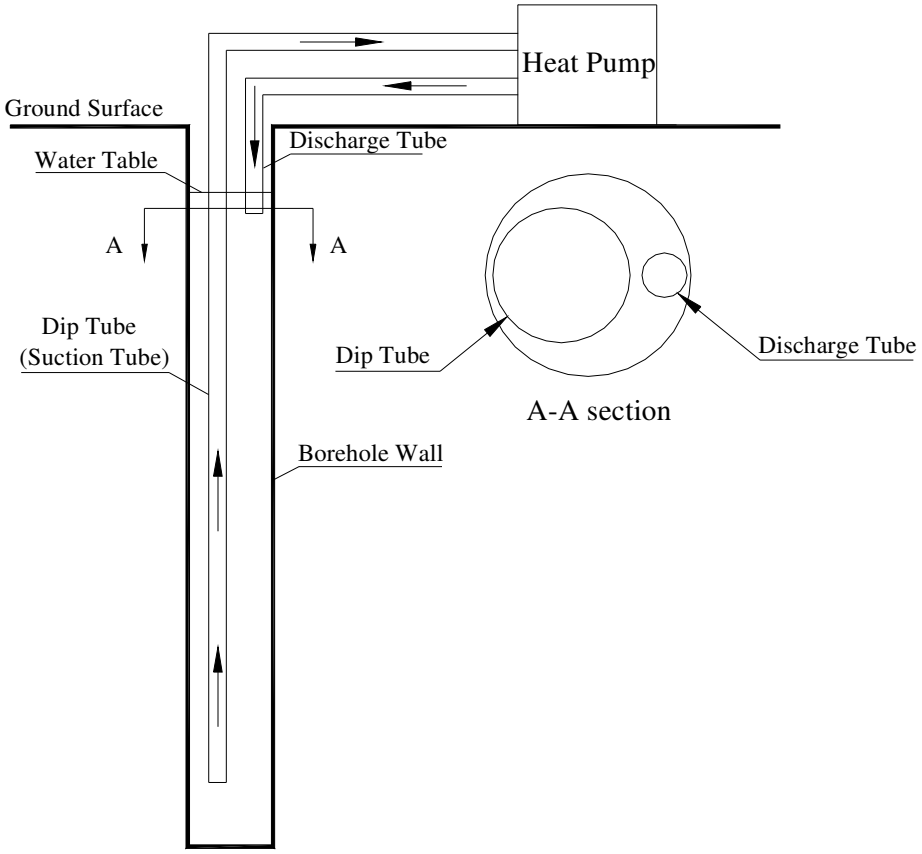

Figure 1-2 A schematic drawing showing the borehole arrangement

During peak heat rejection or extraction periods, if the well-water temperature drops too low or climbs too high, standing column well systems can bleed part of the water rather than returning it all to the well. This causes water to flow to the column from the surrounding formation to make up the flow. This cools the column and surrounding ground during heat rejection in the summer, and heats the column and surrounding ground during heat extraction in the winter, thus restoring the well-water temperature to the normal operating range and improving the system performance. The bleed water can be diverted to a storm sewer, used for domestic water consumption, or otherwise

disposed. Sometimes, SCW systems serve to provide household domestic water, which cause the system to naturally "bleed" the whole year.

1.2. Application (limitations and benefits)

SCW systems are used in geologic areas with abundant ground water. This system can provide the necessary water flows as well as shorter heat transfer lengths (depths) and the ability to return water to the same aquifers. The combination of relatively shallow water table and a deep well (sometimes greater than 300 m or 1000 ft) means that the well has a large water volume, about 1800 L per 100 m (150 gal per 100 ft) for a 152.4 mm (6 in) nominal diameter well (Sachs and Dinse 2000). Based on experience by the Water and Energy Systems Corporation, 50 to 60 feet of water column is needed per ton of building load (4.3m/kW to 5.2m/kW). Commercial systems larger than 350 kW (100 tons) have used multiple standing column wells with success (Orio 1994).

The application of SCW systems is limited to geologic regions with good ground water quality like other ground water heat pump systems. This enables the ground water to be directly circulated through the heat pump. Applications also exist in areas with poorer water quality. In such situations it is common practice to use an intermediate heat exchanger between the well and the heat pump in order to avoid fouling the heat pump heat exchangers.

Sachs and Dinse (2000) suggested that the designer of SCW systems should (1) work with an experienced local hydrologist and (2) avoid any areas with salt bed or other

formation that could be dissolved. Also, any water well including standing column wells must be constructed, developed, and operated according to state and local regulations for water wells. It is imperative that designers and installers of SCW systems be aware of the regulations in their locations (DenBraven 2002).

Generally speaking, SCW systems have some advantages shared with all the other forms of ground source heat pump systems:

- Economy

  When properly designed, a geothermal heat pump system is one of the lowest cost ways of providing heating/cooling because of high equipment efficiency, annual storage/reuse of energy, and availability. However, geothermal heat pump systems have comparatively high capital costs. A geothermal system often has lower life cycle costs than conventional systems due to its reduced energy and maintenance costs. Because there is no outdoor equipment in the geothermal systems, corrosion, weathering and vandalism are not normal problems.

- Environmental benefits

  The need for electricity (pumps) introduces the only credible source of possible environmental concern for a geothermal system. The geothermal system itself produces zero local pollution. This system causes less carbon dioxide emission and other pollutants than its conventional alternatives, thus reducing global warming and other environmental impacts.

- Reduced requirement for mechanical room floor place
- Quiet operation
- Potential for reducing the peak electrical demand

Standing column well systems share the same advantages, in terms of energy efficiency, environmental benefits, low maintenance, etc. with other forms of geothermal heat pump systems. At the same time, the heat exchange rate in a standing column well is enhanced by direct contact and by the pumping action, which promotes ground water flow to and from the borehole. Consequently heat transfer with the surrounding rock takes place by advection in addition to conduction. If a standing column well is considered as a cylinder, the surface area for heat exchange of a 152.4 mm (6 in) borehole with 304 m (1000 ft) long is about 145 m^2 (1570 ft^2), which allows substantial heat exchange. Put another way, SCW systems have substantially heat exchange rate and the fact that such systems are open loop means that the fluid flowing through the heat pump system is closer to the mean ground temperature compared to systems with closed loop U-tube heat exchangers.

SCW systems have a lower initial cost because the borehole depths are in the 50-60 feet per ton compared to closed loops at 150 or more feet per ton. Thus, the borehole in SCW systems could be one-half the depth of closed loop earth coupled methods (Orio, 1994). To date, the typical drill rigs in the regions where SCW system are mainly located (Northeast and Pacific Northwest), can be able to reach 560 m (1800 ft) and the deepest standing column wells are in the range of 460 m (1500 ft). The depth of this cost-effective geothermal coupled method can be extended with the development of rigs.

1.3. Basic physical mechanism in SCWs (heat transfer and mass transfer in porous media)

First, some definitions are given for later use. Above the water table lies the unsaturated zone, where voids between rocks are mostly filled with air. Some water is held in the unsaturated zone by molecular attraction, and it will not flow toward or enter a well. In the saturated zone, which lies below the water table, all the openings in the rocks are full of water that may move through the aquifer to streams, springs, or wells from which water is being withdrawn (see Figure 1-3). This research is mainly focused on the saturated zone.

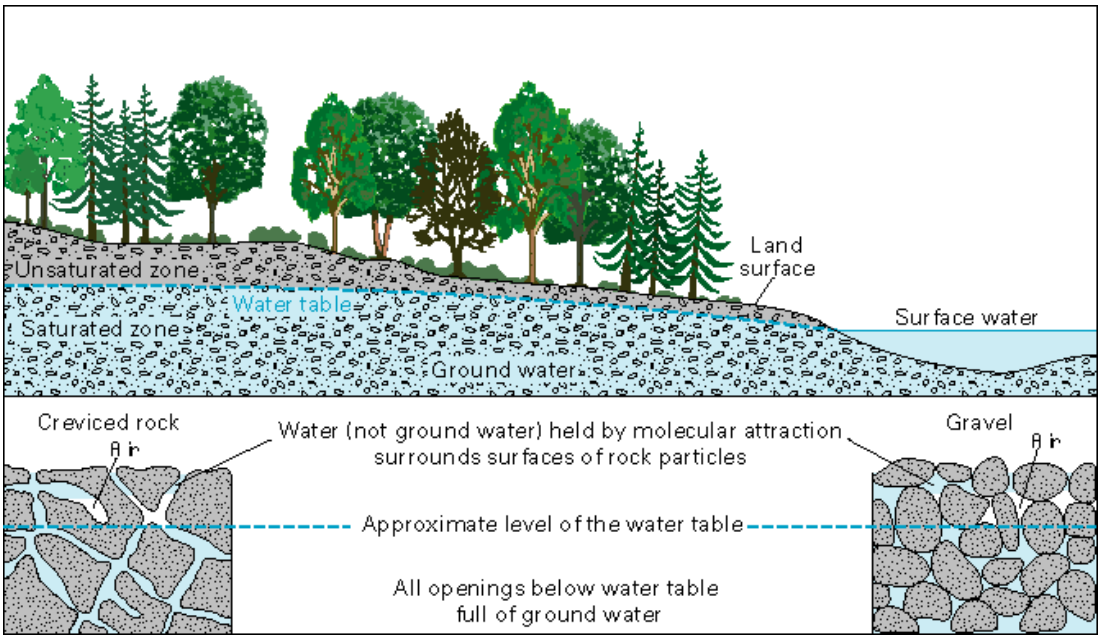

Figure 1-3 How Groundwater occurs in rocks*

(http://capp.water.usgs.gov/GIP/gw_gip/how_occurs.html)

* Public resource provided by USGS website

The energy transport in the ground outside of the standing column well is through a porous media (aquifer). An "aquifer" is defined by Driscoll (1986) as formation, group of formations, or part of a formation that contains sufficient saturated permeable material to yield economical quantities of water to wells and springs. The word aquifer comes from the two Latin words, *aqua*, or water, and *ferre*, to bear or carry. An aquifer literally carries water underground. We can consider an aquifer as a porous medium that consists of a solid phase and an interconnected void space totally filled with groundwater. Transport of groundwater occurs in the interconnected voids. Heat is transported both in the solid matrix and in the void system, forming a coupled heat transfer process with heat diffusion (conduction) and heat advection by moving groundwater. The governing steady state, one-dimensional equations for heat and fluid flow are given by Fourier's law and Darcy's law, which are identical in the form:

Fourier's law:

$$q'' = -k\frac{dT}{dx} \tag{1.1}$$

Where q'' is heat flux (W/m^2 [Btu/hr-ft^2]);

k is the thermal conductivity of the ground (W/m-K [Btu/h-ft-ºF]);

Darcy's law:

$$\vec{q} = -K\frac{dh}{dx} \tag{1.2}$$

Where $\vec{q}$ is the specific discharge (volume flow rate per unit of cross-sectional area)

(m/s [gpd/ft^2]);

K is the hydraulic conductivity of ground (m/s [gpd/ft^2]);

h is the hydraulic head (m [ft]).

The specific discharge $\vec{q}$ is related to average linear ground water velocity v by:

$$v = \frac{\vec{q}}{n} \tag{1.3}$$

Where n is the porosity, which, for a given cross-section of a porous medium, is the ratio of the pore area to the cross-sectional area (Fetter 1988).

The uncased borehole in SCW systems allows the heat exchange fluid to be in direct contact with the earth and allows ground water infiltration over the entire length of the borehole. This direct contact eliminates the conductive resistances of plastic pipe and grout associated with a typical earth-coupled U-tube system. The presence of ground water enhances the usability of the ground as a heat source/sink. The larger heat capacity of the water-saturated soil/rock dampens the temperature changes in the ground compared with unsaturated soil/rock. Furthermore, the movement of ground water enhances the heat transfer. In addition, the rough borehole wall can induce turbulence; so higher heat transfer coefficients can be obtained.

The moisture content of soil has a significant effect on its thermal properties. When water replaces the air between particles it reduces the contact resistance. The thermal conductivity can vary from 0.25 W/m-K for dry soil to 2.5 W/m-K for wet soil (Rawlings and Sykulski 1999). When heat is extracted/rejected, there will be migration of moisture by diffusion, thus the effective thermal conductivity will be increased.

As mentioned above, ground water movement will have a significant impact on heat transfer through the ground because heat is transferred by convection due to moving

groundwater as well as conduction. In the presence of groundwater, buoyancy flows generated by the temperature differences also affect the temperature distribution in the ground. The presence of groundwater flow in SCW systems changes the heat transfer problem from pure heat conduction to a coupled flow and advective-diffusive heat transfer problem.

Accordingly, heat transfer in the ground surrounding SCW systems is much more complicated and much more difficult to simulate. Also, the heat exchange fluid (water) in SCW systems is affected by the transient building thermal loads in addition to the heat transfer in the porous medium (aquifer) around the borehole of SCW systems. Therefore, this problem is characterized by time-varying boundary conditions.

Through this research, we hope to make a more complete and much better understanding of the characteristics of standing column well systems, such as necessary well length per given load, preferred operating strategies (bleed, etc.) The first objective of this work is to analyze and evaluate the currently available research on standing column well systems. The second objective is to develop a detailed numerical model of standing column well systems. The third objective is to use the detailed numerical model to perform a parametric study of the effects and significance of standing column well design parameters. Finally, the fourth objective is to develop a simplified analytical and/or numerical model, which is feasible to be used as a design tool by HVAC engineers.

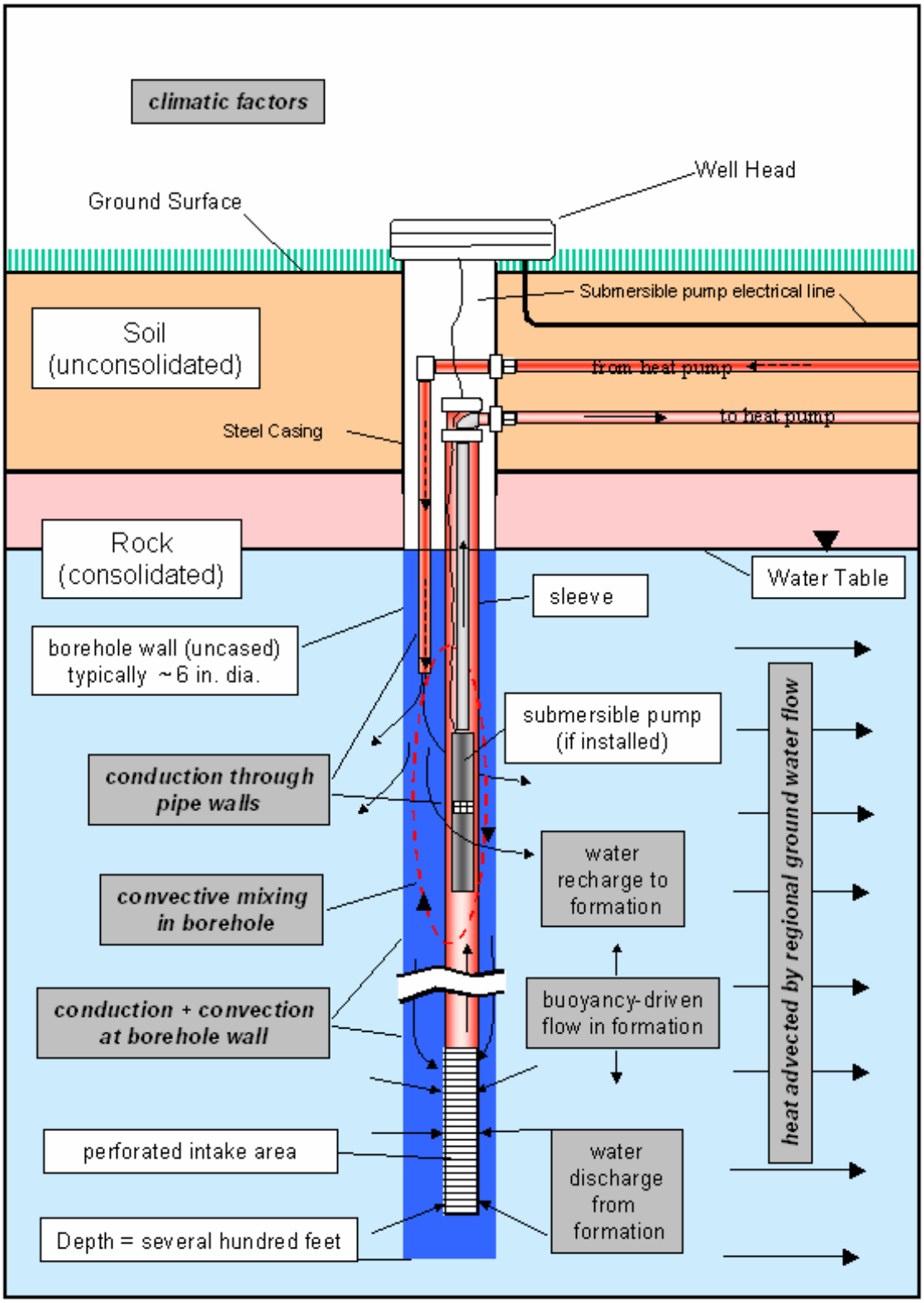

Figure 1-4 A typical schematic of standing column well

(http://www.hvac.okstate.edu/)

2. BACKGROUND AND LITERATURE REVIEW

Although there are numerous SCW systems installations in the United States, very little has been published on the theory of operation and modeling. The literature directly related to the standing column well, is reviewed first. Secondly, related research in the discipline of hydrogeology is reviewed.

2.1. Bose et al. (1979) Geo-thermal well system

The first reported field research on SCW systems is described by Bose et al. (1979). This system was referred to as a "Geo-thermal well system". The Geo-thermal well is somewhat different from the current standing column well (Figure 1-4). While it has a standing column, ground water cannot enter into the well because it is completely cased. A schematic of the Geo-thermal well is shown in Figure 2-1. A 5-inch PVC pipe with cap at both ends, pressurized to about 15 psig (at the top of the well), is the most important component in this vertical heat exchanger. The water may be discharged to the top or bottom, and the discharge tube may be insulated. In the experimental well described by Bose et al. the water exiting the heat pump is discharged into the bottom of the 5-inch PVC pipe by means of $1^{1/4}$-inch tube (the dip tube) running the length of the well.

Regarding the location of the discharge pipe, Bose et al. (1979) did some tests during the summer. From the test results, it was found that the entering water temperature to the heat

pump would be lower when the hot water from the heat pump was discharged to the bottom of the well rather than to the top of the well. Also a series of tests have shown an improvement of approximately 20 % in U-values (overall heat transfer coefficient) for wells by using insulated dip tubes.

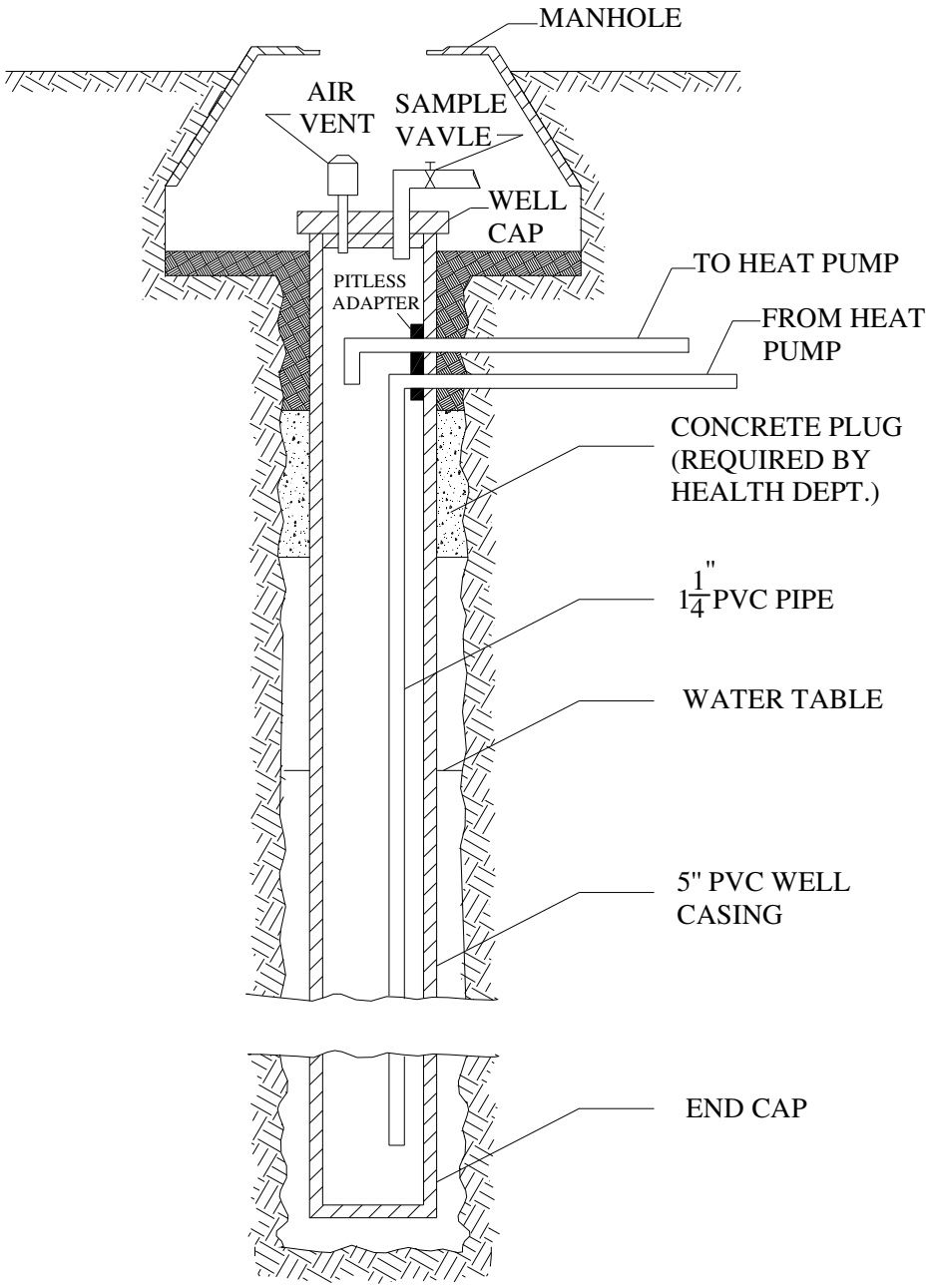

Figure 2-1 Geo-thermal well design (Bose et al. 1979)

Since no exchange of water with the surrounding formation is allowed, this system cannot be expected to perform as well as a modern SCW system.

2.2. Braud and Oliver's research (1980's)

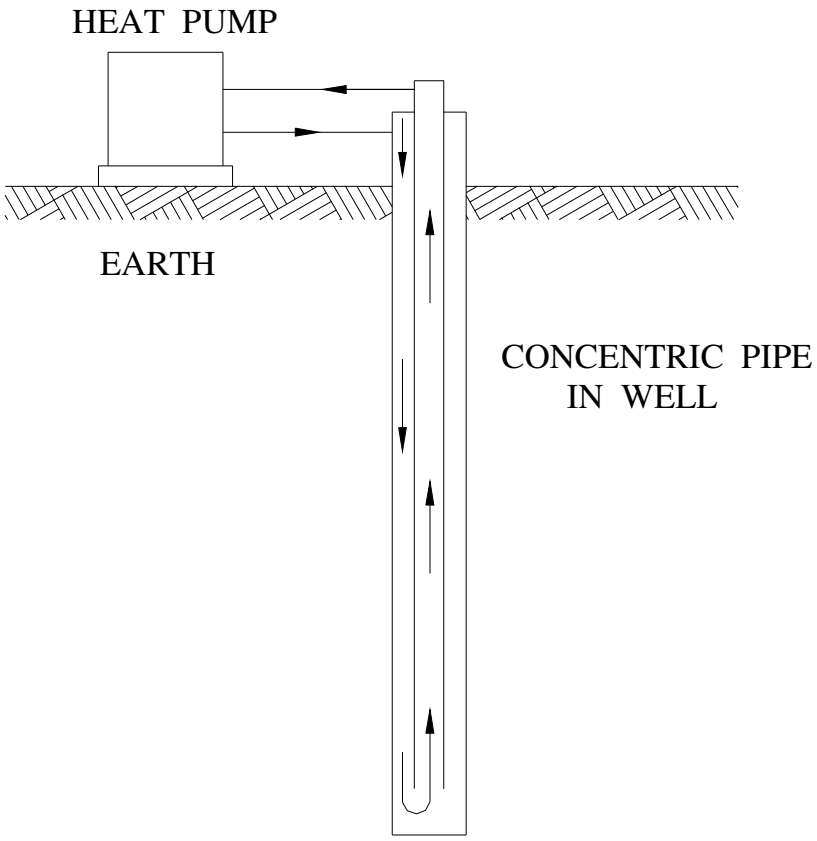

Figure 2-2 Concentric well pipes for thermal exchange to earth with liquid source heat pump (Oliver and Braud 1981)

Analysis of steady-state heat exchange to earth with concentric well pipes and governing equations for fluid temperature distribution in the pipes were given by Oliver and Braud (1981). They derived a closed-form analytical solution for the concentric vertical, ground-coupled heat exchanger under steady-state operation by assuming an isothermal

ground surface 10 m (3.3 ft) away from the center of the heat exchanger. The temperature difference between fluid in the annular area and the earth is the driving force for the heat transfer to the earth mass, and the temperature difference in the two pipes is the driving force for the crossover heat flow.

Oliver and Braud's analysis assumed steady-state, radial, conduction heat flow only. They didn't account for the effect of ground water flow. Their analysis is based on the following assumptions:

- all physical parameters are independent of time, location, pressure and temperature;
- all heat flow is radial in the heat exchanger;
- the only mechanism for heat transfer is conduction (this has the effect of modeling a cased system as described by Bose);
- temperature in the fluid is constant at each cross section (inside pipe).

They derived differential equations from the standpoint of conservation of energy for a control volume of fluid and surrounding ground, and solved them analytically. The general solution was given by:

$$TR(Z) = \frac{\theta_2(Z)}{\theta_1(Z)} = \frac{(\lambda_1 + 1)\exp\{\lambda_1 Z\} - \frac{\lambda_1}{\lambda_2}(\lambda_2 + 1)\exp\{\lambda_2 Z\}}{\exp\{\lambda_1 Z\} - \frac{\lambda_1}{\lambda_2}\exp\{\lambda_2 Z\}} \qquad (2.1)$$

Where $\theta_1 = T_1 - T_0$;

$\theta_2 = T_2 - T_0$;

$Z = \frac{U_{21} x}{\dot{m} C}$;

$\beta = \frac{U_{02}}{U_{21}}$;

x is the coordinate of the position along the axis of the heat exchanger well (m [ft]), (x = 0 at the bottom of well);

T_0 is the earth temperature (ºC [ºF]);

T_1 is the temperature of the fluid in the inner return pipe at position x (ºC [ºF]);

T_2 is the temperature of the fluid in the annular area at position x (ºC [ºF]);

$\dot{m}$ is the fluid circulation rate (kg/s [lbm/hr]);

C is the specific heat of the fluid in the pipe (J/kg-K [Btu/lbm-ºF]);

U_{21} is the fluid to fluid conductance of the inner pipe(W/m-K [Btu/hr-ft-ºF]);

U_{02} is the conductance of the well casing plus earth cylinder (W/m-K [Btu/hr-ft-ºF]), (includes film coefficient if appropriate);

λ_1 , λ_2 are functions of β (the type of function was not described in this paper).

In residential heating and cooling use, the operation of a heat pump is cyclic; the energy exchange to earth is highly transient rather than steady state. The steady state value from Oliver and Braud's model (1981) underestimates the heat transfer during the whole year cyclic operation. It is therefore unrealistic to design the heat exchanger on the basis of its steady–state operation. Moreover, this model does not take into account the beneficial effect of the ground water flow and bleed.

Braud et al. (1983) measured the heat exchange rate of earth-coupled concentric pipe heat exchangers in Louisiana State University. They noted greater conductance values of the

concentric pipes over the single U-tubes when the concentric heat exchanger consisted of a steel outer casing (rather than PVC) and PVC inner pipes. Some thermal "short-circuiting" could occur between the inner and outer flow channel, but this can be reduced with use of a low thermal conductivity inner pipe.

2.3. Tan and Kush's research (1986)

A 152 mm (6 in) diameter, 189 m (620 ft) deep standing column well located at Westchester County, NY, was used for this R&D/field test project. An off-the-shelf, 5-ton water-to –air heat pump intended for groundwater use was installed in this residential building. Tan and Kush (1986) called the SCW a "semi-closed loop" because of the influx/outflow of ground water at fissures in the rock. While it is the first SCW system described with an uncased borehole, no bleed was utilized. Water was withdrawn at a depth of 12.2 m (40 ft) and the return water from the heat pump was re-injected at a depth of 183 m (600 ft). The fluid water flow rate was 0.6935 kg/s (11 gpm) with a 0.25 kW (1/3 hp) circulating pump at the ground level outside the well. The static water table level was at a depth of 1.52 m (5 ft). Water was discharged to the bottom of the well; thus the water supplied to the heat pump does not pass through the region of discharge.

The well, heat pump and system parameters such as water temperature back to the heat pump, and from the heat pump were thoroughly measured and documented for a continuous 22-month period in this field test project. Also, the line-source theory was used to approximately calculate the theoretical long-term seasonal temperature change of the earth surrounding the well as a function of radius. It was found that the best

agreement between the analytical and the actual ground temperature was obtained when a value of thermal conductivity of 2.6 Btu/ft-hr-ºF (an "enhanced" thermal conductivity) was used. This may be compared with the actually averaged one (less than 2.4 Btu/ft-hr-ºF, which was assumed to be the value of granite rock surrounding the well). Tan and Kush (1986) didn't use any in-situ test method to obtain this actually averaged value of thermal conductivity. Presumably, they took the values directly from publicly available handbooks.

Tan and Kush (1986) pointed out that SCW systems performed very well as earth-coupled devices in both heating and cooling season. They measured the entering water temperature (EWT) to the heat pump and found it ranged from 6.9 ºC (44.5 ºF) in early January to slightly over 15.6 ºC (60 ºF) in mid-July of the second cooling season.

According to their field test, Tan and Kush (1986) concluded that SCW systems could give very stable EWT to the heat pump even in severe winter or summer. In their test, the lower limit for the heat pump operation, which was set as leaving water temperature of 3.3 ºC (38 ºF), was never reached.

Regarding the influence of ground water, if the well is uncased, the local hydrology will affect the performance of well. Although in their test, this effect was not quantified, Tan and Kush (1986) pointed out that substantial infiltration/exfiltration can enhance the system performance greatly. No information about bleed was found in Tan and Kush's research.

2.4. Mikler's research (1995)

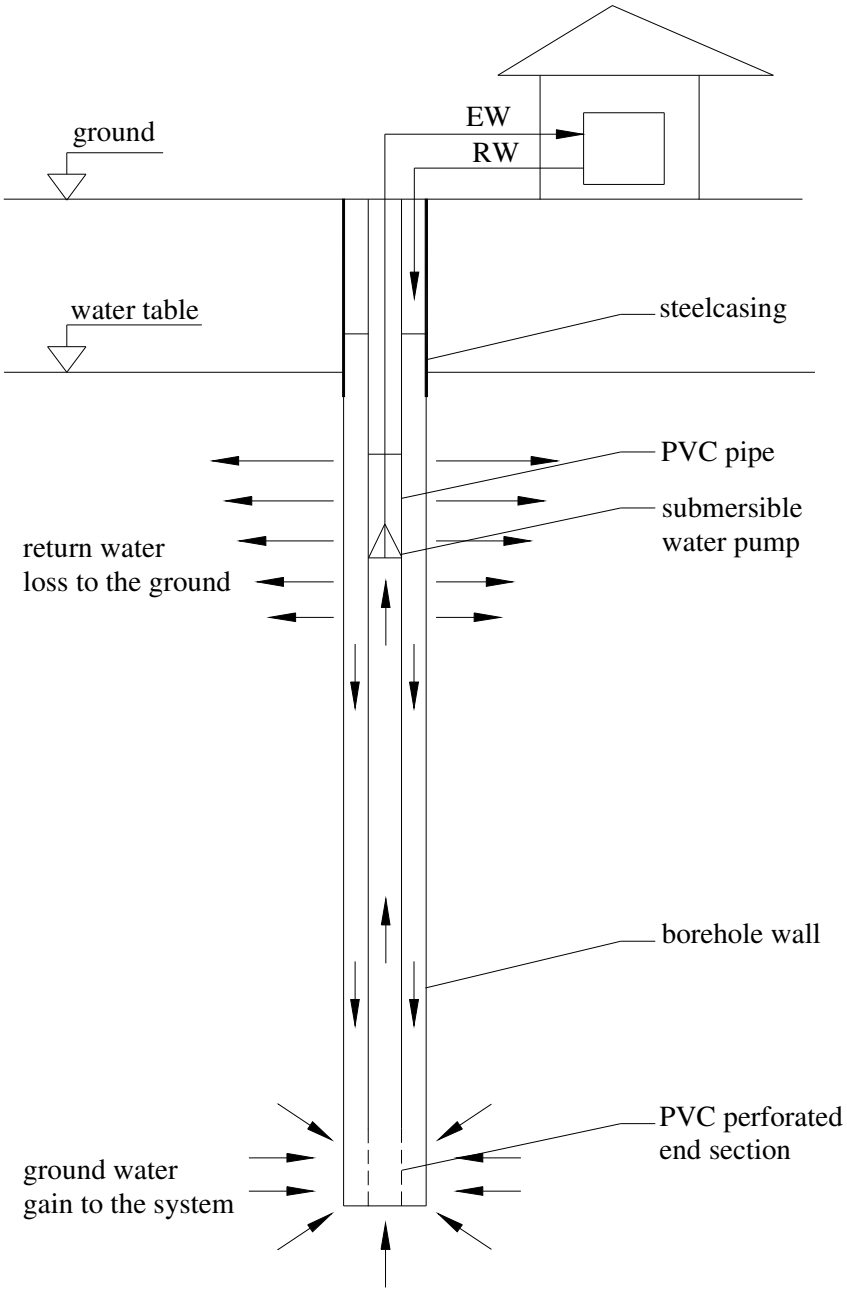

Figure 2-3 A schematic 'thermal well' studied by Yuill and Mikler (1995)

2.4.1. Numerical study

Yuill and Mikler (Mikler 1993; Yuill and Mikler 1995) used a well at Pennsylvania State University to research the performance of standing column well systems. They referred to

the standing column well as a "thermal well." The thermal well serves as a circulation, withdrawal and injection well at the same time. But the well does not bleed; the injection rate always matches the withdrawal rate. They developed a simplified mathematical model to describe the coupled thermo-hydraulic energy transfer by conduction and convection in an aquifer surrounding a thermal well. A schematic of the well system is shown in Figure 2-3.

To simplify the analysis, Yuill and Mikler (1995) used the following assumptions in their study:

- homogeneous and isotropic aquifer
- cylindrical symmetry of the coupled flow around the axis of the borehole
- no heat or ground water flow in the vertical direction
- laminar ground water
- no dispersion (no groundwater diverted to other places)
- thermal well is in the dynamic hydraulic equilibrium with the surrounding groundwater aquifer
- natural hydraulic gradients in the aquifer are neglected; hydraulic gradients caused by pumping are dominant.

Based on these assumptions and by introduction of a "groundwater factor" (G_f), which is the ratio of convection to conduction, the governing partial differential equations are derived, simplified, and solved numerically.

$$\frac{\partial^2 T}{\partial r^2} + \left[\frac{1 \pm G_f}{r}\right]\frac{\partial T}{\partial r} = \frac{1}{\alpha}\frac{\partial T}{\partial t} \qquad (2.2)$$

Where G_f is the groundwater factor (+ denotes flow into the well; - denotes flow out of the well);

$$G_f = \frac{\dot{m}_w C_{pw}}{2\pi \cdot k \cdot dz};$$

$\dot{m}_w$ is the groundwater mass flow rate (kg/s [lbm/hr]), (either discharge groundwater or suction groundwater flow);

C_{pw} is the specific heat of water (J/kg-K [Btu/lbm-ºF]);

k is the thermal conductivity of the ground (W/m-K [Btu/hr-ft-ºF]);

α is the thermal diffusivity of the ground (m^2/s [ft^2/hr]);

z is the vertical coordinate (m [ft]).

The governing equations are converted into explicit forms of finite difference equations by using central difference approximations. To obtain stable solutions, the stability criterion is set as:

$$Fo = \frac{\alpha \Delta t}{(\Delta r)^2} \leq 1/2 \qquad (2.3)$$

Where α is the thermal diffusivity (m^2/s [ft^2/hr]).

Also, Yuill and Mikler (1995) used a new term, equivalent thermal conductivity (k_{eq}), to account for the improved heat transfer due to the induced groundwater flow in the aquifer. To attain the value of k_{eq}, they let heat transfer rates along the borehole wall for the case of coupled thermo-hydraulic flow considering the real ground thermal conductivity (k) equal the ones for the case of pure heat conduction considering the

equivalent thermal conductivity (k_{eq}). They suggested this equivalent thermal conductivity could be used in the existing pure heat conduction design models to determine the depth of the thermal well.

Regarding hydraulic head distribution in the thermal well, Yuill and Mikler (1995) considered this distribution as time independent and used a steady-state solution approach in the thermal well model. They assumed that the hydraulic gradients caused by pumping were dominant with respect to natural hydraulic gradients in the aquifers. Therefore, during their analysis, they neglected the natural hydraulic gradients. The equilibrium well equation relating the groundwater flow rates to the hydraulic gradients in the well was given by:

$$Q_w = -\frac{2\pi \cdot K \cdot \Delta h \cdot dz}{\ln(R / r_b)} \qquad (2.4)$$

Where Q_W is the water flow rate (m^3/s [gpm]);

K is the hydraulic conductivity of the ground (m/s [gpd/ft^2]);

R is the radius of influence (m [ft]);

r_b is the borehole radius (m [ft]).

But this finite difference model that allowed calculation of the radial heat transfer at a particular depth was not truly two-dimensional. Consequently, vertical heat transfer, end effects, and bleed operation could not be considered.

2.4.2. Experimental study

Mikler (1993) did some experimental studies on transient heat and mass transfer in a "thermal well" system installed at Pennsylvania State University.

Well #1 was 0.15 m (6 in) and 325 m (1065 ft) deep and was used in a large commercial system with 70 kW (20 tons) cooling capacity. Another well, #2, with the same diameter but 91 m (300 ft) depth was used to monitor and measure ground temperature changes in the vicinity of well #1. The distance between well #1 and well # 2 was 3.65 m (12 ft). Four 17.6 kW (5 ton) heat pumps were operated at full capacity in parallel in this system during the experimental period.

Thermocouples were used to monitor both the water temperature distribution along the thermal well as well as the ground temperature in the vicinity of the operating well (well #1) at different depths. Also, thermocouples were used to monitor the entering and return temperature of the circulating water, the inlet and outlet air temperatures passing through the heat pumps, and the ambient temperatures. A flow sensor was used for monitoring total flow rate of the circulating water. Thermal and hydraulic properties of the aquifer were estimated based on the available measured data, "drilling log", and basic knowledge about the local geology.

The heat pumps were operated at fully capacity in cooling mode for a period of 48 subsequent days from August 4 to September 20, 1992, with a total of 235.73 GJ

(223.44 MMBtu) of heat injected into the ground. The temperatures of the water flowing down in the annular space and up inside the PVC pipe were measured continuously at five different depths in the well #1 and two depths in well #2. From his experimental data, Mikler (1993) found that the trend of the temperature change confirmed the well known theoretical analysis presented by Eskilson (1987)-"On a time scale, one third of the total temperature drop to steady state conditions occurs during the first day, and two thirds during the first two months". Also, from Mikler's experimental observation, it was shown that the water temperature at some lower depth inside the PVC pipe is lower than the temperature at the bottom of the well. Mikler contributed this phenomenon to the fact that some amount of fresh water was being drawn into the system and mixed with the return water.

After the cooling mode operation, the system was shut off for a period of six weeks from September 21 to December 10, 1992. Temperatures at all monitored locations finally stabilized at a higher level than the corresponding initial undisturbed aquifer temperatures. Then, the heat pumps were operated at full capacity in heating mode for the period of 71 subsequent days from December 10, 1992, to February 19, 1993, with a total of 114.15 GJ (108.20 MMBtu) of heat absorbed from the ground. Temperatures were measured at the same locations in the cooling mode operation. Mikler (1993) observed the temperature difference at the bottom of the well during the heating mode operation, which was proof of the direct interaction between the circulating water in the thermal well and the groundwater.

In their paper, Yuill and Mikler (1995) didn't give any description of bleed. According to their research, they pointed out that the required drilled depth of a 6-in thermal well is about 60% of the depth of the $1^{1/2}$-in, U-tube earth-coupled borehole, assuming that both are properly designed and are installed in the same geological formation. The authors attribute the superior performance to the increased roughness at the wall of the well together with the induced interaction between the circulating water and groundwater. They didn't mention that elimination of grout and pipe resistances contribute to the superior performance.

The limitations of thermal wells are also listed in this paper (Yuill and Mikler 1995). If the groundwater quality is bad and impossible or too costly to treat (for example, groundwater with high mineral and bacterial content,) the thermal well is not preferable. In some states, this type of well can't be installed because the water-well legislation does not permit the "co-mingling of aquifers". Sometimes, drilling problem may be the major obstacle. For example, the borehole may collapse in some geological formations.

According to their experimental and theoretical study, Yuill and Mikler (1995) concluded that properly designed and installed "thermal wells" could compete with any of the closed-loop systems based on their high system performance with smallest borehole depth and lowest combination of installation and operating costs.

2.5. Orio's research

Mr. Carl Orio first designed and employed standing column well systems in 1970's. Since that time, he has been involved in many standing column well systems of Water & Energy System Corporation. Orio (1994, 1995) used the Kelvin line theorem to analyze the heat transfer in this system.

$$T - T_0 = \frac{Q'}{2\pi k_s} \int_X^\infty \frac{e^{-B^2}}{B} dB = \frac{Q'}{2\pi k_s} I(X) \tag{2.5}$$

$$X = \frac{r}{2\sqrt{\alpha t}}$$

Where T is the soil temperature (ºC [ºF]);

T_0 is the initial temperature of the soil (ºC [ºF]);

Q' is heat transfer rate (negative for heat extraction and positive for heat rejection) (W/m [Btu/ft-hr]);

r is the radial distance from line (m [ft]);

k_s is the thermal conductivity of the soil (W/m-K [Btu/hr-ft-ºF]);

α is the thermal diffusivity (m^2/s [ft^2/hr]);

t is the heat pump run time (hr);

B is the integration variable.

The Kelvin line theorem has provided a good correlation with some practical field experience (Orio 1995). But the Kelvin line theorem, offered as a relatively simple treatment of the problem, is not sufficient for the complicated heat transfer in standing column well systems, including conduction, convection, and advection, especially for

systems with ground water bleed. The Kelvin line theorem neglects the advection of heat from the borehole due to groundwater flow. The effect of the ground water flow on performance of SCW systems should be taken into account in a more complete and accurate model. In particular, the process of advection is very important in the modeling of SCW systems with groundwater bleed. Thus, the Kelvin theorem cannot be directly used to correctly calculate the temperature distribution of a "bleed" SCW system. The line source analysis with an "enhanced" thermal conductivity might be used to consider the effect of groundwater (See more discussion about related analytical solutions in section 2.9.).

In this literature review, Orio's papers are the only ones that give some detailed information about bleed. It is reported that in the severity of winter or summer, a relatively small (10%) bleed can reestablish water temperature in the well of SCW system at a rapid rate. According to his observations, Orio (1994, 1995) pointed out that bleed can make the effective thermal conductivity increase by factors of 3 to 5. The homogeneity of the geologic formation, the characteristics of the aquifer, and the density of the fractures affect the performance of SCW systems with bleed. Usually, 80-90% of the water is returned to the standing column well and the balance is returned to the earth some distance away or disposed of.

In some cases, the bleed water is disposed of in a separate return well. The National Ground Water Association (NGWA) provides the following formula to calculate the optimum return well distance:

$$D = \sqrt{0.2 \times Q} \tag{2.6}$$

Where D is the distance in feet to the recharge well (ft);

Q is the design heat transfer rate (Btu/hr) .

In fact, a return well is often not required because of the relatively small amount of bleed water. Instead, the bleed water may be disposed of in storm drains, ponds, streams or other natural routes. In wells that also serve as the household domestic water supply, "bleed" is naturally provided. The "bleed" power of a shower, laundry and other water use makes the average water temperature in the well of the residential SCW systems quite stable (Orio 1995).

Orio (1999) discussed the placement of pumps and the depth of the boreholes. The boreholes could be one-half the depth of the closed loop earth coupling methods. When boreholes get deeper than 152 m (500 ft), there is substantial increase in heating energy because the earth temperature increases with the increasing depth. But placing the pump at the bottom of the borehole has some disadvantages such as installation and service. To eliminate these disadvantages, Orio (1999) proposed that the submersible pump should be placed at the top of the borehole, but a lightweight plastic tube (dip tube or tail pipe) should be inserted to the bottom of the borehole (Figure 2-4b). Thus, the most stable water temperature is achieved, and shorter pipes and wires are required, so the initial investment can be reduced. Deeper wells (depth >152 m [500 ft]) mostly use dip tubes constructed of 100 mm (4 in) diameter PVC pipes to the bottom of the well. The dip tube has a minimum of 120 one-inch perforations in the lowest 12 m (40 ft).

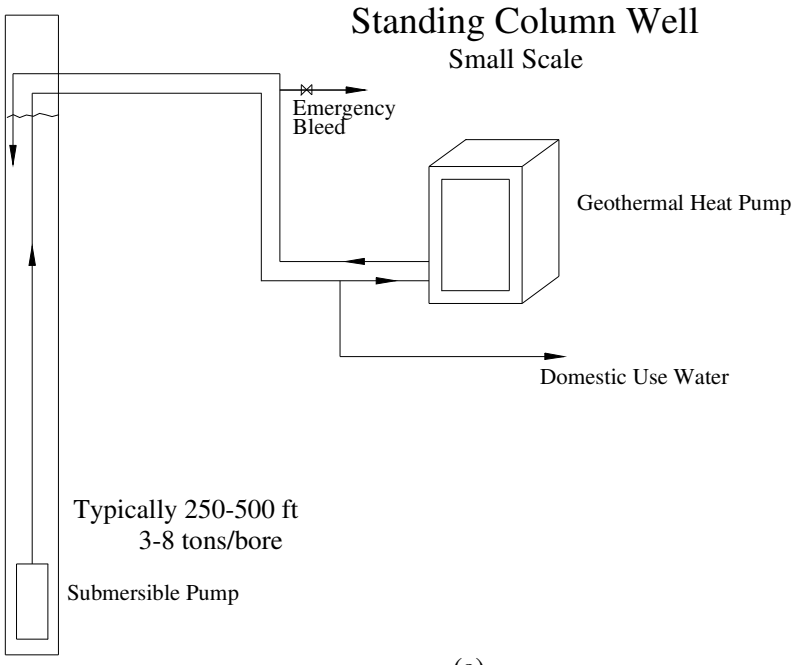

(a)

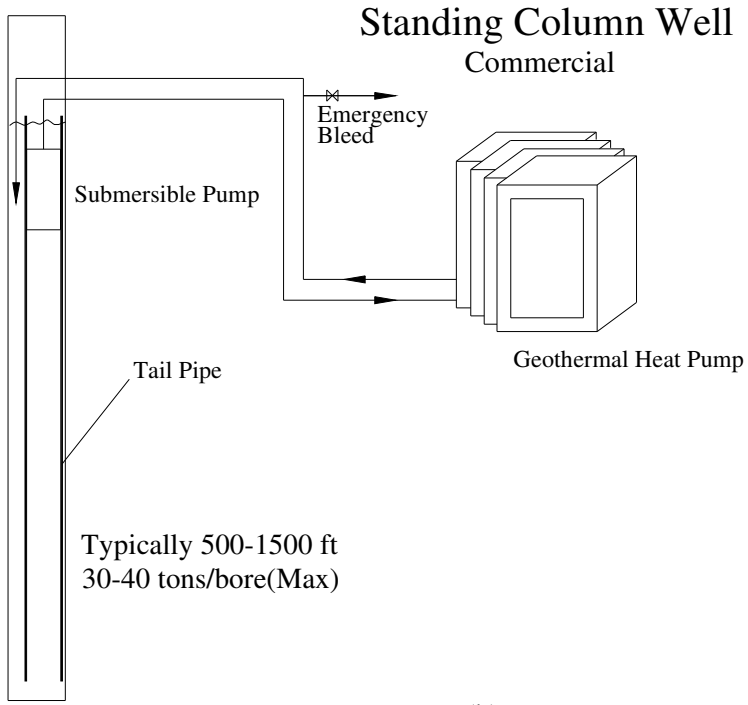

(b)

Figure 2-4 Schematics of standing column well from description of Orio (Orio 1999)

2.6. Some typical installations of SCW systems

There are approximately 1000 SCW installations in the United States. Most of them are located in the Northeast and Pacific Northwest in addition to parts of Canada in heating-dominated residential and light commercial applications. Also there are some installations out of North America.

2.6.1. Haverhill public library

The Haverhill public library is located in Haverhill, Massachusetts. There are four standing column wells to provide a heat sink/source for water-to-water heat pumps (initially two SCWs in 1994 but expansion of the library resulted in two additional SCWs after 1996). Each of the standing column well wells is 457 m (1500 ft) deep. Water is drawn from the bottom of the well, run through the heat pump and discharged at the top of the well.

Whenever the well water temperature drops below 4.44 °C (40 °F), a bleed cycle initiates. This automatic bleed diverts approximately 10 % of the flow from returning to the wells. A bleed cycle typically lasts for 30 minutes. It acts to limit the lower well temperatures by drawing in new warmer groundwater from far field. There is no bleed for high temperatures.

As Figure 2-5 shows the well water temperature remained above 2.78 °C (37 ºF) and generally operated in the lower 40s (ºF) during heating mode. The peak loop temperature reached 21.1 ºC (70 ºF) in June. However system operation changed after June 25th when

the second well pump became active and the maximum well temperature remained below 18.9 ºC (66 ºF) thereafter. There was also less variation in the temperature after June 25th in both heating and cooling mode.

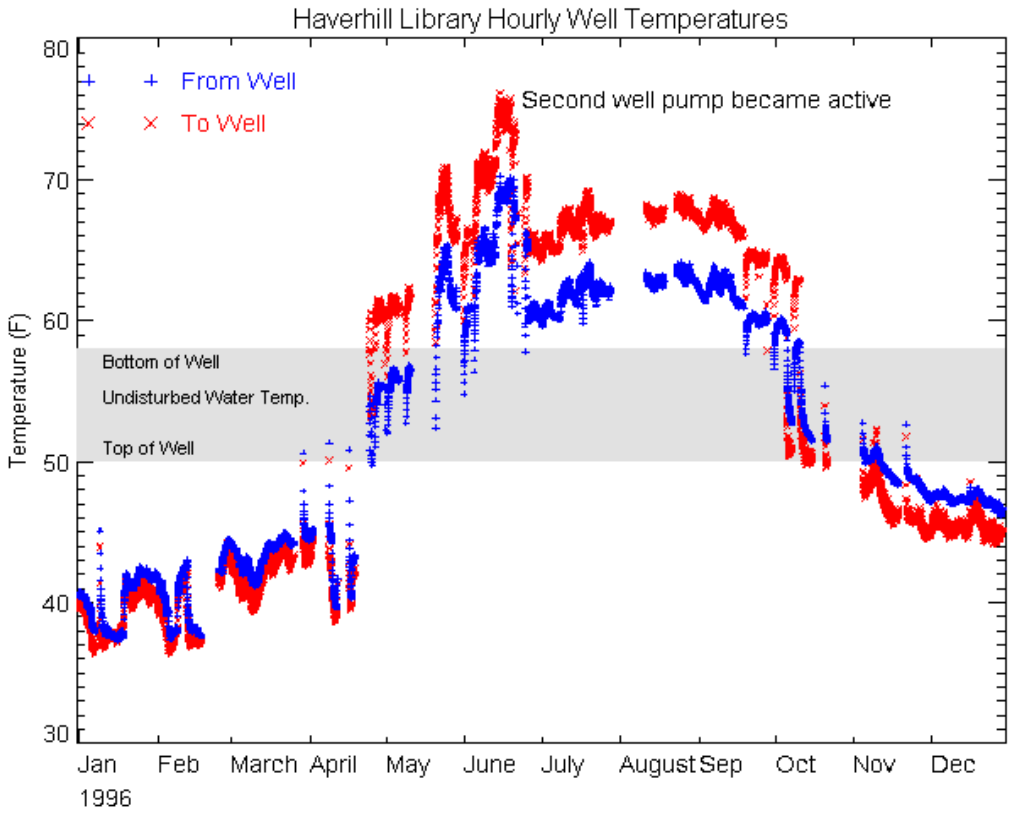

Figure 2-5 Standing column well water temperature trends in Haverhill public library (http://www.cdhenergy.com/ghp/haverhill/haverhill_main.htm)

2.6.2. SCW application in China

From March 2001 to present, Ever Source Science & Technology Development Co. LTD in Beijing, China, has been applying the concept of the standing column well in about two hundred projects, with the name "single well for supply and return." The schematic drawing of the single well is shown in Figure 2-6. A heat exchanger is located at the well

mouth, where the well water and recycle water circulated in separate loops. Therefore, the groundwater from the well is neither consumed nor polluted. According to their experience, this single well system can solve problems such as moving sands, pollution of groundwater, and collapse, which are all related to multi-well systems. More detailed technical information about this system is not available.

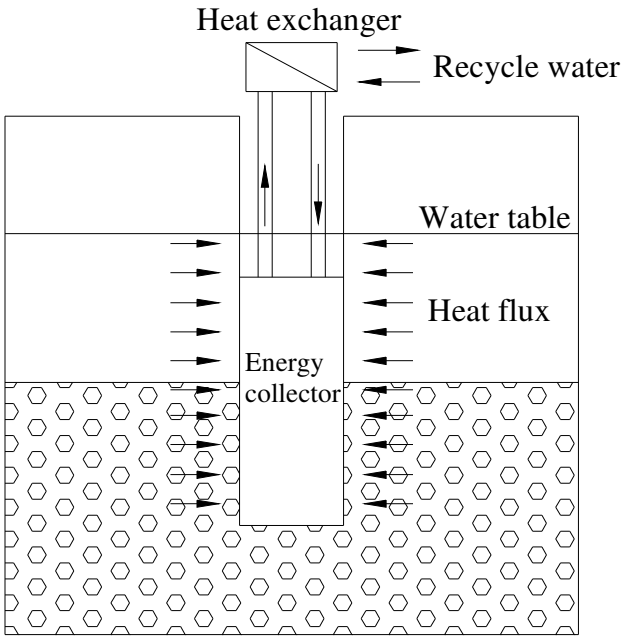

Figure 2-6 The schematic drawing of "single well for supply and return" (HYY 2003)

From December 12, 2003 to March 17, 2004, Ever Source Science & Technology Development Co. LTD measured the energy consumption of eleven different type buildings in Beijing. These buildings use standing column wells as a heat source for heating in winter (Sun 2004). This investigation shows that energy consumptions of seven buildings among the eleven buildings are lower than that of the conventional heating system with a coal boiler. All eleven buildings have lower energy consumptions than other conventional oil/gas/electrical boiler heating system.

2.7. "Geohill"-open hole coaxial thermal well

An open loop concentric well heat exchanger called a "Geohill" has been developed by Geocalor A.G. (Hopkirk and Burkart 1990). The system schematic is shown in Figure 2-7. The borehole is 250 mm (10 in) in diameter and up to 300 m (1000 ft) deep, and it remains open with the exception of a steel casing in the upper part. A central PVC tube is surrounded by graded gravel filling and contains a downhole pump feeding water via an insulated tube to the heat pump. The fluid return is through the gravel-filled annulus. According to this configuration, the gravel filling can increase friction resistance for the return water flowing down, and therefore more groundwater is sucked into the system, especially if the well were drilled in a highly permeable rock formation.

According to Hopkirk and Burkart's research, the "Geohill" system shows much promise, especially in larger commercial installations requiring both heating and cooling.

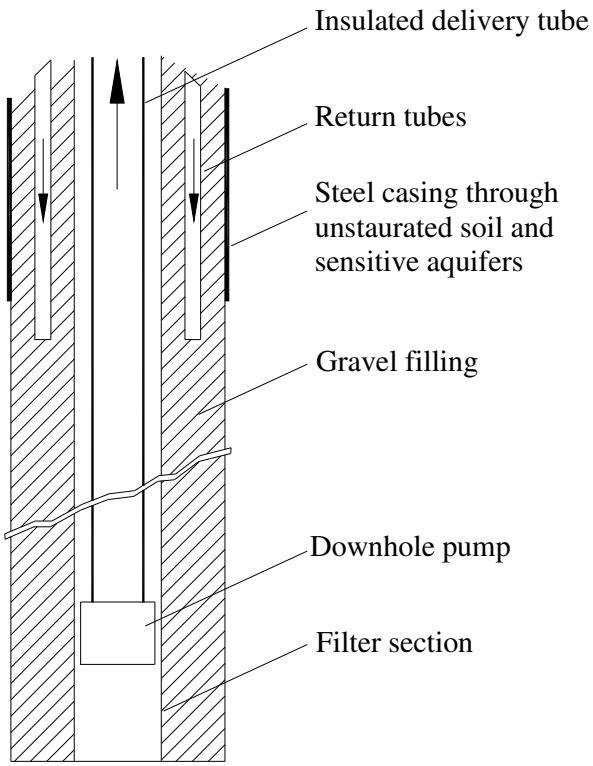

Figure 2-7 Open hole coaxial thermal well "Geohill"

(Hopkirk and Burkart 1990)

2.8. Summary of the different research related to SCWs

Tables 2-1 and 2-2 summarize the research related to SCWs to date.

Table 2-1 Summary of experimental research related to SCWs

Researcher and date	System name	Depth of well	Diameter of well	Placement of well pump	Placement of suction tube	System water mixes with groundwater (i.e., open-loop)	System bleeds some groundwater	Heat pump capacity	ft/ton
Bose et al. (1979)	Geo-thermal well	73 m (240 ft)	127 mm (5 in)	Ground level	Top of the well	No	No	2.25 tons	106
Braud and Oliver (1980, 1983)	Concentric pipe well	154 m (504 ft)	63.5 mm (2.5 in)	Ground level	Bottom of the well	No	No	2 tons	77
Tan and Kush (1986)	Semi-closed loop standing column well	189 m (620 ft)	152.4 mm (6 in)	Ground level	Top of the well	Yes	No	5 tons	124
Hopkirk and Burkart (1990)	Open hole coaxial thermal well "GEOHILL"	305 m (1000 ft)	254 mm (10 in)	Bottom of the well	Bottom of the well	Yes	No	N/A	N/A
Mikler (1993) Yuill and Mikler (1995)	Thermal -well	325 m (1065 ft)	152.4 mm (6 in)	Top of the well (under the water table)	Bottom of the well	Yes	No	20 tons	53
Orio (1988,1995, 1999)	Standing Column Well	73 - 457 m (240-1500 ft)	152.4 mm (6 in)	1. Top of the well (under the water table) 2. Bottom of the well	Bottom of the well	Yes	Yes	5-200 tons	50-60
HYY Beijing (2000s)	Single well for supply and return	80 m	500 mm (19.68in)	N/A	N/A	Yes	No	N/A	N/A

Table 2-2 Summary of the modeling of SCWs

Researcher and date	System Name	Analytical solution	Numerical solution	Include the effect of groundwater (advective heat transfer)	Include the effect of bleed	Comments
Braud and Oliver (1980, 1983)	Concentric pipe well	Yes	No	No	No	1. Steady state solution 2. Only consider heat conduction transfer 3. Cannot simulate cases in bleed operation
Tan and Kush (1986)	Semi-closed loop standing column well	Yes	No	Yes	No	1. Based on line-source theory 2. Use "enhanced" thermal conductivity
Mikler (1993) Yuill and Mikler (1995)	Thermal-well	No	Yes	Yes	No	1. Finite difference method 2. Some inputs in their models are based on their experiments
Orio (1988,1995, 1999)	Standing column well	Yes	No	Yes	Yes	1. Based on line-source theory 2. Use "enhanced" thermal conductivity

2.9. Some related analytical solutions (to ground source heat pump)

Several methods to predict the performance of ground source heat pumps are available, including both analytical (line heat source, cylindrical heat source) and numerical methods. Although numerical solutions are very powerful, they are relatively complex. Much data and computer time are usually required to obtain good results. In contrast, the simplified analytical methods such as the line heat source model and the cylindrical heat source model (first presented by Carslaw and Jaeger [1947] and Ingersoll et al. [1948] and later refined by other researchers [Kavanaugh 1984, Bose et al. 1988]) make it relatively simple to perform annual hour-by-hour simulations of ground-coupled heat pump systems. Because these analytical solutions might be further modified to be employed in SCW system after considering the movement of groundwater, they are reviewed below.

Figure 2-8 shows the cylindrical heat source embedded in an infinite medium, e.g. the earth. In the simplest case, the borehole is subjected to a constant heat transfer rate, q, from (or to) the surrounding ground for which the far field temperature is the undisturbed temperature, T_u. The object of the analytical solution is to calculate the temperature difference between the undisturbed ground temperature, T_u, and the borehole wall temperature, T_w. Based on the work of Carslaw and Jaeger (1947), Ingersoll et al. (1948, 1951, 1954) gave an analytical solution to the transient heat transfer from a line (or cylinder) embedded in an infinite homogeneous medium.

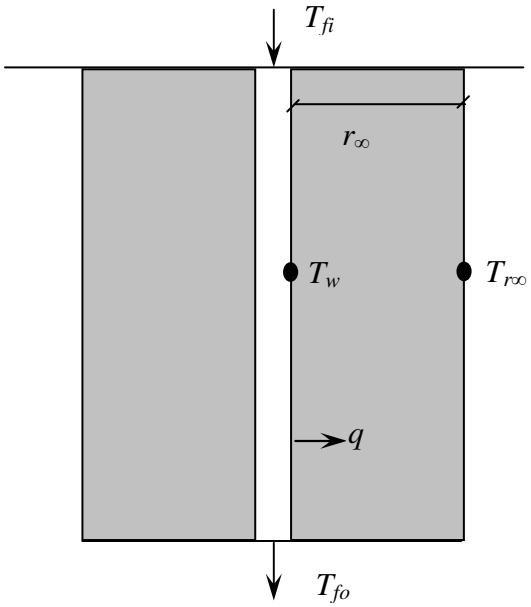

R_∞: the far field radius

$T_{r\infty}$: the far field temperature

$T_{r\infty} = T_u$

T_u: the undisturbed temperature of the ground

Figure 2-8 Schematic drawing showing the cylindrical heat source embedded in an infinite medium *

* When the diameter of the cylinder is zero, the cylindrical heat source becomes line heat source

2.9.1. Kelvin line source solution

The earliest approach to calculating thermal transport around a heat exchanger in the ground was the Kelvin line source theory (Ingersoll et al. 1948,1954). The temperature distribution around a line source of heat buried in a homogenous, infinite media is given by:

$$T_u - T = \frac{q_l}{2\pi k_s} \int_X^\infty \frac{e^{-B^2}}{B} dB = \frac{q_l}{2\pi k_s} I(X) \qquad (2.7)$$

$$X = \frac{r}{2\sqrt{\alpha t}}$$

Where T is the soil temperature (ºC [ºF]);

T_u is the uniform initial temperature of the soil (ºC [ºF]);

q_l is the heat transfer rate applied to the ground (W/m [Btu/ft-hr]) (a positive q value implies heating mode);

r is the radial distance from the line (m [ft]);

k_s is the thermal conductivity of the soil (W/m-K [Btu/hr-ft-ºF]);

α is the thermal diffusivity of the soil (m^2/s [ft^2/hr]);

t is the heat pump run time (hr);

B is the integration variable.

This model is based on approximating the borehole as a line source, assuming end effects are negligible. The soil acts as a heat rejection (absorption) medium that has an assumed uniform and constant initial temperature (T_u).

Let $y = X^2 = \frac{r^2}{4\alpha t}$. Thus Equation (2.7) can be changed into

$$T_u - T = \frac{q_l}{4\pi k_s}\int_y^{\infty}\frac{e^{-\lambda}}{\lambda}d\lambda = \frac{q_l}{4\pi k_s}(y - \ln y - \gamma - \frac{y^2}{2\cdot(2!)} + \frac{y^3}{3\cdot(3!)} + ... + \frac{(-1)^{N+1}y^N}{N\cdot(N!)}) \quad (2.8)$$

Where $\lambda$is the integration variable;

γ is Euler's constant, 0.5772157…

Equation (2.8) can be written as:

$$T_u - T_w = \frac{q_l}{4\pi k_s}\left(\ln\left(\frac{4\alpha t}{r_b^{\,2}}\right) - \gamma + C\right) \quad (2.9)$$

Where T_w is the borehole wall temperature (ºC [ºF]);

r_b is the borehole radius (m [ft]);

C is the summation of the series $\sum_{N=1}^{\infty} \frac{(-1)^{N+1} y^N}{N \cdot (N!)}$.

Actually, the integration of Equation (2.7) is from X to r_∞, where r_∞ is equal to $4\sqrt{\alpha t}$. To find how close T_u is to the value of the temperature at r_∞, a formula was given by Hart and Couvillion (1986):

$$T_{r_\infty} - T_u = \frac{q_l}{2\pi k_s}[0.0019] \qquad (2.10)$$

At typical values of q_l and k_s, $T_{r_\infty} - T_u$ varies from approximately 0.00167 ºC (0.003 ºF) to 0.0167 ºC (0.03 ºF) when r_∞ is equal to $4\sqrt{\alpha t}$.

Considering this correction, Equation (2.9) can be written as

$$T_u - T_w = \frac{q_l}{4\pi k_s}\left(\ln\left(\frac{4\alpha t}{{r_b}^2}\right) - \gamma - 0.0038 + C\right) \qquad (2.11)$$

Ingersoll et al. (1951) stated that the line source equation (Equation [2.9]) is exact only for a *true* line source, but that it can also be applied with negligible error for pipes less than 4 inch in diameter and times longer than 24 hours. The error does not exceed about 2% under these conditions. For the case where the time is too short or the pipe diameter is too large (in general when $\frac{\alpha t}{r^2} < 20$), the use of the line source equation will involve the error greater than 2%. Therefore, the line source cannot effectively and accurately model

systems with normal transient operating performance. Deerman and Kavanaugh (1991) stated that the line source method had a 10% error when using one-hour intervals.

2.9.2. Cylindrical heat source solution

The cylindrical heat source solution was developed using a single isolated pipe surrounded by an infinite solid of constant properties. The following assumptions are used in this solution:

- heat transfer only by pure conduction
- soil acts as an infinite solid
- perfect soil and pipe contact
- no groundwater movement

There are several cylindrical heat source solutions corresponding to different cases of our interest. These include a cylindrical heat source solution with and without considering the thermal mass in the borehole, and a cylindrical heat source solution, which considers two thermal masses in the borehole separated by a thermal resistance.

(a). Cylindrical heat source solution without considering the thermal mass in the borehole

The cylindrical heat source solution without considering the thermal mass in the borehole for a constant heat flux is as follows (Ingersoll et al. 1954):

$$T_u - T = \frac{q_l}{k_s} G(Fo, p) \tag{2.12}$$

Where T is the soil temperature (ºC [ºF]);

T_u is the uniform initial temperature of the soil (ºC [ºF]);

q_l is the heat transfer rate applied to the ground (W/m [Btu/ft-hr]) (a positive q value implies heating);

k_s is the thermal conductivity of the soil (W/m-K [Btu/hr-ft-ºF]);

$G(Fo, p)$ is the analytical solution;

$$G(Fo, p) = \frac{1}{\pi^2} \int_0^{\infty} \frac{\dfrac{e^{-(\beta^2 Fo)} - 1}{J_1^2(\beta) + Y_1^2(\beta)} \left[J_0(p\beta) Y_1(\beta) - J_1(\beta) Y_0(p\beta) \right]}{\beta^2} d\beta \qquad (2.13)$$

p is the ratio of the radius where the temperature is calculated over the borehole radius (r_0) ;

Fo is the Fourier number defined as: $Fo = \alpha t / r_0^{\,2}$.

Values of G are available from Ingersol et al. (1954). For $p = 1$ (i.e., at the cylindrical radius, borehole wall), the following equation is given by Bernier (2001).

$$G(Fo,1) = 10^{\left[-0.89129 + 0.36081 \times \log_{10}(Fo) - 0.05508 \times \log_{10}^2(Fo) + 3.59617 \times 10^{-3} \times \log_{10}^3(Fo)\right]} \qquad (2.14)$$

So, for the temperature at the borehole wall, T_w, Equation (2.12) can be reduced to

$$T_u - T_w = \frac{q_l}{k_s} 10^{\left[-0.89129 + 0.36081 \times \log_{10}(Fo) - 0.05508 \times \log_{10}^2(Fo) + 3.59617 \times 10^{-3} \times \log_{10}^3(Fo)\right]} \qquad (2.15)$$

(b). Cylindrical heat source solution with considering the thermal mass in the borehole

If a cylinder of radius r_b of a thermal massive perfect conductor is surrounded by an infinite medium (e.g. the ground) and is heated at the rate q_l per unit length per unit time for $t > 0$, all initial temperature being zero, the temperature of the perfect conductor is given by Carslaw and Jaeger (1959):

$$T = \frac{q_l}{k_s} G(h, \alpha_1, \infty, Fo) \tag{2.16}$$

$$G(h, \alpha_1, \alpha_2, Fo) = \frac{2\alpha_1^2 \alpha_2^2}{\pi^3} \int_0^\infty \frac{\left[1 - \exp\left(-u^2 Fo\right)\right]}{u^3 \Delta_1(u)} du \tag{2.17}$$

Where $h = 2\pi R_b k_s$, $\alpha_1 = 2\pi r_b^2 \rho C_p / S_1$, $\alpha_2 \to \infty$,

Fo is the Fourier number defined as $Fo = \frac{\alpha t}{r_b^2}$;

$$\Delta_1(u) = \left[u\left(\alpha_1 + \alpha_2 - hu^2\right) J_0(u) - \alpha_2\left(\alpha_1 - hu^2\right) J_1(u)\right]^2 + \left[u\left(\alpha_1 + \alpha_2 - hu^2\right) Y_0(u) - \alpha_2\left(\alpha_1 - hu^2\right) Y_1(u)\right]^2 \tag{2.18}$$

J_i is the Bessel function of order i;

Y_i is the modified Bessel function of order i;

k_s is the thermal conductivity of the ground (W/m-K [Btu/hr-ft-ºF]);

α is the thermal diffusivity of the ground (m^2/s [ft^2/hr]);

ρ is the density of the ground (kg/m^3[lbm/ft^3]);

C_p is the specific heat of the ground(J/kg-K [Btu/lbm-ºF]);

r_b is the radius of the cylindrical conductor (m [ft]);

R_b is the thermal resistance between the conductor and the ground (K/(W/m) [hr-ft-ºF/Btu]);

S_1 is the thermal capacity of the cylinder of perfect conductor

(J/m^3-K [Btu/ft^3-ºF]);

u is the integration variable.

For large values of Fo ($Fo >> 1$) Equation (2.16) can be reduced to:

$$T = \frac{q_l}{4\pi k_s}\left\{2h + \ln(\frac{4Fo}{C}) - \frac{(4h-\alpha_1)}{2\alpha_1 Fo} + \frac{\alpha_1 - 2}{2\alpha_1 Fo}\ln(\frac{4Fo}{C}) + o(\frac{1}{Fo^2})\right\} \qquad (2.19)$$

Where $C = 1.7811 = \exp(\gamma)$, and $\gamma = 0.5772157...$ is Euler's constant. All other variables are defined as the same in the equation (2.16).

The simplified cylindrical solution (considering the thermal mass) to a given borehole with T_u, initial temperature of soil, is given:

$$T_u - T_w = \frac{q_l}{4\pi k_s}\left\{2h + \ln(\frac{4Fo}{C}) - \frac{(4h-\alpha_1)}{2\alpha_1 Fo} + \frac{\alpha_1 - 2}{2\alpha_1 Fo}\ln(\frac{4Fo}{C})\right\} \qquad (2.20)$$

Where T_u is the uniform initial temperature of the soil (ºC [ºF]);

T_w is the borehole wall temperature (ºC [ºF]);

q_l is the heat transfer rate applied to the ground (W/m [Btu/ft-hr]) (a positive q value implies heating);

$h = 2\pi R_b k_s$, $\alpha_1 = 2\pi r_b^2 \rho C_p / S_1$;

Fo is the Fourier number defined as $Fo = \frac{\alpha t}{r_b^2}$;

k_s is the thermal conductivity of the ground (W/m-K [Btu/hr-ft-ºF]);

α is the thermal diffusivity of the ground (m^2/s [ft^2/hr]);

ρ is the density of the ground (kg/m^3[lbm/ft^3]);

C_p is the specific heat of the ground(J/kg-K [Btu/lbm-ºF]);

r_b is the radius of the borehole (m [ft]);

R_b is the thermal resistance of the borehole (K/(W/m) [hr-ft-ºF/Btu]);

S_1 is the thermal capacity of the materials in the borehole (J/m^3-K [Btu/ft^3-ºF]);

$C = 1.7811 = \exp(\gamma)$;

γ is is Euler's constant ($\gamma = 0.5772157...$).

(c). Cylindrical heat source solution to a cylinder of perfect conductor with the sheath surrounded by an infinite medium (soil)

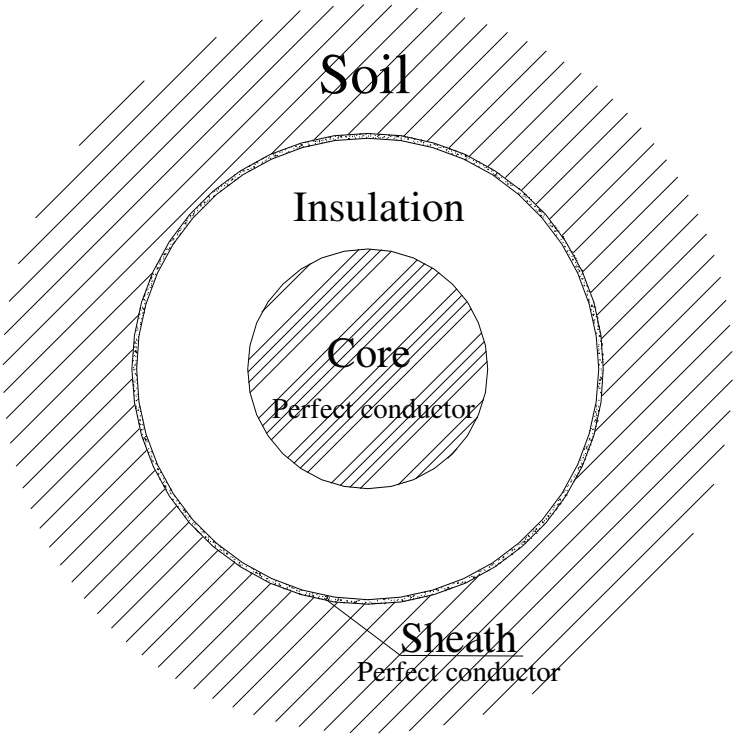

Figure 2-9 A schematic drawing of a core separated by the insulation from the sheath

Figure 2-9 shows a schematic drawing of a cylinder of the core with the sheath surrounded by an infinite medium (soil). The core and the sheath are perfect conductors of thermal capacities S_1 and S_2, respectively. They are separated by the insulation, which is regarded as of negligible thermal capacity and thermal resistance, *R*. The cylinder is also supposed to be buried in the soil of thermal conductivity, k_s, thermal diffusivity, α, and specific heat, C_p. If the whole system is initially at zero temperature and heat is supplied at the rate q_l per unit length per unit time, the temperature of the cylinder is given by Carslaw and Jaeger (1959):

$$T = \frac{q_l}{k_s} G(h, \alpha_1, \alpha_2, Fo) \tag{2.21}$$

$$G(h, \alpha_1, \alpha_2, Fo) = \frac{2\alpha_1^2 \alpha_2^2}{\pi^3} \int_0^\infty \frac{\left[1 - \exp\left(-u^2 Fo\right)\right]}{u^3 \Delta_1(u)} du \tag{2.22}$$

Where $h = 2\pi R_b k_s$, $\alpha_1 = 2\pi r_b^2 \rho C_p / S_1$, $\alpha_2 = 2\pi r_b^2 \rho C_p / S_2$;

Fo is the Fourier number defined as $Fo = \frac{\alpha t}{r_b^2}$;

$$\Delta_1(u) = \left[u\left(\alpha_1 + \alpha_2 - hu^2\right) J_0(u) - \alpha_2\left(\alpha_1 - hu^2\right) J_1(u)\right]^2 + \left[u\left(\alpha_1 + \alpha_2 - hu^2\right) Y_0(u) - \alpha_2\left(\alpha_1 - hu^2\right) Y_1(u)\right]^2 \tag{2.23}$$

J_i is the Bessel function of order i;

Y_i is the modified Bessel function of order i;

k_s is the thermal conductivity of the ground (W/m-K [Btu/hr-ft-ºF]);

α is the thermal diffusivity of the ground (m^2/s [ft^2/hr]);

ρ is the density of the ground (kg/m^3[lbm/ft^3]);

C_p is the specific heat of the ground(J/kg-K [Btu/lbm-ºF]);

r_b is the radius of cylindrical conductor (m [ft]);

R_b is the thermal resistance between the two perfect conductors (the core and the sheath) (K/(W/m) [hr-ft-ºF/Btu]);

S_1 is the thermal capacity of the cylinder of the core (J/m^3-K [Btu/ft^3-ºF]);

S_2 is the thermal capacity of the sheath (J/m^3-K [Btu/ft^3-ºF]);

u is the integration variable.

2.9.3. Analytical solution considering the movement of groundwater (groundwater g-function)

Claesson and Hellström (2000) gave a new analytical solution for the influence of regional groundwater flow in the performance of borehole heat exchangers based on the groundwater g-function.

The temperature $T_b(t)$ at the borehole wall, which is needed to sustain the constant heat injection rate Q_0 from time $t = 0$, is denoted by a corresponding dimensionless g-function:

$$T_b(t) = \frac{q_0}{2\pi k_s} \cdot g_{total}(t,....) \qquad q_0 = \frac{Q_0}{H} \tag{2.24}$$

The g-functions depend on time, thermal properties, etc. Groundwater flow will diminish the g-function. Claesson and Hellström (2000) wrote the total g-function in the following way:

$$g_{total}(t;q_w) = \frac{2\pi k_s}{q_0} T_b(t) = g(t;q_w = 0) - g_{gw}(t) \tag{2.25}$$

Where $T_b(t)$ is the temperature at the borehole wall (ºC [ºF]);

q_w is the constant regional groundwater flow (m^3 of water per m^2 and s);

k_s is the thermal conductivity of the ground (W/m-K [Btu/hr-ft-ºF]);

H is the borehole depth (m [ft]).

The first term on the right-hand side of Equation (2.25) is the ordinary g-function for the given borehole without the effect of groundwater ($q_w = 0$) (Claesson and Eskilson 1987). The second term accounts for the effect of the groundwater flow.

After some calculation, Claesson and Hellström (2000) gave the groundwater g-function g_{gw}:

$$g_{gw}(\tau, h) = \int_0^{\tau} \frac{1}{2s}(1 - e^{-h^2 s/4}) \cdot erfm(1/\sqrt{s}) \cdot ds \tag{2.26}$$

Where $erfm(x) = \frac{1}{x}\int_0^x erf(s)ds = erf(x) - \frac{1 - e^{x^2}}{\sqrt{\pi} \cdot x}$;

$\tau = \frac{4\alpha t}{H^2}$;

$h = \frac{H\rho_w c_w q_w}{2k_s}$;

q_w is the constant regional groundwater flow (m^3 of water per m^2 and s).

k_s is the thermal conductivity of the ground (W/m-K [Btu/hr-ft-ºF]);

α is the thermal diffusivity of the ground (m^2/s [ft^2/hr]);

ρ_w is the density of the groundwater (kg/m^3 [lbm/ft^3]);

c_w is the specific heat of the groundwater(J/kg-K [Btu/lbm-ºF]);

H is the borehole depth (m [ft]).

For $\tau > 1$, the following approximation of groundwater g-function, which is valid for any h, is given by Claesson and Hellström (2000):

$$g_{gw}(\tau, h) \cong \frac{1}{2} Ein\left(\frac{h^2\tau}{4}\right) - \frac{1}{h}\left(\frac{h\sqrt{\tau}}{\sqrt{\pi}} - erf\left(\frac{h\sqrt{\tau}}{2}\right)\right) \qquad \tau > 1 \tag{2.27}$$

Where $Ein(x) = \int_0^x \frac{1-e^{-s}}{s} ds \cong \ln(x + e^{-x}) + 0.577(1 - e^{-7x/4})$

Also, for $\tau < 1$, $h < 1$, the following simple expression is used to estimate the effect of groundwater flow within 3% error:

$$g_{gw}(\tau, h) \cong \frac{h^2\tau}{8}\left(1 - \sqrt{\frac{4\tau}{9\pi}}\right) \qquad \tau < 1,\ h < 1 \tag{2.28}$$

2.10. Related research - aquifer thermal energy storage (ATES)

A related type of system, with similar analytical requirements, is the aquifer thermal energy storage (ATES) system. ATES systems utilize aquifers for the storage of low-grade thermal energy such as solar heat or waste heat during periods of low demand. The low-grade energy is used to heat or chill water, which is injected into an aquifer for storage. Later, during a period of high demand, the water is withdrawn for space heating or cooling. During a period of heat injection, water is extracted from the cold well, heated

and reinjected into the warm well. The pump is reversed during a period of heat recovery. Water is then extracted from the warm well, cooled and reinjected into the cold well (see Figure 2-10). The same type of system may be used to store cold water for cooling purposes in warm climates.

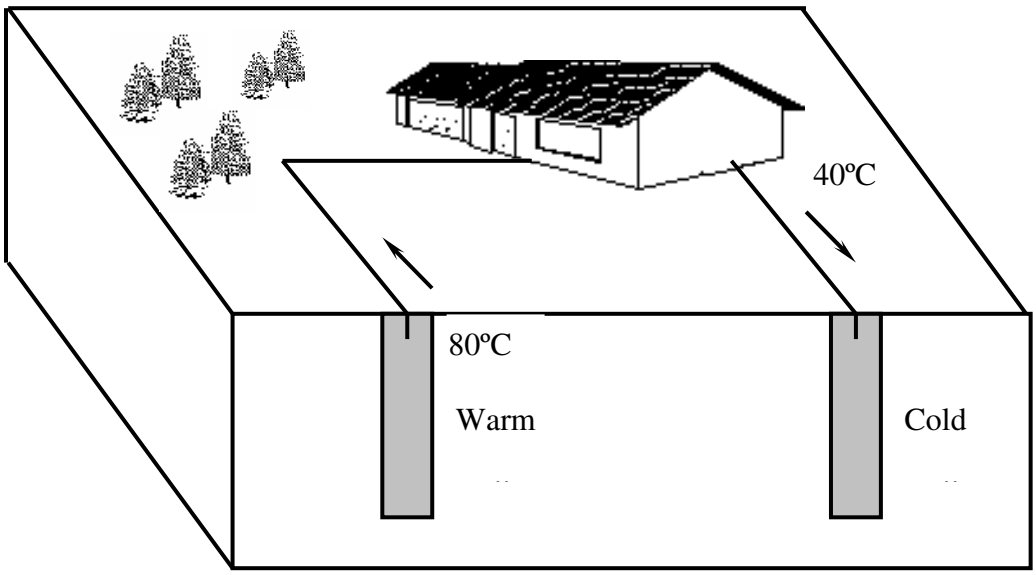

Figure 2-10 Heat storage in an aquifer

Hall and Raymond (1992) gave a schematic of a simplified ATES system used for air conditioning (Figure 2-11). In this system, the cooling tower is used for chilling water drawn from the warm well during the winter. The chilled water is stored in the aquifer by the cold well, and is recovered during the summer and passed through heat exchangers to cool the warm air.

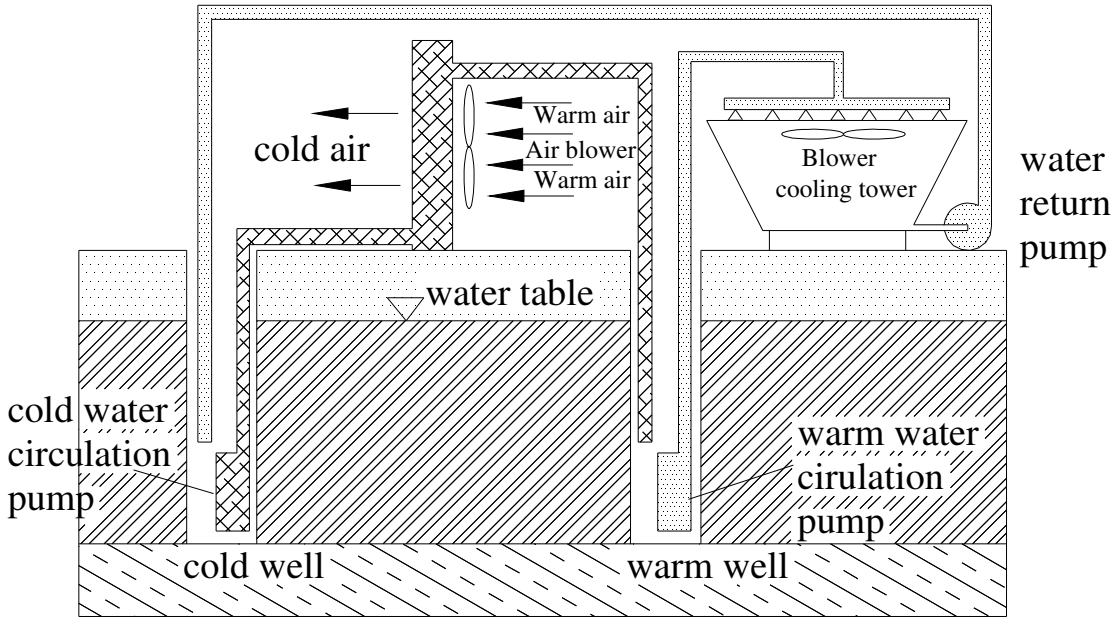

Figure 2-11 Simplified aquifer thermal energy storage system used for air-conditioning (Hall and Raymond 1992)

Numerous studies have been performed concerning the concept of ATES. Hall and Raymond (1992) gave the following three elements, which determine whether the design and operation of an ATES system are successful.

- the presence of a suitable aquifer for groundwater supply and energy storage;
- the availability of a source of low-grade thermal energy;
- a temporal mismatch between thermal energy availability and thermal energy use.

Aquifer characterization is very important to the design of an ATES system. However, unlike other components of the ATES system, the aquifer itself cannot be changed to

meet the design specification. Thus, the ATES system must be designed with regard to the aquifer characterization. So, as the first step in any ATES project, site investigation is necessary and should be combined with the user's specific requirements. Hall and Raymond (1992) also pointed out that the aquifer's hydraulic conductivity, which is dependent on the size and shape of media pores, is of the first-order importance in the design and evaluation of ATES systems. Basically, under ATES conditions, the differences in the thermal conductivities and thermal capacities of earth materials are relatively small. So, thermal conductivity and thermal capacity are of secondary importance.

There are several descriptions of ATES systems in the literature. Midkiff et al. (1992) presented the results of 6 years of study on the long-term performance of an air-conditioning system (a building at University of Alabama) based on ATES. During the cold weather, ambient 18ºC water is pumped from warm wells, chilled to about 6 ºC in a cooling tower, and reinjected into the separated cold storage wells. In warm weather, water is withdrawn from the cold wells and pumped through building heat exchangers for air-conditioning (see also Figure 2-11). This ATES system was operated to provide 100% of the building air conditioning with an annual average COP of about 5.0, about twice that for conventional mechanical air-conditioning equipment of the same capacity (Midkiff et al. 1992).

Marseille and Wilke (1992) provided an overview of an ATES system integrated with a central heating and cooling plant (Mid-Island Postal Facility in Melville, New York).

Cold wells are charged with water that is cooled during the winter by heat pump. Water from these cold wells is then used to meet the facility's cooling load during the summer, before being pumped back into the ground at warm wells. Backup cooling is provided by a heat pump. They described and assessed energy and economic merits of this system. Their studies shown that this ATES system can offer both energy and environmental advantages over more conventional systems.

2.11. Effect of groundwater flow on closed-loop ground-coupled heat exchangers

Although it has been recognized that the convective heat transport by groundwater flow may be an important factor in reducing the necessary size of closed-loop ground-coupled heat exchangers, current design and simulation models for closed-loop systems still assume that heat transfer underground occurs by conduction only. Little work has been done to quantify the effects of groundwater flow on closed-loop systems.

Claesson and Hellström (2000) presented models for the influence of regional groundwater flow based on the assumption that the natural groundwater movement is reasonably homogenously spread over the ground volume. This applies well for homogenous and porous ground materials. The authors used the line source theory to model the groundwater effect on a single vertical borehole (groundwater g-function, see section 2.9.3.) and concluded that under normal conditions, the influence of regional groundwater flow is negligible.

Chiasson (1999) made a preliminary investigation of the effects of groundwater flow on the design and performance of vertical closed-loop ground heat exchangers. A two-

dimensional finite element numerical groundwater flow and heat transport model (AQUA3D) was used to simulate and observe the effects (Chiasson et al. 2000). The relative importance of heat conduction in the ground vs. heat advection by groundwater flow is assessed by using of the dimensionless Peclet number, Pe .

$$Pe = \rho_w c_w qL / K_{eff} \tag{2.29}$$

Where ρ_w is the density of the groundwater (kg/m^3 [lbm/ft^3]);

c_w is the specific heat of the groundwater (J/kg-K [Btu/lbm-ºF]);

K_{eff} is the effective hydraulic conductivity (m/s [ft/s]);

q is the specific discharge (m/s [ft/s]);

L is the characteristic length (m [ft]).

Based on their preliminary work (Chiasson et al. 2000), it is shown that heat advection by groundwater flow is a significant process contributing to heat transfer in geologic formations such as coarse-grained soil and rocks with fractures and solution channels. The value of effective thermal conductivity is greater with a flowing fluid than with a stagnant fluid. The results from this work also show that as groundwater flow velocity increases, the values of the predicted effective thermal conductivity, including the effects of groundwater advection, are significantly different. From their preliminary assessment of the effects of groundwater flow, Chiasson et al. (2000) pointed out that it is difficult to adapt results from current design guidelines and software tools to fully account for the effect of groundwater movement.

Theoretical studies dismiss significant effects of groundwater flow for typical conditions in a porous ground (Chiasson et al. 2000; Claesson and Hellström 2000). However, groundwater flow in standing column well systems, especially when bleeding, results in higher flow velocities. The hydraulic pressure difference between the suction point and discharge point may also be potentially important.

2.12. Numerical groundwater flow and heat transport models

Ground water flow and thermal energy transport in the porous media have been studied in some detail in the discipline of hydrogeology.

Numerical research into groundwater and heat transport has been continuing for more than a decade in North American and Europe. Numerous commercially available and public domain numerical software codes exist. Of these, we focus on the simulation modeling both mass *and* heat transport in groundwater. Table 2-3 lists some numerical models for groundwater flow and energy or solute transport in groundwater. These models can all be used to simulate an ATES system. Models THETA and SUTRA are selected for a more detailed review, since the information about these two models is readily obtained in the public literature.

In assessing the effect of groundwater flow on closed-loop heat exchanger performance, Chiasson (1999) reviewed numerical software code, which can be used to model mass and/or heat transport in groundwater. Finally, Chiasson (1999) selected AQUA3D for his study based on his selection criterion**:**

- the type of boundary conditions handled by the code

- the solution scheme employed by the code
- verification of the code
- cost

Table 2-3 Numerical models for groundwater

Model	Creator	Descriptions
AQUA3D	Vatnaskil Consulting Engineers, Reykjavik, Iceland	Three-dimensional, finite-element method; developed mainly for simulation of mass-transport problems, but can be adapted to model heat transport without density-dependent ground-water flow.
HST3D	United States Geological Survey (USGS)	Three-dimensional, finite-difference method; capable of simulating mass and heat transport in variable-density groundwater flow system.
FEFLOW	WASY Institute for Water Resources Planning and Systems Research, Ltd., Berlin, Germany	Three-dimensional, finite-element method; capable of simulating both mass and heat transport in density-dependent groundwater flow systems.
SUTRA (**S**aturated-**U**nsaturated **Tra**nsport)	Clifford L. Voss	Two-dimensional hybrid finite-element and finite-difference method; simulated fluid movement and the transport of either energy or dissolved substances in the subsurface environment.
THETA 3.0	Kangas and Lund	Three-dimensional, finite-difference method; coupled transport of fluid and energy in porous media.

2.12.1. Numerical model THETA

THETA was developed at Helsinki University of Technology by Kangas (1996). It can be used to accurately simulate the three-dimensional coupled transport of fluid and energy in porous media. Simulations have been performed to evaluate the effect of groundwater on the performance of a ground heat extraction system using vertical wells.

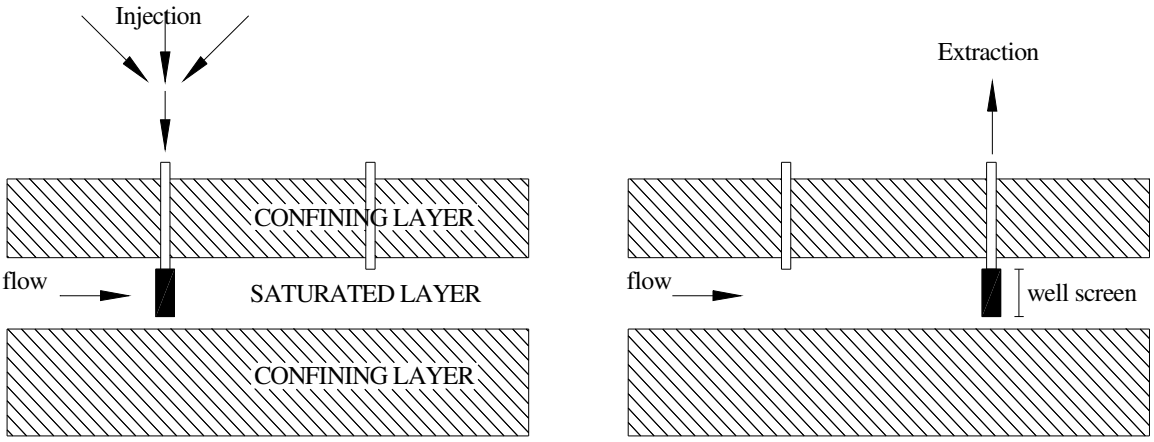

Figure 2-12 A ground heat extraction system using vertical wells (Kangas 1996).

Kangas (1996) used the porous medium approximation to study the groundwater flow. The specific discharge ($\vec{q}$) is given by Darcy equation:

$$\vec{q} = -\frac{\bar{\bar{k}}}{\mu}(\nabla p - \rho\vec{g}), \quad \bar{\bar{k}} = \frac{K\mu}{\rho g} \tag{2.30}$$

Where: $\bar{\bar{k}}$ is the intrinsic permeability (m^2 or Darcy [ft^2]) ($\bar{\bar{k}}$ is a function of the size of the openings through which the fluid moves. It depends only on the geological properties of the ground. $\bar{\bar{k}} = C \cdot d^2$);

C is the shape factor and d is the diameter of the effective grain, they are properties of the porous media (Fetter 1994);

K is the hydraulic conductivity of rock (m/s [gpd/ft^2]) (It depends not only on the geological properties of the ground, but also on the thermal properties of the flowing medium);

p is the pressure (N/m^2 [lbf/ft^2]);

g is the acceleration of gravity (m/s^2 [ft/s^2]);

μ is the dynamic viscosity of water (N-s/m^2 [lbf-s/ft]).

In addition, Kangas (1996) assumed that, locally, the groundwater and the surrounding ground are in the thermal equilibrium to derive the transferred energy equation in groundwater from the principle of conservation of energy. The resulting energy equation with an incompressible fluid is:

$$(\rho c)_s \frac{\partial T}{\partial t} = \nabla \cdot (\lambda \nabla T) - (\rho c)_f \vec{q} \cdot \nabla T + H \qquad (2.31)$$

Where: ρc is the volumetric heat capacity (J/m^3-K [Btu/ft^3-ºF]);

λ is the thermal conductivity (W/m-K [Btu/hr-ft-ºF]);

$\vec{q}$ is the specific discharge (volume flow rate per unit of cross-sectional area) (m/s [gpd/ft^2]);

H is the heat source or sink (W/m^3 [Btu/hr-ft^3]);

and subscripts: f is fluid (water);

s is fluid saturated soil.

The above two governing equations are discretized in THETA using the explicit finite difference method (FDM) and solved numerically.

The results from the THETA simulations of Kangas (1996) suggest that an increase in groundwater flow will result in improved system performance, which results from the energy transfer by groundwater; groundwater constantly replenishes the recoverable energy at the site of extraction. The presence of groundwater flow significantly increases the amount of recoverable energy. Similarly, standing column well systems, especially with groundwater bleed, make use of the energy stored in the aquifer.

The THETA aquifer simulation model has been incorporated into a computer simulation model AQSYST for simulating energy systems employing ATES (Kangas and Lund 1994). This system simulation showed that energy systems employing heat pumps for storage discharge could obtain high performance for the whole range of natural groundwater flow rates from 10 m/year to 600 m/year.

THETA simulates the thermo-hydraulic flow in the aquifer when either injecting water to the well or extracting water from the well. It cannot model simultaneous injection and extraction to/from a single well. The performance of standing column well systems is characterized by circulating, injecting, and extracting water to and from an aquifer at the same time. Therefore, THETA cannot be applied directly to the standing column well system.

2.12.2. Numerical model SUTRA

SUTRA (**S**aturated-**U**nsaturated **Tra**nsport) is a computer program developed by Voss (1984). This numerical model simulates fluid movement and the transport of either

energy or dissolved substances in the subsurface environment (aquifer). A two-dimensional hybrid finite-element and finite difference method is used to approximate the governing equations. SUTRA can solve the two interdependent processes:

1. fluid density-dependent saturated or unsaturated groundwater flow, and either

2a. transport of a solute in the groundwater, or

2b. transport of thermal energy in the groundwater and solid matrix of the aquifer.

SUTRA was primarily intended to simulate two-dimensional flow, and either solute or energy transport in a saturated variable density system. To simulate the groundwater in unconfined aquifers affected by a periodic boundary condition, Ashtiani et al. (1999) modified the SUTRA model in three aspects:

1. the basic flow equation is changed from a pressure-based form to a mixed-form;
2. an automatic under-relaxation method is applied for adjustment of pressure after each iteration to handle the non-linearity of the unsaturated zone equations;
3. the model has been adjusted to handle a seepage-face boundary condition.

The validation tests of this two-dimensional numerical model for density-dependent groundwater flow in unconfined aquifers against experimental data were successful.

Like THETA, SUTRA cannot model simultaneous heat/mass injection and extraction to/from a single well. So, SUTRA cannot be applied directly to the standing column well system, either.

2.12.3. Other Numerical models

A few other models address energy transfer in the aquifer. Here are some brief reviews.

Hellström et al. (1986, 1989) developed a model that simulates the thermal process in the aquifer and in the surrounding ground under certain simplifying assumptions concerning the groundwater flow. The basic assumption of the model is that the groundwater flow is essentially radial in the thermally active region around the well. There are other assumptions that must be fulfilled:

- negligible regional groundwater flow;
- negligible buoyancy flow caused by varying water temperature in the aquifer;
- negligible influence of viscosity differences between different flow paths.

Convective heat transport and three-dimensional heat conduction are accounted for in this model. The combined diffusive and convective heat flow processes in the aquifer and the surrounding layers are solved using the explicit difference method (finite difference method).

Molson et al. (1992) simulated the thermal energy storage in an unconfined aquifer with a three-dimensional finite element numerical model. In their model, the authors coupled the density-dependent groundwater flow and thermal energy transport. A symmetric matrix time integration scheme with the Galerkin finite element method is employed.

Recently, Chevalier and Banton (1999) applied the random walk method to model energy transfer in porous media. The method is based on the concept that cumulative results of

repeated trials with an arbitrary probability distribution tend to a Gaussian distribution. They compared their random results with the analytical solution and the numerical finite difference solution. The results are similar in both cases.

Because the above three models cannot model simultaneous heat/mass injection and extraction to/from a single well, so they cannot be applied directly to the standing column well system.

2.13. Summary of the literature

From the review of the literature discussed in the previous sections, it is clear that research into the operation and design of SCW systems has been very limited. To date, no models have been developed that have come into common use in design procedures for SCW systems. Attempts have been made to adapt conduction heat transfer models to include the effects of groundwater flow. However, these models (e.g., Yuill and Mikler 1995) do not allow representation of bleed from the well. As this is common practice and can have a significant impact on the design and cost of the well, there is a clear need to be able to model this effect.

Based on the existing published research, the following conclusions can be drawn:

1. Because of the direct interaction between the water in the borehole and the groundwater in SCW systems, none of the pure heat conduction models such as Braud's (1980) could be directly applied to the SCW system without any modification.
2. Only Yuill and Mikler (1995) have developed an analytical tool that accounts for heat transfer improvement due to the presence of groundwater. The influence of infiltration/exfiltration of groundwater to the overall heat transfer depends on the local geological formation and performance characteristics of the system. However, this finite difference model allowing calculation of the radial heat transfer at a particular depth is not a true two-dimensional model. A two-dimensional model would be much more appropriate.

3. In Tan and Kush's paper (1986), the effect of groundwater was referenced, but not quantified. Only Yuill and Mikler (1995) discussed this effect in detail by the introduction of the "groundwater factor." But they didn't account for the effect of bleed and buoyancy.
4. Little information about "bleed" is available in the literature, except that Orio (1994, 1995, 1999) provided some initial information based on his experiences. Much more work must be done to evaluate the performance enhancement provided by "bleed." It is essential to predict the safe amount of bleed flow to prevent equipment freeze-up during peak heating periods. Also, during the bleed times, the water table may fluctuate in response to draw down in the well. It may be helpful to numerically track the water table position, which has a huge influence on the power consumption of water pump in SCW systems during bleed operation. In real life, it has a significant effect on the flow rates.
5. Although some field test projects related to SCW systems have been published (Bose et al. 1979; Braud et al. 1983; Tan and Kush, 1986), no computer simulations of a SCW system have been developed, which could be used to predict the hourly heat pump entering water temperature at given hourly building loads. Hourly energy analyses can allow us to examine the transient nature of SCW systems, especially during "bleed" times.
6. Currently available simplified analytical/numerical solutions based on pure heat conduction assumptions cannot be directly coupled into SCW system simulations, in which the movement of groundwater has a significant effect on heat transfer, especially in bleed operation.

The heat transfer and hydrological boundary conditions in SCW systems vary in both time and space and also depend on the mode of operation of the well (e.g., bleed). The full complexity of the boundary conditions associated with standing column well operations can only be dealt with by a numerical model, which considers both ground-water flow and heat transfer. From the review of the literature discussed in Sections 2.10-2.12, we can see that sophisticated numerical models of groundwater flow and contaminant transport in both the saturated zones (rock) and unsaturated zones (soil) have been developed over the last two decades. These models have been applied by practicing hydrogeologists to study large-scale water supply and contaminant transport problems. Although those models effectively model the pumping process and calculation of groundwater flow, they are not adapted to enable the complex time-varying thermal boundary conditions required to model SCW systems over an extended simulation period. The design parameters such as well diameter, dip tube size, insulation, well surface roughness, etc. cannot be studied without a detailed thermal borehole model of the standing column well.

A summary of the different numerical and analytical models of interest is given in Table 2-4**.**

Table 2-4 Summary of the different numerical and analytical models

	Analytical solution	Numerical solution	Effect of groundwater	Effect of bleed	Effect of buoyancy	Comments
Braud and Oliver (1980, 1983)	Yes	No	No	No	No	Steady-state, radial, conduction heat flow only.
Mikler (1993) Yuill and Mikler (1995)	No	Yes	Yes	No	No	1. Introduce "groundwater factor" ($G_f = \frac{\dot{m}_w C_{pw}}{2\pi \cdot k \cdot dz}$) to consider the groundwater effect; 2. Finite difference model that allowed calculation of the radial heat transfer at a particular depth was not two-dimensional. The vertical heat transfer, end effects and bleed operation could not be considered
Kelvin line source	Yes	No	No	No	No	Exact only for a true line source, assuming end effects are negligible. The soil has an assumed uniform and constant initial temperature.
Cylindrical heat source (a)	Yes	No	No	No	No	Without considering the thermal mass in the borehole.
Cylindrical heat source (b)	Yes	No	No	No	No	Considering the thermal mass in the borehole.
Analytical solution with g-function	Yes	No	Yes	No	No	1. Based on superposition of steady state, periodic and extraction step analytical solutions; 2. Introduce the groundwater g-function ($g_{gw}(\tau, h) \cong \frac{h^2 \tau}{8}\left(1 - \sqrt{\frac{4\tau}{9\pi}}\right)$) to consider the constant regional groundwater flow.
AQUA3D	No	Yes	Yes	N/A	No	1. Three-dimensional, finite-element method; 2. Developed mainly for simulation of mass-transport problems, but can be adapted to model heat transport without density-dependent ground-water flow; 3. Used by Chiasson (1999) to simulate and observe the effects of groundwater flow on the vertical closed-loop system.
SUTRA	No	Yes	Yes	N/A	No	1. Two-dimensional hybrid finite-element and finite-difference method; 2. Simulated fluid movement and the transport of either energy or dissolved substances in the subsurface environment.

3. DEFINITION OF THE PROBLEM AND OBJECTIVES

The goals of this research have been briefly discussed in the introduction section. In more detail, the specific objectives of this research into standing column well systems will be subdivided into several major stages:

The first stage concerns the review, analysis and evaluation of currently available research related with standing column well systems. The strengths and shortcomings of currently available research are to be analyzed and evaluated. The literature review of this research attempts to provide this.

The second stage involves analysis of the mechanism of heat transfer and characteristics of hydrological flow about the standing column well systems. As we know, the heat transfer in standing column well systems is very complicated because of the presence of groundwater. The detailed two-dimensional numerical model of the standing column well system will consist of two parts:

1) Borehole sub model (using nodal model)

   The thermal model for the borehole can be described by a series of resistance network.

2) Porous medium model describing heat transfer and groundwater flow in the rock (using finite volume model).

The third stage will deal with computer algorithms. The mathematical and physical model will be converted into computer model. The programming language will be *Fortran 90/95*. At this stage, some experimental data (Mikler 1993; Henderson 2003) will be used to validate and calibrate the numerical models.

The fourth stage is a parametric study and energy consumption analysis based on the detailed model. Using the numerical model, the effect of key parameters and operating strategies (e.g., bleed) will be evaluated.

This research will be helpful in the design of standing column well systems by providing:

- simulation of standing column well systems to predict fluid temperature (entering fluid temperature to the heat pump, exiting fluid temperature from the heat pump, average fluid temperature in the well);
- determination of the necessary well depth per given load in specified hydrogeological conditions;
- influence of “bleed”.

Anticipating that the detailed model will take extensive computing resources, the last stage of this work is to develop a simplified numerical one-dimensional model. This should be feasible for use by engineers in HVAC application areas. This simplified model should be compared with the detailed numerical model and experimental data for accuracy. An economic performance analysis based on this simplified model is the last objective of this research.

The validation of the models against the experimental data is carried out along the development of the models.

The detailed numerical two-dimensional model with the experimental validation will be described in Chapter 4. Chapter 5 will focus on a parametric study of standing column well systems using the detailed model. Chapter 6 will discuss the simplified numerical one-dimensional model. Economic performance analysis of standing column well systems will be discussed is Chapter 7. Finally, conclusions and recommendations will be presented in Chapter 8.

4. DETAILED MODEL FOR STANDING COLUMN WELL SYSTEMS

Previous models of standing column well systems (Oliver and Braud 1981; Mikler 1993) make a number of assumptions about the heat transfer between the different components of SCW system (Section 2.2, Section 2.4). They either treat groundwater flow in the surrounding rock in a very simplified manner or neglect it entirely. The objective of the detailed numerical model in this work is to predict the transient operation of the standing column well heat exchanger under the varying load and flow conditions.

Since the groundwater flow surrounding the borehole has a significant effect on the operation of SCW system, the model must be extended beyond the borehole. A big difference exists between the flow inside and outside the borehole. Inside the borehole, the flow is a kind of turbulent pipe flow, and outside the borehole, the fluid is flowing through a porous medium. Also, the heat transfer processes in SCW systems should be considered on two physical scales: inside the borehole and outside the borehole. Accordingly, we need to model rather different physical scales and fluid regions inside and outside the borehole. The numerical model used in this work is composed of two parts:

- Thermal energy transport in the borehole is handled by a nodal model of the borehole components.

- Flow equations in both the borehole and in the surrounding rock, and thermal energy transport in the surrounding rock are handled by a finite volume model.

In the following sections, firstly this detailed numerical model is described. Then, this model is validated against the limited experimental data. Finally, the simulation results from the base case are provided.

4.1. Descriptions of the model

First, the hydrological and heat transfer flow in standing column well systems will be elaborated, then computer algorithm.

4.1.1. Hydrological flow in the SCW systems

In the broadest sense, all the subsurface water is groundwater, but more commonly, "groundwater" refers to the subsurface water in the saturated zone. The surface separating the saturated zone from the unsaturated zone is known as the water table. At the water table, the pore water pressure is equal to atmospheric pressure. In the saturated zone under the water table, pores are fully saturated and water pressure is greater than atmospheric pressure owing to the weight of overlying water. In the unsaturated zone above the water table, pores are partly saturated and water pressure is less than atmospheric pressure (Figure 4-1).

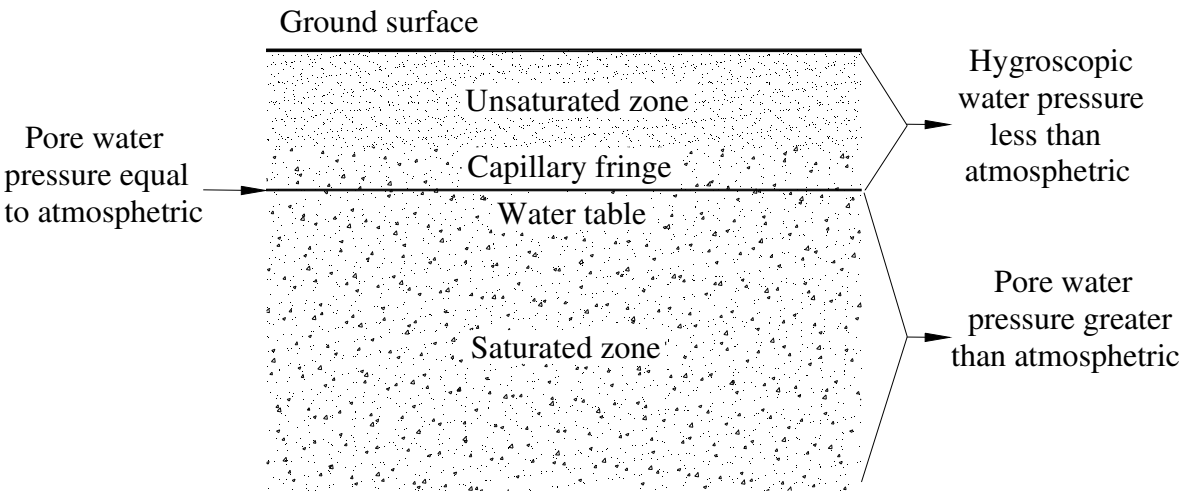

Figure 4-1 Distribution of the fluid pressure in the ground with respect to the water table (Fetter 1994)

The groundwater flow can be studied using the porous medium approximation (Bear, 1979), in which the flow of groundwater in individual pores is described macroscopically using average parameter values representing the group of pores as a whole. In this approximation, the Darcy equation (Equation (1.2)) can be used.

4.1.1.1. Hydrological flow in the aquifer (porous medium)

By applying the law of mass conservation to a control volume and using Darcy's Law (Equation (1.2)), the governing equation defining the hydraulic head distribution in the porous medium can be derived as:

$$S_s \frac{\partial h}{\partial t} = \frac{\partial}{\partial x_i}\left(K_{ij} \frac{\partial h}{\partial x_i} \right) + R \qquad (4.1)$$

Where h is the hydraulic head (m [ft]);

$S_s = \rho_w g(\alpha + n\beta)$,

S_s is the specific storage (m^{-1} [ft^{-1}]), specific storage is the amount of water per unit volume of a saturated formation that is stored or expelled from storage owing to compressibility of the mineral skeleton and the pore water per unit change in head. It is also called the elastic storage coefficient (Fetter 1994).

ρ_w is the density of water (kg/m^3 [lbm/ft^3]);

g is the acceleration of gravity (m/s^2 [ft/s^2]);

α is the compressibility of aquifer ($1/(N/m^2)$ [$1/(lbf/ft^2)$]);

β is the compressibility of water ($1/(N/m^2)$ [$1/(lbf/ft^2)$]);

n is the porosity.

K_{ij} is the hydraulic conductivity tensor(m/s [gpd/ft^2]);

R is the source/sink ([s^{-1}]).

It should be noticed that the water table is free to rise or fall depending on the amount of available water in the aquifer. But a preliminary calculation of well drawdown for hydraulic conductivities of interest in SCW systems shows it to be typically less than one meter. Compared with the depth of the standing column well, which is usually hundreds of meters, this well drawdown is very small, and can be neglected. Hence during this work, the water table fluctuations are ignored and Equation (4.1) is used.

4.1.1.2. Hydrological flow in borehole

The flow in the borehole of SCW systems is often non-Darcy flow (the relationship between the flux and gradient is non-linear), but by introducing the effective hydraulic conductivity (EHC) K_{eff}, we still use the equation 4.1 to describe the water flow in the

borehole just replacing K_{ij} with K_{eff}. Here, we use the formulas recommended by Chen and Jiao (1999):

$$K_{eff} = \begin{cases} K & Darcy\ flow\ in\ the\ aquifer \\ \dfrac{d^2 \rho g}{32\mu} & Laminar\ pipe\ flow\ in\ the\ borehole \\ \dfrac{2gd}{uf} & Transitional\ and\ turbulent\ flow\ in\ the\ borehole \end{cases} \quad (4.2)$$

Where: d is the diameter (m [ft]);

ρ is the density of water(kg/m^3 [lbm/ft^3]);

g is the acceleration of gravity (m/s^2 [ft/s^2]);

μ is the dynamic viscosity(Pa-s [lbm/ft-sec]);

u is the average water velocity in the borehole(m/s [ft/sec]}

f is the friction factor.

For the dip tube walls in the well, $K = 0$.

4.1.2. Heat transfer mechanism in SCW systems

Different mechanisms are used to describe heat transfer in the aquifer (porous medium) and heat transfer in the borehole of SCW systems. Figure 4-2 shows all the heat transfer mechanism in SCW systems.

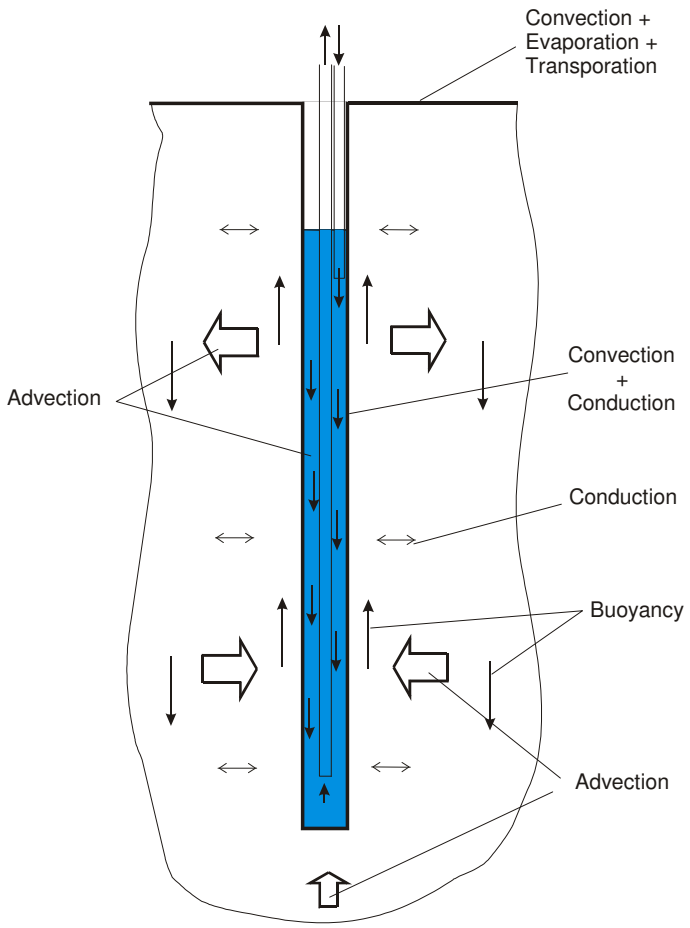

Figure 4-2 Heat transfer mechanisms in SCW systems (Rees 2001)

4.1.2.1. Heat transfer in the aquifer (porous medium)

There are several heat transfer processes affecting the heat transferred through an aquifer:

a. heat conduction through the fluid phase,

b. heat conduction through the solid phase,

c. particle to particle radiation,

d. heat convection from the fluid phase to the solid phase,

e. convection through the fluid phase (advection).

Figure 4-3 shows the relationship between the actual thermal conductivity and the four mechanisms that contribute to it. None of the first three processes is affected by fluid

flow, and the last two processes are dependent on fluid velocity. At large velocities, the last two processes are dominant.

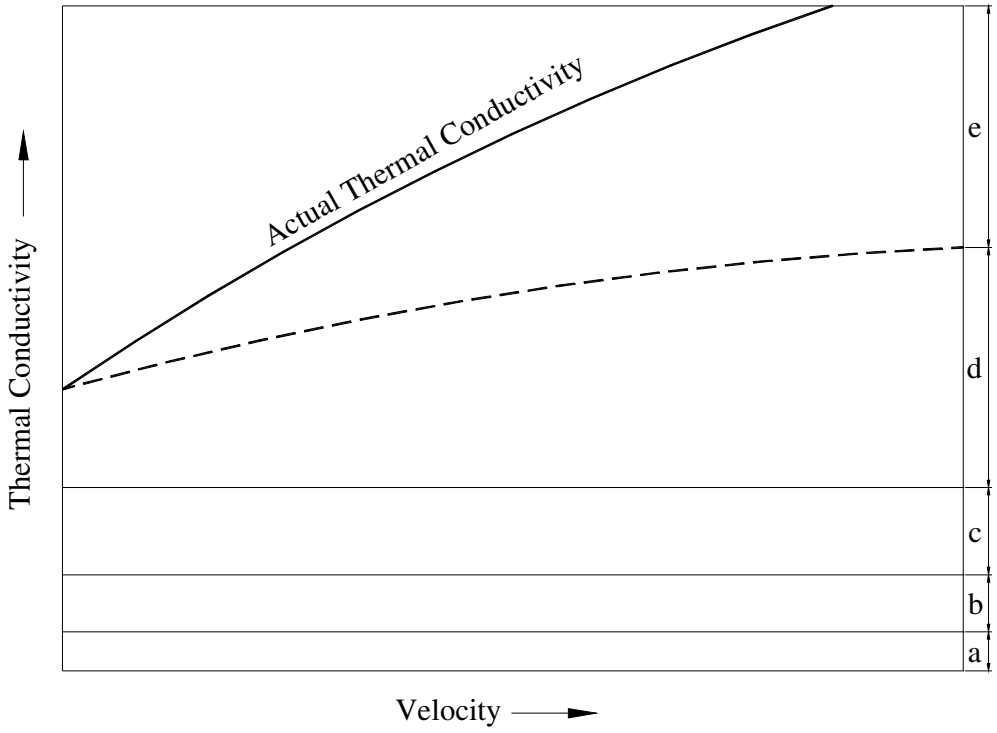

Figure 4-3 The relationship between the actual thermal conductivity and the mechanisms that contribute to it* (Domenico and Schwartz 1990)

* a. heat conduction through the fluid phase, b. heat conduction through the solid phase, c. particle to particle radiation, d. heat convection from the fluid phase to the solid phase, e. convection through the fluid phase (advection).

We assume that the solid phase and fluid phase in the aquifer are at the same temperature (in thermal equilibrium) so that we consider the temperature as an average temperature of both phases. An effective thermal conductivity k_{eff} is expressed as:

$$k_{eff} = nk_l + (1-n)k_s \tag{4.6}$$

Where n is the porosity;

k_l is the thermal conductivity of the fluid (W/m-K [Btu/hr-ft-ºF]);

k_s is the thermal conductivity of the solid (W/m-K [Btu/hr-ft-ºF]).

In general, the more porous the medium, the lower the effective thermal conductivity, just since water has a lower thermal conductivity than most solids.

The control volume for the solid –liquid phase system (a saturated porous medium) is shown in Figure 4-4:

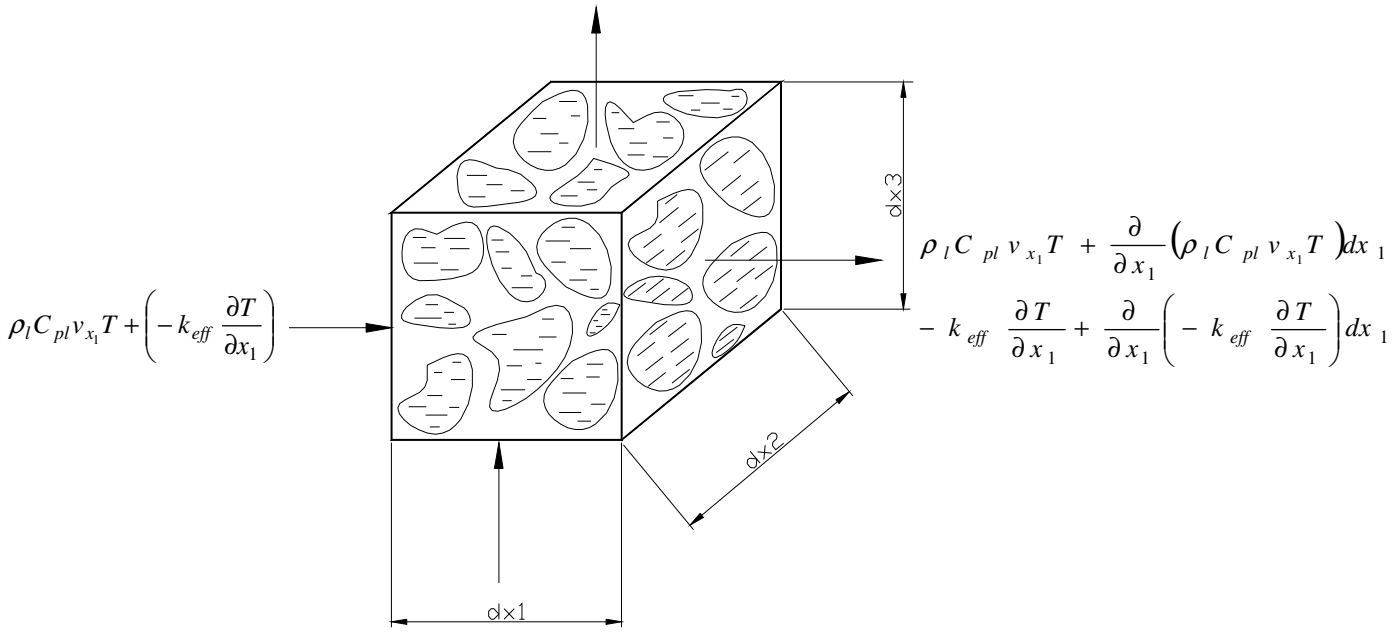

Figure 4-4 Control volume for the solid-liquid phase

Strictly speaking, enthalpy is defined as: $h = u + pv$. In the given system with temperatures below 100ºC that are not pressurized, the "flow work" term, pv, is ignored. So the advection-diffusion equation can be used where enthalpy is thermal energy content only.

Since heat is transported by advection in the liquid phase and by both advection and diffusion in both phases, the net flux of energy in x_1 direction is written as:

$$\left[\rho_l C_{pl} v_{x_1} T + \frac{\partial}{\partial x_1}\left(\rho_l C_{pl} v_{x_1} T\right)dx_1 - k_{eff}\frac{\partial T}{\partial x_1} + \frac{\partial}{\partial x_1}\left(-k_{eff}\frac{\partial T}{\partial x_1}\right)dx_1\right]dx_2 dx_3$$
$$-\left[\rho_l C_{pl} v_{x_1} T - k_{eff}\frac{\partial T}{\partial x_1}\right]dx_2 dx_3 = \left[\frac{\partial}{\partial x_1}\left(\rho_l C_{pl} v_{x_1} T\right) - \frac{\partial}{\partial x_1}\left(k_{eff}\frac{\partial T}{\partial x_1}\right)\right]dx_1 dx_2 dx_3 \tag{4.7}$$

After considering the same form for the x_2 and x_3 directions, the energy balance equation of this control volume gives:

$$\begin{aligned}&\left[\frac{\partial}{\partial x_1}\left(\rho_l C_{pl} v_{x_1} T\right) + \frac{\partial}{\partial x_2}\left(\rho_l C_{pl} v_{x_2} T\right) + \frac{\partial}{\partial x_3}\left(\rho_l C_{pl} v_{x_3} T\right)\right]dx_1 dx_2 dx_3 \\ &-\left[\frac{\partial}{\partial x_1}\left(k_{eff}\frac{\partial T}{\partial x_1}\right) + \frac{\partial}{\partial x_2}\left(k_{eff}\frac{\partial T}{\partial x_2}\right) + \frac{\partial}{\partial x_3}\left(k_{eff}\frac{\partial T}{\partial x_3}\right)\right]dx_1 dx_2 dx_3 \\ &- Q dx_1 dx_2 dx_3 + \frac{\partial}{\partial t}\left(\rho C_p T\right)_{cv}\cdot dx_1 dx_2 dx_3 \\ &= 0\end{aligned} \tag{4.8}$$

Dividing by the volume ($dx_1 dx_2 dx_3$), taking constants out of the derivative and simplifying gives:

$$\left(\rho C_p\right)_{cv}\frac{\partial T}{\partial t} + \rho_l C_{pl} V_i \frac{\partial T}{\partial x_i} = k_{eff}\frac{\partial^2 T}{\partial x_i^2} + Q \tag{4.9}$$

The effective thermal mass of the control volume is defined by $\left(\rho C_p\right)_{cv} = [n\rho_l C_{pl} + (1-n)\rho_s C_{ps}]$ where C_{pl} and C_{ps} are the specific heats of the liquid and the solid, respectively.

Thus, after applying the principle of energy conservation to the given control volume, the energy equation in a density-dependent porous medium is:

$$[n\rho_l C_{pl} + (1-n)\rho_s C_{ps}]\frac{\partial T}{\partial t} + \rho_l C_{pl} V_i \frac{\partial T}{\partial x_i} = k_{eff} \frac{\partial^2 T}{\partial x_i^2} + Q \qquad (4.10)$$

Where k_{eff} is the effective thermal conductivity (W/m-K [Btu/hr-ft-ºF]);

V_i is the average linear groundwater velocity vector (m/s [ft/s]), which will be determined from the Darcy's law;

n is the porosity;

k is the thermal conductivity (W/m-K [Btu/hr-ft-ºF]) ;

ρ is the density (kg/m^3 [lbm/ft^3]);

C_p is the specific heat (J/kg-K [Btu/lbm-ºF]);

Q is the source/sink (W/m^3 [Btu/hr-ft^3]);

and the subscripts: l is water;

s is solid (water saturated rock).

The second term of Equation (4.10) only contains the thermal mass of the liquid because heat is only advected by the liquid phase. The energy equation (4.10) and the head equation (4.1) are coupled by the fluid velocity. The fluid velocity is obtained from the Darcian groundwater flux as follows:

$$v = -\frac{K}{n}\nabla h \qquad (4.11)$$

Where v is the average linear ground water velocity (m/s [ft/s]);

K is the hydraulic conductivity of ground (m/s [gpd/ft^2]);

h is the hydraulic head (m [ft]);

n is the porosity.

Hence the solution to the energy equation depends on the velocity data calculated from Darcy's equation.

4.1.2.2. Heat transfer in the borehole

Heat transfer in the borehole of SCW systems is characterized in the r direction by convection from the pipe walls and borehole wall, plus advection at the borehole surface, and in the z direction by advection only. The thermal model for the borehole can be described by a series of resistance networks as shown in Figure 4-5.

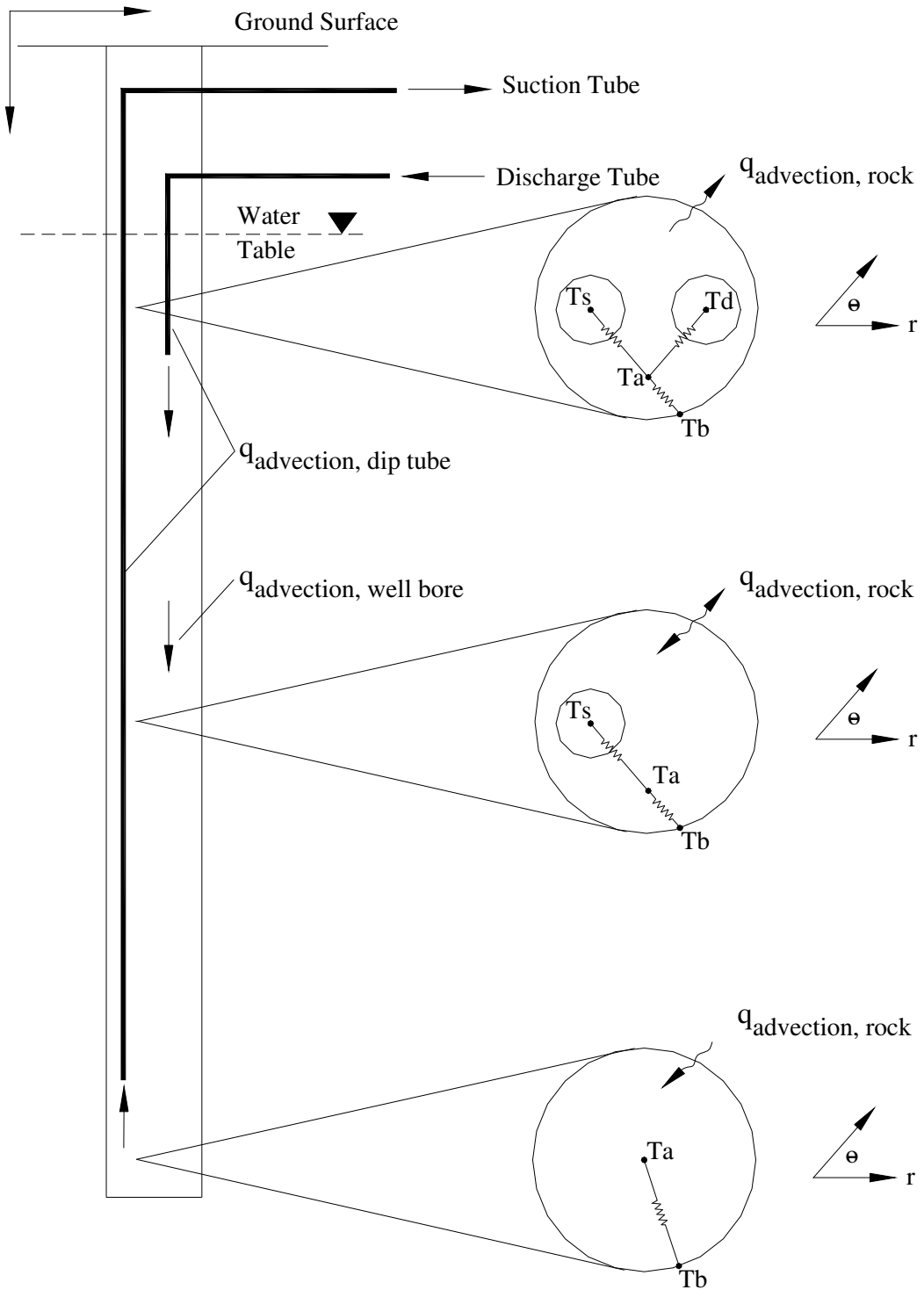

Figure 4-5 The borehole thermal model

An energy balance on the water in the annular region can be formulated in each z plane. Figure 4-6 shows a schematic control volume in the borehole.

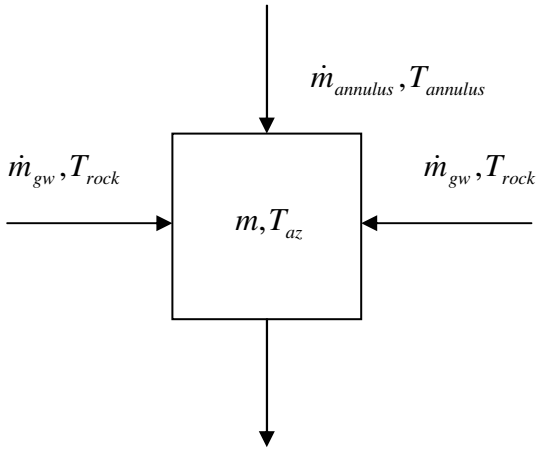

Figure 4-6 A schematic control volume in the borehole

The energy balance equation can be written as:

$$\frac{d(m \cdot C_P \cdot T_{a,z})}{dt} = q_{convection,suction\,tube} + q_{convection,discharge\,tube} + q_{convection,rock} + q_{1-advection,rock} + q_{1-advection,annulus} \tag{4.12}$$

The left hand side of Equation (4.12) can be reduced to:

$$\begin{aligned} \frac{d(m \cdot C_P \cdot T_{a,z})}{dt} &= \frac{dm \cdot C_p \cdot T_{az}}{dt} + \frac{m \cdot C_p \cdot dT_{az}}{dt} \\ &= \frac{\dot{m} \cdot dt \cdot C_p \cdot T_{az}}{dt} + \frac{m \cdot C_p \cdot dT_{az}}{dt} = \dot{m} \cdot C_p \cdot T_{az} + m \cdot C_p \cdot \frac{dT_{az}}{dt} \\ &= \dot{m}_{gw} \cdot C_p \cdot T_{az} + \dot{m}_{annulus} \cdot C_p \cdot T_{az} + V\rho \cdot C_p \cdot \frac{dT_{az}}{dt} \end{aligned} \tag{4.13}$$

The right hand side of Equation (4.12) can be reduced to:

$$\begin{aligned} RHS = q_{convection,suction\,tube} + q_{convection,discharge\,tube} + q_{convection,rock} \\ + \dot{m}_{gw} \cdot C_p \cdot T_{rock} + \dot{m}_{annulus} \cdot C_p \cdot T_{annulus} \end{aligned} \tag{4.14}$$

Thus, the energy balance equation (4.12) can be written as

$$\frac{dT_{az}}{dt} \cdot V\rho \cdot C_p = q_{convection,suction\,tube} + q_{convection,discharge\,tube} + q_{convection,rock} + \dot{m}_{gw} \cdot C_p \cdot (T_{rock} - T_{az}) + \dot{m}_{annulus} \cdot C_p \cdot (T_{annulus} - T_{az}) \quad (4.15)$$

After the new definitions, Equation (4.15) can be written as:

$$\frac{dT_{az}}{dt} \cdot V\rho \cdot C_p = q_{convection,suction\,tube} + q_{convection,discharge\,tube} + q_{convection,rock} + q_{advection,rock} + q_{advection,annulus} \quad (4.16)$$

Where,

$$q_{advection,rock} = \dot{m}_{gw} \cdot C_p \cdot (T_{rock} - T_{az}) \quad (4.17)$$

$$q_{advection,annulus} = \dot{m}_{annulus} \cdot C_p \cdot (T_{annulus} - T_{az}) \quad (4.18)$$

and $T_{a,z}$ is the water temperature in the annular region at node z (ºC [ºF]);

V is the volume of water in the annular region (m^3 [ft^3]);

ρ is the density of water in the annular region (kg/m^3 [lbm/ft^3]);

C_p is the specific heat of water (J/kg-K [Btu/lbm-ºF]);

$\dot{m}_{gw}$ is the mass flow rate of ground water in/out of the borehole (kg/s [lbm/sec]);

$\dot{m}_{annulus}$ is the mass flow rate of water in the annulus of the borehole (kg/s [lbm/sec]).

Similarly, for the water in each of the tubes the energy balance is given by:

$$\frac{dT_{tube.z}}{dt} V\rho C_p = q_{convection,annular\ region} + q_{advection,tube} \quad (4.19)$$

Where $T_{tube,z}$ is the water temperature in the tube (discharge tube or suction tube) at node z (ºC [ºF]);

V, ρ, C_p are the same terms expressed in Equation (4.16).

The advection heat transfer rates in Equations (4.16) and (4.19) can be given by:

$$q_{advection,n} = \dot{m} C_p (T_n - T_{a,z}) \tag{4.20}$$

Where $\dot{m}$ is the mass flow rate of the water (kg/s [lbm/sec]);

n refers to each of the rock and annular fluid at nodes $z-1$ and $z+1$.

The convection heat transfer rates in Equations (4.16) and (4.19) are given by:

$$q_{convection,m} = \frac{1}{R_m}(T_m - T_{a,z}) \tag{4.21}$$

Where R is the thermal resistance (ºC/W [ºF-hr/Btu]);

m is an index referring to the discharge tube, the suction tube or the rock.

The thermal resistance in Equation (4.21) is defined as the following:

$$R_m = \frac{1}{A_{i,m}}\left[\frac{1}{h_{i,m}} + \frac{r_i}{k_{pipe}}\ln\left(\frac{r_i}{r_o}\right) + \frac{r_i}{r_o}\left(\frac{1}{h_o}\right)\right] \tag{4.22}$$

Where A is the area (m^2 [ft^2]);

r is the radius (m [ft]);

k is the thermal conductivity (W/m-K [Btu/hr-ft-ºF]);

h is the heat transfer coefficient (W/m^2-K [Btu/hr-ft^2-ºF]);

and subscript: i is the inner surface, o is the outer surface.

The heat transfer coefficient, h, is defined as

$$h = \frac{Nu \cdot k_{water}}{D_h} \tag{4.23}$$

Where D_h is the hydraulic diameter (m [ft]).

4.1.2.2.1. Convective heat transfer in the borehole

A literature review regarding convective heat transfer correlations in annular spaces has been performed. The literature review suggests that the difference between concentric pipe configurations and eccentric pipe configurations may not be significant (Bhatti and Shah 1987). Also, the correlations applicable to eccentric configurations are limited, and most of them are in tabular forms, not explicit correlations that can be directly used in the computer code. So, the correlations will be based on concentric configurations. In the standing column well, to obtain good heat transfer, the annular area in the well is usually smaller than the area inside the dip tube, so the velocity near the wall is high enough to produce turbulent flow. Here, the attention is put on the turbulent flow.

Friction factor correlations, which may be used in convective heat transfer coefficient correlations, are reviewed first. Second, convective heat transfer correlations for smooth and rough surfaces are reviewed respectively. Finally, we focus on free convection correlations, applicable when the circulating pump is off.

(a). As discussed above, the circular duct correlations for friction factors will be used. For smooth surfaces, the Techo's correlation (Techo et al. 1965) has least relative error compared to the PKN empirical formula[+].

$$\frac{1}{\sqrt{f}} = 1.7372 \ln \frac{\mathrm{Re}}{1.964 \ln \mathrm{Re} - 3.8215} \qquad \text{For smooth surfaces, } 10^4 < \mathrm{Re} < 10^7 \quad (4.24)$$

[+] PKN(Prandtl, Kármán, Nikuradse) correlation: $\frac{1}{\sqrt{f}} = 1.7372 \ln(\mathrm{Re}\sqrt{f}) - 0.3946$

And for rough surface, the explicit equation with least relative error compared to the Colebrook-White empirical formula[+] is given by Chen (1979):

$$\frac{1}{\sqrt{f}} = 3.48 - 1.7372 \ln[\frac{\varepsilon}{a} - \frac{16.2426}{\mathrm{Re}} \ln A_2] \quad \text{For rough surfaces, apply to all values of Re and } \frac{\varepsilon}{a} \qquad (4.25)$$

Where f is the Fanning friction factor;

Re is the Reynolds number, $\mathrm{Re} = \frac{D_h V}{\nu}$;

D_h is the hydraulic diameter (m [ft]);

V is the fluid velocity (m/s [ft/s]);

ν is the kinematic fluid viscosity (m^2/s [ft^2/s]);

ε is the height of the surface roughness (m [ft]);

$A_2 = \frac{(\varepsilon / a)^{1.1098}}{6.0983} + (\frac{7.149}{\mathrm{Re}})^{0.8981}$;

a is the radius of duct (m [ft]).

In the above formula, for more accuracy, the laminar equivalent diameter, D_l, can be substituted for the hydraulic diameter, D_h.

$$\frac{D_l}{D_h} = \frac{1 + r^{*2} + (1 - r^{*2}) / \ln r^*}{(1 - r^*)^2} \qquad (4.26)$$

Where $r^* = \frac{r_i}{r_0}$;

[+] Colebrook-White correlation: $\frac{1}{\sqrt{f}} = 3.48 - 1.7372 \ln(\frac{\varepsilon}{a} + \frac{9.35}{\mathrm{Re}\sqrt{f}})$

r_0, r_i are the radius of outer and inner pipe, respectively (m [ft]);

D_h is the hydraulic diameter (4*area/wet perimeter) (here, $D_h = 2(r_0 - r_i)$) (m [ft]) ;

(b). The circular duct correlations for Nusselt number could be used for both inner and outer walls of the pipes in standing column well systems. But the hydraulic diameter ($D_0 - D_i$) should be used in those correlations. The correlation by Gnielinski is used for smooth surfaces such as the discharge and suction tube:

$$Nu = \frac{(f/2)(\mathrm{Re}-1000)\,\mathrm{Pr}}{1+12.7(f/2)^{1/2}(\mathrm{Pr}^{2/3}-1)} \tag{4.27}$$

For rough surfaces such as the borehole wall, we may use the correlation proposed by Bhatti and Shah (1987) because the range of Reynolds number, *Re*, in this correlation is very wide (i.e., $R_e > 2300$):

$$Nu = \frac{(f/2)(\mathrm{Re}-1000)\,\mathrm{Pr}}{1+(f/2)^{1/2}[(17.42-13.77\,\mathrm{Pr}_t^{\,0.8})\,\mathrm{Re}_\varepsilon^{0.2}\,\mathrm{Pr}^{0.5}-8.48]} \tag{4.28}^{+}$$

Where Pr is the Prandtl number:

$$\mathrm{Pr}_t = \begin{cases} 1.01-0.09\,\mathrm{Pr}^{0.36} & for 1 \le \mathrm{Pr} \le 145 \\ 1.01-0.11\ln \mathrm{Pr} & for 145 < \mathrm{Pr} \le 1800 \\ 0.99-0.29(\ln \mathrm{Pr})^{1/2} & for 1800 < \mathrm{Pr} \le 12500 \end{cases};$$

Re_ε is the roughness Reynolds number, $\mathrm{Re}_\varepsilon = \dfrac{\mathrm{Re}\sqrt{f/2}}{D/\varepsilon}$;

[+]A correction of the printed version based on personal communication with Dr. Shah.

ε is the height of surface roughness (m [ft]);

a is the radius of the pipe (m [ft]).

(c). The borehole wall of standing column well systems is always rougher than the surface of a plastic or steel pipe. The roughness depends on the local geological conditions and drilling methods. Increased roughness increases the borehole wall's surface area and promotes local turbulent flow at the rough wall of borehole, which augments heat transfer. But at the same time, it also increases the friction factor. Norris (1971) suggested the following correlation for heat transfer in rough pipes:

$$\frac{Nu}{Nu_{smooth}} = (\frac{f}{f_{smooth}})^n \qquad \text{for} \qquad \frac{f}{f_{smooth}} \le 4 \tag{4.29}$$

Where $n = 0.68\,\mathrm{Pr}^{0.215}$.

For $\frac{f}{f_{smooth}} > 4$, Norris (1971) also found that Nusselt number no longer increased with the increasing roughness. This was attributed to the fact that when roughness becomes very large ($\frac{f}{f_{smooth}} > 4$), the heat transfer resistance has become essentially a conduction resistance at the surface between the roughness elements.

(d). Free convection is the motion that results from the density difference within a fluid. The density differences in heat transfer result from temperature gradients. In standing column well systems, free convection may occur at the bottom of the borehole or when the pump is off. A few papers deal with free convection in vertical eccentric annulus.

Churchill and Chu (1975) recommend a correlation for the vertical cylinder. Their correlation may be used as an approximation of our problem.

$$Nu = \{0.825 + \frac{0.387 Ra^{1/6}}{[1 + (0.492/\mathrm{Pr})^{9/16}]^{8/27}}\}^2 \tag{4.30}$$

Where Rayleigh number $Ra = \frac{g\beta(T_s - T_\infty)L^3}{\nu\alpha}$

L is the characteristic length L of the cylinder (m [ft]), this is the height of the borehole;

β is the expansion coefficient;

ν is the kinematic viscosity (m^2/s [ft^2/s]);

α is the thermal diffusivity (m^2/s [ft^2/s]).

Equation (4.30) has a condition to be satisfied, which is usually satisfied for our case.

$$\frac{D}{L} \geq \frac{35}{Gr_L^{1/4}} \tag{4.31}$$

Where Grashof number $Gr_L = \frac{gL^3\beta\Delta t}{\nu^2}$.

4.1.3. Computer algorithm

The detailed model consists of two components:

1) A nodal model is used to solve heat transfer in the borehole.

   A set of discretization equations is simultaneously solved by the Gauss-Seidel method. Upon convergence of the fluid temperatures, the heat flux to the borehole wall is calculated and passed to the finite volume model and used to set the flux boundary conditions along the wall of the well.

2) A finite volume model (FVM) with boundary-fitted coordinates is used to solve both the flow equation (Equation (4.1)) in the borehole and the aquifer, and the energy equation (Equation (4.10)) in the aquifer. GEMS2D (General Elliptical Multi-block Solver), a finite volume program, is used in this work. This program was initially developed by Building and Environmental Thermal Systems Research Group at Oklahoma State University (Rees, 2000). The borehole wall temperatures are calculated in this finite volume model and passed to the nodal model and used to set the temperature boundary conditions along the wall of the well.

GEMS2D is capable of solving the general advection-diffusion equation on two dimensional boundary fitted grids. The FVM starts from the integral form of the partial differential equation:

$$\frac{\partial}{\partial t}\int_{\mathbf{V}} \phi d\mathbf{V} + \int_{\mathbf{S}} \rho\phi\mathbf{v}\cdot\mathbf{n}d\mathbf{S} = \int_{\mathbf{S}} \Gamma\nabla\phi\cdot\mathbf{n}d\mathbf{S} + \int_{\mathbf{V}} Qd\mathbf{V} \qquad (4.32)$$

Where ϕ is the dependent variable (head or temperature in this work), Γ is the diffusivity, $\mathbf{V}$ is the volume, $\mathbf{S}$ is the surface of a control volume, and $\mathbf{n}$ is a vector normal to the surface. The left-hand term of the equation is the temporal term, the second term represents the advective fluxes, the third term represents the diffusion fluxes, and the fourth term represents sources and sinks. A physical space approach for dealing with complex geometries can be derived from the vector form of the equation above. This generic form of the advection-diffusion equation can be used to represent both the heat transfer and groundwater flow equations used in this work.

A second order approximation is to assume that the value of the variable on a particular face is well represented by the value at the centroid of the cell face. The diffusion flux at the east face of a cell can be written as:

$$F_e^D = \int_{\mathbf{S}_e} \Gamma \nabla \phi \cdot \mathbf{n} d\mathbf{S} \approx (\Gamma \nabla \phi \cdot \mathbf{n})_e S_e \tag{4.33}$$

Where S_e is the area of the east face.

Our main difficulty is in calculating the gradient of the variable $(\nabla \phi)$ at each cell face when grids are not orthogonal. The formula $F_e^D \approx \Gamma_e S_e (\partial \phi / \partial \xi)_{e'}$ is only accurate if the grid is orthogonal. We defined local coordinates at the cell face as shown in Figure 4-7. In the direction normal to the face at its centroid, the coordinate *n* is defined, and on the line between neighboring centroids the coordinate ξ which passes through the face at point *e′* is defined.

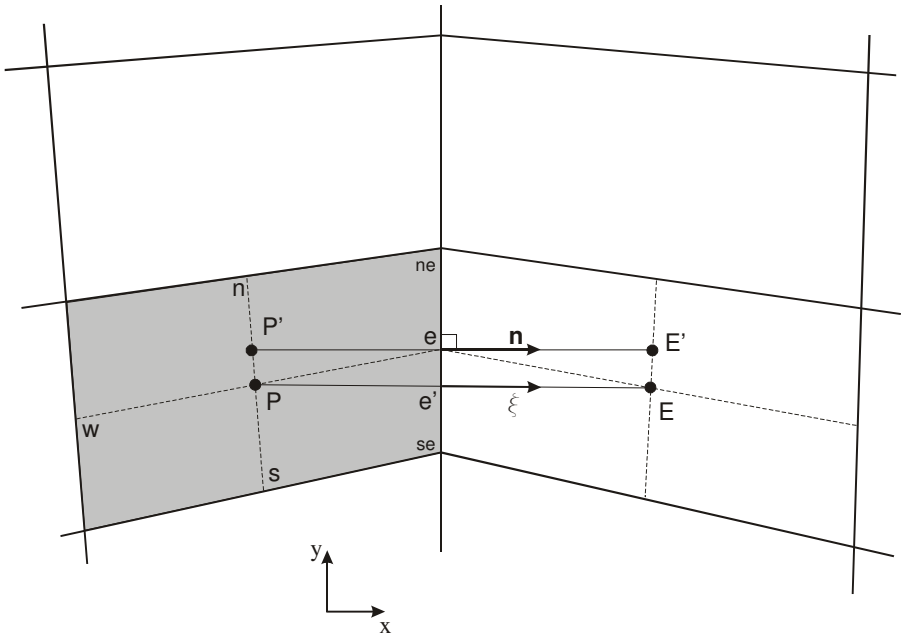

Figure 4-7 The geometry of a typical cell in the mesh showing the relationship between the face and cell centroids.

To preserve second-order accuracy, the calculation of the gradient should be along the normal to the face and at the centroid of the face using the values of the variable at points *P′* and *E′*. However, in GEMS2D, the values of the variables at the cell centroid *P* and *E* are still used to calculate the gradient of the variable. A 'deferred correction' approach is used to calculate the flux as follows:

$$F_e^D = \Gamma_e S_e \left(\frac{\partial \phi}{\partial \xi}\right)_{e'} + \Gamma_e S_e \left[\left(\frac{\partial \phi}{\partial n}\right)_e - \left(\frac{\partial \phi}{\partial \xi}\right)_{e'}\right]^{old} \tag{4.34}$$

The gradients are calculated by central differencing. The terms with "old" on the right hand side are calculated explicitly using previous values of the variable. As the solution approaches convergence, the terms $(\partial\phi/\partial\xi)_{e'}$ and $(\partial\phi/\partial\xi)_{e'}^{old}$ cancel out, leaving

$(\partial\phi/\partial n)_n$. $(\partial\phi/\partial n)_n$ is calculated explicitly from the central difference.

Interpolation is required to get $\phi_{p'}$ and $\phi_{E'}$. Finally, Equation (4.34) can be written as

$$F_e^D = \frac{\Gamma_e S_e}{L_{P,E}}(\phi_E - \phi_P) + \frac{\Gamma_e S_e}{L_{P,E}}\left[\nabla\phi_E \cdot (\mathbf{r}_{E'} - \mathbf{r}_E) - \nabla\phi_P \cdot (\mathbf{r}_{P'} - \mathbf{r}_P)\right]^{old} \quad (4.35)$$

Where the right hand terms are calculated as a deferred correction. If the grid is orthogonal, then it can be seen that the deferred correction becomes zero and the discrete equation becomes equivalent to that for orthogonal grids.

To formulate a finite volume solution in FVM, the partial differential equation should be integrated with respect to volume. In a transient problem it should be integrated with respect to time, also. A first-order backwards differencing approach is used in a fully implicit formulation. The fully implicit approach results in the following discretized equation:

$$\rho\Delta V\left(\phi_P^{n+1} - \phi_P^n\right) = \left[F_n^D + F_s^D + F_w^D + F_e^D\right]^{n+1}\Delta t \quad (4.36)$$

Where the superscript is the index in time level. The discretized equation can then be said to be first-order accurate in time and second-order accurate in space. This scheme is unconditionally stable. After integrating the PDE and applying the discretization procedures discussed, an algebraic equation is obtained for each control volume of the form,

$$a_P\phi_P = \Sigma a_{nb}\phi_{nb} + b \quad (4.37)$$

For a two-dimensional model, this results in a set of algebraic equations that are coupled via neighboring cells. There are several solvers for discretization equations in GEMS2D, but currently, the Semi-Implicit Method (SIP) along with Biconjugate Gradient Stabilized (BiCGSTAB) algorithm are preferred considering the time consumed.

Model organization.

The physical and mathematical models discussed above have been implemented in *Fortran90/95* computer models. Figure 4-8 shows the flowchart of the Fortran program.

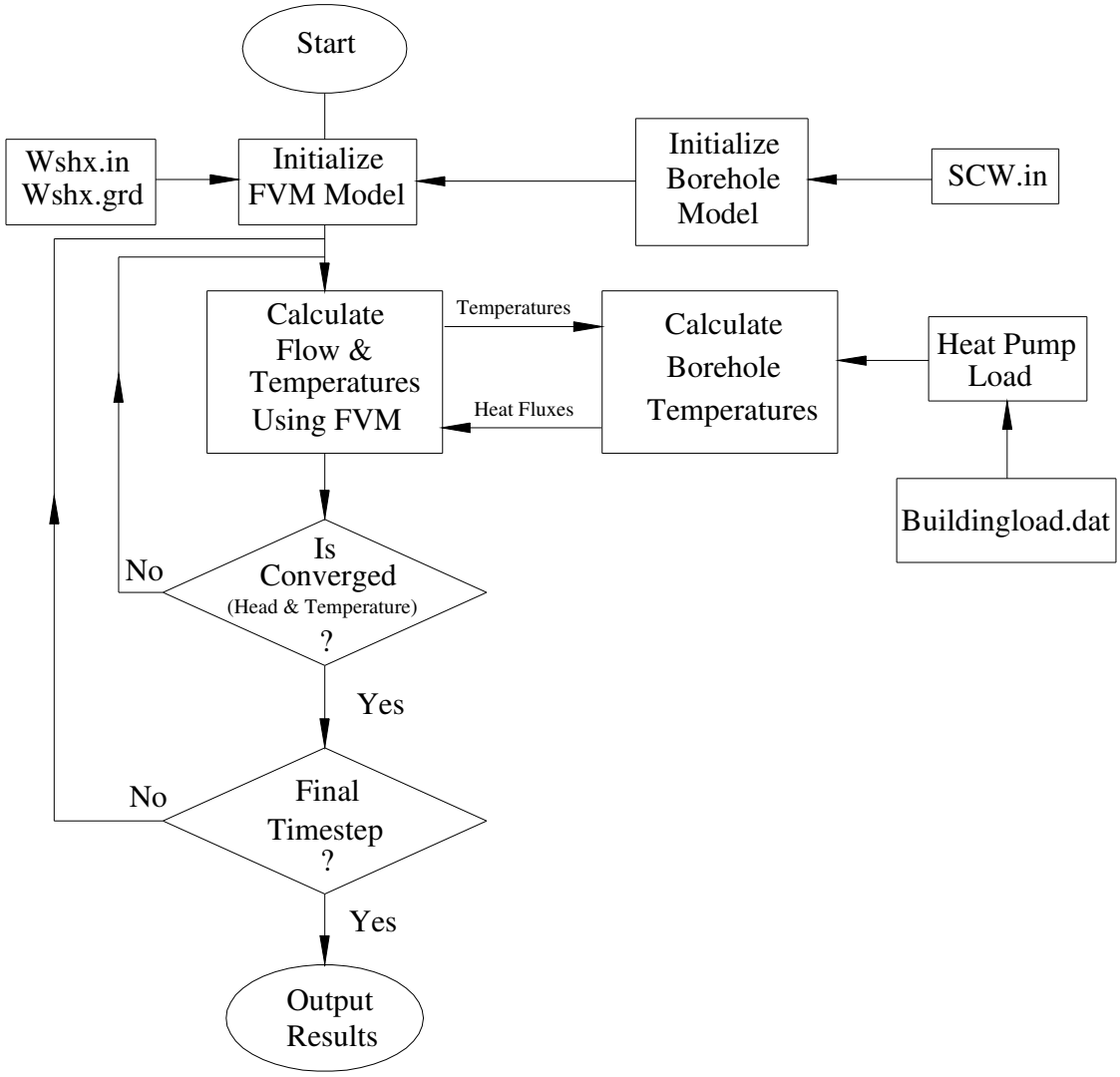

Figure 4-8 Flowchart of computer algorithm for the overall SCW systems

An energy balance is formulated at each z-plane in the borehole of the SCW, corresponding to the z-plane in the FVM numerical model of flow and heat transfer in the aquifer. The borehole model is used to calculate the heat fluxes along the borehole wall for a given set of borehole wall temperatures. To couple the borehole model and FVM, heat fluxes calculated from the borehole model are used to set boundary conditions at the borehole wall in the FVM. In turn, the FVM calculates both the groundwater flow and the

temperature field in the aquifer and passes the borehole wall temperature back to the borehole model. Therefore, the borehole wall temperatures are inputs to the borehole model and heat fluxes along the borehole wall are output, and vice versa for the FVM. It is necessary to under-relax the temperatures passed to the borehole model. This requires considerable iteration before the two models converge at each z-level.

There are four input files for the numerical models: SCW.in, Wshx.in, Wshx.grd and Buildingload.dat.

File SCW.in includes:

1) the geometric information about the borehole, such as the diameters of borehole and tubes, the depth of well, bleed rate, etc;
2) the physical properties of the borehole, such as roughness of different surfaces, and thermal conductivity of tubes and casing.

File Wshx.grd is generated by a grid generation code PGRID_2D (Rees 2000), which was initially developed for generation of two-dimensional multi-block structured grids. A two-dimensional cylindrical grid of single standing column well is shown in Figure 4-9.

After conducting some grid independence calculations, a final grid size of 160x70 was chosen as the best compromise between accuracy and computational speed. There will be some discussions of the domain size, the grid size and time-step size in Appendix A.

File Wshx.in is the input file for FVM. In this file, the boundary conditions, solver control flag, and initial values of each variable are set.

File Buildingload.dat contains annular building load for a given building and is generated by building energy simulation software (BLAST 1986).

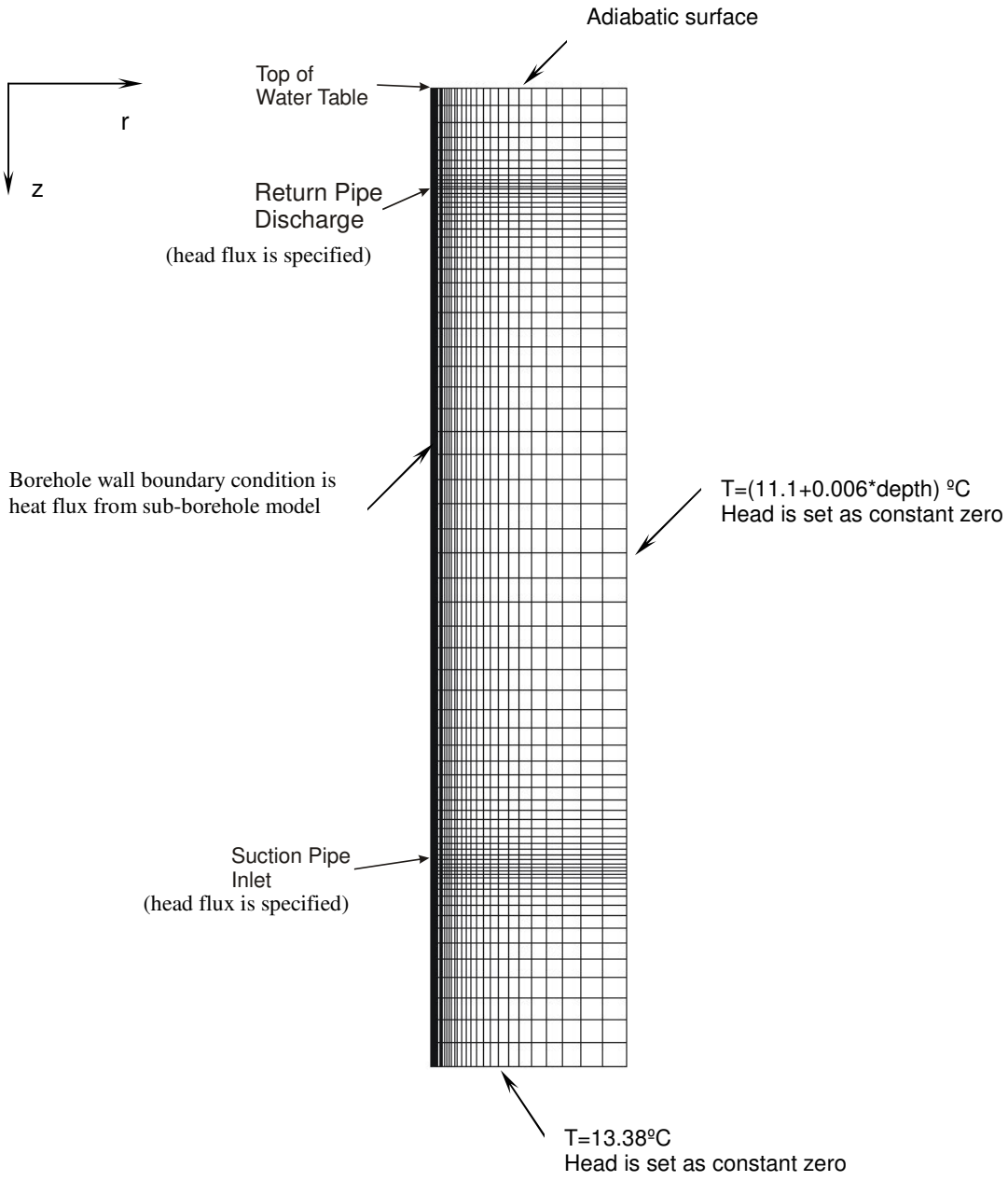

Figure 4-9 A 2D cylindrical grid of single standing column well

(with boundary conditions in the base case)

4.2. Experimental validation

Detailed experimental validation of the model is highly desirable. As construction and monitoring of a standing column well system is beyond the scope of this study, existing data from standing column well systems in the United States have been sought. The following discussion first sets out "ideal" experiment. Using data collected by others may necessarily result in some compromise. Experimental validations against data, which are available from two exiting standing column well systems, are described in sections 4.2.2 and 4.2.3.

4.2.1. Ideal experiment

At first, information about the aquifer characteristics in the region where the standing column well is located should be obtained, particularly thermal and hydraulic properties. The thermal conductivity can be determined by *in-situ* measurement (Austin et al. 2000). A well drawdown test for determining the hydraulic conductivity of the aquifer should be made too.

Following the *in-situ* thermal conductivity and well drawdown tests, the standing column well would be connected to a heat pump providing cooling and heating to a building. Thermocouples will be used to monitor the entering and return temperatures of the water circulating to the heat pump and back to the well. Flow meters will be used to measure the flow rate of the water circulating to the heat pump and back to the well. Heat transfer rates can then be established. Wattmeters will be used to measure power consumption of

the heat pump and the water pump. Also, the water table depth in the well should be recorded.

Additional information that would be useful in verifying model performance would include several temperature measurements made along the length of the well.

- borehole wall temperature
- water temperature in the annular space
- water temperature in the dip tube
- ground water temperatures in the vicinity of the standing column well

All the temperatures and flow rates should be monitored continuously from the beginning of the operation of SCW system. All the thermocouples and flow meters should be connected to a computerized data acquisition system.

Although there are approximately 1000 SCW installations in the Unites States, monitored data are rarely available. To date, two sets of data from existing standing column well systems have been identified. Because these data do not completely satisfy the requirements listed above, it is necessary to estimate some parameters used during the validation. The experimental validations with these two data sets are described below.

4.2.2. Validation with data from SCW system at Pennsylvania State University

Mikler (1993) performed experimental studies of transient heat and mass transfer in one standing column well system installed at Pennsylvania State University (see Figure 2-3 in

section 2.4). The standing column well was in non-bleed operation during the whole experimental period.

4.2.2.1. Experimental data

Thermocouples were used to monitor both the water temperature distribution along the well as well as the ground temperature in the vicinity of the SCW at different depths. Also, thermocouples were used to monitor the entering and return temperatures of the circulating water, the inlet and outlet air temperatures passing through the heat pumps, and the ambient temperatures. A flow sensor was used for monitoring total flow rate of the circulating water. Thermal and hydraulic properties of the aquifer were determined based on knowledge of the local geology.

Cooling mode operation

The heat pumps were operated at full capacity in cooling mode for the period of 48 subsequent days from August 4 to September 20, 1992. The distributions of ground load, total water flow rate, and entering and return water temperatures T_{WE} and T_{WR} in time during the whole cooling mode operation are shown in Figures 4-10, 4-11, and 4-12. There are some fluctuations of ground loads shown in Figure 4-10. To some extent, those fluctuations correspond to flow rate changes shown in Figure 4-11.

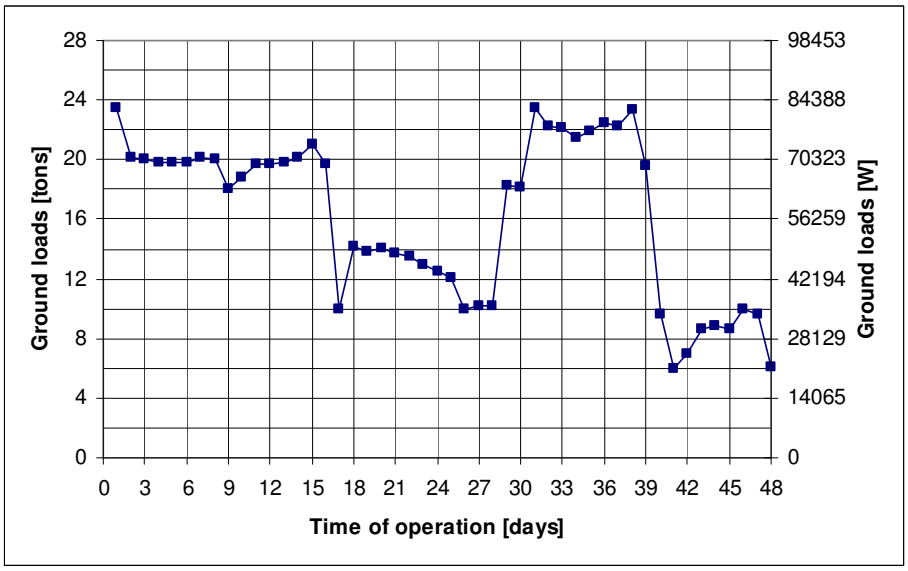

Figure 4-10 Cooling mode-ground load (Mikler 1993)

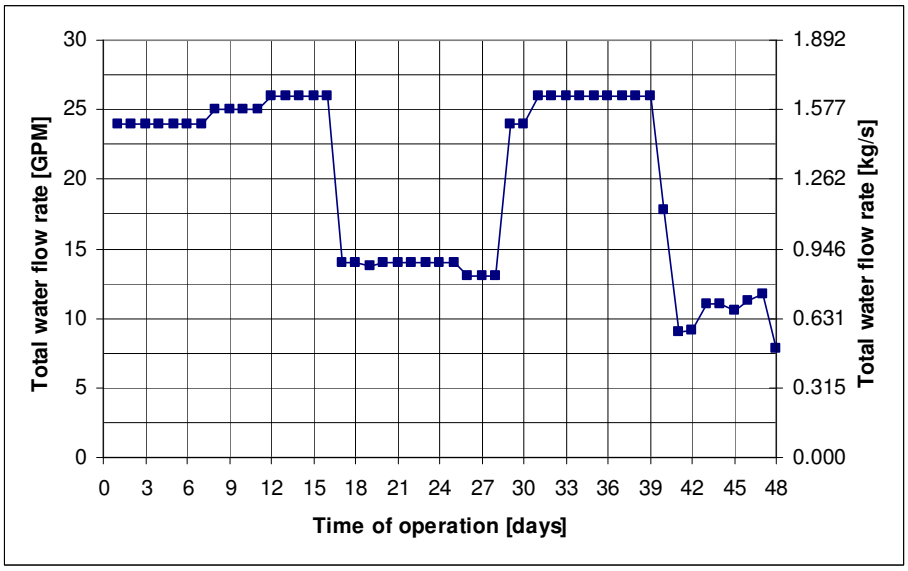

Figure 4-11 Cooling mode-total water flow rate (Mikler 1993)

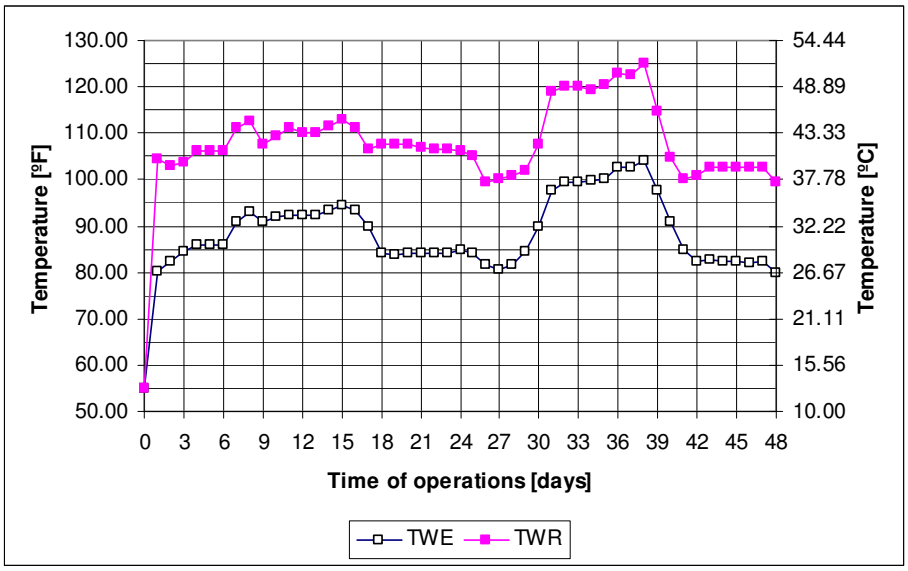

Figure 4-12 Cooling mode-entering and return water temperatures (Mikler 1993)

Heating mode operation

After the completion of the cooling mode operation, the system was shut off for the period of six weeks from September 21 to December 10, 1992, and the aquifer temperature recovered. On average, the initial aquifer temperatures for the heating mode operation (December) were 4 to 5 ºF (2.5 ºC) higher compared with the initial undisturbed conditions for the cooling mode operation (August).

The heat pumps were operated at full capacity in heating mode for 71 days from December 10, 1992 to February 19, 1993. The distribution of ground load, total water flow rate, and entering and return water temperatures T_{WE} and T_{WR} in time during the whole heating mode operation are shown in Figures 4-13, 4-14 and 4-15. System flow rate were fluctuated much for the first 9 days, and then became almost constant for the

rest days during the operations. Fluctuations of ground load correspond to flow rates fluctuations in Figure 4-14.

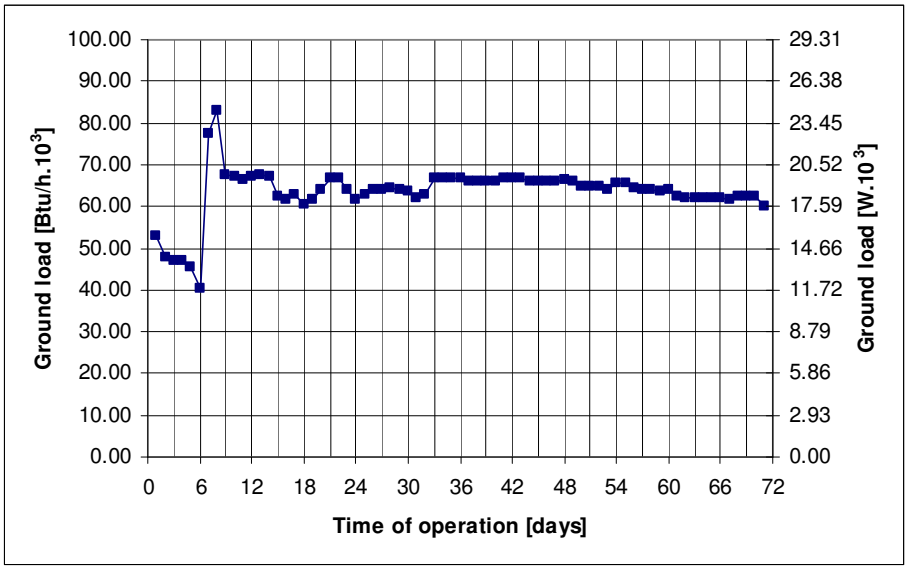

Figure 4-13 Heating mode-ground load (Mikler 1993)

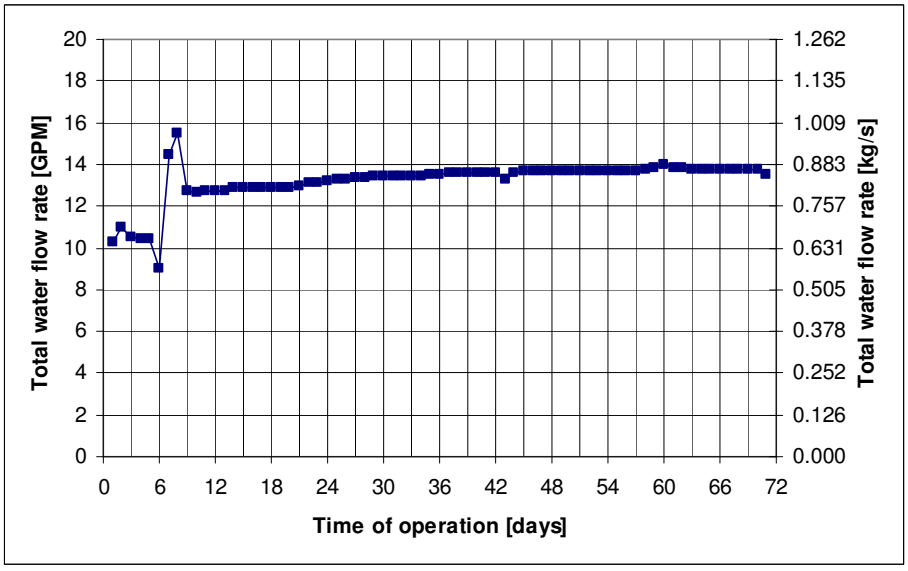

Figure 4-14 Heating mode-total water flow rate (Mikler 1993)

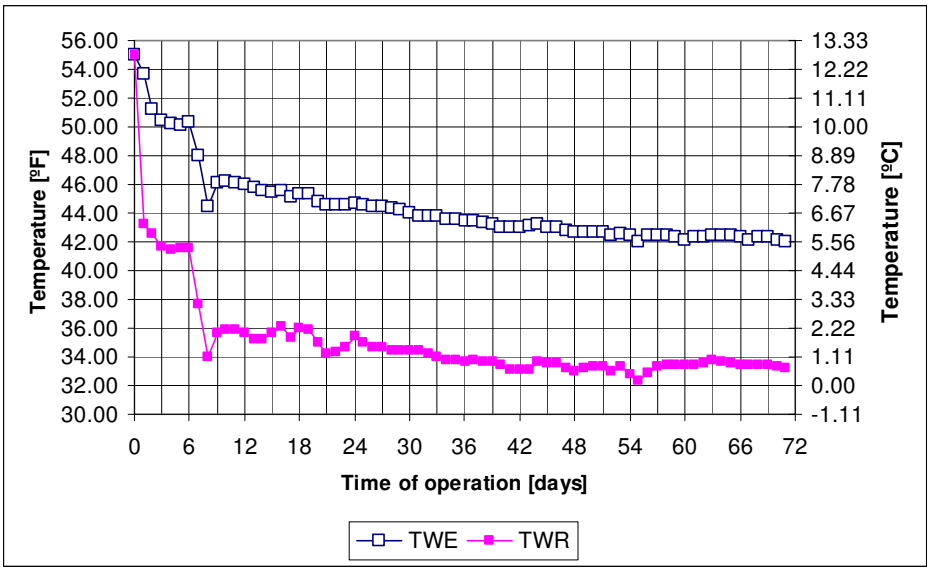

Figure 4-15 Heating mode-entering and return water temperatures (Mikler 1993)

4.2.2.2. Methodology for validation

The experimental results presented by Mikler (1993) are compared with the detailed model using a subset of the experimental data as input parameters.

Experimental data are available for different validation procedures depending on which data are treated as model inputs:

Procedure A -The ground loads are used as input parameters;

Procedure B -The return water temperatures into the standing column well are used as input parameters.

The validation results from the above two procedures are almost identical, so only the validation from the procedure A is provided and discussed in the followings.

All the other parameters used in the simulation in both procedures are same, which are given in Tables 4-1 and 4-2.

Table 4-1 Hydraulic and thermal properties of the rock (Karst limestone)

Hydraulic Properties		
Hydraulic Conductivity (K) **m/s** **(gal/day/ft^2)**	**Porosity (n)** **(---)**	**Specific Storage (Ss)** **m^{-1}** **(ft^{-1})**
7.00E-05 (148.23)	0.275	1.00E-05 (3.28E-05)
Thermal Properties		
Thermal Conductivity (k) **W/m-K** **(Btu/hr-ft-^{o}F)**	**Density (ρ)** **kg/m^3** **(lbm/ft^3)**	**Specific Heat (Cp)** **J/kg-K** **(Btu/lbm-^{o}F)**
Estimated during the validation	2700 (168.56)	1000 (0.2389)

Table 4-2 Properties of the borehole

Parameter	**Depth**	**Diameter**	**Wall Thickness**	**Thermal Conductivity**	**Surface Roughness**
Units	**m** **(ft)**	**mm** **(in)**	**m** **(in)**	**W/m-^{o}C** **(Btu/hr-ft-^{o}F)**	**mm** **(in)**
Borehole	320 (1049.6)	152.4 (6)	-----	----	1.5 (0.06)
Discharge pipe	2 (6.56)	33.4 (1.3)	3.05 (0.12)	4 (2.31)	1.5 (0.06)
Suction pipe	318 (1043)	101.6 (4)	6.35 (0.25)	0.1 (0.0578)	1.5 (0.06)

Mikler (1993) measured the undisturbed ground temperatures before the actual heat pump operation started. According to this experimental data:

$$T = 10.05 + 0.006 \times depth \qquad (4.38)$$

Where T is the ground temperature at the given depth (ºC);

Depth is the distance for the surface of the ground to the given point under the ground (m).

The thermal conductivity of the aquifer should be determined based on the available measured data, "drill log", and the basic knowledge about the local geology. However, Mikler (1993) took the value of thermal conductivity from the published data of the independent source (Hellström 1991). This value was *not* measured by *in-situ* test, so it doesn't necessarily consider the effect of the actual geology or movements of groundwater in the aquifer. The parameter estimation method was used to find the actual value of this thermal conductivity.

Estimation of thermal conductivity

The objective of the estimation is to find the actual value of thermal conductivity, using data from the first 50 hours of operation in lieu of a separate *in-situ* test. It should be noticed that since the heat pumps were run full-out, they approximated the constant load of an *in-situ* test. This estimation includes the effects of groundwater movement during the operation of the standing column well system. The objective function used in conjunction with the golden section search method is given as the following:

$$\sum_{i=1}^{N} (T_{Mikler,i} - T_{model,i})^2 \tag{4.39}$$

Where i is the time step;

N is the total time steps (the first 50 hours);

$T_{Mikler,i}$ is the exiting water temperature recorded during Mikler's experiments;

$T_{model,i}$ is the exiting water temperature obtained from the models.

The objective is to find the value of actual thermal conductivity, which minimizes the difference between the experimental data from Mikler and the model.

By minimizing the objective function given in Equation (4.39), the estimated effective thermal conductivity for this given area (Karst limestone) is found to be about 3.0 W/m-K. From the definition of the effective thermal conductivity:

$$k_{eff} = nk_l + (1-n)k_s \tag{4.40}$$

Where n is the porosity;

k_l is the thermal conductivity of the water (W/m-K [Btu/hr-ft-ºF]);

k_s is the thermal conductivity of the solid (W/m-K [Btu/hr-ft-ºF]).

The porosity of Karst limestone is 0.275. Therefore, from Equation (4.40), the thermal conductivity of Karst limestone is calculated to be 3.81 W/m-K. The range of thermal conductivity of Karst limestone is from 2.5 W/m-K to 4.3 W/m-K (Chiasson et al. 2000). Thus, the estimated thermal conductivity, 3.81 W/m-K, is in this range.

4.2.2.3. Validation results and conclusions

A comparison of the temperatures back to the heat pump in both cooling and heating mode from the detailed model and Mikler's data is shown in Figures 4-16 and 4-17. The validation results show that the SCW system simulated in the detailed model responds a

little slower to the ground load changes than the real system in Mikler's experiment. The possible reasons for this difference are listed as follows:

1. In reality, it is possible that there are some rock fractures near the well. Also, the aquifer surrounding the well is not homogenous or isotropic. These effects cannot be considered in the detailed model, which is a model for the continuous medium.

2. The thermal and hydrogeological properties of the surrounding rock used in this validation such as thermal conductivity and hydraulic conductivity are *not* measured by *in-situ* tests.

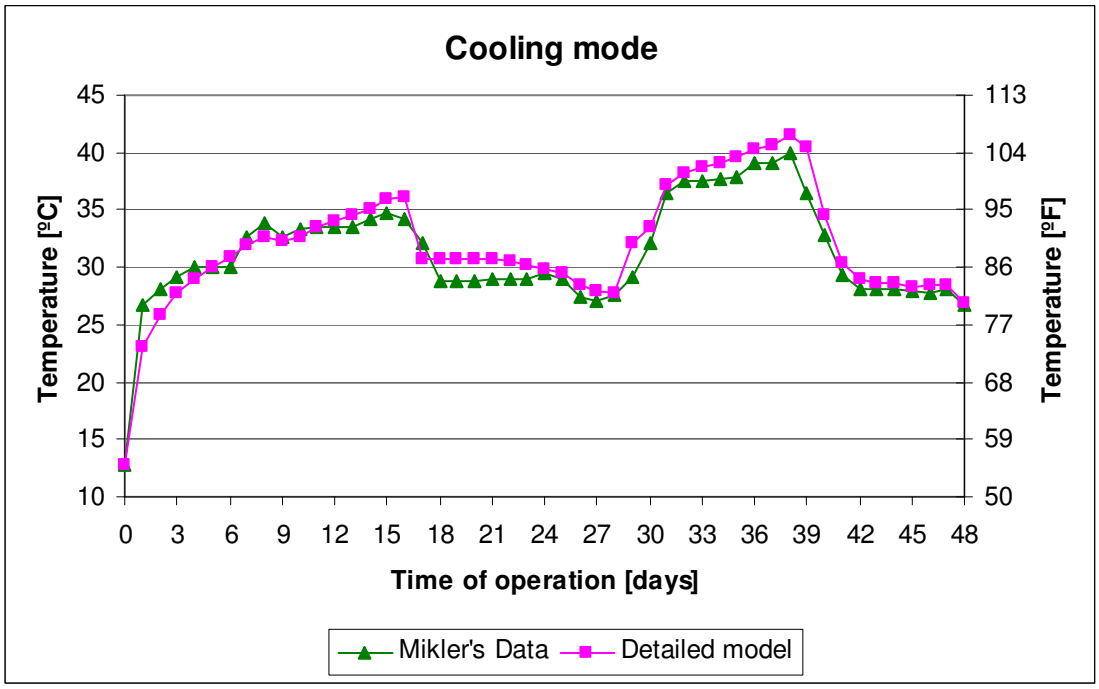

Figure 4-16 Comparisons of temperatures back to the heat pump for the detailed model and Mikler's data in cooling mode

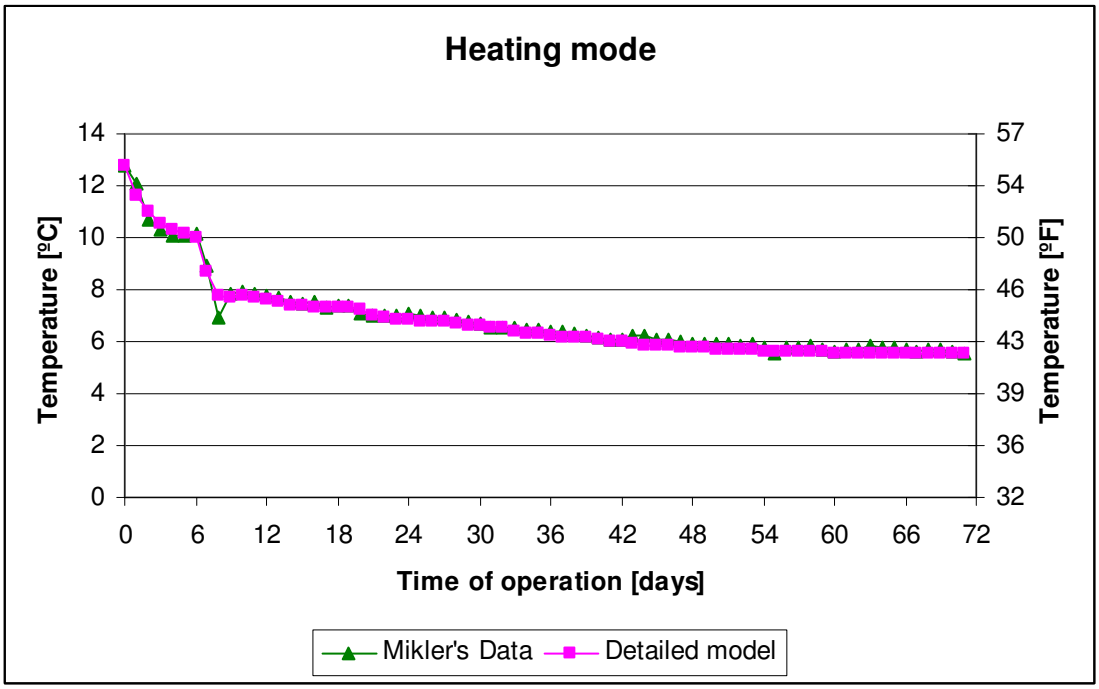

Figure 4-17 Comparisons of temperatures back to the heat pump for the detailed model and Mikler's data in heating mode

Figures 4-16 and 4-17 show that there is a good agreement between the temperatures back to the heat pump predicted by the detailed model and Mikler's data. This preliminary validation shows that the detailed model can be used to adequately simulate the standing column well systems in non-bleed operation.

The maximum deviation of the temperature predictions is observed when water flow rate changes abruptly. The best agreement between the predicted and measured temperatures is observed when water flow rate in the loop is relatively continuous as in the heating mode after the 9^{th} day. The goodness of the agreement between the predicted and the actual temperatures back to the heat pump depends on the continuity of the experimental

data. The reason for this may be explained as follows: All the available data in this experiment were provided as daily average values; therefore the time-step size set in the model for this validation is 24 hours. As shown in Appendix A, the sensitivity of the simulation results to the time-step size is small for a typical standing column well system. In the numerical model for the transient problem, it is supposed that all the input data (i.e., the flow rate and the entering fluid temperature) and boundary conditions do not fluctuate much during the time-step, thus the average values can be used. For the transient model with large time-step size, it is desirable that the input data (i.e., flow rate and the entering fluid temperature) and boundary conditions (i.e., ground load) are continuous and constant in this give time-step period. Otherwise, the transient characteristics of the system can not be accurately modeled by using the average values. In Mikler's data set, experimental data including ground load (thermal boundary conditions for the model) and water flow rate fluctuate less in the heating experiment than in the cooling experiment. This may explain why better agreement is obtained for the validation in heating mode.

The bleed operation, which is a very important strategy for SCW system, is not included in Mikler's experiment. To validate whether this detailed model can correctly predict the performance of a SCW system in bleed operation, another set of SCW system experimental data with bleed is necessary.

4.2.3. Validation with data from a SCW system in the Haverhill public library

A SCW system was used to provide heating/cooling to Haverhill public library, Massachusetts. Currently, there are four standing column wells to provide a heat sink/source for the water-to-water heat pumps. Initially two SCWs were installed in 1994, but expansion of the library resulted in two additional SCWs after 1996. Each of the standing column well wells is 457 m (1500 ft) deep, 0.1524 m (6 in) in diameter. Water is drawn from the bottom of the well, run through the heat pump and discharged at the top of the well. ClimateMaster WE120 heat pumps were used in this system.

The SCW system was placed in service in January of 1995. Until June 25th, 1996, only one standing column well was used. After that, the second well pump became active. The validation will focus on the time period before June 25th, 1996, when only one standing column well was operating. During the winter or whenever the well temperature drops below 4.44 ºC (40 ºF), a bleed cycle initiates. This automatic bleed diverts approximately 10 % of the flow from returning to the wells. A bleed cycle typically lasts for 30 minutes. It acts to limit the lower well temperature by drawing in new warmer ground water. There is no bleed during summer operation.

4.2.3.1. Experimental data

CDH Energy Corp. (Henderson 2003) provided hourly data for the year 1996 on the following:

- Total power use of the heat pumps
- Total power use of the well pumps

- Outdoor air temperature
- Water temperatures entering and leaving the wells

Figure 4-18 shows temperatures entering and leaving the well in the year of 1996.

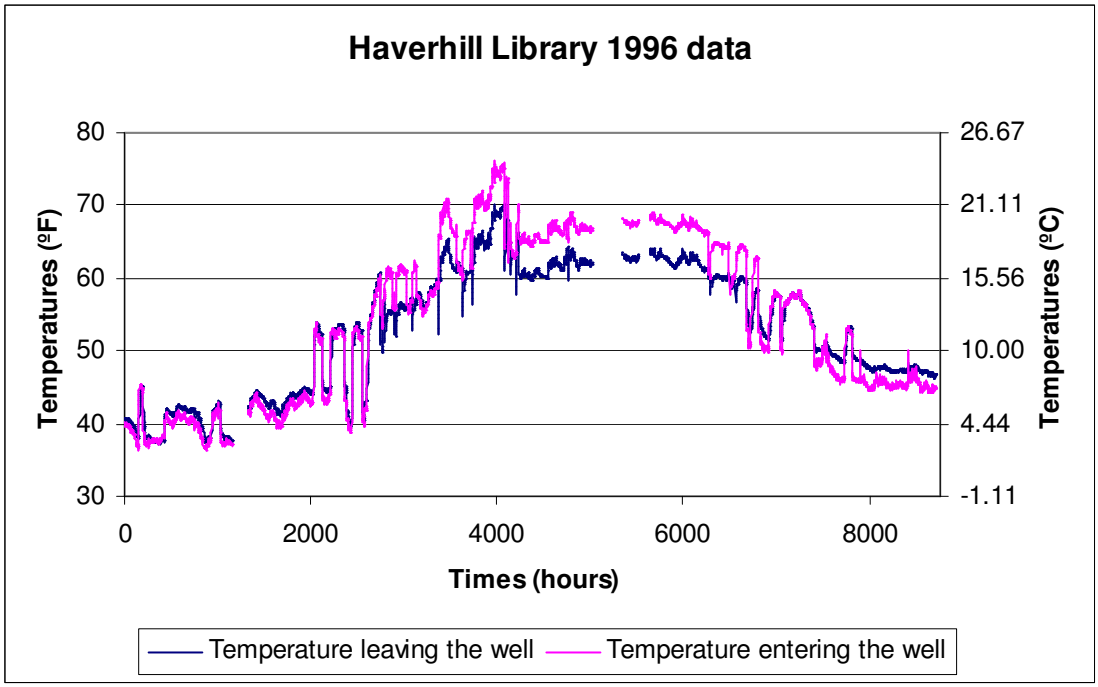

Figure 4-18 Water temperatures entering and leaving the well in Haverhill library (Henderson 2003)

Water and Energy Systems Corp. (Johnson 2003) provided the Haverhill library well logs. Unfortunately, the well drawdown tests were not reported in these well logs. The efforts have been tried to look for any well logs in the general vicinity of Haverhill public library that has drawdown tests, and then the hydraulic conductivity can be calculated. However, nobody can provide such logs. Therefore, thermal and hydraulic properties of the aquifer are estimated based on knowledge of the local geology.

According to the general information provided by the U.S. Geological Survey (USGS), the rock type for Haverhill region is Ordovician and Cambrian sedimentary rock. The thermal and hydraulic properties of the rock are taken from Domenico and Schwartz (1990).

4.2.3.2. Methodology for validation

The existing hourly experimental data set is only for the year 1996. The models will be used to predict the hourly performance of the SCW system for this year. Since the thermal history of the system operation is important and the system has been in operation since January 1995, some approximation for the year 1995 operation must be made. The best approach is likely to run the model for the year 1995 to provide the initial boundary conditions for the year 1996 simulation. Thus, first, a one-year simulation is run for the year 1995. Building loads are used as input parameters for the models. The daily building loads for the year 1995 are available from CDH Energy Corp.; however, some of loads are not reported. Therefore, it is necessary to calibrate the building loads.

After the simulation for the year 1995 is finished, the results of this simulation such as ground temperatures, groundwater velocities are used as the initial conditions of the simulation for the year 1996. The real data (i.e., water temperatures entering the well) recorded during the experiment are used as input parameters. The water temperatures leaving the well predicted by the models will be compared with the experimental data.

Parameters used in the simulation are given in Tables 4-3 and 4-4. The bleed control strategy is set as the following according to data provided by CDH Energy Corp (Henderson 2003):

- Whenever the well water temperature drops below 40 ºF (4.44 ºC), a bleed cycle with bleed rate 10 % initiates.
- The bleed cycle lasts for 30 minutes.

Table 4-3 Hydraulic and thermal properties of the Ordovician and Cambrian sedimentary rock (Domenico and Schwartz 1990)

Hydraulic Properties		
Hydraulic Conductivity (K) **m/s** **(gal/day/ft^2)**	**Porosity (n)** **(---)**	**Specific Storage (Ss)** **m^{-1}** **(ft^{-1})**
1.00E-05 (21.18)	0.10	1.00E-05 (3.28E-05)
Thermal Properties		
Thermal Conductivity (k) **W/m-K** **(Btu/hr-ft-ºF)**	**Density (ρ)** **kg/m^3** **(lbm/ft^3)**	**Specific Heat (Cp)** **J/kg-K** **(Btu/lbm-ºF)**
Estimated during the validation	2200 (137.35)	1000 (0.2389)

Table 4-4 Properties of the borehole in Haverhill library (Henderson 2003)

Parameter	**Depth**	**Diameter**	**Wall Thickness**	**Thermal Conductivity**	**Surface Roughness**
Units	**m** **(ft)**	**mm** **(in)**	**m** **(in)**	**W/m-ºC** **(Btu/hr-ft-ºF)**	**mm** **(in)**
Borehole	457 (1499.42)	152.4 (6)	-----	----	1.5 (0.06)
Discharge pipe	2 (6.56)	33.4 (1.3)	3.05 (0.12)	4 (2.31)	1.5 (0.06)
Suction pipe	455 (1492.86)	101.6 (4)	6.35 (0.25)	0.1 (0.0578)	1.5 (0.06)

The thermal conductivity is estimated to be 2.32 W/m-K (1.34 Btu/hr-ft-ºF) for the detailed model by using the same parameter estimation method described in section 4.2.2.2. The time period for the estimation is set to be the first 200 hours of operation to include the bleed operation.

The undisturbed ground temperatures are set according to the data provided by CDH Energy Corp:

$$T = 10.0 + 0.009 \times depth \qquad (4\text{-}41)$$

Where T is the ground temperature at the given depth (ºC);

Depth is the distance for the surface of the ground to the given point under the ground $0 \le depth \le 457$ (m).

4.2.3.3. Pre-processing the data

There are some corrupt or missing data in the data set provided by CDH energy Corp. Among these data, water temperatures entering the well and flow rates are used as the inputs for the numerical model during the validation, so it is necessary to pre-processing those data to have continuous inputs for the model. Then, the validation process could be continuous for a given time period.

Flow rate

Hourly flow rate is not available for the given data set. In this validation, flow rate is calculated based on the energy balance. Appendix C gives the calculation process in detail. Figure 4-19 shows system flow rates for the first 2000 hours.

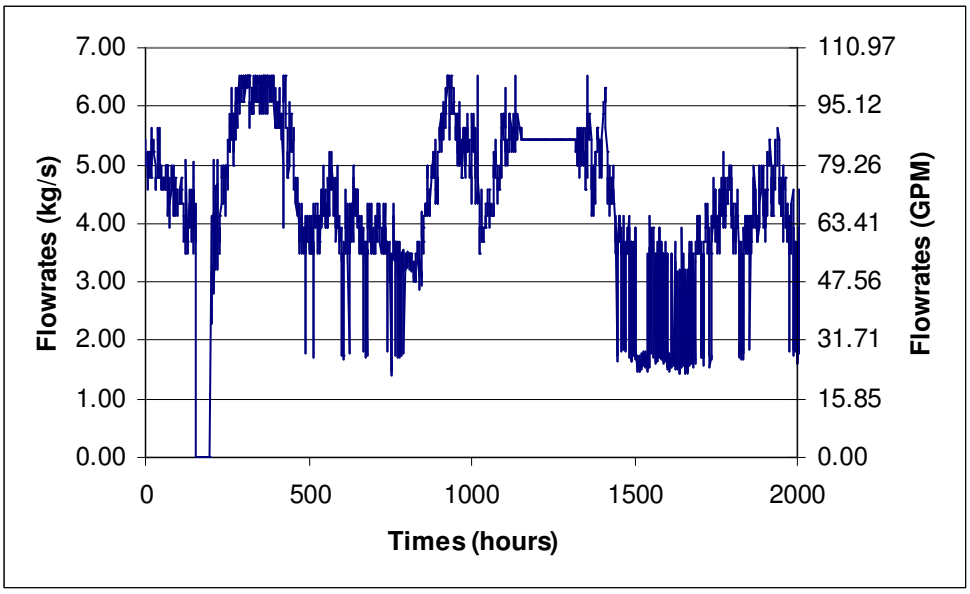

Figure 4-19 System flow rates in Haverhill library

Missing data

From Feb. 18th to Feb. 24th (i.e., from the 1152nd hour to the 1319th hour), the temperature data, including temperatures entering/leaving the well and outdoor air temperatures, are not available. But, the daily building loads for these 7 days are available.

Firstly, ground loads are estimated from building load (COP of heat pump is available), and then those ground loads are used as input parameters of the model to estimate water temperatures entering the well. Finally, these estimated water temperatures entering the well are used during the validation.

Corrupt data

From the 156th hour to the 199th hour, outside air temperatures were below zero, which means the standing column well system should be in heating mode. However, the power consumption measurements indicate that the system was off.

Also, from the 250th hour to the 424th hour, outside air temperatures were below zero, which means the standing column well system should be in heating mode. However, water temperatures leaving the well are less than water temperatures entering the well, which shows that the system was in cooling mode.

The corrupt data are not used during the validation. The system is assumed to be off, so zero heat flux is directly applied in the validation. The simulation results shown in the following section have justified this assumption.

4.2.3.4. Validation results and conclusions

Comparisons of temperatures back to the heat pump from the detailed model and Haverhill data are shown in Figures 4-20. There are lots of missing data for the post-2000 hour data, so only the data from the first 2000-hour operation are chosen for the validation. The corrupt and missing data are excluded from the experimental validation.

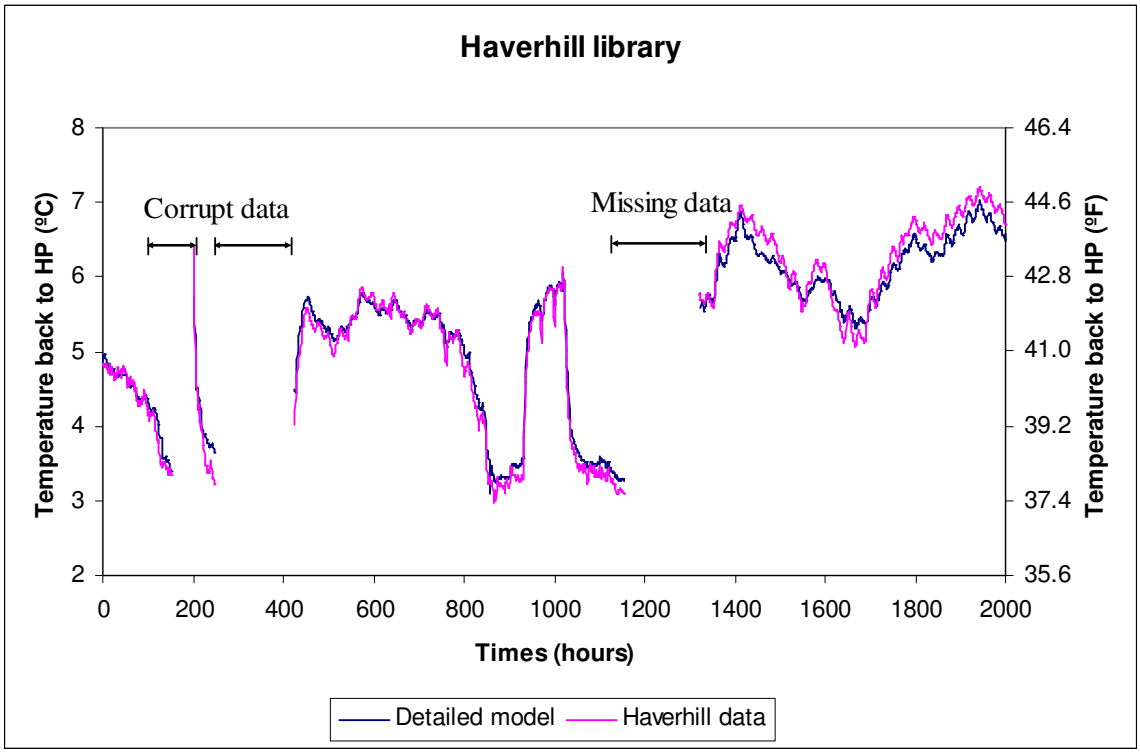

Figure 4-20 Comparison of temperatures back to heat pump for the detailed model and Haverhill data

Figure 4-20 shows that there is a good agreement between experimental measurements of temperature and temperatures predicted by the detailed model. The maximum temperature difference between the model and the experiment is 0.45 ºC (0.85 ºF), which is an acceptably small error. From this validation, it may be inferred that the detailed numerical model can also be used to adequately simulate the standing column well systems in bleed operation.

The Haverhill data is a little bit closer to the correspondingly predicted temperatures from the detailed model than Mikler's data. This improvement probably comes from increased measurement frequency.

Mikler's data (Mikler 1993) is given as daily average values; on the contrary, the data from Haverhill library are hourly instantaneous values, which are more desirable for the validation of the transient model.

At this point, this detailed numerical model has been validated with limited experimental data. How might this model be applied? What are typical temperatures and velocity fields in and around a standing column well? In the next section, this detailed numerical model will be used to study the performance of a typical system. This system is also utilized as the base case in the parametric study described in Chapter 5, and also is referred to as "the base case."

4.3. The base case

This section describes how the detailed numerical model is applied to model a standing column well system. The system performance for a typical case, to be used as the base case in a parametric study in Chapter 5, is calculated. The configuration of this standing column well is set according to an existing standing column well at Pennsylvania State University (Mikler 1993). One year of hourly building loads from a prototype building have been used to provide thermal boundary conditions for the SCW model. Simulations have been made using a whole year of load data. This allows the highly transient nature of the SCW system to be examined.

4.3.1. Building loads

All the simulations are made using building loads calculated for a building (the Meridian Technology Center Incubator) located in Stillwater, OK with a Boston, MA, weather file (Figure 4-21). The building loads are determined using building energy simulation software (BLAST 1986). The total area of the building is approximately 1,320 m^2 (14,205 ft^2). This building has previously been used in other energy studies (Yavuzturk 1999), and several assumptions have been made to determine the annual building loads:

1) The building is divided into eight different thermal zones.
2) For each zone, a single zone draw through fan system is specified. The total coil loads obtained from system simulation are equal to the loads to be met with ground source heat pump system.
3) Assume one person with a 70% radiant heat gain of 131.9 W (450 Btu/hr).
4) A 11.8 W/m^2 (1.10 W/ft^2) of equipment plug load is used.
5) The lighting loads vary between 10.04 W/m^2 (0.93 W/ft^2) and 15.88 W/m^2 (1.48 W/ft^2) in the different zones.
6) Schedules for people occupancy, lighting, equipment are specified.

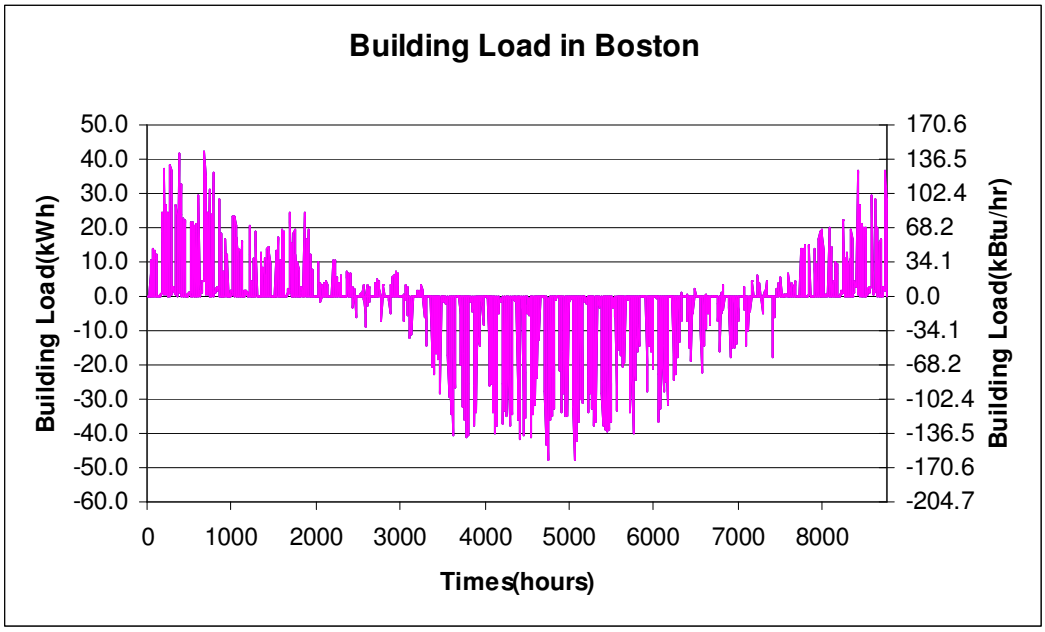

Figure 4-21 Building load of a building in Boston (Positive loads are heating load)

Compared to loads for the same building with Houston, TX, and Tulsa, OK, weather data (Yavuzturk 1999), the heating and cooling loads for this building are reasonably balanced – see Figure 4-21. The maximum exiting water temperature (back to the heat pump) occurs during the day of the peak cooling-load (July 15). The minimum temperature back to heat pump occurs during January 15, but does not coincide with the day of peak heating load (January 28). This is caused by the distribution of building load. High heating loads for several days leading up to January 15 caused a successive reduction in the borehole temperature. In contrast, the loads are relatively small immediately before the peak building heating load on January 28.

4.3.2. Base case SCW design

The design data for the base case well design comes mostly from the well used by Mikler (1993). The geometric arrangement of the well is shown in Figure 4-22. This well has a

dip tube extending to very near the bottom of the well, and discharge from the heat pump system is near the top. The ground conditions are assumed to be similar to that in the Northeastern U.S. The ground surface temperature used was 11.1 °C (52 °F), and the natural geothermal gradient is 0.6 °C/100m (0.34 °F/100 ft). The base case thermal and hydraulic properties are taken from the mean values for Karst limestone (Chiasson et al. 2000). Hydraulic and thermal properties in the base case are listed in Table 4-1 in section 4.2. Some properties of the borehole are given in Table 4-2 in section 4.2. too.

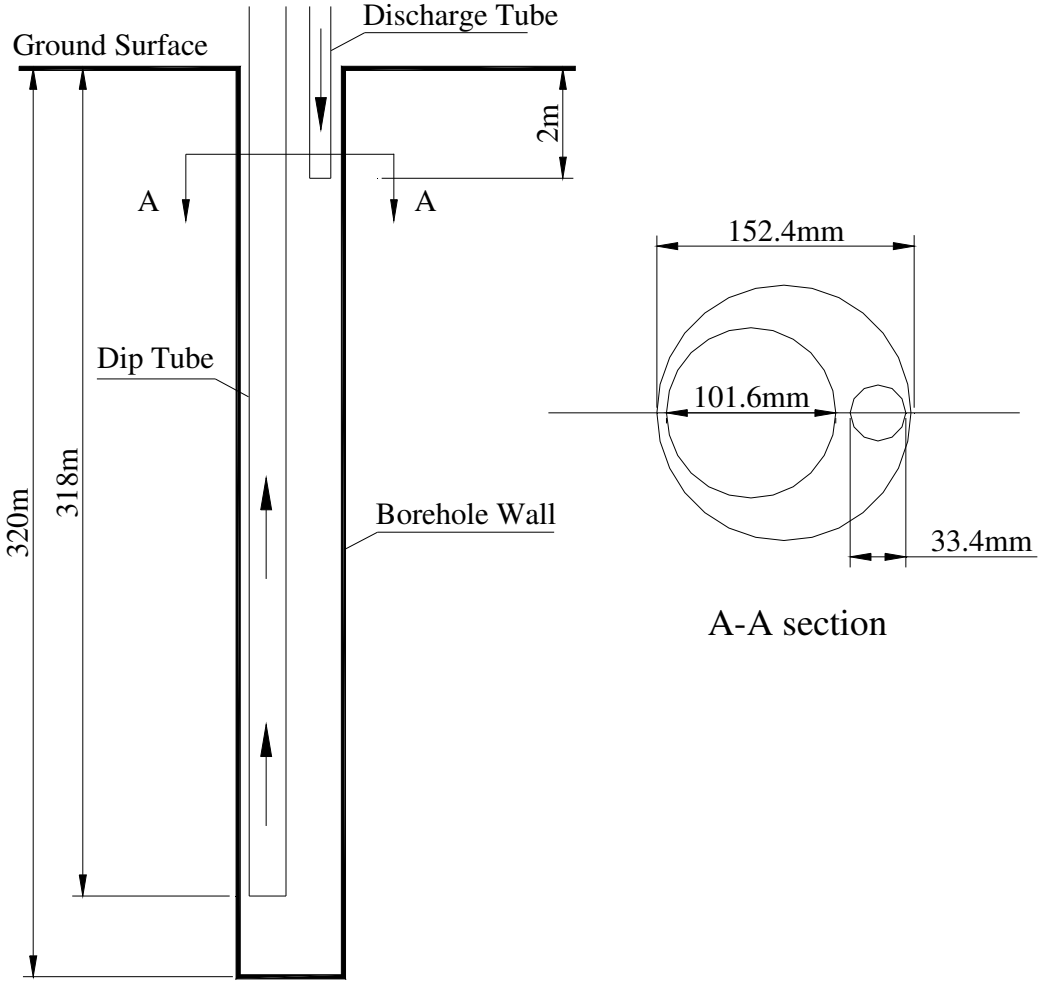

Figure 4-22 A schematic drawing showing the borehole geometric arrangement for the base case

4.3.3. Results for base case

Figures 4-23 and 4-24 show simulation results of borehole operations of the base case. Figure 4-23 shows borehole temperatures over the depth of the borehole on January 28, when the peak heating load occurs. Figure 4-24 shows borehole temperatures over the depth of the borehole on July 15, when peak cooling load occurs. The temperature in the dip tube (suction temperature) variation along the borehole can be seen to be non-linear. This variation in temperature is due to heat transfer between the water in the dip (suction) pipe and the surrounding water in the borehole. This heat transfer is generally detrimental to SCW efficiency.

Figure 4-25 shows the suction and discharge temperature over the whole year of operation, along with the building loads. The difference between suction and discharge temperatures coincide with the building loads shown in the lower part of Figure 4-25. Notice that the water temperatures at the end of the year are very similar to those at the start of the year. This is due to the relatively balanced nature of the building load.

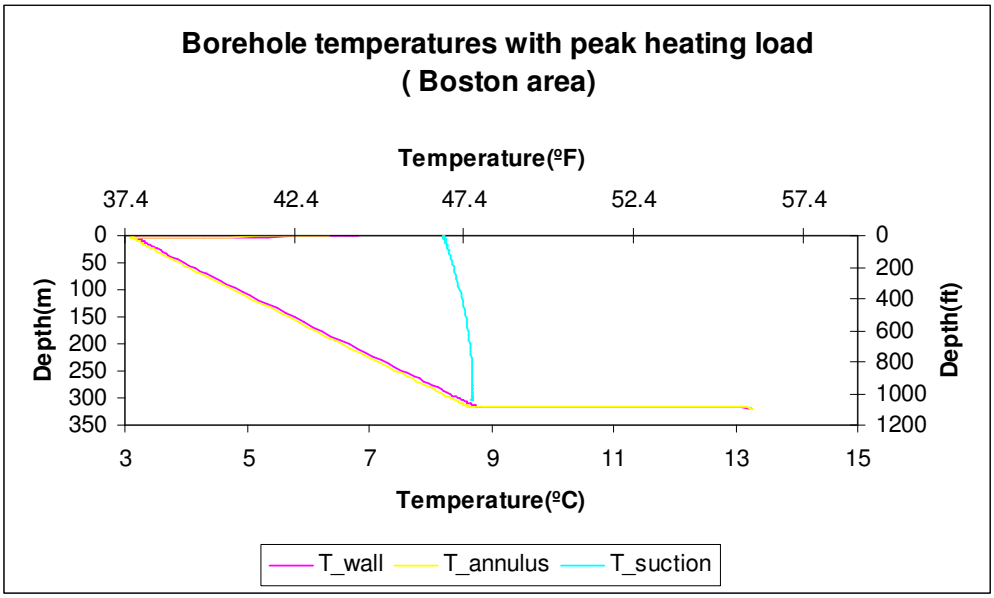

Figure 4-23 Borehole temperatures when peak heating load occurs

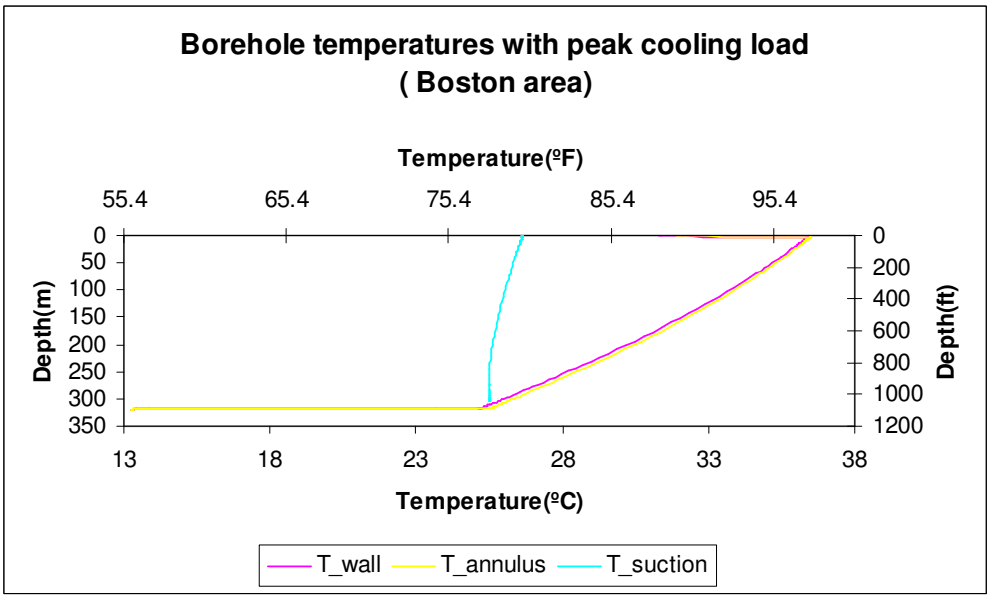

Figure 4-24 Borehole temperatures when peak cooling load occurs

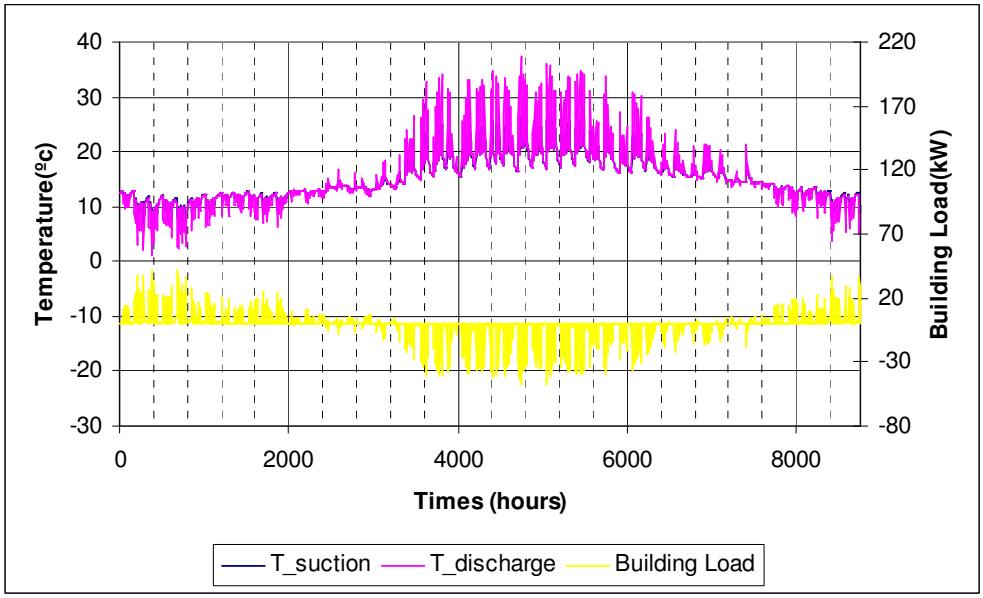

Figure 4-25 Borehole suction and discharge temperatures and building loads for the base case

Figure 4-26 shows the dynamic head distribution after one year of normal operation for the base case. The axis of the borehole is at the left-hand edge of this figure. In this figure the neutral point is indicated by the zero head contour intersecting with the borehole wall approximately halfway down its length. Above this point there is flow from the borehole into the rock, and below this point the flow is into the borehole from the rock.

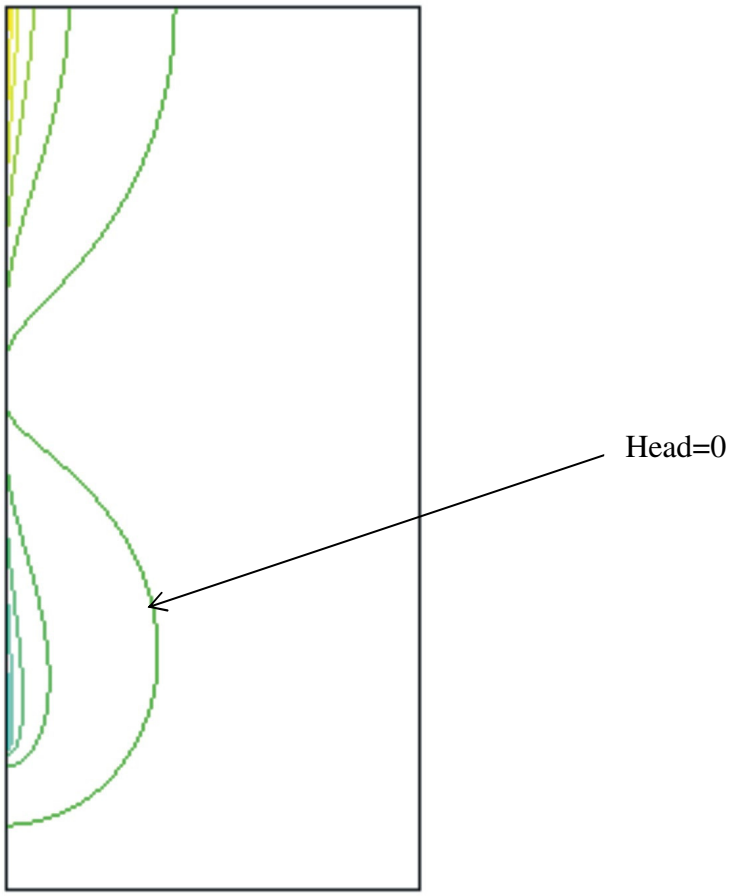

Figure 4-26 Head contours for the base case (after one year of operation)

5. PARAMETRIC STUDY

A parametric study was planned to determine the effect of key parameters on the performance of SCW systems. Currently, one-year hourly building loads have been used to provide thermal boundary conditions for the numerical models. This allows the highly transient nature of SCW systems to be examined, especially during the "bleed on" times.

5.1. Organization of parametric study

The parametric study has been organized using a base case and calculating the system performance (e.g., water temperature back to the heat pump) for this and other cases where a single parameter is varied from its corresponding value in a "base case". Variations in the following parameters have been studied:

- rock thermal conductivity
- rock specific heat capacity
- ground temperature gradient
- borehole surface roughness
- borehole diameter
- borehole casing depth
- dip tube diameter and conductivity
- system bleed
- borehole depth

- rock hydraulic conductivity
- different bleed strategy
- pipe configuration

In addition to the calculations of well performance with constant rates of bleed, additional calculations were made using two strategies for controlling bleed operation:

1. Deadband control: In winter, when the water temperature back to the heat pump is lower than 5.83 ºC (42.5 ºF), bleed is started. When the water temperature back to the heat pump is higher than 8.6 ºC (47.5 ºF), bleed is stopped. In summer, bleed is started when water temperature back to the heat pump is higher than 29.2 ºC (84.5 ºF), and stopped when water temperature back to the heat pump is lower than 26.4 ºC (79.5 ºF)[+].
2. Temperature-difference control: The temperature difference (ΔT) between water back to and from HP was used as a controlled parameter. The temperature difference (ΔT) was set to give the same number of hours of operation as the deadband bleed control case: 4.6 ºC (8.3 ºF).

In both cases the rate of bleed was 10%.

5.2. Methodology of parametric study

As shown in Table 5-1 in Section 5.3, there are currently 36 cases to be studied. The procedure for the parametric study includes:

[+] Personal communication with Mr. Carl D. Orio in Water and Energy System Corporation.

- Write suitable input files (Wshx.in, SCW.in, Wshx.grd) for each case.
- Adjust and find the appropriate under-relaxation factor for each case by trial and error. This factor is used to under-relax the borehole wall temperatures passed to the borehole model.
- Run the program.
- Post-processing the data.

5.3. Parameter values

The parameter values for the different cases in addition to the base case are shown in Table 5-1.

Table 5-1 Parametric study parameter values

(Values changed from the base case are shaded)

Parameter		Thermal conductivity of rock	Natural geothermal gradient of rock	Specific heat capacity of rock	Hydraulic conductivity of rock	Surface roughness	Borehole diameter	Casing depth	Dip tube diameter	Borehole length	Bleed rate	Porosity	Thermal conductivity of dip tube
No.	Case	W/m-K (Btu/hr-ft-ºF)	ºC/100m (ºF/100m)	J/m^3-K (Btu/ft^3-ºF)	m/s (gal/day/ft^2)	m (in)	m (in)	m (in)	m (in)	m (ft)	(%)	(-)	W/m-K (Btu/hr-ft-ºF)
1	**Base**	3 (1.73)	0.6 (0.329)	2.70E+06 (40.27)	7.00E-05 (148.23)	1.50E-03 (0.06)	0.1524 (6)	0 (0)	0.1016 (4)	320 (1050)	0	0.275	0.1 (0.0577)
2	**kt2**	2.5 (1.44)	0.6 (0.329)	2.70E+06 (40.27)	7.00E-05 (148.23)	1.50E-03 (0.06)	0.1524 (6)	0 (0)	0.1016 (4)	320 (1050)	0	0.275	0.1 (0.0577)
3	**kt3**	4.3 (2.48)	0.6 (0.329)	2.70E+06 (40.27)	7.00E-05 (148.23)	1.50E-03 (0.06)	0.1524 (6)	0 (0)	0.1016 (4)	320 (1050)	0	0.275	0.1 (0.0577)
4	**s2**	3 (1.73)	0.6 (0.329)	2.13E+06 (31.77)	7.00E-05 (148.23)	1.50E-03 (0.06)	0.1524 (6)	0 (0)	0.1016 (4)	320 (1050)	0	0.275	0.1 (0.0577)
5	**s3**	3 (1.73)	0.6 (0.329)	7.40E+06 (82.03)	7.00E-05 (148.23)	1.50E-03 (0.06)	0.1524 (6)	0 (0)	0.1016 (4)	320 (1050)	0	0.275	0.1 (0.0577)
6	**n2**	3 (1.73)	0.3 (0.17)	2.70E+06 (40.27)	7.00E-05 (148.23)	1.50E-03 (0.06)	0.1524 (6)	0 (0)	0.1016 (4)	320 (1050)	0	0.275	0.1 (0.0577)
7	**n3**	3 (1.73)	1.8 (0.99)	2.70E+06 (40.27)	7.00E-05 (148.23)	1.50E-03 (0.06)	0.1524 (6)	0 (0)	0.1016 (4)	320 (1050)	0	0.275	0.1 (0.0577)
8	**kh2**	3 (1.73)	0.6 (0.329)	2.70E+06 (40.27)	1.00E-04 (211. 8)	1.50E-03 (0.06)	0.1524 (6)	0 (0)	0.1016 (4)	320 (1050)	0	0.275	0.1 (0.0577)
9	**kh3**	3 (1.73)	0.6 (0.329)	2.70E+06 (40.27)	1.00E-06 (2.118)	1.50E-03 (0.06)	0.1524 (6)	0 (0)	0.1016 (4)	320 (1050)	0	0.275	0.1 (0.0577)
10	**h2**	3 (1.73)	0.6 (0.329)	2.70E+06 (40.27)	7.00E-05 (148.23)	3.00E-04 (0.01)	0.1524 (6)	0 (0)	0.1016 (4)	320 (1050)	0	0.275	0.1 (0.0577)
11	**h3**	3 (1.73)	0.6 (0.329)	2.70E+06 (40.27)	7.00E-05 (148.23)	9.00E-03 (0.35)	0.1524 (6)	0 (0)	0.1016 (4)	320 (1050)	0	0.275	0.1 (0.0577)
12	**h4**	3 (1.73)	0.6 (0.329)	2.70E+06 (40.27)	7.00E-05 (148.23)	3.00E-03 (0.12)	0.1524 (6)	0 (0)	0.1016 (4)	320 (1050)	0	0.275	0.1 (0.0577)

Table 5-1 (continued)

Parametric study parameter values (values changed from the base case are highlighted with shading)

Parameter		Thermal conductivity of rock	Natural geothermal gradient of rock	Specific heat capacity of rock	Hydraulic conductivity of rock	Surface roughness	Borehole diameter	Casing depth	Dip tube diameter	Borehole length	Bleed rate	Porosity	Thermal conductivity of dip tube
No.	Case	W/m-K (Btu/hr-ft-ºF)	ºC/100m (ºF/100m)	J/m^3-K (Btu/ft^3-ºF)	m/s (gal/day/ft^2)	m (in)	m (in)	m (in)	m (in)	m (ft)	(%)	(_)	W/m-K (Btu/hr-ft-ºF)
13	**d2**	3 (1.73)	0.6 (0.329)	2.70E+06 (40.27)	7.00E-05 (148.23)	1.50E-03 (0.06)	0.1398 (5.5)	0 (0)	0.1016 (4)	320 (1050)	0	0.275	0.1 (0.0577)
14	**d3**	3 (1.73)	0.6 (0.329)	2.70E+06 (40.27)	7.00E-05 (148.23)	1.50E-03 (0.06)	0.1778 (7)	0 (0)	0.1016 (4)	320 (1050)	0	0.275	0.1 (0.0577)
15	**d4**	3 (1.73)	0.6 (0.329)	2.70E+06 (40.27)	7.00E-05 (148.23)	1.50E-03 (0.06)	0.1524 (6)	0 (0)	0.0762 (3)	320 (1050)	0	0.275	0.1 (0.0577)
16	**d5**	3 (1.73)	0.6 (0.329)	2.70E+06 (40.27)	7.00E-05 (148.23)	1.50E-03 (0.06)	0.1524 (6)	0 (0)	0.1143 (4.5)	320 (1050)	0	0.275	0.1 (0.0577)
17	**d6**	3 (1.73)	0.6 (0.329)	2.70E+06 (40.27)	7.00E-05 (148.23)	1.50E-03 (0.06)	0.1524 (6)	0 (0)	0.1016 (4)	320 (1050)	0	0.275	0.4 (0.2308)
18	**c2**	3 (1.73)	0.6 (0.329)	2.70E+06 (40.27)	7.00E-05 (148.23)	1.50E-03 (0.06)	0.1524 (6)	160 (525)	0.1016 (4)	320 (1050)	0	0.275	0.1 (0.0577)
19	**c3**	3 (1.73)	0.6 (0.329)	2.70E+06 (40.27)	7.00E-05 (148.23)	1.50E-03 (0.06)	0.1524 (6)	90 (295)	0.1016 (4)	320 (1050)	0	0.275	0.1 (0.0577)
20	**c4**	3 (1.73)	0.6 (0.329)	2.70E+06 (40.27)	7.00E-05 (148.23)	1.50E-03 (0.06)	0.1524 (6)	60 (197)	0.1016 (4)	320 (1050)	0	0.275	0.1 (0.0577)
21	**b1**	3 (1.73)	0.6 (0.329)	2.70E+06 (40.27)	7.00E-05 (148.23)	1.50E-03 (0.06)	0.1524 (6)	0 (0)	0.1016 (4)	320 (1050)	10	0.275	0.1 (0.0577)
22	**b2**	3 (1.73)	0.6 (0.329)	2.70E+06 (40.27)	7.00E-05 (148.23)	1.50E-03 (0.06)	0.1524 (6)	0 (0)	0.1016 (4)	320 (1050)	15	0.275	0.1 (0.0577)
23	**b3**	3 (1.73)	0.6 (0.329)	2.70E+06 (40.27)	7.00E-05 (148.23)	1.50E-03 (0.06)	0.1524 (6)	0 (0)	0.1016 (4)	320 (1050)	20	0.275	0.1 (0.0577)
24	**b4**	3 (1.73)	0.6 (0.329)	2.70E+06 (40.27)	7.00E-05 (148.23)	1.50E-03 (0.06)	0.1524 (6)	0 (0)	0.1016 (4)	320 (1050)	2.5	0.275	0.1 (0.0577)
25	**b5**	3 (1.73)	0.6 (0.329)	2.70E+06 (40.27)	7.00E-05 (148.23)	1.50E-03 (0.06)	0.1524 (6)	0 (0)	0.1016 (4)	320 (1050)	5	0.275	0.1 (0.0577)

Table 5-1 (continued)

Parametric study parameter values (values changed from the base case are highlighted with shading)

Parameter		Thermal conductivity of rock	Natural geothermal gradients of rock	Specific heat capacity of rock	Hydraulic conductivity of rock	Surface roughness	Borehole diameter	Casing depth	Dip tube diameter	Borehole length	Bleed rate	Porosity	Thermal conductivity of dip tube
No.	Case	W/m-K (Btu/hr-ft-ºF)	ºC/100m (ºF/100m)	J/m^3-K (Btu/ft^3-ºF)	m/s (gal/day/ft^2)	m (in)	m (in)	m (in)	m (in)	m (ft)	(%)	(_)	W/m-K (Btu/hr-ft-ºF)
26	**L1**	3 (1.73)	0.6 (0.329)	2.70E+06 (40.27)	7.00E-05 (148.23)	1.50E-03 (0.06)	0.1524 (6)	0 (0)	0.1016 (4)	240 (787)	0	0.275	0.1 (0.0577)
27	**L2**	3 (1.73)	0.6 (0.329)	2.70E+06 (40.27)	7.00E-05 (148.23)	1.50E-03 (0.06)	0.1524 (6)	0 (0)	0.1016 (4)	280 (919)	0	0.275	0.1 (0.0577)
28	**L3**	3 (1.73)	0.6 (0.329)	2.70E+06 (40.27)	7.00E-05 (148.23)	1.50E-03 (0.06)	0.1524 (6)	0 (0)	0.1016 (4)	360 (1181)	0	0.275	0.1 (0.0577)
29	**L4**	3 (1.73)	0.6 (0.329)	2.70E+06 (40.27)	7.00E-05 (148.23)	1.50E-03 (0.06)	0.1524 (6)	0 (0)	0.1016 (4)	400 (1312)	0	0.275	0.1 (0.0577)
30	**kt4**	1.5 (0.865)	0.6 (0.329)	2.13E+06 (31.77)	5.00E-07 (1.059)	1.50E-03 (0.06)	0.1524 (6)	0 (0)	0.1016 (4)	320 (1050)	0	0.1	0.1 (0.0577)
31	**kt5**	5 (2.88)	0.6 (0.329)	2.20E+06 (32.81)	1.50E-06 (3.176)	1.50E-03 (0.06)	0.1524 (6)	0 (0)	0.1016 (4)	320 (1050)	0	0.05	0.1 (0.0577)
32	**kh4**	4 (2.30)	0.6 (0.329)	2.70E+06 (40.27)	7.00E-10 (0.00148)	1.50E-03 (0.06)	0.1524 (6)	0 (0)	0.1016 (4)	320 (1050)	0	0.18	0.1 (0.0577)
33	**L1_bt1**	3 (1.73)	0.6 (0.329)	2.70E+06 (40.27)	7.00E-05 (148.23)	1.50E-03 (0.06)	0.1524 (6)	0 (0)	0.1016 (4)	240 (787)	10	0.275	0.1 (0.0577)
34	**L1_bt3**	3 (1.73)	0.6 (0.329)	2.70E+06 (40.27)	7.00E-05 (148.23)	1.50E-03 (0.06)	0.1524 (6)	0 (0)	0.1016 (4)	240 (787)	5	0.275	0.1 (0.0577)
35	**L1_bt1-t**	3 (1.73)	0.6 (0.329)	2.70E+06 (40.27)	7.00E-05 (148.23)	1.50E-03 (0.06)	0.1524 (6)	0 (0)	0.1016 (4)	240 (787)	10	0.275	0.1 (0.0577)
36	**reverse**	3 (1.73)	0.6 (0.329)	2.70E+06 (40.27)	7.00E-05 (148.23)	1.50E-03 (0.06)	0.1524 (6)	0 (0)	0.1016 (4)	320 (1050)	0	0.275	0.1 (0.0577)

Note: Karst limestone was assumed as the rock type for all cases except case kt4 (dolomite), case kt5 (fractured ingenious and metamorphic), and case kh4 (sandstone).

5.4. System energy calculations

For each case in the parametric study, the annual energy consumption of the heat pump and well pump has been calculated. Fluid temperatures and well pump operating hours are output from the annual system simulations. To calculate the energy consumption, the pump head, hourly water pump power consumption, and hourly heat pump power consumption also have to be calculated. This procedure is described below.

5.4.1. System pressure drop without bleed

A schematic of the pipe work system applicable to cases without bleed is shown in Figure 5-1.

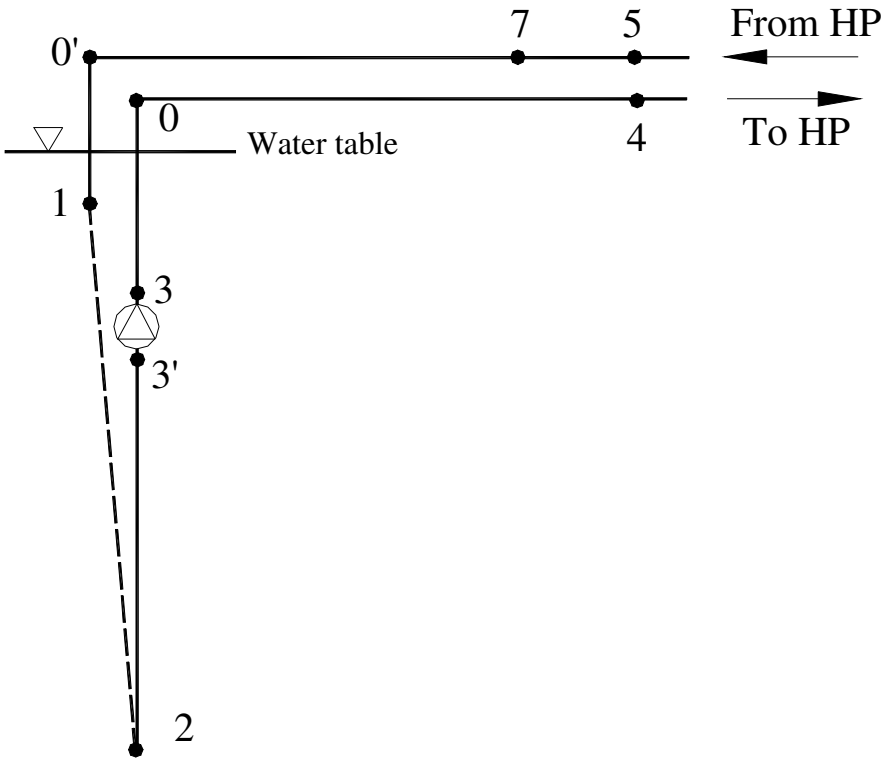

Figure 5-1 Pipe system schematic for cases without bleed

We assume that p_w is the atmosphere pressure at the water table, and the elevation here is z_w. The mechanical energy equation can be applied to a number of points in the system and used to find the pump head.

Between the water table section and node 1 (neglecting the frictional losses):

$$p_w + \rho g z_w = p_1 + \frac{\rho v_1^2}{2} + \rho g z_1 \tag{5.1}$$

Rearranging gives:

$$p_1 = p_w - \rho g z_w - \frac{\rho v_1^2}{2} - \rho g z_1 \tag{5.1a}$$

Between the water table section and node 2:

$$p_w + \rho g z_w = p_2 + \frac{\rho v_2^2}{2} + \rho g z_2 + \Delta p_{1-2loss} \tag{5.2}$$

Rearranging gives:

$$p_2 = p_w - \rho g z_w - \frac{\rho v_2^2}{2} - \rho g z_2 - \Delta p_{1-2loss} \tag{5.2a}$$

Between the water table section and node 3':

$$p_w + \rho g z_w = p_{3'} + \frac{\rho v_{3'}^2}{2} + \rho g z_{3'} + \Delta p_{2-3'loss} \tag{5.3}$$

Rearranging gives:

$$p_{3'} = p_w + \rho g z_w - \frac{\rho v_{3'}^2}{2} - \rho g z_3' - \Delta p_{2-3'loss} \tag{5.3a}$$

Between node 3 and node 1:

$$p_3 + \frac{\rho v_3^2}{2} + \rho g z_3 = p_1 + \frac{\rho v_1^2}{2} + \rho g z_1 + \Delta p_{3-4-5-1loss} \tag{5.4}$$

Now substituting $p_w = p_1 + \frac{\rho v_1^2}{2} + \rho g z_1 - \rho g z_w$ into Equation (5.4):

$$p_3 = p_w + \rho g z_w - \frac{\rho v_3^2}{2} - \rho g z_3 + \Delta p_{3-4-5-1loss} \tag{5.4a}$$

Assuming $z_3 = z_3^{'}$ and $v_3 = v_3^{'}$, the total dynamic head for the pump is

$$H = p_3 - p_3^{'} = \Delta p_{3-4-5-1loss} + \Delta p_{2-3^{'}loss} \tag{5.5}$$

5.4.2. System pressure drop with bleed

A schematic of the pipe work system applicable to cases with bleed is shown in Figure 5-2.

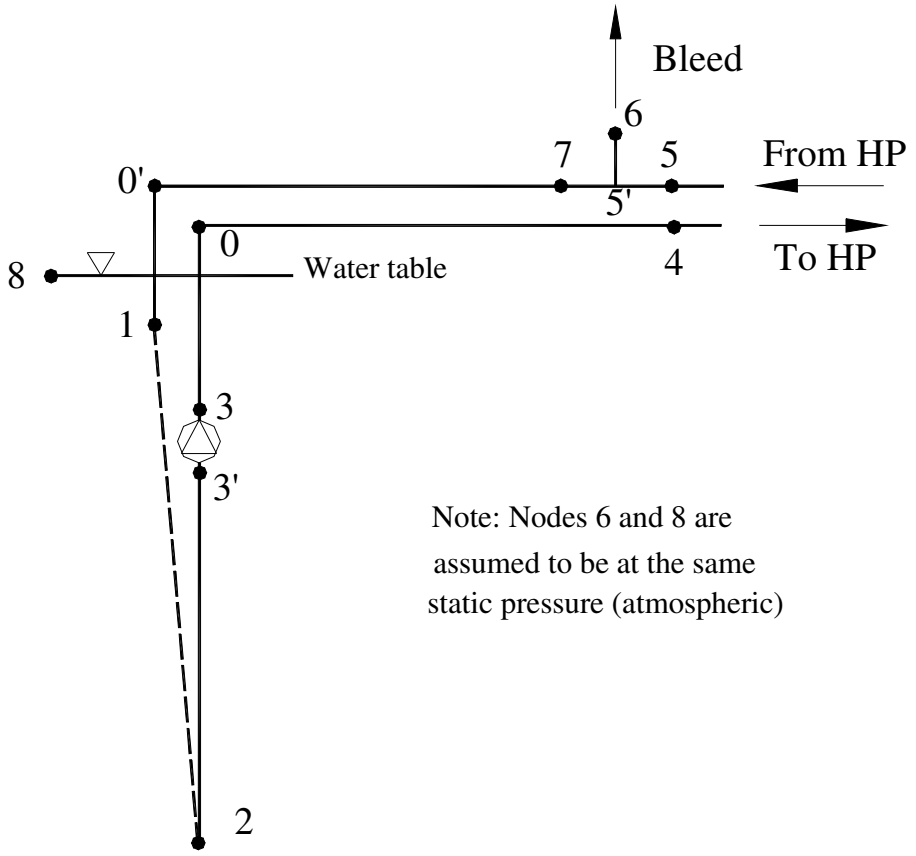

Figure 5-2 Pipe system schematic for cases with bleed

Bernoulli's equation can be applied to a number of points in the system and used to find the pump head.

Between the water table section and node 3':

$$p_w + \rho g z_w = p_{3'} + \frac{\rho v_{3'}^2}{2} + \rho g z_{3'} + \Delta p_{w-3'loss} \tag{5.6}$$

Between node 3 and node 5':

$$p_3 + \frac{\rho v_3^2}{2} + \rho g z_3 = p_{5'} + \frac{\rho v_{5'}^2}{2} + \rho g z_{5'} + \Delta p_{3-5'loss} \tag{5.7}$$

Applying energy conservation, yields:

$$\begin{aligned} m \cdot (p_{5'} + \frac{\rho v_{5'}^2}{2} + \rho g z_{5'}) = m \cdot (1-r).(p_w + \rho g z_w + \Delta p_{5'-wloss}) \\ + m \cdot r \cdot (p_6 + \rho g z_6 + \Delta p_{5'-6loss}) \end{aligned} \tag{5.8}$$

Where m is the mass flow rate and r is the fractional (normalized) rate of bleed.

The pressure loss from nodes 5' to 6 is equal to the pressure loss from node 5' to the water table. Applying a mass balance at node 5' and a pressure balance enables the loss from 5'to 6 to be calculated for a given flow rate and return pipe size.

We assume that p_w is the atmosphere pressure at the water table, and the elevation here is z_w and is used as the datum elevation ($z_w = 0$). The aboveground pipework is assumed to be at the same elevation, z_{ground}. If the water level is used as a datum ($z_w = 0$), then $z_6 = z_{ground} = h_{watertable}$. Assuming $p_6 = p_w$, $z_{5'} = z_3 = z_{3'}$ and $v_{5'} = v_3 = v_{3'}$, the total dynamic head for the pump can be shown to be,

$$H = p_3 - p_3^{'} = \Delta p_{5'-6loss} + bleedrate \cdot \rho g h_{watertable} + \Delta p_{8-5'loss} \tag{5.9}$$

In Equations (5.1) to (5.9),

p is the static pressure (Pa);

$\frac{\rho v^2}{2}$ is the velocity pressure (Pa);

ρgz is the elevation pressure (Pa);

Δp is the total pressure loss (fitting +friction) (Pa);

H is the total dynamic head for the water pump (Pa);

r is the bleed fraction in the system (-);

m is the mass flow rate of the water pump (kg/s).

5.4.3. Heat pump model

To match the peak building loads of the hypothetical building, two Climate Master HL Horizontal 072 heat pumps (water to air) were selected. Curve fits describing capacity vs. entering water temperature and power consumption vs. entering water temperature, at a range of flow-rates, were derived from the catalogue data. The following functions were used:

$HP\_capacity = 22410.37 + 1122.66 * EWT - 3.0345 * EWT^2$ (Heating mode)

$HP\_capacity = 97442.70 - 332.76 * EWT - 0.1491 * EWT^2$ (Cooling mode)

$HP\_power = 6130.83 - 16.30 * EWT + 0.3305 * EWT^2$ (Heating mode)

$HP\_power = 3198.09 + 39.03 * EWT + 0.0247 * EWT^2$ (Cooling mode)

It was assumed that the heat pump performance only changed with entering water temperatures.

5.4.4. Circulating pump model

To calculate the pump power consumption, a pump with sufficient capacity to match the system flow and pressure drop was selected. A Munro 4in. submersible well pump (18GPM series) was chosen. This pump is capable of meeting the flow and head requirements in bleed and non-bleed modes of operation.

Assuming constant pump efficiency, the following equation can be used to calculate the power consumption of the circulating water pump:

$$w = \frac{\gamma Q H}{\eta} \tag{5.10}$$

Where: $\gamma = \rho g$

ρ is the water density (kg/m^3);

Q is the volume flow rate (m^3/s);

H is the total dynamic head (m);

η is the efficiency of the circulating water pump;

taken as 0.65 during this calculation (Rafferty ,1998);

w is the power consumption of the circulating water pump (W).

5.4.5. Frictional Pressure Losses

Frictional pressure losses are calculated for each section of the pipe work. Losses for straight pipe are calculated from the Moody friction factor, and fitting losses are estimated from standard loss coefficients. To calculate the total pressure loss:

$$\Delta p_m = \sum (f \frac{L}{D} + K) \frac{V^2}{2g} \tag{5.11}$$

Where Δp_m is the total pressure loss (fitting +friction) (m [ft]);

f is the Moody friction factor;

L is the length of the given pipe section(m [ft]);

D is the diameter of the given pipe (m [ft]);

K is the resistance coefficient;

V is the mean velocity in the given pipe(m/s [ft/s]);

g is the acceleration due to the gravity (m/s^2 [ft/s^2]).

For the Moody friction factor, the following correlations are used during the calculation (Techo et al. 1965, Colebrook 1939, Chen 1979).

$$\frac{1}{\sqrt{f}} = 1.7372 \ln \frac{\mathrm{Re}}{1.964 \ln \mathrm{Re} - 3.8215} \quad \text{for smooth surfaces, } 10^4 \le \mathrm{Re} < 10^7 \quad (5.12)$$

$$\frac{1}{\sqrt{f}} = 1.5635 \ln(\frac{\mathrm{Re}}{7}) \quad \text{for smooth surfaces, } \mathrm{Re} < 10^4 \quad (5.13)$$

$$\frac{1}{\sqrt{f}} = 3.48 - 1.7372 \ln[\frac{\varepsilon}{a} - \frac{16.2426}{\mathrm{Re}} \ln A_2] \quad \text{for rough surfaces, apply to all values of Re and } \frac{\varepsilon}{a} \quad (5.14)$$

Where f is the Fanning friction factor;

Re is the Reynolds number, $\mathrm{Re} = \frac{D_h V}{\nu}$;

D_h is the hydraulic diameter (m [ft]);

V is the fluid velocity (m/s [ft/sec]);

ν is the kinematic fluid viscosity (m^2/s [ft^2/sec]);

ε is the height of surface roughness (m [ft]);

$$A_2 = \frac{(\varepsilon / a)^{1.1098}}{6.0983} + (\frac{7.149}{\mathrm{Re}})^{0.8981};$$

a is the radius of pipe (m [ft]).

Piping fittings are shown in Figure 5-3. Resistance coefficients are taken from available tables (ASHRAE Handbook, Fundamental, 2001).

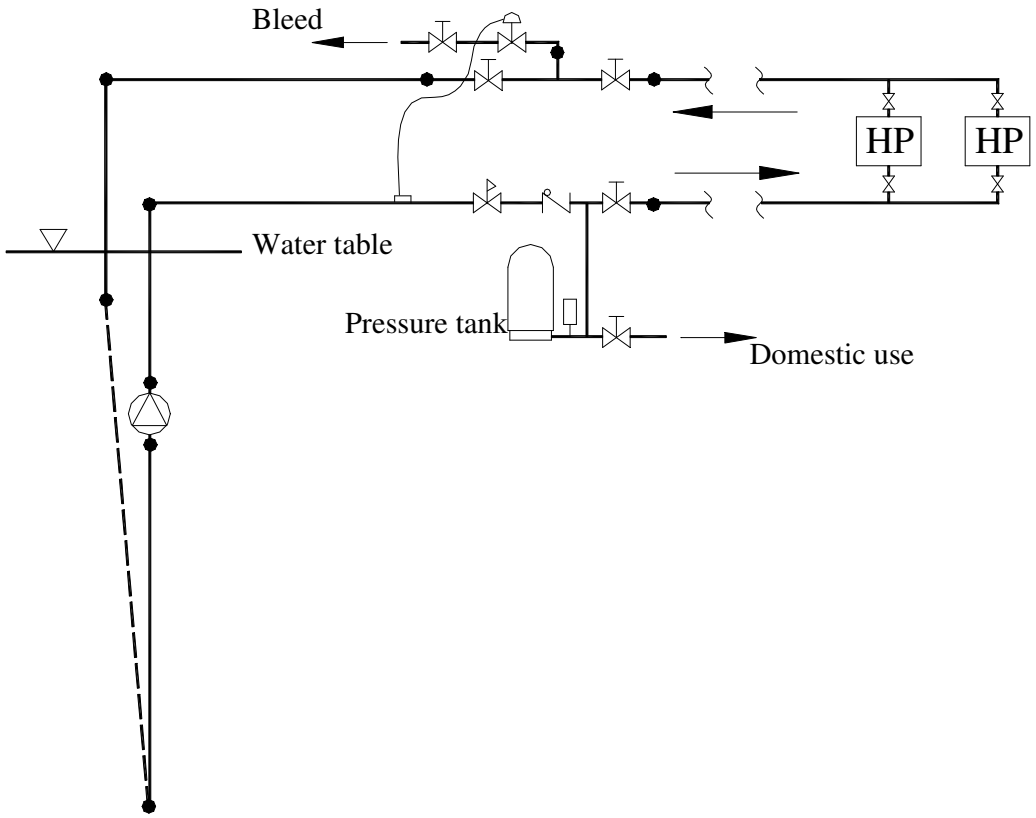

Figure 5-3 Schematic diagram of the pipe work showing the arrangement of fittings

5.4.6. Electricity costs

The cost of energy consumed by the well pump and heat pump has been calculated using the monthly schedule in Table 5-2 (commercial rate), which was applicable to the state of Massachusetts in the year 2000.

Table 5-2 Electric utility monthly average cost per kilowatt-hour for Massachusetts (cents per kilowatt-hour)*

Building Type	Jan.	Feb.	March	April	May	June	July	Aug.	Sep.	Oct.	Nov.	Dec.
Residential	10.2	9.7	10.2	11.0	11.1	11.3	11.0	10.8	11.5	11.2	11.1	11.0
Commercial	7.8	7.5	7.8	8.5	8.7	9.8	10.2	10.1	10.7	9.5	8.6	8.7

*data from http://www.eia.doe.gov/cneaf/electricity/page/at_a_glance/sales_tabs.html

5.5. Parametric study results

The parametric study results have been processed to find the maximum and minimum exiting water temperatures from the standing column well. This data is given in Table 5-3. These temperatures have also been plotted against each parameter and are discussed in the sections that follow.

In an attempt to correlate changes in parameter values with effective changes in design borehole length, a number of simulations were made using the base case but with different borehole lengths. The results of these calculations are shown in Figure 5-4 in terms of the corresponding minimum and maximum exiting temperatures. These data have been used to find linear relationships between minimum and maximum temperatures and borehole length. We can then estimate (assuming this relationship to be

linear in all cases) the effect that each parameter variation has in terms of the design well depth. This data is presented in the right-hand column of Table 5-3.

The method used to calculate and apply the relationship between temperatures and equivalent borehole length is described as follows. The linear correlation between the exiting water temperatures and length are assumed to have the form:

$$EWT_{\max} = C_1 + C_2 \cdot L \tag{5.15}$$

$$EWT_{\min} = C_3 + C_4 \cdot L \tag{5.16}$$

The constants found from the data shown in Figure 7-4 have the values:

$C_1 = 46.67$, $C_2 = -0.0604$; $C_3 = -5.78$, $C_4 = 0.00372$

The design conditions are:

Summer: $EWT_{max} = 32°C$,

Winter: $EWT_{min} = 6°C$.

$L_{design} = 317m$

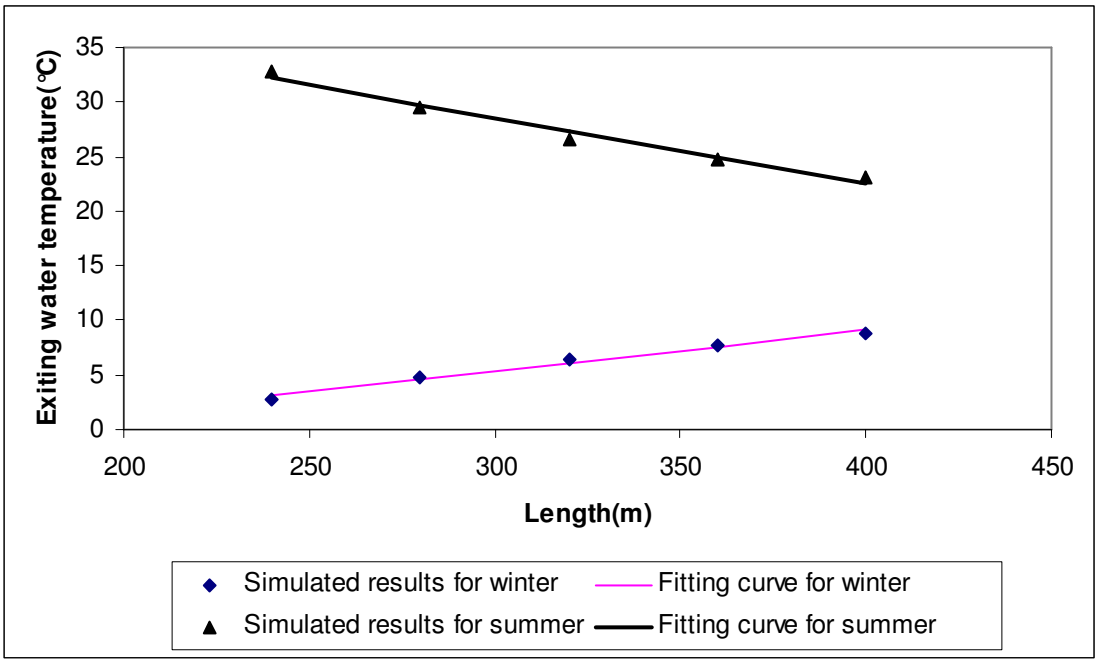

Figure 5-4 Relationship between EWT and length of borehole

For other cases, the slopes of all the curves are assumed to be the same with the base case, so that:

$$EWT_{\max,i} = C_{1,i} + C_2 \cdot L \tag{5.17}$$

$$EWT_{\min,i} = C_{3,i} + C_4 \cdot L \tag{5.18}$$

The constants $C_{1,i}, C_{3,i}$ for each case are obtained from the maximum/minimum EWT difference between the given case and the base case. Equations (5.17) and (5.18) can then be used to find the equivalent length.

Table 5-3 Parametric study results – effect of parameter variations on minimum and maximum exiting water temperatures and design length

Parameter Varied	Case Name	Parameter Values (Units)	Maximum Temperature Back to HP ºC (ºF)	Minimum Temperature Back to HP ºC (ºF)	Equivalent Design Length m (ft)
Thermal conductivity		**W/m-K (Btu/hr-ft-ºF)**			
	kt2	2.5 (1.44)	27.92 (82.26)	5.70 (42.26)	331 (1086)
	Base	3.0 (1.73)	26.62 (79.92)	6.44 (43.58)	317 (1040)
	kt3	4.3 (2.48)	23.48 (74.27)	7.75 (45.95)	281 (922)
Natural geothermal gradients		**ºC/100m (ºF/100ft)**			
	n2	0.3 (0.17)	26.60 (79.89)	6.42 (43.55)	317 (1040)
	Base	0.6 (0.329)	26.62 (79.92)	6.44 (43.58)	317 (1040)
	n3	1.8 (0.99)	29.97 (85.94)	9.58 (49.25)	298 (978)
Specific heat capacity		**J/m^3-K(Btu/ft^3-ºF)**			
	s2	2.13E+06 (31.769)	27.03 (80.65)	6.24 (43.23)	322 (1056)
	Base	2.70E+06 (40.27)	26.62 (79.92)	6.44 (43.58)	317 (1040)
	s3	5.50E+06 (82.03)	25.34 (77.62)	7.15 (44.88)	297 (974)
Borehole diameter		**m (in)**			
	d2	0.1398 (5.5)	26.20 (79.16)	6.31 (43.36)	320 (1050)
	Base	0.1524 (6)	26.62 (79.92)	6.44 (43.58)	317 (1040)
	d3	0.1778 (7)	26.20 (79.16)	7.75 (45.98)	281 (922)
Bleed rate		**bleed rate (%)**			
	Base	0	26.62 (79.92)	6.44 (43.58)	317 (0140)
	b4	2.5	24.15 (75.47)	7.58 (45.64)	286 (938)
	b5	5.0	21.88 (71.38)	8.36 (47.05)	265 (870)
	b1	10.0	19.30 (66.74)	9.21 (48.58)	242 (795)
	b2	15.0	17.66 (63.78)	9.83 (49.69)	225 (740)
	b3	20.0	16.49 (61.68)	10.32 (50.58)	212 (696)
Casing depth		**m (ft)**			
	Base	0 (0)	26.62 (79.92)	6.44 (43.58)	317 (1040)
	c4	60 (197)	26.88 (80.39)	6.54 (43.77)	320 (1050)
	c3	90 (295)	27.11 (80.80)	6.44 (43.59)	317 (1040)
	c2	160 (525)	27.33 (81.19)	6.33 (43.39)	314 (1030)
Surface roughness		**m (in)**			
	Base	1.50E-03 (0.06)	26.62 (79.92)	6.44 (43.58)	317 (1040)
	h2	3.00E-04 (0.01)	26.95 (80.51)	6.06 (42.92)	327 (1073)
	h4	3.00E-03 (0.12)	26.79 (80.22)	6.37 (43.46)	319 (1047)
	h3	9.00E-03 (0.35)	26.23 (79.22)	6.51 (43.71)	315 (1033)

Table 5-3 (continued)

Parametric study results-effect of parameter variations on minimum and maximum exiting water temperatures and design length

Parameter Varied	Case Name	Parameter Values	Maximum Temperature Back to HP ºC (ºF)	Minimum Temperature Back to HP ºC (ºF)	Equivalent Design Length m (ft)
Hydraulic conductivity		**m/s (gal/day/ft^2)**			
	kh3	1.00E-06 (2.118)	25.01 (77.19)	7.25 (45.04)	295 (968)
	Base	7.00E-05 (148.23)	26.62 (79.92)	6.44 (43.58)	317 (1040)
	kh2	1.00E-04 (211.8)	24.64 (76.35)	7.09 (44.76)	299 (981)
Dip tube diameter		**m (in)**			
	d4	0.0762 (3)	26.45 (79.61)	6.54 (43.78)	314 (1030)
	Base	0.1016 (4)	26.62 (79.92)	6.44 (43.58)	317 (1040)
	d5	0.1143 (4.5)	26.79 (80.23)	6.33 (43.39)	320 (1050)
	d6	0.1016 (insulation different)	28.48 (83.26)	5.56 (42.01)	340 (1115)
Depth of borehole		**m (ft)**			
	L1	240 (787)	32.85 (91.14)	2.81 (37.06)	
	L2	280 (919)	29.43 (84.97)	4.78 (40.61)	
	Base	320 (1050)	26.62 (79.92)	6.44 (43.58)	317 (1040)
	L3	360 (1181)	24.65 (76.38)	7.74 (45.93)	
	L4	400 (1321)	23.16 (73.68)	8.76 (47.77)	
Rock type		**Rock type**			
	Base	Karst limestone	26.62 (79.92)	6.44 (43.58)	317 (1040)
	kt4	Dolomite	34.41 (93.94)	4.23 (39.62)	376 (1234)
	kt5	Fractured igneous and metamorphic	19.43 (66.97)	9.38 (48.89)	238 (781)
	kh4	Sandstone	21.26 (70.27)	8.57 (47.43)	259 (850)
Bleed control		**Bleed rate (%)**			
	L1	0.0	32.85 (91.14)	2.81 (37.06)	
	L1_bt3	5.0	31.30 (88.34)	3.66 (38.59)	
	L1_bt1	10.0	32.01 (89.62)	3.49 (38.28)	
	L1_bt1_t	10.0	21.39 (70.50)	6.12 (43.02)	
Reverse		**Reverse**			
	No reverse	Base	26.62 (79.92)	6.44 (43.58)	317 (1040)
	Reverse	Reverse A	25.8 (78.4)	5.66 (42.2)	335 (1099)

5.5.1. The effect of thermal conductivity

Figure 5-5 shows the variation of the minimum and maximum exiting water temperatures with rock thermal conductivity. When extracting heat from the ground in the winter, the higher the thermal conductivity, the higher the temperature back to heat pump. Conversely, when rejecting heat into the ground in the summer, the higher the thermal conductivity, the lower the temperature back to heat pump. This trend can be expected and is similar to the behavior of closed-loop U-Tube heat exchangers. Increasing thermal conductivity allows greater heat fluxes along the borehole wall for the same temperature rise. Therefore, higher thermal conductivities are advantageous in SCW systems.

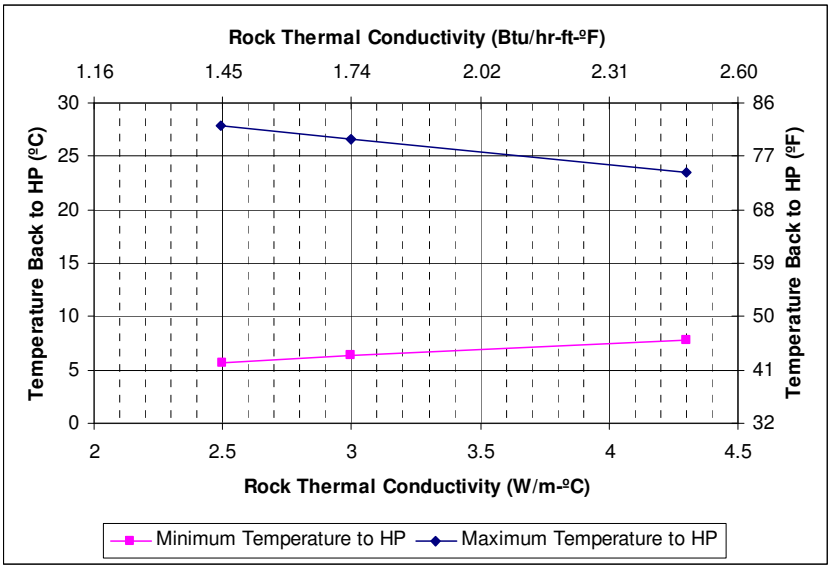

Figure 5-5 The effect of thermal conductivity of rock on the water temperature back to the heat pump

5.5.2. The effect of specific heat capacity

Figure 5-6 shows the variation of the minimum and maximum exiting water temperatures with rock specific heat capacity. When extracting heat from the ground in the winter, the higher the specific heat capacity, the higher the temperature back to the heat pump.

Conversely, when rejecting heat into the ground in the summer, the higher the specific heat capacity, the lower the temperature back to heat pump. The higher specific heat capacity means the thermal inertia of the rock is larger, and under a given heat flux (load), the temperature change of the rock is small. The higher specific heat capacity leads to increased damping of dynamic changes in the borehole temperatures.

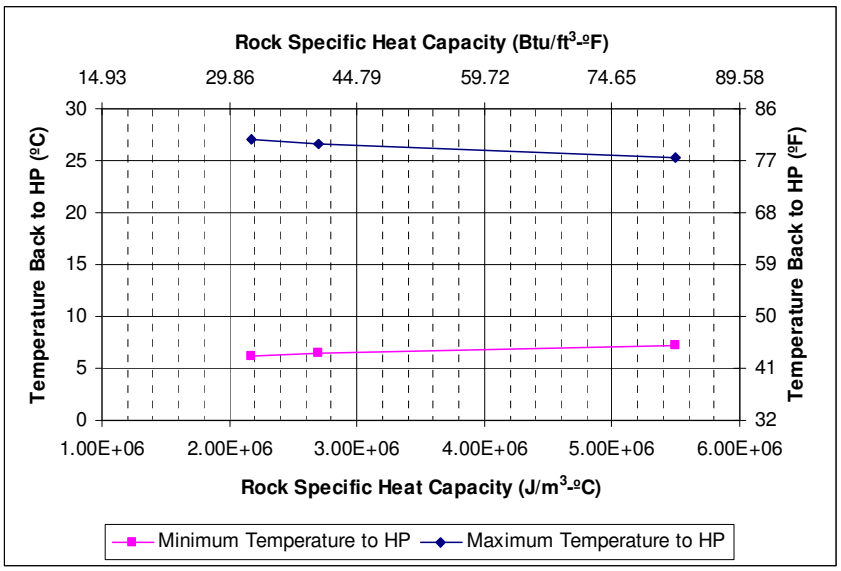

Figure 5-6 The effect of specific heat capacity of rock on the water temperature back to the heat pump

5.5.3. The effect of natural geothermal gradients

Figure 5-7 shows the variation of the minimum and maximum exiting water temperatures with a rock thermal temperature gradient. Higher thermal gradients result in higher mean rock temperatures over the length of the borehole. This would be particularly true for deep wells. The data show that when heat is extracted or rejected, the higher natural geothermal gradients lead to higher water temperatures back to heat pump. The performance of the SCW would be improved (in the winter) or degraded (in the summer).

This is probably advantageous in most applications of SCW systems, in which the design considerations are based on heating conditions.

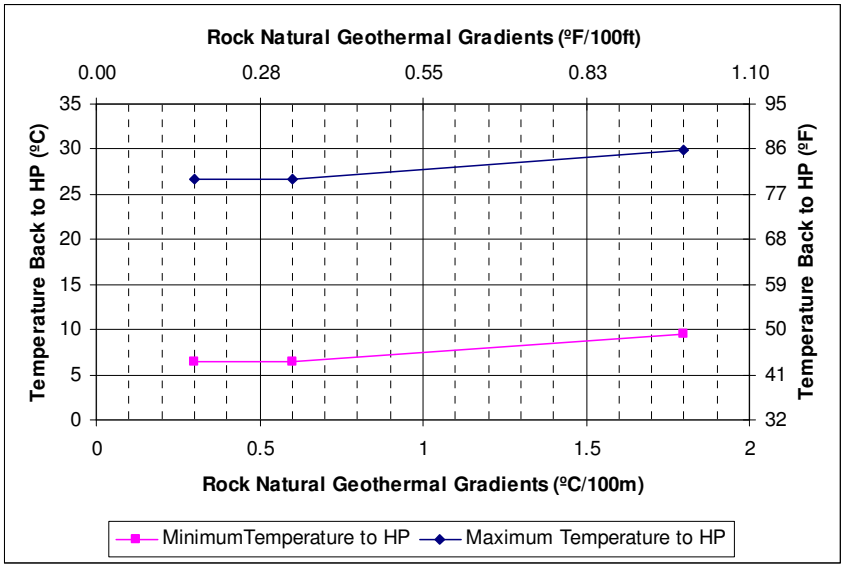

Figure 5-7 The effect of natural geothermal gradients of rock on the water temperature back to the heat pump

5.5.4. The effects of hydraulic conductivity

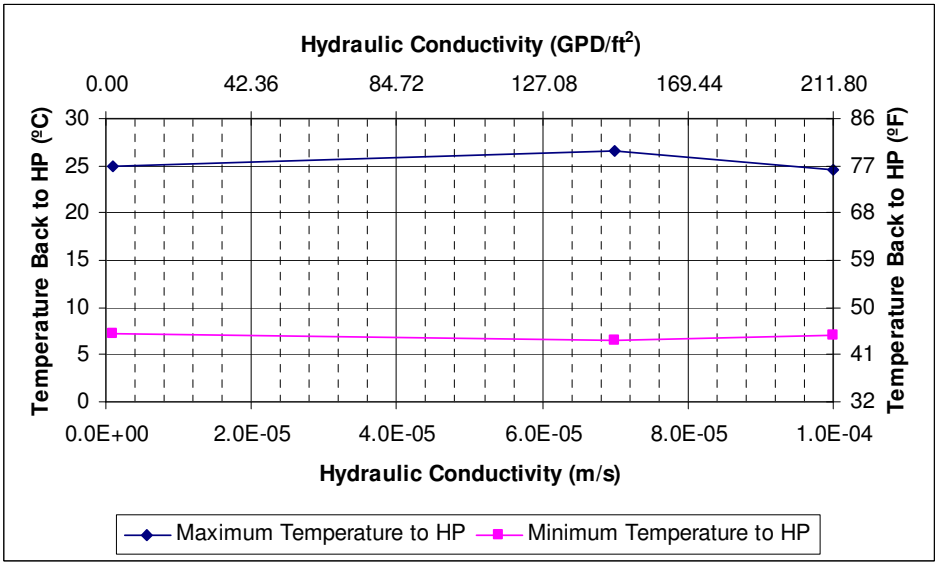

Figure 5-8 The effect of hydraulic conductivity of rock on the water temperature back to the heat pump

Figure 5-8 shows the variation of the minimum and maximum exiting fluid temperature with changes in rock hydraulic conductivity. A moderate effect on the maximum and minimum exiting water temperature can be seen from both higher hydraulic conductivity (i.e. case kh2, [K =1.00E-04 m/s]) and lower hydraulic conductivity (i.e., Case kh3, [K =1.00E-06m/s]). It might be expected that at higher hydraulic conductivities the resulting increased advective flow would lead to improved performance. However, the results show that when hydraulic conductivity is increased or decreased from the base case, the performance decreases. To further investigate the effect of the hydraulic conductivity in this given borehole configuration, calculations were made for five cases using a two-week operation period. Figure 5-9 shows the variation of heat transfer rates with rock hydraulic conductivity.

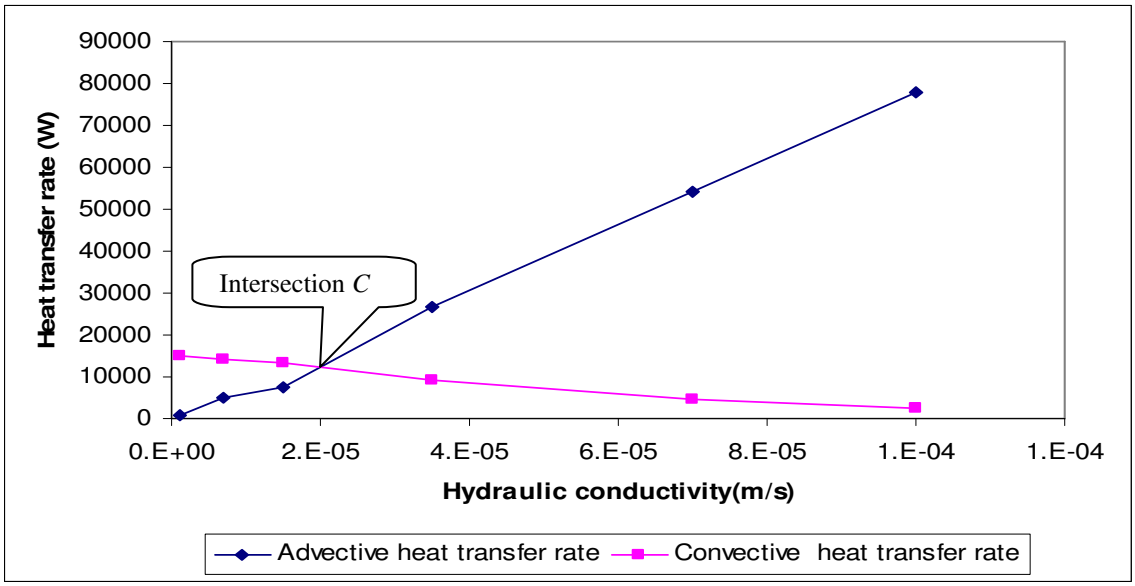

Figure 5-9 Total heat transfer rates along the borehole wall in the different cases of varied hydraulic conductivity *

*All the data in Figure 5-9 are generated by two-week (336 hours) simulations with fixed entering water temperatures. All the data correspond to the last time step.

The advective heat transfer rate and the convective heat transfer rate in Figure 5-9 are calculated from the following equations:

$$Q_{advective} = \dot{m} \cdot C_p \cdot T \tag{5.19}$$

$$Q_{convective} = h \cdot \Delta T \cdot A \tag{5.20}$$

Where $Q_{advective}$ is the advective heat transfer rate (W [Btu/hr]);

$Q_{convective}$ is the advective heat transfer rate (W [Btu/hr]);

$\dot{m}$ is the mass flow rate (kg/s);

C_p is the specific heat of the water (J/kg-K [Btu/lbm-ºF]);

T is the temperature of the advective water(ºC [ºF]);

h is the convection heat transfer coefficient(W/m^2-K [Btu/hr-ft^2-ºF]);

A is the area where convection heat transfer happens (m^2 [ft^2]).

There are two mechanisms of heat transfer along the borehole wall between fluid and rock: advective and convective heat transfer. As fluid flows down the borehole a boundary layer is formed at the borehole wall resulting in convective heat transfer. As the borehole wall is porous, additional heat transfer takes place by advection of fluid into and out of the rock. As the hydraulic conductivity increases, the corresponding advective heat transfer increases. However, as the flow into and out of the rock increases, the vertical fluid flow in the borehole reduces.

Figure 5-9 shows the variation of the two heat transfer rates with different hydraulic conductivities. If hydraulic conductivities are greater than approximately 2.0E-5 m/s (Intersection *C*), advective heat transfer is dominant. If hydraulic conductivities are less

than 2.0E-5 m/s, convective heat transfer is dominant. In the first region, where advective heat transfer is dominant, higher hydraulic conductivities result in the exiting water temperature back to heat pump being higher when extracting heat from the ground in winter. Conversely, when rejecting heat into the ground in summer, higher hydraulic conductivities result in the exiting water temperature back to heat pump being lower. In the region where convective heat transfer is dominant (i.e., $K <$ 2.0E-5 m/s), the variation of the exiting water temperatures with hydraulic conductivity is opposite to that associated with the first region.

This phenomenon can be explained as follows. From mass conservation, as the flow into and out of the rock increases, the vertical fluid flow in the borehole reduces. As can be expected from the linear nature of Darcy's equation, the higher hydraulic conductivities result in higher water flow rates leaving the borehole, so that less vertical water flows in the borehole. Thus, the smaller convective heat transfer coefficients along the borehole wall are the result of smaller water velocities (axial) in the borehole. The higher hydraulic conductivities lead to enhanced advective heat transfer from rock, but reduced convective heat transfer along the borehole wall. Therefore, there are trade-offs in these two processes.

It should be noted that different borehole configuration (e.g. borehole diameter) would give a different critical value of Intersection *C*. Higher rock hydraulic conductivity is still preferable because the drawdown of the water table will be greater with a lower hydraulic conductivity.

5.5.5. The effect of surface roughness of borehole wall

The increased roughness increases the borehole wall's surface area and promotes local turbulent flow along the wall of the borehole, which augments the heat transfer and results in a moderating effect on maximum and minimum exiting temperatures. So, in the winter the temperature back to the heat pump would be higher with the higher roughness, and in the summer the temperature back to the heat pump would be lower with the higher roughness. This trend can be observed from Figure 5-10. Table 5-4 lists the average heat transfer coefficients along the borehole wall at the time when minimum water temperature back to the heat pump occurs. The rough borehole wall abets turbulence and enhances heat transfer, but the effect does not seem to be significant compared to that associated with other design parameters.

Table 5-4 Results for different roughness height cases

Case name	Case h2	Case h4	Case h3
Surface roughness (m)	3×10^{-4}	3×10^{-3}	9×10^{-3}
Minimum temperature back to HP (°C)	6.06	6.37	6.51
Average heat transfer coefficient along the borehole wall (W/m^2-K)	456.14	905.29	1751.61

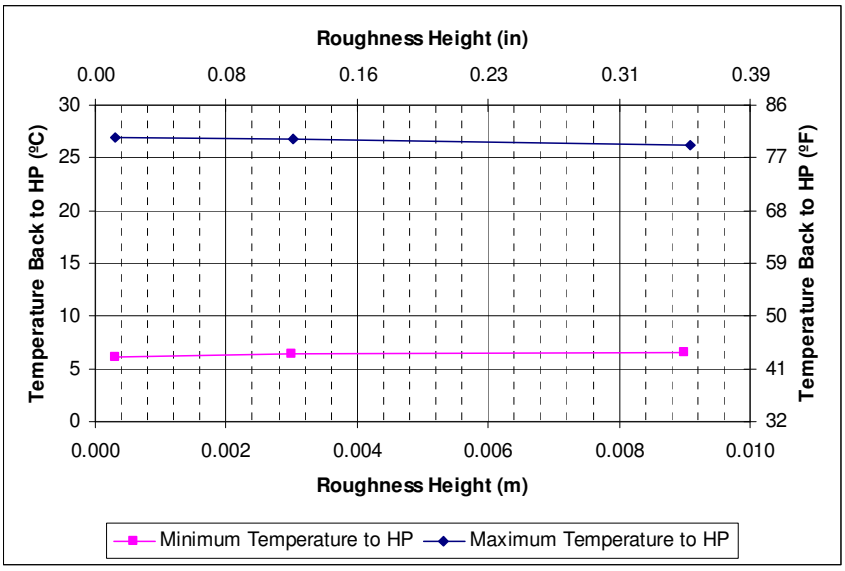

Figure 5-10 The effect of roughness height of borehole wall on the water temperature back to the heat pump

5.5.6. The effect of borehole diameter

Figure 5-11 shows the variation of the minimum and maximum exiting water temperatures with borehole diameter. To enhance the turbulent flow in the annular area in the borehole, it is desirable that the annular area be smaller than the area inside the tubes. Figure 5-11 shows that there is only little difference between cases with different borehole diameter. For a given time step, the Reynolds numbers for different cells during the simulation were in the range from 4800-6000 for case d2 (borehole diameter 5.5 in [0.1398 m]), and from 4800-5800 for the base case (borehole diameter 6.0 in [0.1524 m]). The differences in Reynolds numbers from the given cases are minor and have minimal impact on heat transfer rates along the borehole wall.

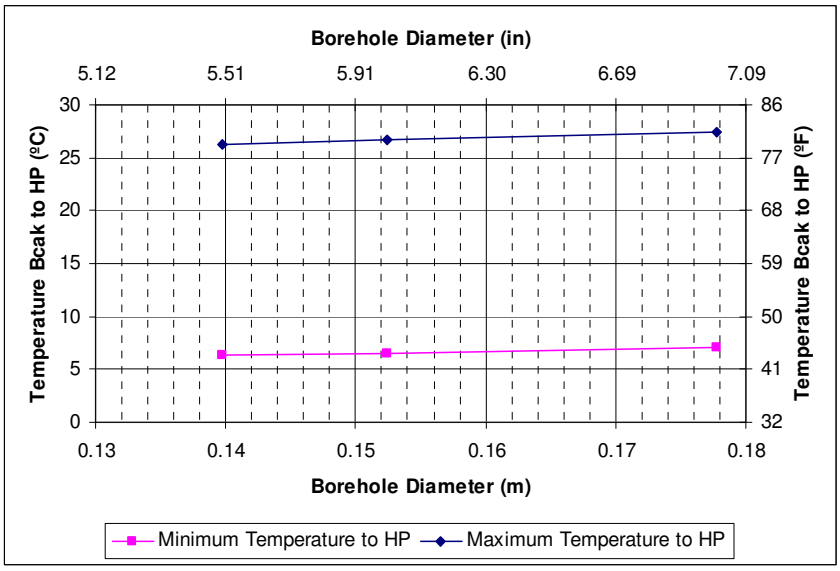

Figure 5-11 The effect of borehole diameter on the water temperature back to the heat pump

5.5.7. The effect of casing (liners)

Because casings act as a barrier to infiltration of groundwater, the transfer of heat by advection is severely reduced over those parts of the borehole where a casing is present. The effect of the depth of casing can be seen in Figure 5-12. Increasing the casing depth can lead to increased maximum and decreased minimum exiting water temperatures. The heat exchanger performance is degraded with increased casing depths. The effect, however, is not as significant as might be expected, though this effect might be more noticeable in rocks with higher hydraulic conductivities.

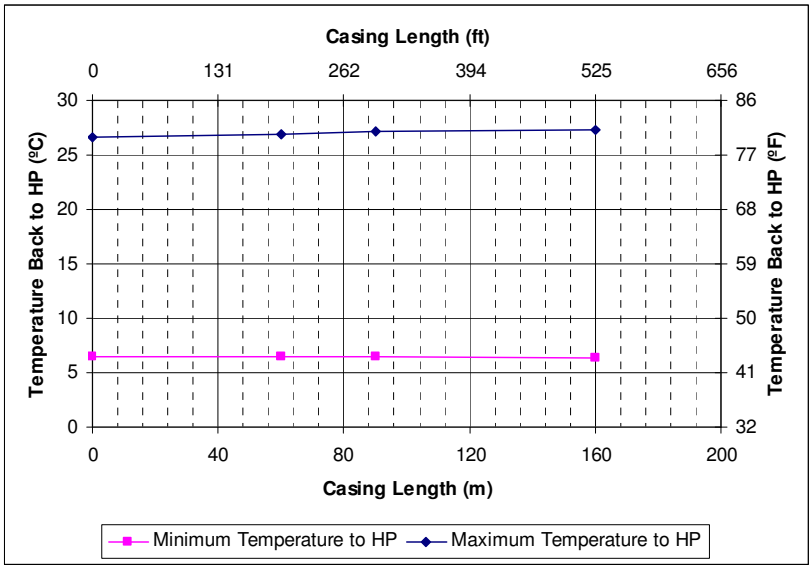

Figure 5-12 The effect of casing length on the water temperature back to the heat pump

5.5.8. The effects of dip tube insulation and diameter

Two cases were used to examine the effects of dip tube insulation (i.e., thermal conductivity of the dip tube). PVC (polyvinyl chloride) dip tube with thermal conductivity, 0.1 W/m-K (0.0577 Btu/hr-ft-ºF), is used in the base case. HDPE (high-density polyethylene) dip tube with thermal conductivity, 0.4 W/m-K (0.2308 Btu/hr-ft-ºF), is used in Cased6. The variation of the minimum and maximum exiting water temperatures for these cases is shown in Figure 5-13. The variation of the minimum and maximum exiting water temperatures with dip tube diameter is shown in Figure 5-14.

The results for Case d6-with higher dip tube thermal conductivity-show higher maximum and lower minimum exiting water temperatures compared to the base case. This is because heat transfer (i.e., short-circuiting heat flux) between the water in the dip tube

and the water surrounding the dip tube is detrimental. Consequently, higher dip tube thermal conductivities may be expected to show poorer SCW performance.

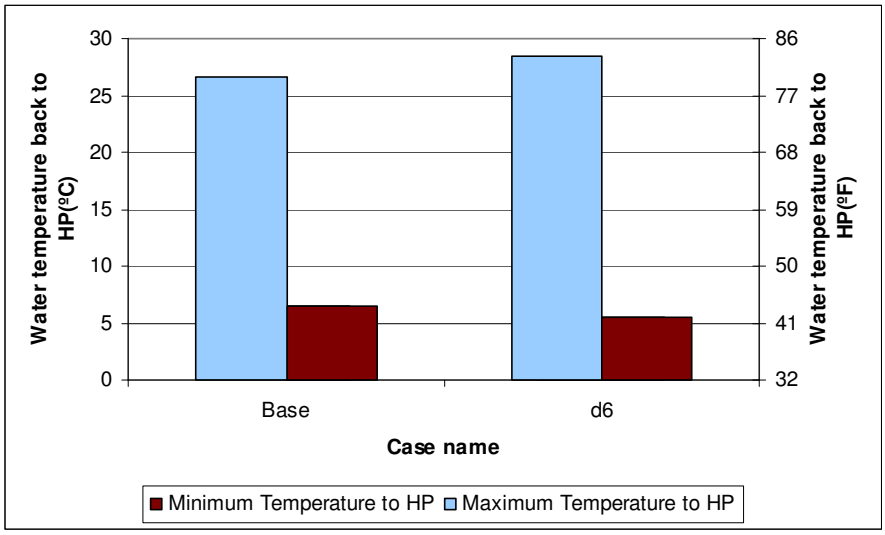

Figure 5-13 The effect of thermal insulation of the dip tube on the water temperature back to the heat pump

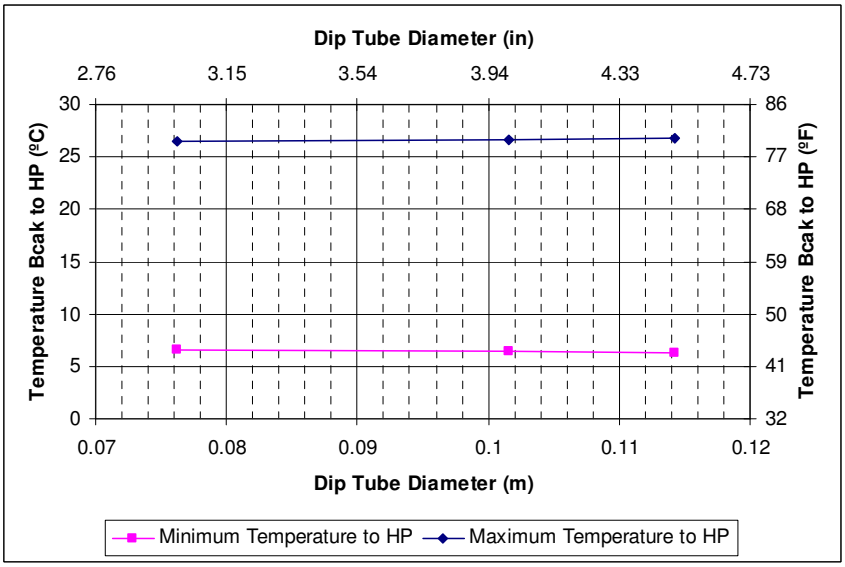

Figure 5-14 The effect of diameter of dip tube on the water temperature back to the heat pump

The dip tube diameter was varied between 76 and 114 mm (3-4.5 in) in the parametric study. The annular areas are noticeably changed when the borehole diameter is 152 mm (6 in). However, the results shown in Figure 5-14 show that this parameter has little effect on the temperature back to heat pump when varied in this given range.

5.5.9. The effect of bleed

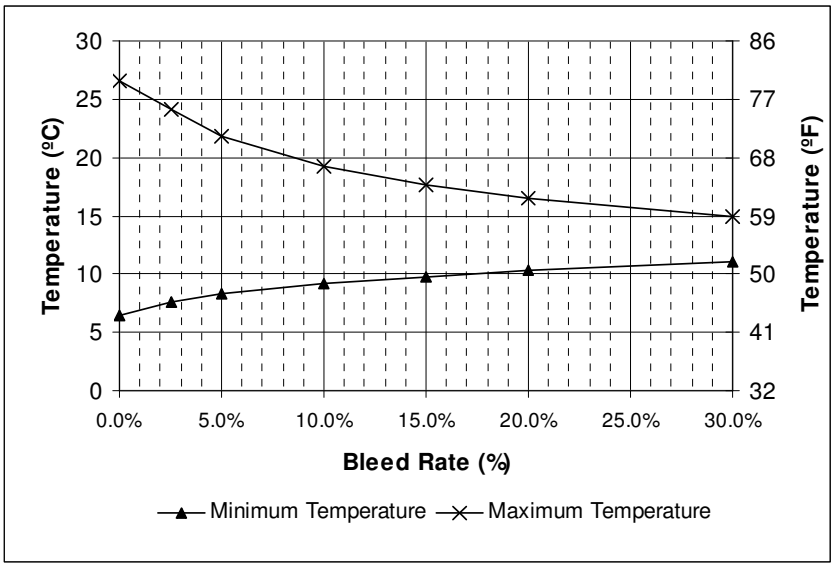

Figure 5-15 The effect of bleed rate on the water temperature back to the heat pump

The bleed parameter calculations were made by making a one-year simulation with a constant bleed rate. Figure 5-15 shows how significantly the minimum and maximum temperatures can be affected by introducing bleed. The performance of the SCW is generally enhanced by a "bleed" strategy, especially in the severity of summer or winter because more groundwater from the formation is drawn into the borehole. As the bleed rate is increased, the minimum and maximum temperatures approach the far field temperature. This affect is non-linear, which is expected due to the advection term of

Equation (4.10). The most significant rate of changes occurs in the 0-15% range. Even a small bleed rate can be seen to be highly effective in moderating the maximum and minimum water temperatures. From this data it could be argued that there is little advantage in increasing the bleed rate beyond fifteen percent. However, energy savings and reduction in well depth might justify higher bleed rates. Non-constant bleed cases will be discussed later in this Chapter.

5.5.10. The effect of the depth of borehole

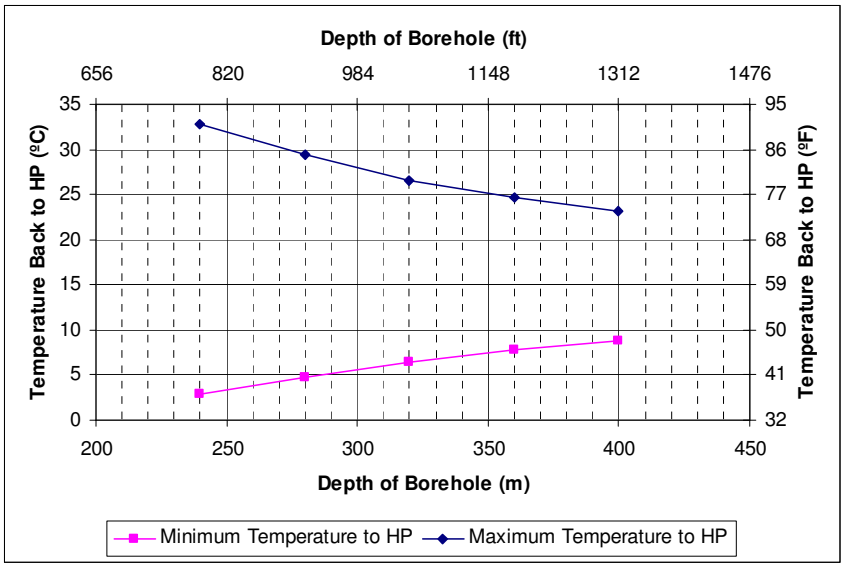

Figure 5-16 The effect of depth of borehole on the water temperature back to the heat pump

The deeper the borehole, the more heat can be exchanged with the ground. The variation of the minimum and maximum exiting water temperatures with borehole depth is shown in Figure 5-16. In our parametric study, borehole depth was varied from 240 to 400 m (787 to1312 ft) with the loads kept the same. As borehole depth is reduced, the amount of load applied per unit length of borehole increases accordingly. Changing the borehole

length in this range has a significant affect on exiting water temperatures. The trend is also slightly non-linear. This might be expected as, in addition to the load per unit depth changing, end effects become more significant at reduced depths. Also, as a temperature gradient is applied, the mean ground temperature becomes lower with shorter depths.

5.5.11. The effect of varied depth with different bleed rate

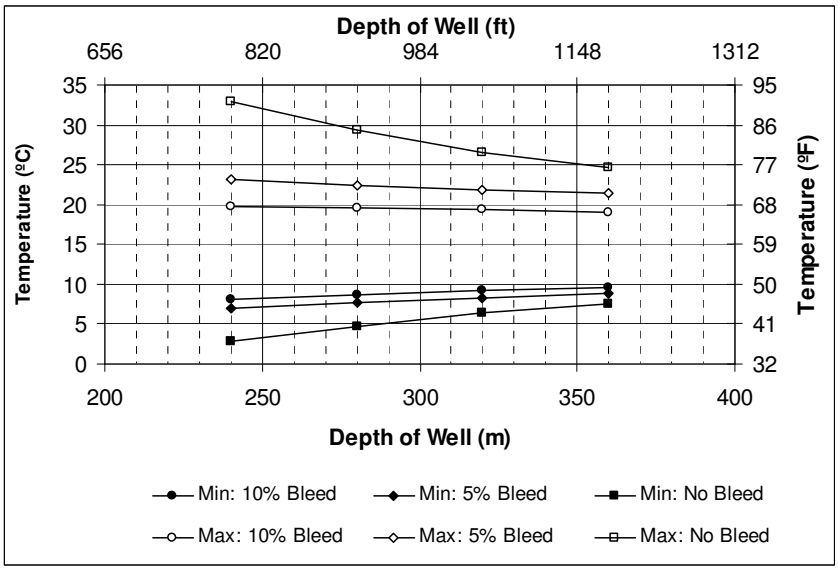

Figure 5-17 The effect of depth of borehole on the water temperature back to the heat pump

The combined effects of different rates of bleed and different well depths are summarized in Figure 5-17. In these cases, borehole depth varied from 240-360 m (787-1181 ft), and bleed rates were 0 %, 5 % and 10 % with a constant load. The variation of borehole depth in this range can be seen to have a significant effect on the exiting water temperature if bleed rate is zero. But if bleed rate is set as 5 % or higher, the borehole depth can be seen to have a little effect on the SCW performance; different borehole depths show almost the

same exiting water temperatures. As bleed rate is increased, the flow to the heat pump approaches the temperature of the far-field groundwater. Correspondingly, the borehole depth becomes less significant. This trend is seen in the results. Figure 5-17 shows clearly how bleed can be used to moderate the temperature of the water drawn from the well. This can be very important in protecting the system against freezing in heating mode. It also shows how well depth might be reduced-along with initial cost-by reliance on bleed. However, there are practical considerations that also determine the minimum depth of borehole and maximum bleed. First, the pumping capacity of a well is limited and also dependent on depth. Consequently, it may not be possible to have a shorter well with a high rate of bleed. Second, high rates of bleed require significant amounts of water be discharged appropriately.

5.5.12. The effect of different rock type

Besides the previous cases deal with variations in individual rock thermal property variations (i.e., thermal conductivity or specific heat), three additional cases have been included where the hydraulic conductivity, thermal conductivity, and porosity are all varied. All those values have been chosen to correspond to a particular rock type. The base case is representative of karst limestone, and other cases are representative of dolomite (Case kt4), fractured igneous rock (Case kt5), and sandstone (Case kh4).

The simulation results (Figure 5-18) show that a SCW installed in igneous or metamorphic rock (Case kt5) will have better performance (higher water temperature back to the heat pump in the winter, lower water temperature back to the heat pump in the

summer). Also, the thermal conductivity of rock plays a more important role in predicting SCW performance. The effect of thermal conductivity is more dominant than that of hydraulic conductivity.

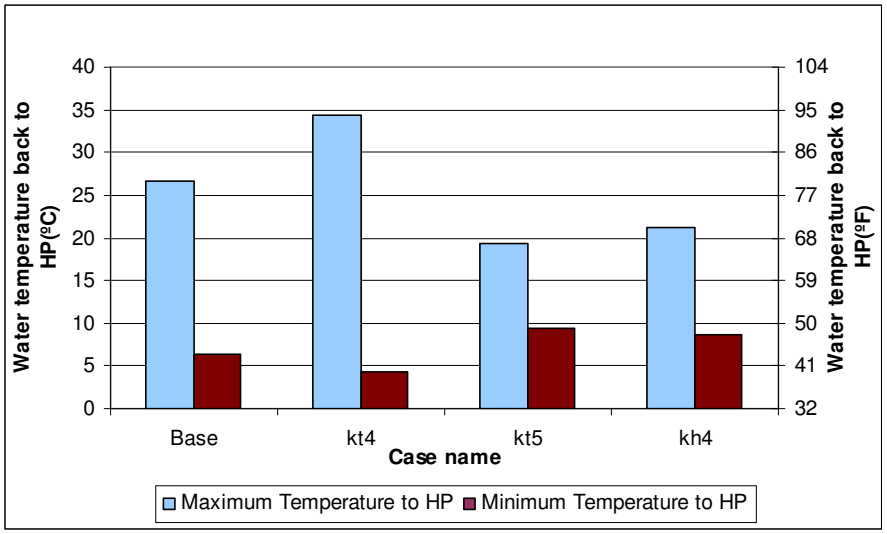

Figure 5-18 The effect of rock type on the water temperature back to the heat pump

5.5.13. The effect of bleed control strategy

In most cases, it is not necessary to continuously apply bleed, and some form of bleed control is used. There are two strategies for controlling bleed operation:

1. Deadband control: In winter, when the water temperature back to the heat pump is lower than 5.83 ºC (42.5 ºF), bleed is started. When the water temperature back to the heat pump is higher than 8.6 ºC (47.5 ºF), bleed is stopped. In summer, bleed is started when water temperature back to the heat pump is higher than 29.2 ºC (84.5 ºF), and stopped when water temperature back to the heat pump is lower than 26.4 ºC (79.5 ºF).
2. Temperature-difference control: The temperature difference (ΔT) between water back to and from HP was used as a controlled parameter. The temperature

difference (ΔT) was set to give the same number of hours of operation as the deadband bleed control case: 4.6 ºC (8.3 ºF).

The variation of the minimum exiting water temperature with different bleed control strategies is shown in Figure 5-19. Although the deadband control and temperature-difference control strategies were arranged to give bleed for the same number of hours, the temperature difference control gave a slightly higher minimum temperature. The minimum water temperature back to heat pump with no bleed was calculated to be 3.7 ºC (38.7 ºF). This implies, in fact, that at this time water temperatures in the annulus of the well are below freezing point.

For the calculations where deadband and temperature-difference bleed control was modeled, the minimum water temperature back to the heat pump was increased to 5.4 ºC (41.6 ºF) and 6.0 ºC (42.8 ºF) respectively. In these cases, the minimum temperature in the borehole annulus was always above freezing point. The result for the calculation with constant bleed is included in Figure 5-19 for comparison. The minimum temperature in that case was 7.7 ºC (45.8 ºF). If the primary concern is to avoid freezing of the borehole intermittent bleed may suffice and constant bleed is probably unnecessary.

Although the total hours the pump ran were the same in controlled bleed cases, the hours when the pump ran were different. Small differences in the results could then be expected due to the dynamic nature of the system and changing loads. The results may show lower

return temperatures for the temperature-difference control in other cases with different load profiles.

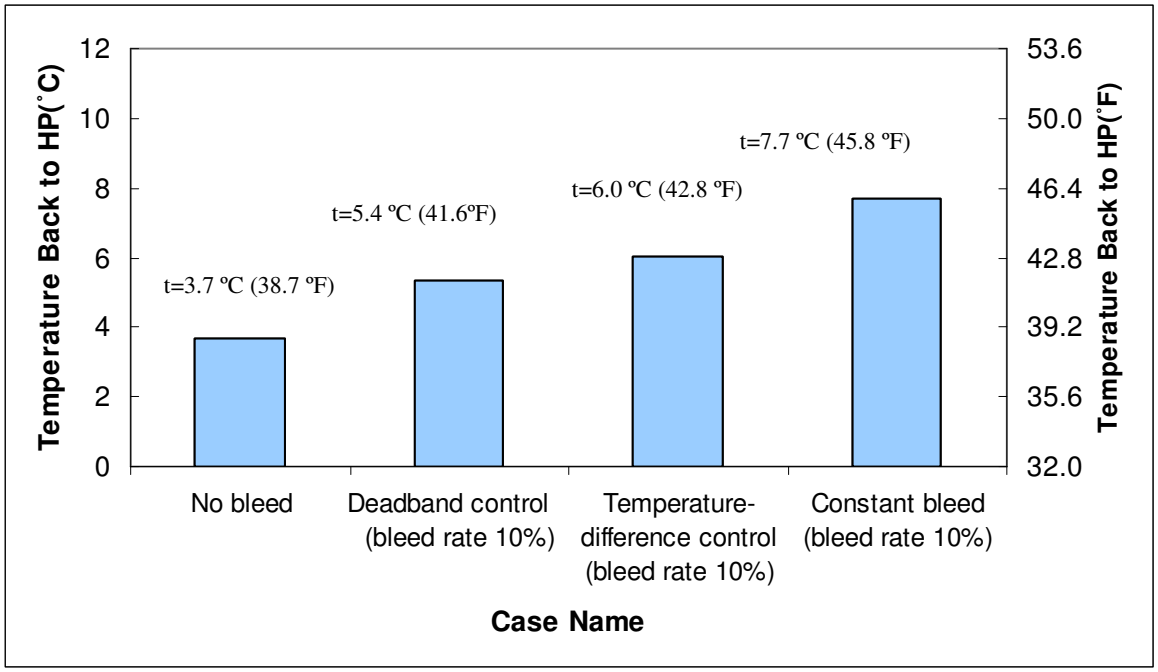

Figure 5-19 The effect of bleed control strategy on the minimum water temperature back to the heat pump in winter (January and February)

Figure 5-20 compares the exiting water temperature in non-bleed operation with deadband bleed control operation over the first 800 hours. The times at which bleed begins or stops are also indicated. Figure 7-21 shows the relations between the temperature difference and the bleed period in temperature-difference bleed control case.

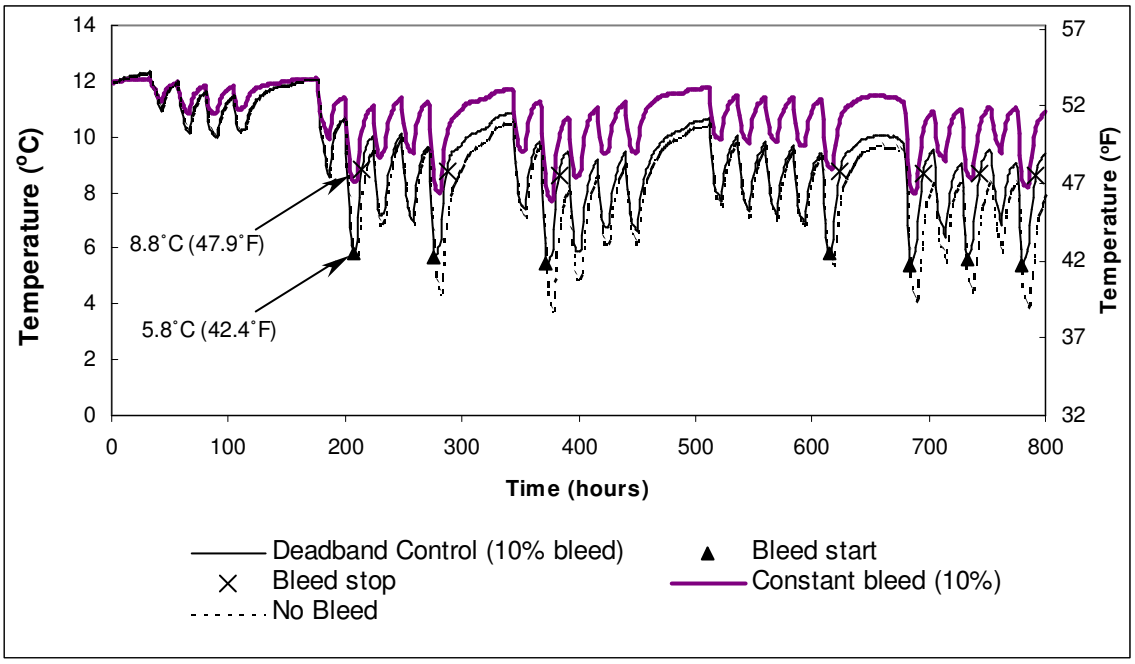

Figure 5-20 Comparison water temperatures back to the heat pump between non-bleed case, constant bleed and deadband bleed control case

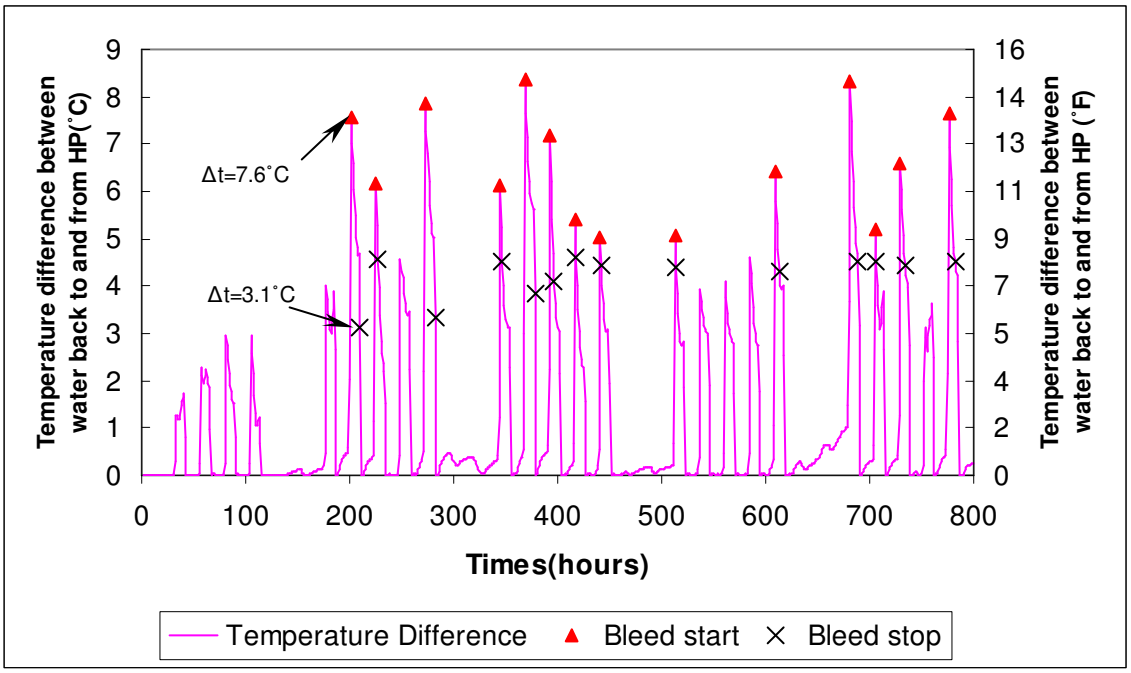

Figure 5-21 Entering and exiting fluid temperature difference during the heating season under temperature-difference bleed control showing the points at which bleed was activated

5.5.14. System energy consumption and costs

System energy consumption (heat pump and water circulating pump) and associated costs have been calculated for each case using the method described in Section 5.4. The calculation results are presented for water table depths of 5 m and 30 m to show the effect of increased pumping power at lower water tables. The results are shown in Table 5-5 for a water table depth of 5 m, and in Table 5-6 for a water table depth of 30 m. The power consumption has been expressed in terms of peak power consumption per unit of cooling (kW/ton). With a water table depth of 5 m (16 ft) the base case operating cost is $1482 per annum with a peak power consumption ratio of 1.13 kW/ton. With a water table

depth of 30 m (98 ft) the base case operating cost is $1504 per annum with a peak power consumption ratio of 1.13 kW/ton.

Table 5-5 Energy calculation results (water table = 5.0 m)

Parameter	Case Name	Parameter Value	Power Consumption /Cooling Capacity (kW/ton)	One Year Operating Cost ($)
Thermal conductivity		W/m-K(Btu/hr-ft-ºF)		
	kt2	2.5 (1.44)	1.14	1500
	Base	3.0 (1.73)	1.13	1482
	kt3	4.3 (2.48)	1.09	1446
Natural geothermal gradients		ºC/100m (ºF/100ft)		
	n2	0.3 (0.17)	1.13	1482
	Base	0.6 (0.329)	1.13	1482
	n3	1.8 (0.99)	1.17	1519
Specific heat capacity		J/m^3-K (Btu/ft^3-ºF)		
	s2	2.13E+06 (31.769)	1.13	1486
	Base	2.70E+06 (40.27)	1.13	1482
	s3	5.50E+06 (82.03)	1.11	1470
Borehole diameter		mm (in)		
	d2	139.8 (5.5)	1.14	1472
	Base	152.4 (6)	1.13	1482
	d3	177.8 (7)	1.12	1481
Bleed rate		Bleed rate (%)		
	Base	0	1.14	1482
	b4	2.5	1.09	1457
	b5	5.0	1.06	1427
	b1	10.0	1.03	1394
	b2	15.0	1.00	1375
	b3	20.0	0.98	1362
Casing depth		m (ft)		
	Base	0 (0)	1.13	1482
	c4	60 (197)	1.13	1487
	c3	90 (295)	1.13	1490
	c2	160 (525)	1.14	1493
Surface roughness		mm (in)		
	h2	0.3(0.01)	1.13	1488
	Base	1.5 (0.06)	1.13	1482
	h4	3.0 (0.12)	1.13	1484
	h3	9.0 (0.35)	1.12	1480

Table 5-5 (continued)

Energy calculation results (water table = 5.0m)

Parameter	Case Name	Parameter Value	Power Consumption /Cooling Capacity (kW/ton)	One Year Operating Cost ($)
Hydraulic conductivity		**m/s (gal/day/ft^2)**		
	kh3	1.00E-06 (2.118)	1.11	1472
	Base	7.00E-05 (148.23)	1.13	1482
	kh2	1.00E-04 (211.8)	1.10	1454
Dip tube diameter		**mm (in)**		
	d4	76.2 (3)	1.12	1485
	Base	101.6 (4)	1.13	1482
	d5	114.3 (4.5)	1.13	1484
	d6	101.6(4) (insulation different)	1.15	1503
Depth of borehole		**m (ft)**		
	L1	240 (787)	1.21	1569
	L2	280 (919)	1.16	1521
	Base	320 (1050)	1.13	1482
	L3	360 (1181)	1.10	1461
	L4	400 (1321)	1.08	1443
Different rock type		**Rock type**		
	Base	Karst limestone	1.13	1482
	kt4	Dolomite	1.24	1600
	kt5	Fractured igneous and metamorphic	1.07	1399
	kh4	Sandstone	1.07	1423
Bleed control		**Bleed rate (%)**		
	L1	0	1.21	1569
	L1_bt3	5.0(Dead-band)	1.19	1540
	L1_bt1	10.0(Dead-band)	1.20	1541
Reverse		**Reverse**		
	No reverse	Base	1.13	1482
	Reverse	Reverse	1.12	1469

Table 5-5 (continued)

Energy calculation results (water table =5.0m)

Parameter	Case Name	Parameter Value		Power Consumption /Cooling Capacity (kW/ton)	One Year Operating Cost ($)
Depth of borehole and Bleed rate		m (ft)	Bleed rate(%)		
	L1_bleed(5)	240 (787)	5	1.08	1441
	L2_bleed(5)	280 (919)	5	1.07	1434
	b5(2)	320 (1050)	5	1.06	1427
	L3_bleed(5)	360 (1181)	5	1.06	1424
Depth of borehole and Bleed rate		m (ft)	Bleed rate(%)		
	L1_bleed(10)	240 (787)	10	1.04	1399
	L2_bleed(10)	280 (919)	10	1.03	1397
	b1(2)	320 (1050)	10	1.03	1394
	L3_bleed(10)	360 (1181)	10	1.03	1394

Table 5-6 Energy calculation results (water table = 30.0 m)

Parameter	Case Name	Parameter Value	Power Consumption /Cooling Capacity (kW/ton)	One Year Operating Cost ($)
Thermal conductivity		W/m-K (Btu/hr-ft-ºF)		
	kt2	2.5 (1.44)	1.15	1521
	Base	3.0 (1.73)	1.13	1503
	kt3	4.3 (2.48)	1.09	1467
Natural geothermal gradients		ºC/100m (ºF/100ft)		
	n2	0.3 (0.17)	1.13	1503
	Base	0.6 (0.329)	1.13	1503
	n3	1.8 (0.99)	1.17	1540
Specific heat capacity		J/m^3-K (Btu/ft^3-ºF)		
	s2	2.13E+06 (31.769)	1.14	1507
	Base	2.70E+06 (40.27)	1.13	1503
	s3	5.50E+06 (82.03)	1.11	1491
Borehole diameter		mm (in)		
	d2	139.8 (5.5)	1.14	1493
	Base	152.4 (6)	1.13	1503
	d3	177.8 (7)	1.12	1502
Bleed rate		Bleed rate (%)		
	Base	0	1.13	1503
	b4	2.5	1.09	1488
	b5	5.0	1.06	1467
	b1	10.0	1.03	1453
	b2	15.0	1.01	1458
	b3	20.0	1.00	1469
Casing depth		m (ft)		
	Base	0 (0)	1.13	1503
	c4	60 (197)	1.13	1508
	c3	90 (295)	1.14	1511
	c2	160 (525)	1.14	1514
Surface roughness		mm (in)		
	h2	0.3(0.01)	1.13	1509
	Base	1.5 (0.06)	1.13	1503
	h4	3.0 (0.12)	1.13	1505
	h3	9.0 (0.35)	1.13	1501

Table 5-6 (continued)

Energy calculation results (water table = 30.0 m)

Parameter	Case Name	Parameter Value	Power Consumption /Cooling Capacity (kW/ton)	One Year Operating Cost ($)
Hydraulic conductivity		**m/s (gal/day/ft^2)**		
	kh3	1.00E-06 (2.118)	1.11	1493
	Base	7.00E-05 (148.23)	1.13	1503
	kh2	1.00E-04 (211.8)	1.10	1475
Dip tube diameter		**mm (in)**		
	d4	76.2 (3)	1.13	1506
	Base	101.6 (4)	1.13	1503
	d5	114.3 (4.5)	1.13	1505
	d6	101.6(4) (insulation different)	1.15	1524
Depth of borehole		**m (ft)**		
	L1	240 (787)	1.21	1591
	L2	280 (919)	1.17	1542
	Base	320 (1050)	1.13	1503
	L3	360 (1181)	1.10	1483
	L4	400 (1321)	1.08	1463
Different rock type		**Rock type**		
	Base	Karst limestone	1.13	1503
	kt4	Dolomite	1.24	1622
	kt5	Fractured igneous and metamorphic	1.07	1421
	kh4	Sandstone	1.07	1444
Bleed control		**Bleed rate (%)**		
	L1	0	1.21	1591
	L1_bt3	5.0(Dead-band)	1.19	1563
	L1_bt1	10.0(Dead-band)	1.20	1564
Reverse		**Reverse**		
	No reverse	Base	1.13	1503
	Reverse	Reverse	1.15	1505

Table 5-6 (continued)

Energy calculation results (water table = 30.0 m)

Parameter	Case Name	Parameter Value		Power Consumption /Cooling Capacity (kW/ton)	One Year Operating Cost ($)
Depth of borehole and Bleed rate		m (ft)	Bleed rate(%)		
	L1_bleed(5)	240 (787)	5	1.08	1482
	L2_bleed(5)	280 (919)	5	1.07	1474
	b5(2)	320 (1050)	5	1.06	1467
	L3_bleed(5)	360 (1181)	5	1.06	1464
Depth of borehole and Bleed rate		m (ft)	Bleed rate(%)		
	L1_bleed(10)	240 (787)	10	1.04	1458
	L2_bleed(10)	280 (919)	10	1.04	1456
	b1(2)	320 (1050)	10	1.03	1453
	L3_bleed(10)	360 (1181)	10	1.03	1452

The parameters that had little effect on the minimum and maximum well temperatures correspondingly change the annual costs insignificantly. The most significant factors influencing the cost are length of borehole, thermal conductivity of surrounding rock and bleed rate. In the cases with different well depth and thermal conductivity, the energy consumption is improved by increasing the heat pump efficiency when the well temperatures are improved (i.e., longer length and higher conductivity).

The energy costs and efficiency can be most significantly improved by introducing higher rates of bleed. In these cases, the water table depth has a significant effect on energy costs. The costs for the cases with different bleed rates and water table depths are compared in Figure 5-22. When the water table is at a depth of 5 m the higher cost of pump energy consumption at higher rates of bleed is outweighed by reduced heat pump

energy costs. Similarly, there appears little benefit in controlling the system to reduce the number of hours operating with bleed (i.e., just to guard against freezing of the borehole). When the water table is at a depth of 30 m, for higher rates of bleed (> 10 %), the higher cost of pump energy consumption starts to outweigh the benefit of improved heat pump efficiency.

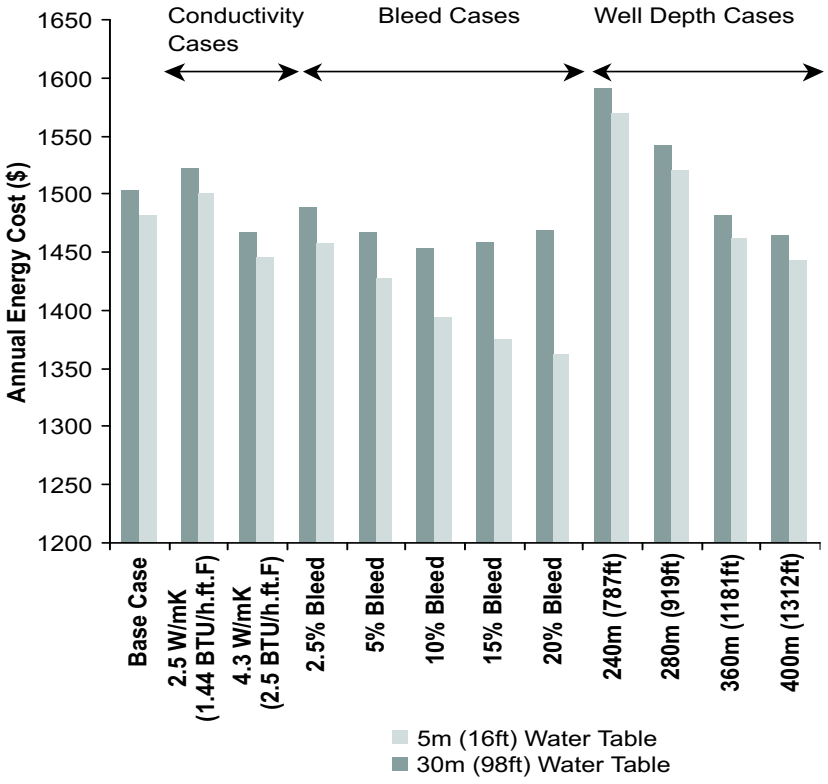

Figure 5-22 Comparison of annual energy costs for water table depths of 5 m and 30 m

The lowest energy costs are found in cases where bleed is introduced and heat pump efficiency is improved. Where the water table is high (5 m) the increased water pump power when bleeding is not significant and the great efficiencies are when bleed rate is maximized (i.e., case with 20 % bleed rate in Figure 5-22). However, when the water

table is lower (30 m), water pump power requirements increase more significantly when bleed is introduced. The benefits of higher rates of bleed (>10 % in this study) are then outweighed by the increased pumping costs.

5.5.15. Summary of parametric study

A numerical model has been employed in a parametric study of standing column well performance. The performance has been characterized by minimum and maximum exiting fluid temperature. The performance is found to be most sensitive to the following parameters:

- bleed rate
- borehole length
- rock thermal conductivity
- hydraulic conductivity
- dip tube thermal conductivity

A number of other parameters affect the convective heat transfer in the borehole but in them have only a secondary effect of the SCW performance:

- borehole wall roughness
- ground thermal gradient
- borehole casing depth

Also, some interesting characteristics can be identified from this parametric study

1. Bleed serves the following purposes:

- Reduces the required well depth for a given heat transfer rate, and consequently reduces initial costs.
- Improves energy consumption by moderating the fluid temperatures and increasing the efficiency of the heat pump.
- Guards against freezing in the standing column well during system heating operation.

2. The performance of SCW systems can be improved dramatically by introducing bleed. However, at higher bleed rates (greater than 15 % in this study), there is little further gain in performance. Also, the performance depends on the depth of water table.
3. As hydraulic conductivity increases, there is a trade-off between convective and advective heat transfer at the borehole wall-increasing advection through the wall reduces convection along the wall. This means that a very high hydraulic conductivity does not necessarily result in better performance than moderate values.

6. SIMPLIFIED MODEL FOR STANDING COLUMN WELL SYSTEMS

The amount of time required to simulate a full year using the detailed numerical model described in Chapter 4 is rather large. It takes a 1.8GHZ 586 machine two weeks to finish an annual simulation. Due to the computationally intensive nature of the calculations required for the detailed study of standing column well performance, it is unlikely that the detailed model would be directly suitable for use in design tools of energy calculation programs. Therefore, a simplified model has been developed and validated against the detailed model and experimental data.

In this simplified model, several assumptions are made regarding the domain outside the borehole in standing column well systems:

- homogenous and isotropic aquifer;
- no explicit consideration of density dependent flow;
- no vertical heat or water flow (the effect of vertical flow is implicitly accounted for by enhanced thermal conductivity);
- zero natural ground temperature gradient (one-dimensional model).

The first assumption of homogenous and isotropic aquifer is necessary for this simplified one-dimensional (radial) model. The term isotropic is used to describe materials where

the permeability or conductivity is same in all different directions (Domenico and Schwartz 1990). A porous material is homogeneous if the permeability is the same from point to point (Domenico and Schwartz 1990). While modeling complex anisotropic geometries is beyond the scope of this thesis, a limiting case representing a borehole where all bleed flow comes through a large fracture is considered here. Figure 6-1 shows two possible limiting cases for the standing column well system:

Case A: Homogeneous flow around a borehole surrounded by a porous medium.

Case B: Groundwater flow in an impermeable medium with a large fracture in it.

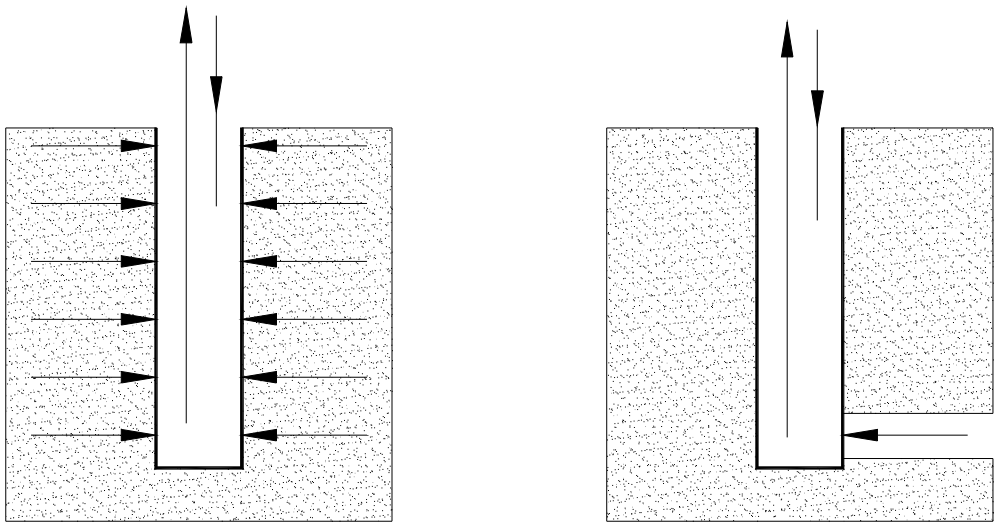

Case A Case B

Figure 6-1 Two limiting cases for standing column well system

The first limiting case (i.e., case A in Figure 6-1) regards the surrounding rock as a homogenous, isotropic, and porous. The groundwater flow is evenly spread over the surrounding rock. This continuum approach is a conceptually simple and commonly used approach in estimated flow and transport in hydrogeology. Much research has shown that

flow in a fractured medium can be reasonably well represented by flow through a porous medium (Singhal and Gupta 1999).

The second limiting case (i.e., case B in Figure 6-2) regards the ground as completely impermeable, but with a fracture zone in it. All groundwater passes through this fracture and enter into the borehole.

Heterogeneous and anisotropic aquifers are beyond the scope of this research because of its complexity. The simplified model to be developed in this chapter will focus on the first limiting case. The second limiting case will be simply solved by "by-pass" approximation, which will be discussed in section 6.3.

The assumption of radial flow and no heat or water flow in the vertical direction is reasonable if the well depth is much larger than the well diameter, which is the case for most practical applications. The vertical water flow may be considered negligible. Actually, both the temperature and hydraulic gradients in the horizontal direction are much larger than those in the vertical direction.

Both the natural groundwater movement and the induced groundwater flow by "bleed" are considered in this simplified model. An "enhanced" thermal conductivity is used to consider the natural water flow caused by the pumping and buoyancy. However, bleed-driven advection is represented explicitly. When bleed occurs, the effect of bleed is

superimposed on top of the effects of pumping and buoyancy. The simplified one-dimensional numerical model to be described in this chapter has two sub-models:

- Thermal and fluid energy transport in the surrounding rock are handled by a one-dimensional (radial) finite difference model, which solves a general one-dimensional advection-diffusion equation with enhanced thermal conductivity. Borehole wall temperature is determined by this model.
- Thermal energy transport in the borehole is handled by a thermal network model, where the fluid in the borehole is treated as one lump. Water temperature back to heat pump is calculated by this model.

First, the simplified model is presented, and then this simplified model is validated against the detailed model and experimental data.

6.1. Simplified one-dimensional model

In this section, the governing energy equation in the surrounding rock is given first, and then borehole heat transfer including short-circuiting is analyzed. Second, numerical solutions to the problem are provided. Finally, the enhanced thermal conductivity, which is used in the simplified model to consider groundwater movement in the absence of bleed, is discussed.

6.1.1. Governing energy equation

Assuming that the vertical heat and water flow can be neglected in standing column well systems whether or not bleed is occurring, then the one-dimensional energy equation (in radial direction) in a porous medium can be reduced from Equation (4.10):

$$\alpha \frac{\partial T}{\partial t} + \beta V_r \frac{\partial T}{\partial r} = \frac{1}{r} \frac{\partial}{\partial r} \left(\Gamma r \frac{\partial T}{\partial r} \right) \tag{6.1}$$

$$\alpha \frac{\partial T}{\partial t} + \beta V_r \frac{\partial T}{\partial r} = \Gamma \left[\frac{\partial^2 T}{\partial r^2} + \frac{1}{r} \frac{\partial T}{\partial r} \right] \tag{6.2}$$

α, β, Γ are given :

$$\alpha = n\rho_l C_{pl} + (1-n)\rho_s C_{ps} \tag{6.3}$$

$$\beta = \rho_l C_{pl} \tag{6.4}$$

$$\Gamma = k_{eff} = nk_l + (1-n)k_s \tag{6.5}$$

Where k_{eff} is the effective thermal conductivity (W/m-K [Btu/hr-ft-ºF]);

n is the porosity of the surrounding rock;

k is the thermal conductivity (W/m-K [Btu/hr-ft-ºF]) ;

ρ is the density (kg/m^3 [lbm/ft^3]);

C_p is the specific heat (J/kg-K [Btu/lbm-ºF]);

V_r is the average linear groundwater velocity vector (m/s [ft/s]);

and subscripts: l is water;

s is solid (water saturated rock).

6.1.2. Groundwater velocity

In this simplified one-dimensional model, the average groundwater velocity, V_r, at location r_i is not determined from Darcy's law, as it is in the detailed two-dimensional model. Instead, assuming homogeneous conditions in the surrounding rock, conservation of mass may be used to calculate this velocity in bleed cases.

$$V_{ri} = -\frac{1}{n}\frac{\dot{m}r}{\rho A} = -\frac{1}{n}\frac{\dot{m}r}{\rho}\frac{1}{2\pi r_i L} \qquad (6.6)$$

Where n is the porosity of the surrounding rock;

$\dot{m}$ is the mass flow rate out of the borehole (kg/s[lbm/sec]);

ρ is the water density (kg/m^3 [lbm/ft^3]);

L is the borehole depth (m [ft]);

r_i is the radius at location i (m [ft]);

r is the bleed rate (-).

In this one-dimensional model, there is an assumption that the groundwater is always flowing into the borehole when bleeding. Therefore, the sign of the groundwater velocity, V_r, is always negative.

In the absence of bleed, the average groundwater velocity, V_r, is set to be zero, which means the second term (advective term) in the left side of Equation (6.1) will be zero. This effectively turns the advection-diffusion equation into a pure diffusion (heat conduction) equation again.

Because this is a one-dimensional simplified model, the influence of the hydraulic conductivity cannot directly be taken into account. It must be assumed that the specified bleed can be obtained without significant drawdown of the water table. This is a key assumption that should be checked with an *in-situ* well drawdown test. A preliminary calculation of well drawdown for hydraulic conductivities of interest in SCW systems shows it to be typically less than one meter, which is very small compared to the below-water-table well depth.

6.1.3. Boundary conditions

To solve the given partial differential equation, necessary boundary conditions are established:

- A constant temperature is set at the far field ($R_\infty = 65$ m[+]), $T_{far} = 12$ ˚C, for the example case here.
- The heat flux q (W/m^2) is set at the borehole wall. This heat flux is determined using the borehole resistance so that:

$$q = \frac{T_b - T_f}{R_b} \cdot \frac{1}{2\pi r_b L} \qquad (6.7)$$

Where q is the heat transfer flux applied to the ground per unit area of the borehole at the given time step (W/m^2 [Btu/ft^2-hr]) (a positive q value implies heat extraction in winter);

T_f is the average water temperature (ºC [ºF]);

[+] The value of R_∞ is taken from a sensitivity analysis of domain radius for 10-year simulation.

R_b is the borehole resistance (K/(W/m) [hr-ft-ºF/Btu]);

r_b is the borehole radius (m [ft]);

L is the borehole depth (m [ft]).

Figure 6-2 shows a schematic drawing of the one-dimensional model for the standing column well, assuming that groundwater is always flowing inwards. There is a heat flux applied to the borehole wall per unit area of the borehole. The solution domain to get the

borehole wall temperature is the surrounding rock in the shaded region, i.e., from the borehole wall to the far field. The partial differential equation (6.1) can be numerically solved with the given boundary conditions. In this study, the fully implicit Finite Difference Method (FDM) is used.

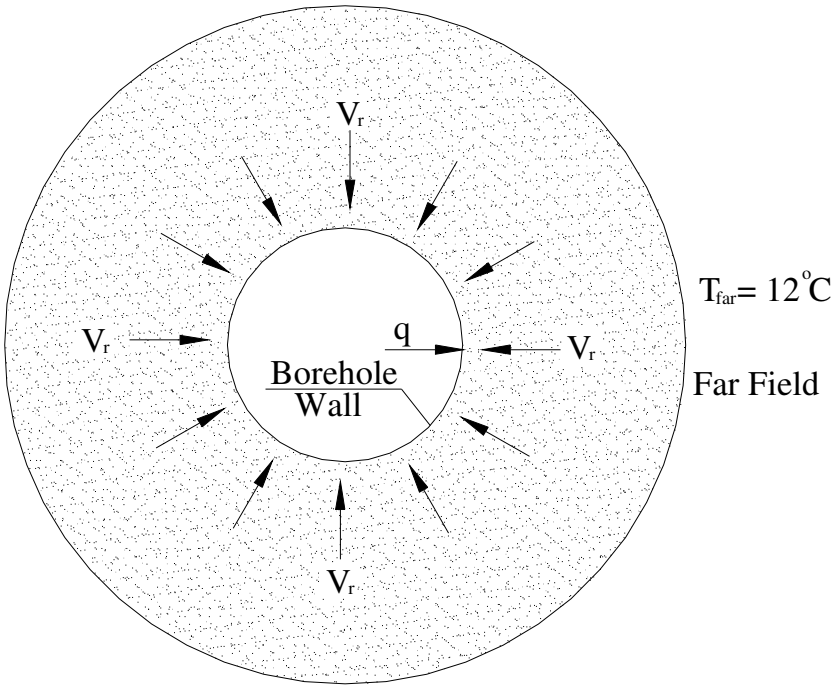

Figure 6-2 Schematic drawing showing 1-D model for the SCW system

(with boundary conditions)

6.1.4. Borehole heat transfer

If the water temperature in the borehole is a linear function of the borehole depth, the arithmetic mean value of water temperatures (leaving and returning to the well) might be used to approximately represent the temperature of the water in the whole borehole. This approximation is commonly used in the simulation and design of U-tube ground heat exchangers. From the previous detailed two-dimensional model, a nearly linear relationship may be shown in cases where there is no natural ground temperature gradient. In this simplified one-dimensional model, a mean surrounding ground temperature is used, rather than a local ground temperature that varies with the depth.

Figure 6-3 shows water temperature variation along borehole depth without bleed. And Figure 6-4 shows water temperature variation along borehole depth with bleed. These two figures verify there is a nearly linear relationship between water temperatures and the borehole depth. All the data in Figures 6-3 and 6-4 were generated by 400-hour simulation of the detailed model. All the data correspond to the last time step. The natural ground temperature gradient was set to be zero, and all the other parameters were set up according to the base case in section 4.3.

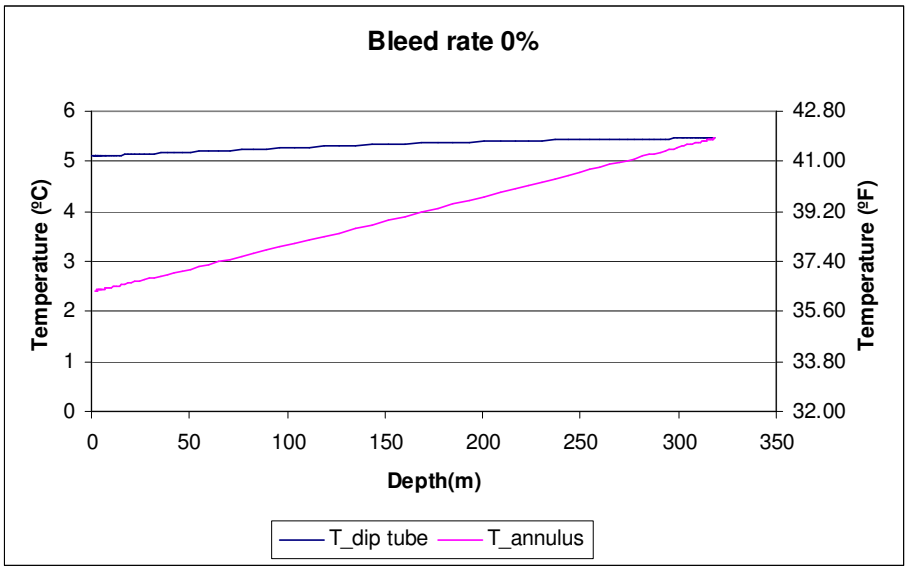

Figure 6-3 Water temperature variation along borehole depth without bleed

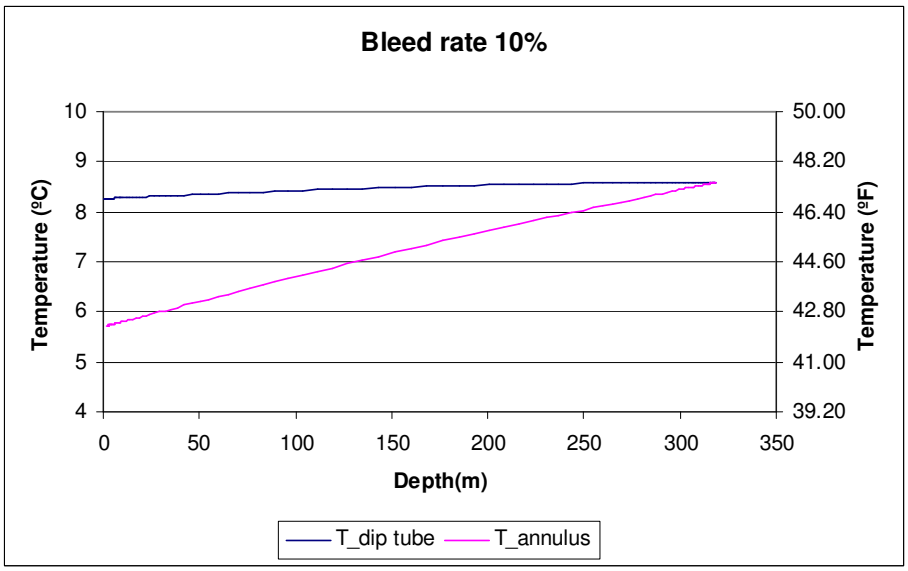

Figure 6-4 Water temperature variation along borehole depth with bleed

After considering the bleed, the average water temperature in the standing column well, T_f, is given as:

$$T_f = \frac{(1-r)T_{fi} + rT_{gw} + T_{fo}}{2} \tag{6.8}$$

Where T_{fo} is the water temperature leaving the well (returning to the heat pump) (ºC [ºF]);

T_{fi} is the water temperature returning to the well (ºC [ºF]);

T_{gw} is the temperature of groundwater entering into the well (ºC [ºF]);

T_f is the average water temperature in the well (ºC [ºF]).

Rearranging equation (6.8):

$$T_{fo} = 2T_f - (1-r)T_{fi} - rT_{gw} \tag{6.9}$$

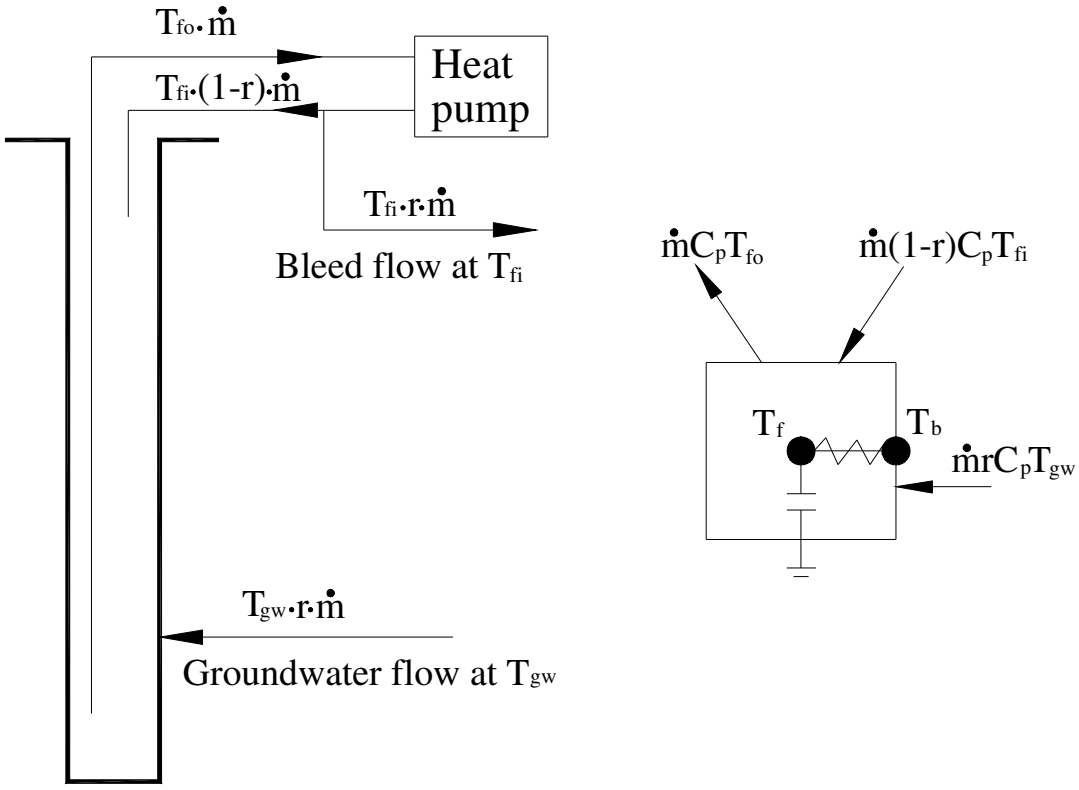

Figure 6-5 The simplified thermal borehole model

The energy balance can be formulated for the borehole, assuming that the water in the borehole is well mixed and there is only one lump in the borehole, where the lump includes water inside the dip tube (Figure 6-5). The heat transfer (short-circuiting) due to temperature difference between the water flowing up in the dip tube and the water flowing down in the annulus will be considered in the next section.

$$mC_p \frac{dT_f}{dt} = \dot{m}(1-r)C_p T_{fi} + \dot{m}rC_p T_{gw} - \dot{m}C_p T_{fo} + \frac{T_b - T_f}{R_b} \cdot L \qquad (6.10)$$

Equation (6.10) states that the net energy entering the well by advection plus the energy entering the well by convection equals the time rate of change of internal energy within the well.

There is an assumption mentioned at the beginning of this chapter that surrounding rock is homogenous, which means that groundwater enters into the well with the borehole wall temperature, T_b. Therefore, $T_{gw} = T_b$. Then, substituting Equation (6.9) into Equation (6.10) and rearranging:

$$mC_p \frac{dT_f}{dt} = 2\dot{m}(1-r)C_p T_{fi} + 2\dot{m}rC_p T_b - 2\dot{m}C_p T_f + \frac{T_b - T_f}{R_b} \cdot L \qquad (6.11a)$$

Let T_{f_old} denote the known value of T_f at time *t*. The quantity T_f stands for the unknown temperature at time $t + \Delta t$. The term on the left side of Equation (6.11a) can be discretized as:

$$mC_p \frac{dT_f}{dt} = mC_p \frac{T_f - T_{f\_old}}{\Delta t} \qquad (6.11b)$$

Substitute Equation (6.11b) into Equation (6.11a) and rearrange:

$$T_f = \frac{\frac{\dot{m}C_p R_b}{L}\left[2(1-r)T_{fi} + 2rT_b\right] + \frac{R_b}{L}mC_p\frac{T_{f\_old}}{\Delta t} + T_b}{1 + \frac{2\dot{m}C_p R_b}{L} + \frac{R_b}{L}mC_p\frac{1}{\Delta t}} \tag{6.11c}$$

After the average water temperature, T_f, is calculated from Equation (6.11c), the water temperature leaving the well, T_{fo}, can be obtained from Equation (6.9)

$$T_{fo} = 2T_f - (1-r)T_{fi} - rT_{gw} \tag{6.9}$$

Where T_{fo} is the water temperature leaving the well (returning to the heat pump) (ºC [ºF]);

T_{fi} is the water temperature returning to the well (ºC [ºF]);

T_f is the average water temperature at the time step $t + \Delta t$ (ºC [ºF]);

T_{f_old} is the average water temperature at the previous time step (ºC [ºF]);

T_b is the borehole wall temperature (ºC [ºF]), which can be obtained from the numerical solution of Equation (6.1);

T_{gw} is the temperature of groundwater entering into the well (ºC [ºF]), in this simplified model, this temperature is set to be T_b;

r is the bleed fraction (-);

R_b is the borehole resistance (K/(W/m) [hr-ft-ºF/Btu]);

m is the mass of water in the standing column well (kg [lbm]);

r_b is the borehole radius (m [ft]);

L is the borehole depth (m [ft]);

$\dot{m}$ is the mass flow rate of water through the heat pump system (kg/s [lbm/sec]).

C_p is the specific heat of water (J/kg-K [Btu/lbm-ºF]);

Δt is the time increment(sec [sec]).

6.1.5. Short-circuiting

The configuration of pipes in a standing column well introduces a complication since there is a short-circuiting heat transfer within the standing column well due to temperature differences between the water flowing up in the dip tube and the water flowing down in the annulus.

In this section, first, calculation of the borehole resistance including short-circuiting resistance is described, and then the correction of the water temperature leaving the well (returning to the well) with the consideration of short-circuiting is discussed.

Borehole resistance

A thermal circuit is used to describe the local heat flow in the annular duct between the flow channels and the borehole wall in the SCW system, which is shown in Figure 6-6.

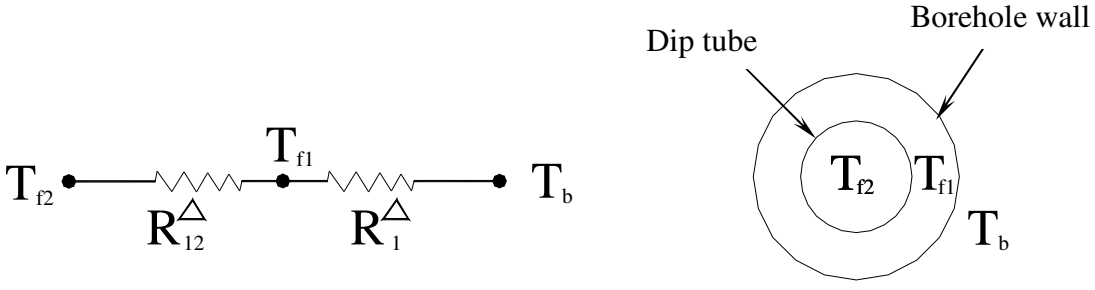

Figure 6-6 Cross-section of the borehole in SCW system and the corresponding thermal circuit

Where, T_w is the temperature of the borehole wall (ºC [ºF]);

T_{f1} is the temperature of the downward flowing water in the annulus (ºC [ºF]);

T_{f2} is the temperature of the upward flowing water in the dip tube (ºC [ºF]).

In Figure 6-6, the thermal resistance R_{12}^{Δ} between the inner and the outer flow channel consists of three parts:

- convective heat transfer resistance between the bulk water in the dip tube and the inner surface of the dip tube (K/(W/m) [hr-ft-ºF/Btu]);
- thermal resistance of the dip tube wall (K/(W/m) [hr-ft-ºF/Btu]);
- convective heat transfer resistance between the outer surface of the dip tube and the bulk water in the annular area (K/(W/m) [hr-ft-ºF/Btu]).

The thermal resistance R_1^{Δ} between the outer flow channel and borehole wall is composed of the convective heat transfer resistance between the water in the annulus and the borehole wall.

The Borehole resistance, R_b, may be determined by considering an application to the approach given by Hellström (1991) for a U-tube.

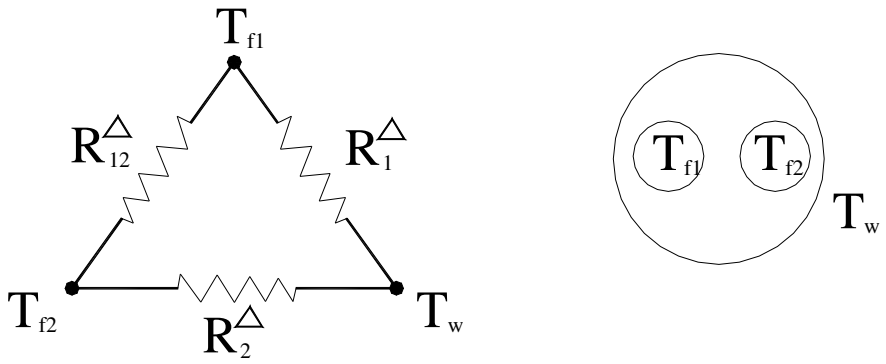

Figure 6-7 Thermal resistances of a Δ-circuit

The thermal resistances of Δ-circuit shown in Figure 6-7 are given by Hellström (1991):

$$R_1^{\Delta} = \frac{R_{11}^0 R_{22}^0 - (R_{12}^0)^2}{R_{22}^0 - R_{12}^0} \tag{6.12}$$

$$R_2^{\Delta} = \frac{R_{11}^0 R_{22}^0 - (R_{12}^0)^2}{R_{11}^0 - R_{12}^0} \tag{6.13}$$

$$R_{12}^{\Delta} = \frac{R_{11}^0 R_{22}^0 - (R_{12}^0)^2}{R_{12}^0} \tag{6.14}$$

Where, R_{mn}^0, the thermal resistance coefficients, are calculated approximately by representing each pipe with a line source. The steady-state heat flow problem is then solved by use of the superposition technique (Hellström 1991).

For the given thermal circuit in the SCW system shown in Figure 6-6, no direct connection exists between the inner flow channel and the borehole wall, which implies: $R_2^{\Delta} = \infty$, $R_{11}^0 = R_{12}^0$. Thus Equations (6.12) to (6.14) can be reduced to:

$$R_1^{\Delta} = R_{11}^0 \tag{6.15}$$

$$R_2^{\Delta} = \infty \tag{6.16}$$

$$R_{12}^{\Delta} = R_{22}^{0} - R_{11}^{0} \tag{6.17}$$

The fluid-to-ground thermal resistance, R_b, is obtained by setting $T_{f1} = T_{f2}$ (Hellström 1991). The resistance between the fluid temperature, T_f, and the borehole wall, T_b, then becomes R_1^{Δ} (Figure 6-6). So, the borehole resistance $R_b = R_1^{\Delta} = R_{11}^{0}$, where R_{11}^{0} is given by

$$R_{11}^{0} = \frac{1}{2\pi\lambda_b}\left[\ln\left(\frac{r_b}{r_{p1}}\right)\right] + R_{p1} \tag{6.18}$$

Where r_b is the radius of the borehole (m [ft]);

r_{p1} is the radius of pipe 1 (m [ft]);

R_{p1} is the thermal resistance between the fluid in pipe 1 and the material immediately outside pipe 1, and R_{p1} is equal to R_1^{Δ} in Figure 6-4 (K/(W/m) [hr-ft-ºF/Btu]).

Figure 6-6 shows that r_b is equal to r_{p1}, so Equation (6.18) can be reduced to:

$$R_{11}^{0} = R_{p1} \tag{6.19}$$

Substitute Equation (6.19) into $R_b = R_1^{\Delta} = R_{11}^{0}$. Finally, we have

$$R_b = R_{p1} = R_1^{\Delta} \tag{6.20}$$

Therefore, in the SCW system, the borehole thermal resistance without considering short-circuiting is given by:

$$R_b = R_1^{\Delta} = \frac{1}{2\pi r_b h_{borehole}} \tag{6.21}$$

The short-circuiting thermal resistance, R_{sc}, is equal to the thermal resistance, R_{12}^{Δ}, shown in Figure 6-6. The short-circuiting resistance is the sum of the dip tube interior film resistance, the pipe wall resistance, and the dip tube exterior film resistance. The correction for the short-circuiting phenomenon will be discussed soon.

The following equation is used to determine the inside convective heat transfer coefficient along the borehole wall:

$$h_{borehole} = Nu \frac{k_{water}}{D_{borehole}} \tag{6.22}$$

Where: $h_{borehole}$ is the heat transfer coefficient (W/m^2-K [Btu/hr-ft^2-ºF]);

k_{water} is the thermal conductivity of water (W/m-K [Btu/hr-ft-ºF]);

$D_{borehole}$ is the hydraulic diameter of borehole (m [ft]);

Nu is local Nusselt number.

The local Nusselt number (Nu) in Equation (6.22) is given by Bhatti and Shah (1987). The detailed discussions about convection heat transfer coefficient in the standing column well system were described in section 4.1.2.1.1.

$$Nu = \frac{(f/2)(\mathrm{Re}-1000)\,\mathrm{Pr}}{1+(f/2)^{1/2}[(17.42-13.77\,\mathrm{Pr}_t^{\,0.8})\,\mathrm{Re}_{\varepsilon}^{0.2}\,\mathrm{Pr}^{0.5}-8.48]} \tag{6.23}$$

Where: Pr is the Prandtl number;

$$\mathrm{Pr}_t = \begin{cases} 1.01 - 0.09\,\mathrm{Pr}^{0.36} & \text{for } 1 \le \mathrm{Pr} \le 145 \\ 1.01 - 0.11 \ln \mathrm{Pr} & \text{for } 145 < \mathrm{Pr} \le 1800 \\ 0.99 - 0.29(\ln \mathrm{Pr})^{1/2} & \text{for } 1800 < \mathrm{Pr} \le 12500 \end{cases};$$

Re_ε is the roughness Reynolds number, $\mathrm{Re}_\varepsilon = \dfrac{\mathrm{Re}\sqrt{f/2}}{D/\varepsilon}$;

ε is the height of the surface roughness(m [ft]).

To consider the short-circuiting phenomenon in the standing column well system, the proposed method is to correct the water temperature leaving the well (returning to the heat pump), T_{fo}, by the temperature difference caused by the short-circuiting as follows:

$$\Delta T_{sc} = \frac{q_{sc} L}{\dot{m}_w C_{p_w}} \tag{6.24}$$

Where ΔT_{sc} is the temperature difference caused by the short circuiting (ºC [ºF]);

q_{sc} is the short circuiting flux (W/m [Btu/hr-m]);

L is the borehole depth (m [ft]);

$\dot{m}_w$ is the mass flow rate of water through the heat pump system (kg/s [lbm/sec]);

C_{pw} is the specific heat of water (J/kg-K [Btu/lbm-ºF]).

The short-circuiting heat flux is calculated by an integral method, where the short-circuiting effect is considered in a general heat transfer equation from an element of differential depth. This equation is integrated over the entire length of the borehole. The detailed description of this integral method is given in Appendix D.

After considering the short-circuiting, the water temperature leaving the well (returning to the heat pump), T_{fo_sc}, can be obtained from:

$$T_{fo\_sc} = T_{fo} - \Delta T_{sc} \tag{6.25}$$

Where T_{fo} is the water temperature leaving the well (returning to the heat pump) without considering the short-circuiting (ºC [ºF]);

T_{fo_sc} is the water temperature leaving the well (returning to the heat pump) after considering short-circuiting (ºC [ºF]);

ΔT_{sc} is the temperature difference caused by the short circuiting (ºC [ºF]).

6.1.6. Solution of equations

The finite difference model applied to the surrounding rock is used to calculate the borehole wall temperature. The borehole model is used to get the water temperature leaving the well (water temperature back to the heat pump). To couple the borehole model and the finite difference model, the borehole model calculates the heat flux applied to the borehole wall. Then, this heat flux is used to set a boundary condition at the borehole wall in the finite difference model. In turn, the finite difference model calculates the borehole wall temperature and passes this back to the borehole model. The equations are then solved iteratively, repeating this process until convergence is reached, as shown in Figure 6-8.

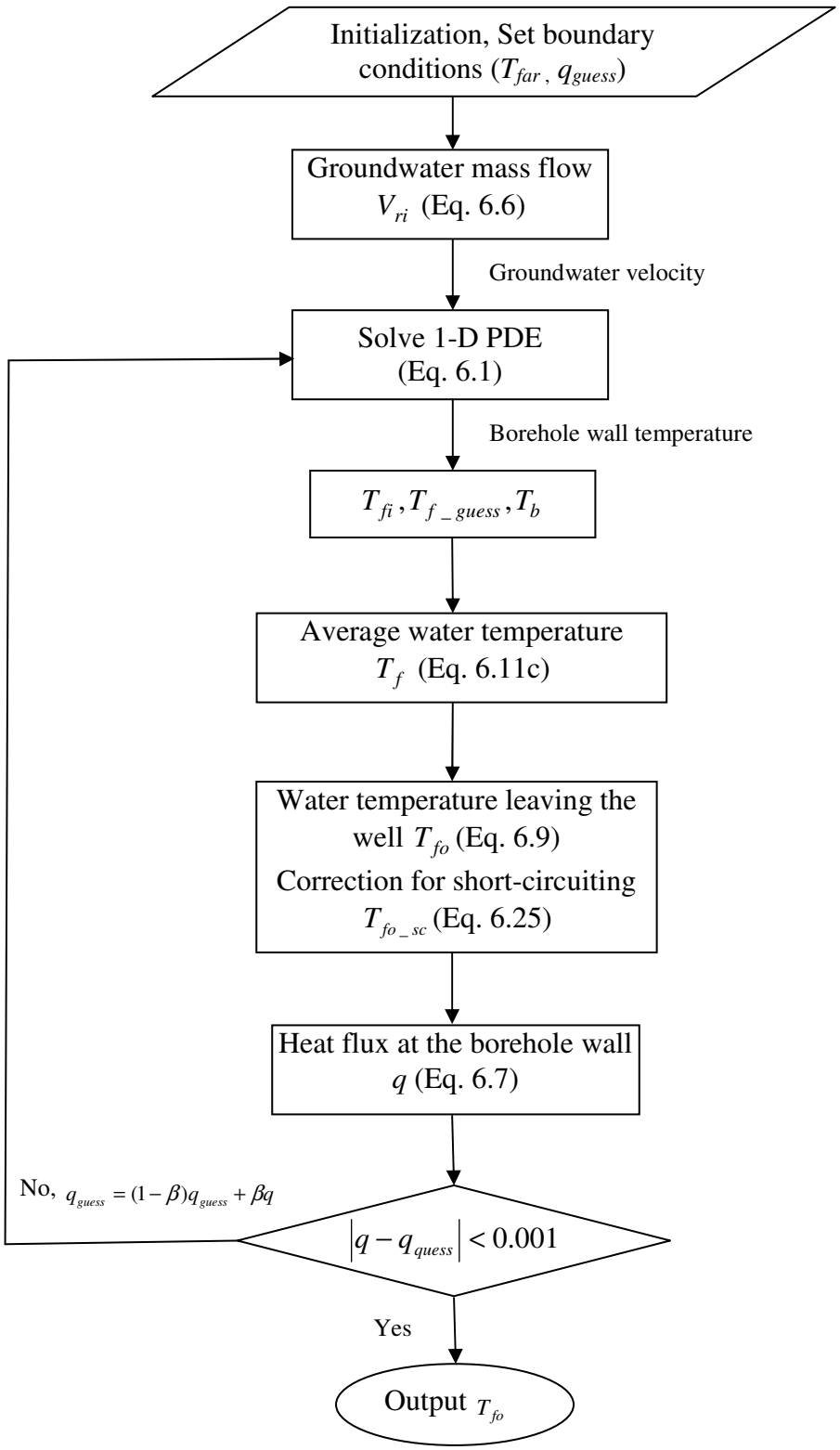

Figure 6-8 Flow chart for the simplified one-dimensional model

First, a guessed heat flux with other parameters is plugged into the finite difference model. Plugging the resulting temperature into the borehole model gives a new guess of the heat flux for this iteration step. The new guess of the heat flux might be used directly, except that experience has shown that the solution may diverge. Therefore, under-relaxation is used:

$$q_{guess} = (1-\beta)q_{guess} + \beta q \tag{6.26}$$

Where q is the heat transfer rate applied to the ground per unit area of the borehole (W/m^2 [Btu/ft^2-hr]);

q_{guess} is the guessed heat transfer rate applied to the ground per unit area of the borehole (W/m [Btu/ft^2-hr]);

β is the under-relaxation factor; a value of 0.01 has been found to work well for all cases.

The partial differential equation (6.1) is solved with the fully implicit Finite Difference Method (FDM). The solution of the discretization equations for this one-dimensional problem is obtained by the Thomas algorithm or the TDMA (TriDiagonal Matrix Algorithm). After conducting some grid independence calculations, the final grid size was chosen to be 130 as the best compromise between the accuracy and computational speed (see Figure 6-9). The numerical solution domain has a radius of 65 m, based on a sensitivity analysis of domain radius for a 10-year simulation. The grid is fine near the borehole wall (Δr = 5.67 mm) and expands in the direction of the far field.

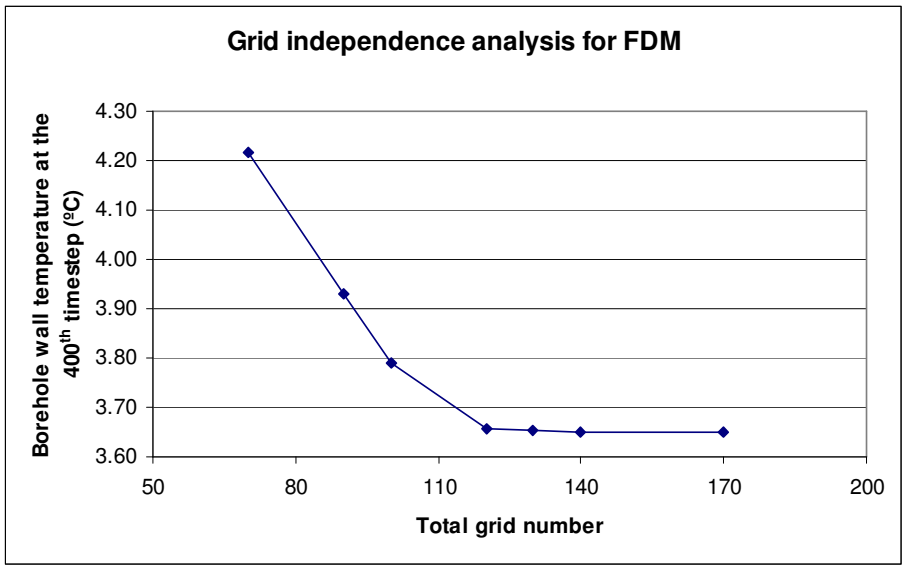

Figure 6-9 Sensitivity of borehole wall temperatures to the grid number in FDM

Solve Equation (6.1) by the Fully Implicit Finite Difference Method (FDM)

Recall the governing partial differential Equation (6.1):

$$\alpha \frac{\partial T}{\partial t} + \beta V_r \frac{\partial T}{\partial r} = \Gamma \left[\frac{\partial^2 T}{\partial r^2} + \frac{1}{r} \frac{\partial T}{\partial r} \right] \tag{6.1}$$

Rearrange:

$$\frac{\partial^2 T}{\partial r^2} + \left(\frac{1}{r} - \frac{\beta}{\Gamma} V_r \right) \frac{\partial T}{\partial r} = \frac{\alpha}{\Gamma} \frac{\partial T}{\partial t} \tag{6.27}$$

The fully implicit finite difference method is utilized in this study, so that all temperatures on the left hand side of Equation (6.27) should be evaluated at the next time step ($p+1$ time step). This method is unconditionally stable. After discretization by the fully implicit finite difference method, Equation (6.27) can be changed into:

$$\frac{\dfrac{T^{p+1}(I+1)-T^{p+1}(I)}{\Delta(I)}-\dfrac{T^{p+1}(I)-T^{p+1}(I-1)}{\Delta(I-1)}}{\Delta(I)}+\left(\frac{1}{r_i}-\frac{\beta}{\Gamma}V_{ri}\right)\frac{T^{p+1}(I+1)-T^{p+1}(I-1)}{\Delta(I)+\Delta(I-1)}=\frac{\alpha}{\Gamma}\frac{T^{p+1}(I)-T^{p}(I)}{\Delta t} \tag{6.28}$$

Given $\eta_1=\dfrac{\Gamma\Delta t}{\alpha\Delta(I)^2}$, $\eta_2=\dfrac{\Gamma\Delta t}{\alpha(\Delta(I)+\Delta(I-1))}$;

$\lambda=\dfrac{\beta\Delta t}{\alpha(\Delta(I)+\Delta(I-1))}$, $\gamma=\dfrac{\Gamma\Delta t}{\alpha(\Delta(I)+\Delta(I-1))}$;

p represents the previous time step;

$p+1$ represents the current time step.

Equation (6.28) can be simplified to:

$$(1+\eta_1+\eta_2)T^{p+1}(I)=T^{p}(I)+\left(\eta_2-\gamma\frac{1}{r_i}+\lambda V_{ri}\right)T^{p+1}(I-1)+\left(\eta_1+\gamma\frac{1}{r_i}-\lambda V_{ri}\right)T^{p+1}(I+1) \tag{6.29}$$

Where $\Delta(I)$ is the grid size in the radial direction at location i;

Δt is the time increment (sec);

r_i is the radius at location i (m [ft]);

V_{ri} is the velocity of groundwater at location i (m/s [ft/sec]).

When Equation (6.28) is applied at the boundary node (i.e., the borehole wall, $i=1$), there is an equation to describe the Neumann boundary condition, where the flux at the boundary is specified.

$$q=-\Gamma\frac{T^{p+1}(I-1)-T^{p+1}(I+1)}{2\Delta(I)} \tag{6.30a}$$

$$\Rightarrow \qquad T^{p+1}(I-1) = T^{p+1}(I+1) - \frac{2q \cdot \Delta(I)}{\Gamma} \tag{6.30b}$$

Substituting Equation (6.30b) into Equation (6.29):

$$\begin{aligned}(1+\eta_1+\eta_2)T^{p+1}(I) = T^{p}(I) &+ \left(\eta_2 - \gamma\frac{1}{r_i} + \lambda V_{ri}\right)\left(T^{p+1}(I+1) - \frac{2q \cdot \Delta(I)}{\Gamma}\right) \\ &+ \left(\eta_1 + \gamma\frac{1}{r_i} - \lambda V_{ri}\right)T^{p+1}(I+1)\end{aligned} \tag{6.31}$$

Where Γ is the effective thermal conductivity given by Equation (6.5);

I is equal to 1 in this equation.

The solution of the discretization equations for this one-dimensional problem is obtained by the Thomas algorithm or the TDMA (*TriDiagonal Matrix Algorithm*).

6.1.7. One dimensional numerical model with enhanced thermal conductivity

Three different effects of water on the heat transfer in standing column well systems may be differentiated:

1. Water filling the pores of otherwise dry rock increases the thermal conductivity from the value associated with dry rock. The water is static and no advection occurs. This increased thermal conductivity is referred to as the "effective thermal conductivity".
2. The pumping of water in and out of the well and buoyancy both drive some water flow in the surrounding rock. With this natural water flow, the advection heat transfer augments the conductive heat transfer. Although this is now an advection-conduction problem, it is possible to treat it as only having conduction by using an "enhanced thermal conductivity". This is the value of thermal conductivity

that, in a pure conduction analysis, approximates the heat transfer rate in the convection-diffusion process.

3. When bleed occurs, the advection effects can become quite significant, and it is no longer feasible to treat the process as a pure-conduction process with an increased thermal conductivity. Therefore, the simplified numerical model represents bleed-driven advection explicitly, but simply, by assuming it is one-dimensional and the water moves only in the inward direction.

Equation (6.6), utilized by the simplified one-dimensional numerical model necessitates that, when the bleed rate is zero, the advection term in the energy equation will be reduced to zero. However, since we still wish to account for the increased heat transfer due to pumping and buoyancy effects, the simplified model uses an enhanced thermal conductivity. Then, when bleed occurs, the effect of bleed is superimposed on top of the effects of pumping and buoyancy.

Accordingly, it is necessary to have some ways of estimating the enhanced thermal conductivity. Three procedures, as summarized in Figure 6-10, are proposed.

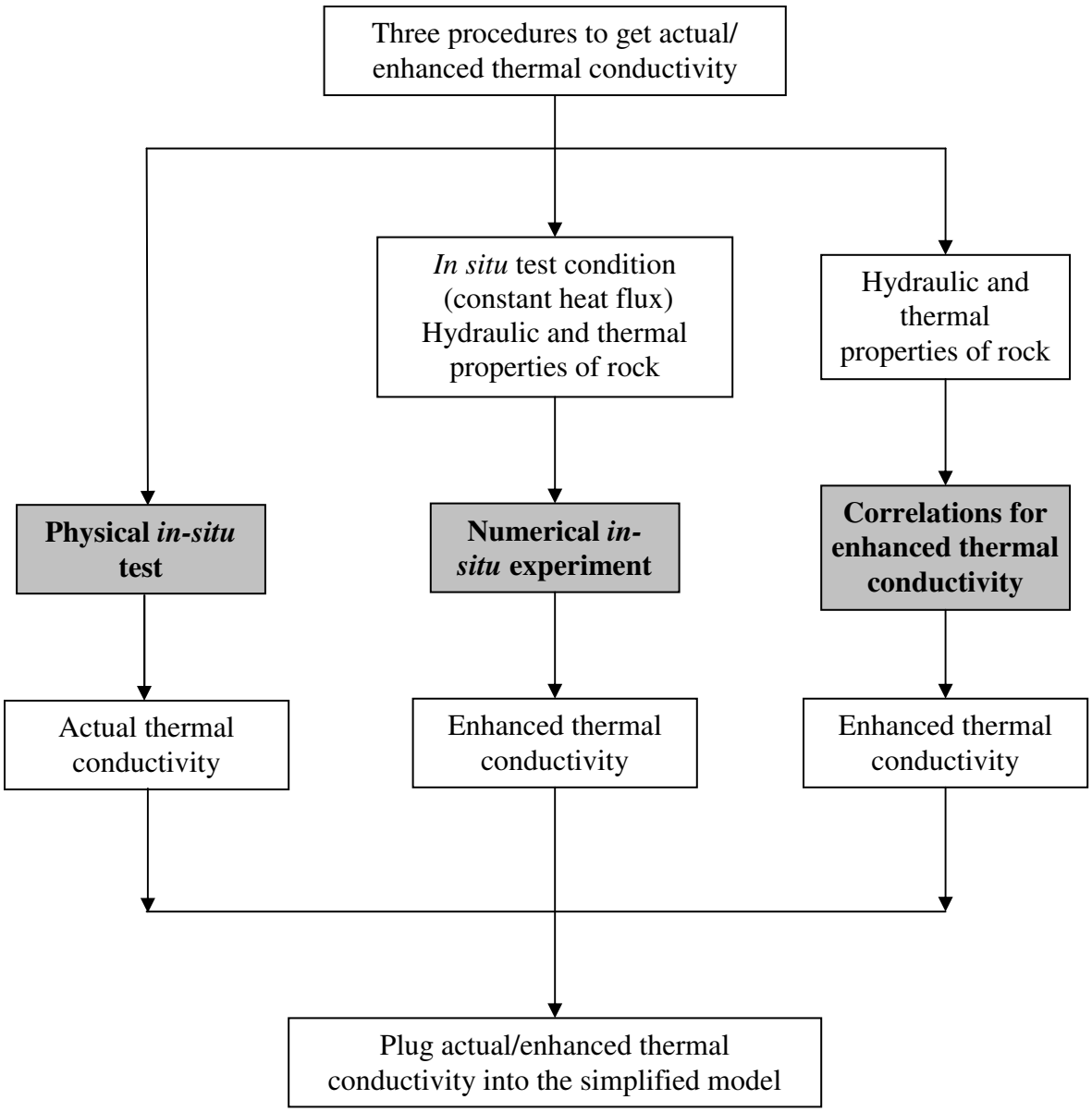

Figure 6-10 The flow chart to get actual /enhanced thermal conductivity

The physical *in-situ* test (Austin et al. 2000) is the best way to estimate the actual enhanced thermal conductivity. The temperature response to a pulse heat input, typically of duration 50 hours, is inversely analyzed to estimate the thermal conductivity. The analysis assumes only conduction, so the estimated value under conditions with

groundwater flow is the enhanced thermal conductivity. If an *in-situ* test of thermal conductivity is performed, the measured thermal conductivity at the well site under the influence of groundwater movement may be estimated and directly plugged into the simplified model.

A second approach would be appropriate if the effective thermal conductivity and hydraulic conductivity are known or estimated. Then, to find the enhanced thermal conductivity a "numerical *in-situ* experiment" might be run using the detailed numerical model described in Chapter 4. This would be done by numerically simulating the temperature response to a pulse heat input, again of duration approximately 50 hours. As in the above step, the enhanced thermal conductivity is estimated by inversely analyzing the temperature response.

A third approach would be to perform a series of numerical *in-situ* tests, then correlate the results. An enhancement factor (ratio of enhanced thermal conductivity to effective thermal conductivity) may be fitted as a function of thermal conductivity and hydraulic conductivity. Then, the enhanced thermal conductivity found with the correlation can be directly used in this simplified model. A correlation for enhancement factor of thermal conductivity is given in the Appendix E.

The simplified numerical model with enhanced thermal conductivity was first validated against the detailed model developed in Chapter 4.

A set of annual simulations has been made by using one year's worth of hourly building loads as thermal boundary conditions. The building loads are determined by using building energy simulation software (BLAST, 1986). The building types selected for this study are an office, school, and motel. The building loads have been calculated for three locations (including Boston, MA, Tulsa, OK, and Houston, TX) with typical meteorological weather data. There are several assumptions have been made to determine the annual building loads (Table 6-1). Further details of the building, systems and loads are given by Yavuzturk and Spitler (2000), and Chen (1996).

Table 6-1 Some information for determining building loads*

	Office	**Motel**	**School**
Areas	1,320 m^2 (14,205 ft^2)	710 m^2 (7,646 ft^2)	2,022 m^2 (21,766 ft^2)
Number of thermal zones	8	12	15
People load	70% radiant heat gain of 131.9 W (450 Btu/hr)	70% radiant heat gain of 104 W (355 Btu/hr)	70% radiant heat gain of 131.9 W (450 Btu/hr)
Equipment plug load	11.8 W/m^2 (1.10 W/ft^2)	7.08W/m^2 (0.66 W/ft^2)	2 W/m^2 (0.186 W/ft^2)
Lights load	varied between 10.04 W/m^2(0.93 W/ft^2) and 15.88 W/m^2(1.48 W/ft^2)	varied between 5.38 W/m^2 (0.5 W/ft^2) and 18.3W/m^2 (1.70 W/ft^2)	8.61 W/m^2 (0.80 W/ft^2)
Windows	Double pane and single pane with varied shading coefficient	Double pane with shading coefficient of 0.88 and overall U factor of 3.80 W/m^2-K (0.67 Btu/hr-ft^2-ºF)	Double pane with shading coefficient of 1.00 and overall U factor of 6.25 W/m^2-K (1.1 Btu/hr-ft^2-ºF)
Exterior wall	Brick construction	Wood frame construction with overall U factor of 0.613 W/m^2-K (0.108 Btu/hr-ft^2-ºF)	Concrete construction with overall U factor of 1.64 W/m^2-K (0.288 Btu/hr-ft^2-ºF)

* Schedules for people occupancy, lighting, and equipment are specified.

The design data for the well comes mostly from the standing column well used by Mikler (1993). All the parameters used in the simulation are given in Tables 4-1 and 4-2. This well has a dip tube (suction tube) extending to very near the bottom of the well and the

discharge from the heat pump system is near the top. The ground conditions are assumed to be similar to those in the northeast of the U.S.

Totally, 34 different cases with bleed rates between 0 % and 30 %, borehole diameters of 0.14 m (5.5 in) and 0.15 m (6 in), borehole depths of 240 m (787 ft) and 320 m (1050 ft), and thermal/hydraulic conductivities shown in Table 6-2 have been analyzed.

The enhanced thermal conductivities for these cases are obtained from the previously described "numerical *in-situ* experiment". The resulting enhanced thermal conductivities are summarized in Table 6-2. Then, the enhanced thermal conductivities are used in the simplified one-dimensional numerical model (SCW1D) to perform a one year simulation with hourly time step. The maximum and minimum water temperatures back to the heat pump for the year, calculated by the simplified model, are compared to those calculated by the detailed model. The results are shown in Figures 6-11 and 6-12. Points lying along the line show perfect agreement between these two models. The relatively small errors indicated that the simplified model is reasonably accurate. However, on a 2.8 GHz Pentium PC, the detailed model took approximately 7 days to perform the annual simulation; the simplified model took less than two seconds!

Table 6-2 Enhanced thermal conductivity from numerical *in-situ* experiment

Hydraulic conductivity (m/s [gal/day/ft^2])	**Effective thermal conductivity ($k_{effective}$) (W/m-K [Btu/hr-ft-°F])**	**Enhanced thermal conductivity ($k_{enhanced}$) (W/m-K [Btu/hr-ft-°F])**
7.0E-05 (148.23)	1.97 (1.14)	2.41 (1.39)
5.0E-04(1057.79)	1.97(1.14)	2.98(1.72)
1.0E-03 (2117.57)	1.97 (1.14)	3.68 (2.12)
1.0E-05 (21.18)	2.33 (1.34)	2.64 (1.52)
7.0E-05 (148.23)	2.33 (1.34)	2.73 (1.57)
1.0E-04 (211.76)	2.33 (1.34)	2.78 (1.60)
2.5E-04 (529.39)	2.33 (1.34)	3.00 (1.73)
3.5E-05(74.12)	3.27(1.89)	3.48(2.01)
7.0E-05 (148.23)	3.27 (1.89)	3.55 (2.05)
2.5E-04 (529.39)	3.27 (1.89)	3.94 (2.27)
7.0E-05 (148.23)	4.78 (2.76)	5.26 (3.03)
1.0E-04 (211.76)	4.78 (2.76)	5.36 (3.09)

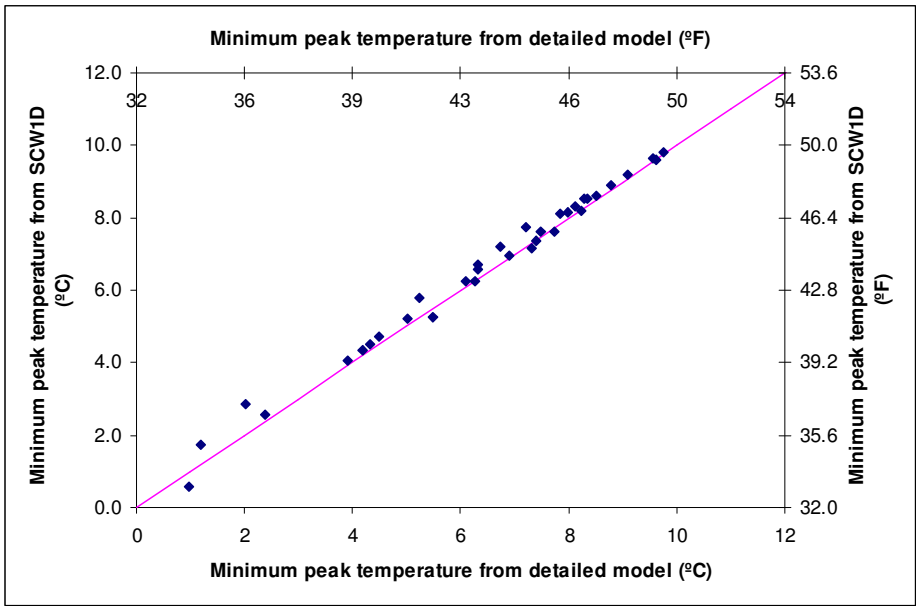

Figure 6-11 Comparison of minimum temperatures back to the heat pump in different models

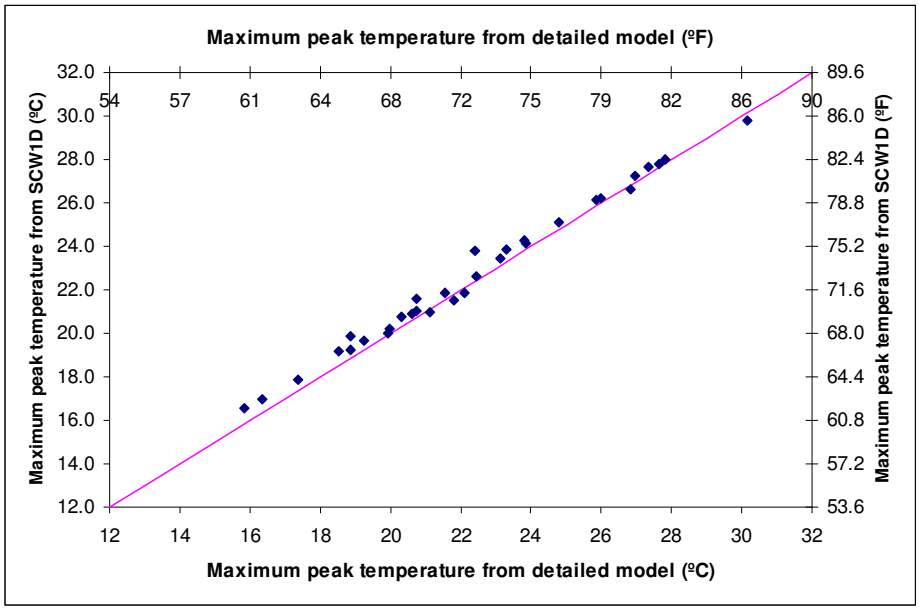

Figure 6-12 Comparison of maximum temperatures back to the heat pump in different models

The biggest errors between the detailed model and the simplified model occur for the cases with shallower depth (240 m). This is presumed to be caused by end effects, which become more significant at reduced depths in the detailed two-dimensional model. The simplified one-dimensional model cannot consider this effect.

The data show a reduction in temperature error with increasing bleed rate. This might be explained by the way the velocity term is treated in Equation (6.6).

$$V_{ri} = -\frac{1}{n}\frac{\dot{m}r}{\rho A} = -\frac{1}{n}\frac{\dot{m}r}{\rho}\frac{1}{2\pi r_i L}$$

In the simplified one-dimensional model, the groundwater is assumed to be always flowing into the borehole when bleeding. So, the sign of the groundwater velocity, V_r, is always negative. However, based on the numerical solutions of the governing two-

dimensional partial differential equation of head (see Chapter 4), this assumption is valid only if the bleed rate is large (i.e., greater than 5 % in the base case). In the cases with bleed rate less than 5 %, there is a point where the groundwater velocity is zero. Above this point, the sign of the groundwater velocity, V_r, is positive, and below this point the sign is negative.

This simplified model is a one dimensional (radial) model, which cannot account for the vertical ground temperature gradient. Currently, mean surrounding ground temperature is used in the model. Simulation results from the simplified model with ground temperature gradient of 0.3 ºC/100m (0.17 ºF/100 ft), 0.6 ºC/100m (0.33 ºF/100 ft), and 1.8 ºC/100 m (0.99 ºF/100 ft), are compared with results from the detailed model. Figure 6-13 compares the minimum exiting water temperatures from the well in the simplified model with temperatures in the detailed model. The results show that ground temperature gradient does cause the difference, in particular when gradient is large. However, when gradient is less than 0.6 ºC/100 m (0.33 ºF/100 ft), the difference is less than 0.2 ºC (0.36 ºF), and could be neglected.

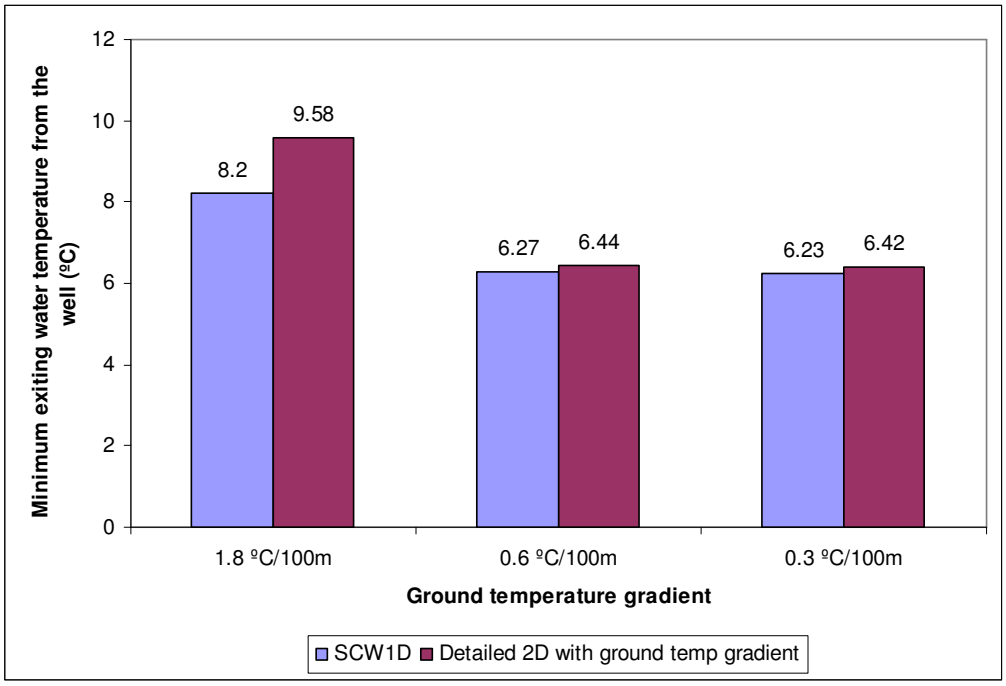

Figure 6-13 Comparison of the minimum exiting water temperatures from the well in different models with ground temperature gradient

6.2. Experimental validation

The simplified one-dimensional model is validated against the same two data sets, which were used to validate the detailed two-dimensional model in Chapter 4. The first data set is for non-bleed operation of one SCW system at Pennsylvania State University (Mikler 1993), and the second data set is for bleed operation of the SCW system at the Haverhill library, Massachusetts (Henderson 2003). The same validation procedure for the detailed model described in Chapter 4 is used in this Chapter. Water temperatures back to the heat pump are used to evaluate the performance of the SCW system.

Tables 6-3 and 6-4 give values of the enhanced rock thermal conductivity for the simplified model in these two data sets. These two enhanced thermal conductivities are obtained from "numerical *in-situ* experiments".

Table 6-3 Rock thermal conductivity for different models using Mikler's data

Model	Rock thermal conductivity used in the models (W/m-K [Btu/hr-ft-°F])
Detailed two-dimensional numerical model	3.0 (1.73)
Simplified one-dimensional numerical model	3.80 (2.19) (Enhanced thermal conductivity)

Table 6-4 Rock thermal conductivity for different models using Haverhill data

Model	Rock thermal conductivity used in the models (W/m-K [Btu/hr-ft-°F])
Detailed two-dimensional numerical model	2.32 (1.34)
Simplified one-dimensional numerical model	2.71 (1.56) (Enhanced thermal conductivity)

Tables 6-3 and 6- 4 show that the values of thermal conductivity used in the detail model are smaller than those from the simplified model. This could be explained as followings. The advection-diffusion equation used in the detailed model can explicitly account for the influence from any groundwater movements. The groundwater velocity field was obtained by solving the head equation. The advection heat transfer from groundwater is considered by the advection term (i.e. , $\rho_l C_{pl} V_i \frac{\partial T}{\partial x_i}$). The thermal conductivity used in the detailed model is the *effective* thermal conductivity, which just considers the porosity of rock. Actually, an effective thermal conductivity accounts for the volume fractions

and conductivities of the individual phases (i.e., water and dry rock). On the contrary, the thermal conductivity used in the simplified models is *enhanced* thermal conductivity, which considers natural groundwater movements because of pumping and buoyancy.

Comparisons of temperatures back to the heat pump for the simplified model (SCW1D), the detailed model and Mikler's data (Milker 1993) are shown in Figures 6-14 and 6-15 for the cooling mode and heating mode respectively. There is a good agreement between the models and the experimental data in non-bleed operation. This validation shows that the simplified model can be used to adequately simulate the standing column well systems in non-bleed operation.

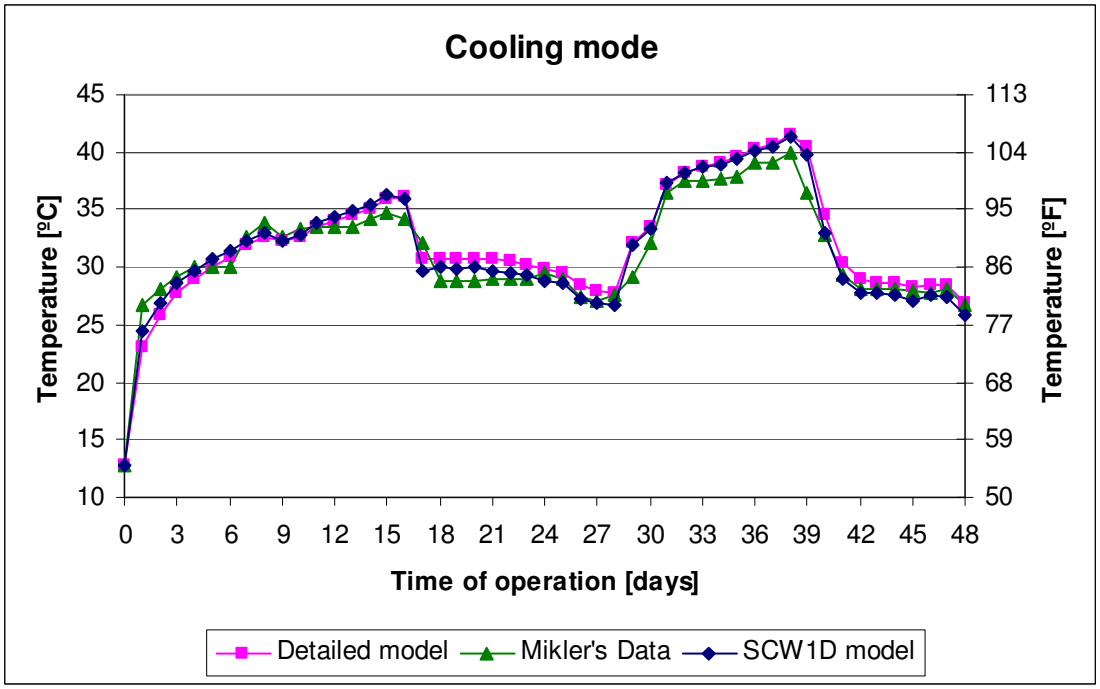

Figure 6-14 Comparisons of temperatures back to the heat pump for the simplified model (SCW1D), the detailed model, and Mikler's data in cooling mode

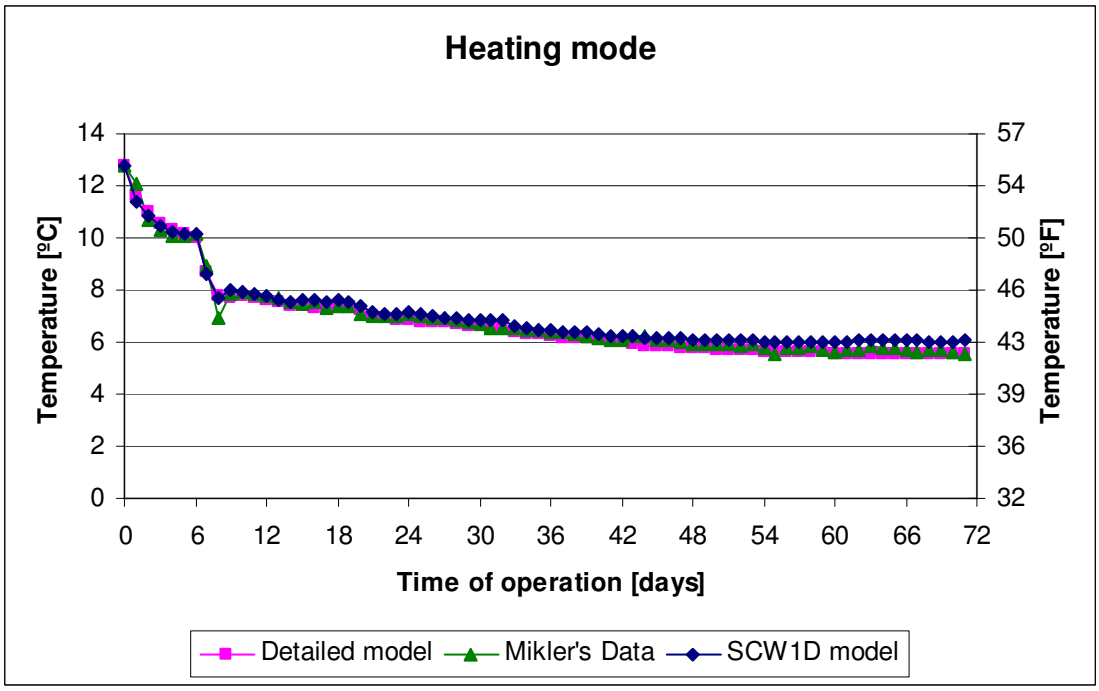

Figure 6-15 Comparisons of temperatures back to the heat pump for the simplified model (SCW1D), detailed model, and Mikler's data in heating mode

The small difference between the models and experimental data could be caused by the assumption of homogenous and isotropic rock surrounding the well, which was discussed in the validation of the detailed model in the section 4.2.2.3. The mean square error $(\frac{1}{N}\sum_{i=1}^{N}(T_{Model,i} - T_{Mikler,i})^2)$ is 0.58 ºC and 0.26 ºC for the simplified model and the detailed model respectively. Both the detailed model and the simplified model work well. The simulation results from the detailed model match the experimental data better than those from the simplified model, though. This is because the simplified model is one-dimensional, and neglects end effect, ground temperature gradient, and vertical heat and fluid flow.

Comparisons of the temperatures back to the heat pump from simplified model (SCW1D), the detailed model, and experimental data from the Haverhill library (Henderson 2003) are shown in Figures 6-16. This validation shows that the simplified model could be used to simulate the performance of standing column well system in bleed operation.

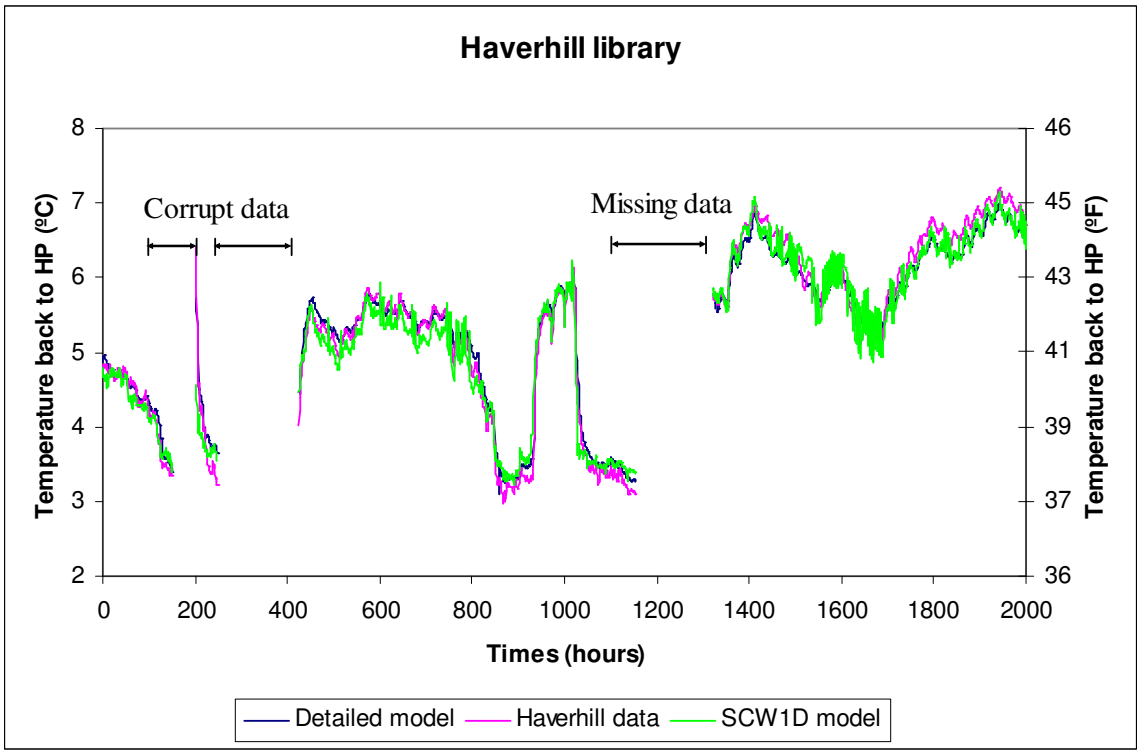

Figure 6-16 Comparisons of temperatures back to the heat pump for the simplified model (SCW1D), the detailed model, and Haverhill data

6.3. Simplified "by-pass" approximation

In this section, the "by-pass" approximation will be used to solve the continuous and constant bleed cases in the second limiting case B mentioned at the beginning of this chapter. In this limiting case, the surrounding rock is impermeable and the groundwater

flow occurs only within the fracture. Therefore, the heat transfer in the surrounding rock is pure heat conduction.

The borehole in an SCW system might be thought of as a cylindrical heat source with water storage, where the water in the borehole can be treated as some combination of groundwater flowing directly into the borehole from the fracture and water returned from the heat pump. The "by-pass" refers to water that bypasses the surrounding ground and comes straight into the borehole at the undisturbed temperature (Figure 6-17). Although this is physically unrealistic, it does represent the limiting case.

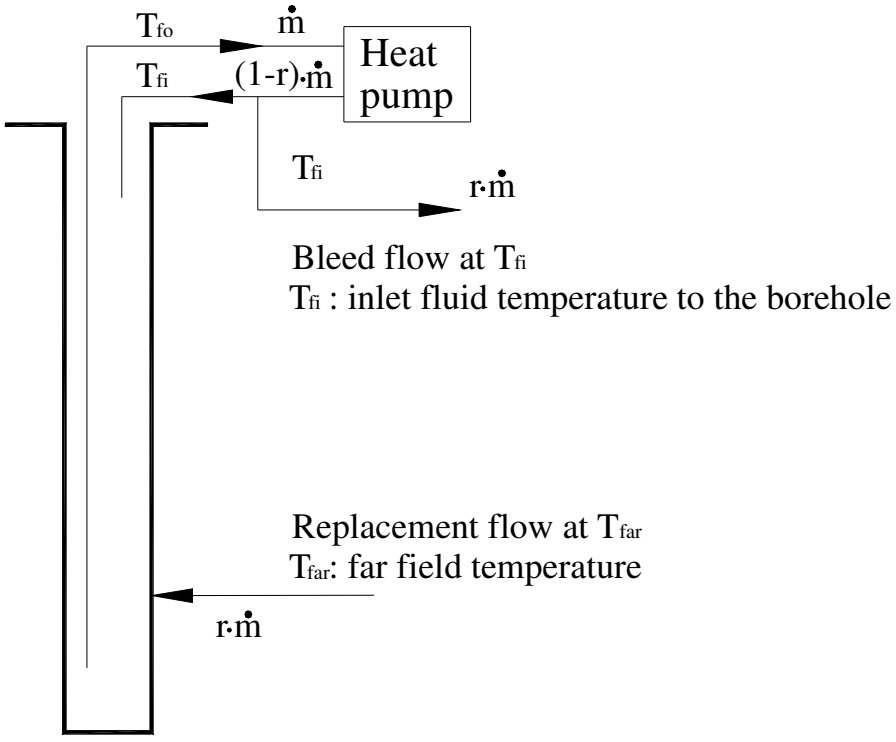

Figure 6-17 Standing column well showing bleed and by-pass flows

After considering the "by-pass" approximation, the energy balance equation is given as:

$$mC_p \frac{dT_f}{dt} = \dot{m}(1-r)C_p T_{fi} + \dot{m}rC_p T_{far} - \dot{m}C_p T_{fo} + \frac{T_b - T_f}{R_b} \cdot L \qquad (6.32)$$

Solution procedure of the equations in this by-pass approximation is the same one described in section 6.1.6. A comparison of simulation results (i.e., temperature back to the heat pump) for the same standing column well with the two different limiting cases is shown from Figures 6-18 through 6-20. All the simulations use the annual building loads for a small office building in Boston, MA shown in Figure 4-21. This building was described in section 4.3.1. All the parameters about the properties of the borehole can be found in Table 4-2. The preliminary study shows that the differences between performances of standing column well system in intermittent bleed (bleed rate 10 %) in the two different limiting case is not big. Therefore, the case with constant bleed rate was chosen for the further study. Constant bleed rate 10 % was applied in the simulation. The differences between the two limiting cases are summarized in Table 6-5.

Table 6-5 Difference between two limiting cases

Case name	Difference
Limiting case A	1. Homogeneous flow around a borehole surrounded by a porous medium. 2. Advection-conduction heat transfer in the surrounding rock
Limiting case B	1. Groundwater flow in an impermeable medium with a fracture in it. 2. Conduction heat transfer in the surrounding rock

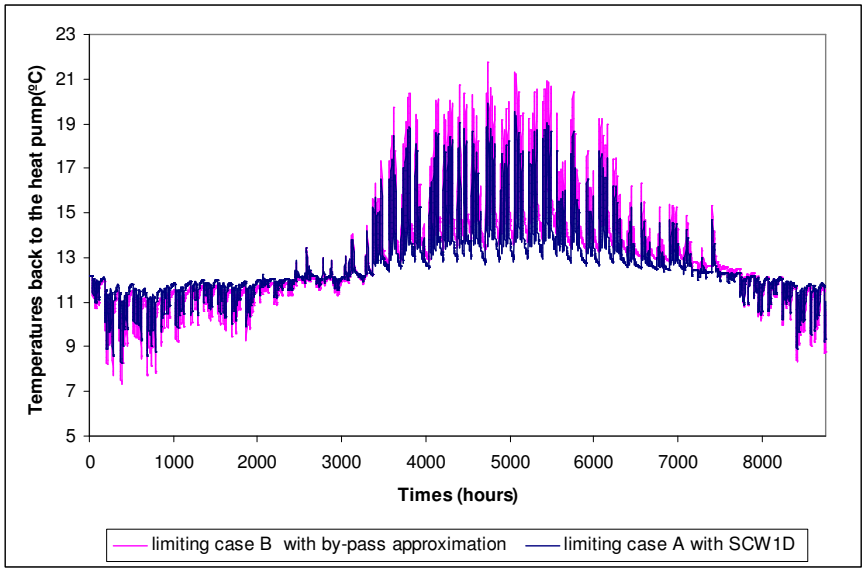

Figure 6-18 Comparison of temperatures back to the heat pump in limiting cases

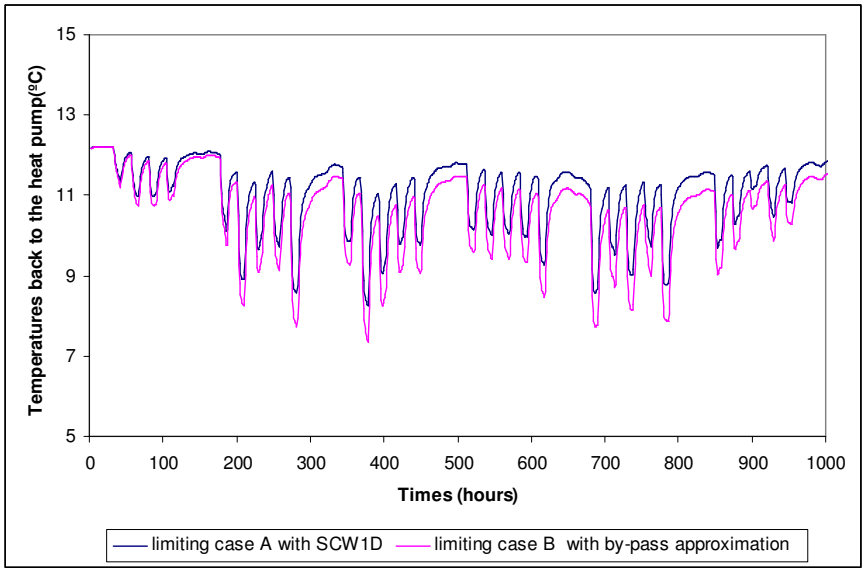

Figure 6-19 Comparison of temperatures back to the heat pump in limiting cases (winter)

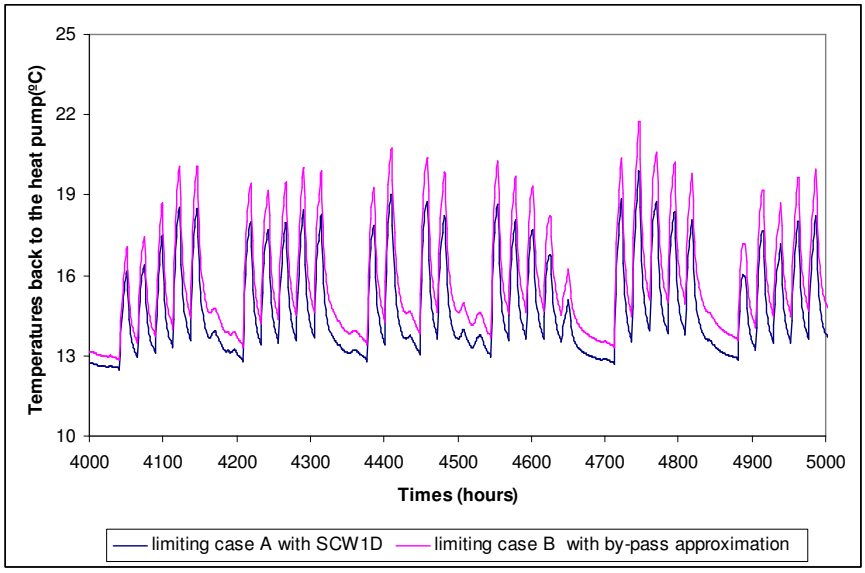

Figure 6-20 Comparison of temperatures back to the heat pump in limiting cases (summer)

Figures 6-18 through 6-20 show that the performance of the standing column well system in the limiting case A with the assumption of homogenous medium is better than that of the limiting case B with a fracture flow in impermeable medium. This is presumably because in the medium, the groundwater flow, which enhances heat transfer, is spread over the surrounding ground volume. The maximum temperature difference in these two limiting case is 1.98 ºC (3.56 ºF), and the average temperature difference is 0.55 ºC (0.99 ºF).

Gehlin (2002) did a preliminary study about the influences on thermal response test by groundwater flow. Her fracture flow model results in higher effective thermal conductivity than the continuous and porous model only with specific flow rates in the

interval 2.5×10^{-8} m/s to 5×10^{-7} m/s. Otherwise, the continuum model gives a higher effective thermal conductivity.

The by-pass approximation is a simplified model for the limiting case B, where groundwater flows in an impermeable medium with a large fracture in it. Without additional research about groundwater flows in the fracture, it appears that 2 ºC (3.6 ºF) safety factor might be prudent for designers of systems operating near the freezing point. However, this is probably excessive given the simplified and conservative analysis done for the limiting case.

Future research that investigates combined heat and mass transfer for specific fracture geometries would be useful to more accurately determine the safety factor required. A reduction in the required safety factor would allow for more cost effective systems.

7. ECONOMIC PERFORMANCE ANALYSIS

In this chapter, the thermal and economic performance of standing column well systems in different regions of the U.S. are examined. This examination is made by means of system simulation using the standing column well model developed in Chapter 6. At the same time, the performance of standing column well systems is compared to the single U-tube closed-loop systems, which are mainly based on a short-time step ground heat exchanger model developed by Yavuzturk and Spitler (1999).

First, the simulation environment HVACSIM+ and component models in this environment are described, and then a simplified design procedure for standing column well system is provided. Finally, simulation results and conclusions from economic analysis are depicted.

7.1. HVACSIM+ models

In this study, the performance comparison of standing column well systems is accomplished by means of a system approach using the HVACSIM+ modeling environment. The core component models are a simplified standing column well model described in Chapter 6, a simple water-to-air- heat pump model and a simple circulating water pump. These three-component models were created using Visual Modeling Tool for HVACSIM+ (Clark 1985), and they are displayed in Figure 7-1. The system simulations are performed using a small office building located in the different climatic

regions of the U. S. The hourly heating and cooling building loads are determined by a building energy simulation program (BLAST 1986) and are treated as thermal boundary conditions in the HVACSIM+ environment.

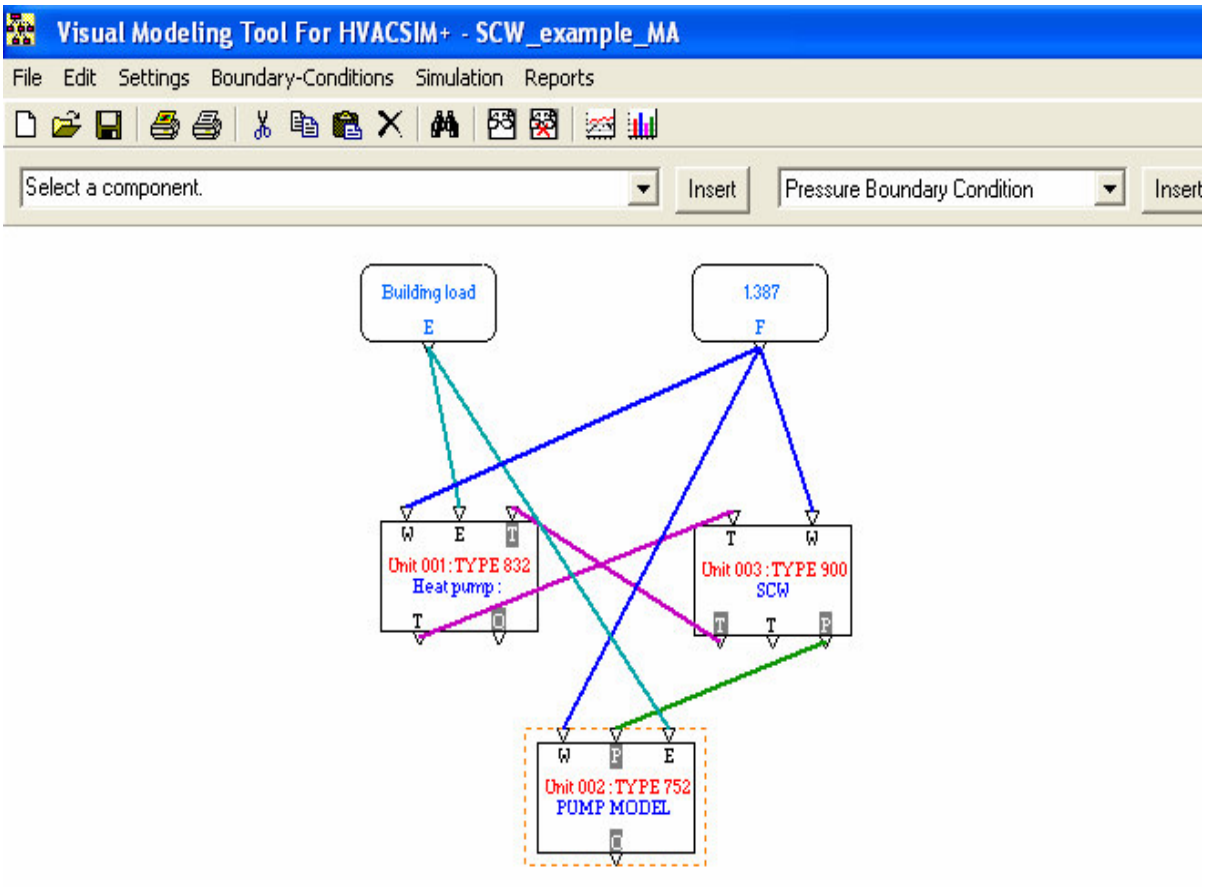

Figure 7-1 Three-component models of a standing column well system in HVACSIM+

There are three component models – standing column well model, heat pump model, and water pump model in this system. The two inputs to the system are the fluid flow rate and hourly building loads. The mass flow rate is constant through the entire length of the simulation. Water temperatures leaving the well calculated by the standing column well model are used as inputs (water temperatures returning to the heat pump) to the heat pump model. At the same time, water temperatures leaving the heat pump are treated as

inputs to the standing column well model. The water pump model uses the system pressure drop calculated from the standing column well model to calculate energy consumption from water pump. In the following subsections, these component models are described in detail.

7.1.1. The standing column well model

The standing column well model used in this study is the simplified one-dimensional numerical model developed in Chapter 6. This simplified one-dimensional numerical model simulates groundwater flow and heat transfer in and around a standing column well. Both the natural groundwater movement and the "induced" groundwater flow by "bleed" are considered in this model. An "enhanced" thermal conductivity is used to consider the natural water flow caused by the pumping and buoyancy. Bleed-driven advection is modeled explicitly as an advection term is included in the governing energy equation. When bleed occurs, the effect of bleed is superimposed on top of the effects of pumping and buoyancy. This component model configuration is shown in Figure 7-2.

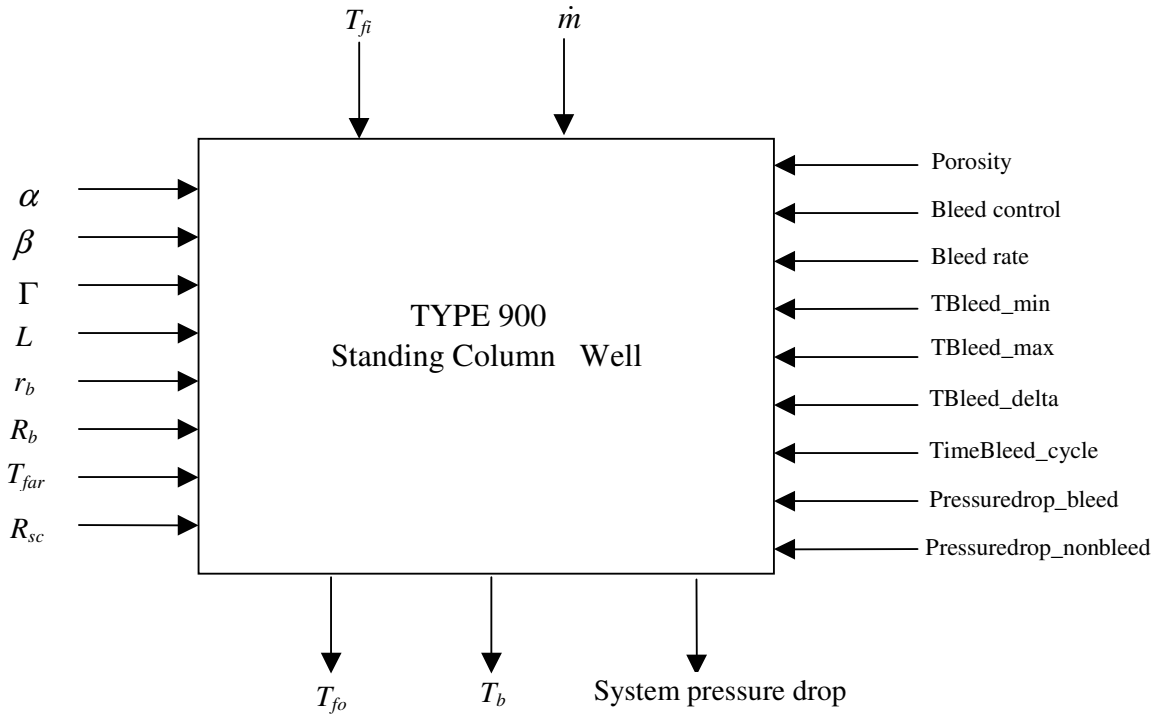

Figure 7-2 Component configuration of standing column well model

In Figure 7-2, inputs are shown at the top; parameters at the sides; and outputs at the bottom. The nomenclature may be summarized as follows:

Inputs:

$\dot{m}$ is the mass flow rate of water through the heat pump system (kg/s);

T_{fi} is the inlet water temperature (ºC).

Parameters:

α is the ground heat capacity (J/m^3-K);

β is the water heat capacity (J/m^3-K);

Γ is the ground (Enhanced) thermal conductivity (W/m-K);

L is the borehole depth (m);

r_b is the borehole radius (m);

R_b is the borehole resistance (K/(W/m));

R_{sc} is the short-circuiting resistance (K/(W/m)).

Bleed-control-strategy:

0: no bleed;

1: Constant bleed ;

2: Deadband bleed control;

3: Timed bleed cycle control;

4: Temperature difference bleed control;

T_{Bleed_min} is the minimum temperature set point for deadband bleed control/ Timed bleed cycle;

T_{Bleed_max} is the maximum temperature set point for deadband bleed control/ Timed bleed cycle;

T_{bleed_delta} is the temperature range for deadband bleed control/temperature difference bleed control;

$Time_{Bleed\_cycle}$ is the bleed cycle time (second);

Pressuredrop_bleed is the system pressure drop in bleed operation (kPa);

Pressuredrop_nonbleed is the system pressure drop in non bleed operation (kPa).

Outputs:

T_{fo} is the outlet water temperature (ºC) ;

T_b is the borehole wall temperature (ºC);

$Pressure_{system\ drop}$ is the system pressure drop (kPa).

Bleed control strategy

Five different bleed control strategies are available, which are described as follows:

No bleed: During the whole operation period of the standing column well system, the bleed rate is zero at any time.

Constant bleed: During the whole operation period of the standing column well system, the bleed rate is a given value greater than zero at any time.

Deadband bleed control: In winter, when the water temperature leaving the well (returning to the heat pump) is lower than a given temperature, T_{bleed_min}, bleed is started. When the water temperature leaving the well is higher than a given temperature, $T_{bleed\_min}+T_{bleed\_delta}$, bleed is stopped. In summer, bleed is started when the water temperature leaving the well is higher than a given temperature, T_{bleed_max}. And bleed is stopped when the water temperature leaving the well is lower than a given temperature, $T_{bleed\_max} - T_{bleed\_delta}$.

Timed bleed cycle control: In winter, when the water temperature leaving the well is lower than a given temperature, T_{bleed_min}, bleed is started and this bleed cycle lasts for the given period, $Time_{bleed\_cycle}$, and then stopped. In summer, bleed is started when the water temperature leaving the well is higher than a given temperature, T_{bleed_max}, bleed is started and this bleed cycle lasts for the given period, $Time_{bleed\_cycle}$, and then stopped.

Temperature difference control: The temperature difference between the water temperature leaving and returning to the well was used as a controlled parameter. When this temperature difference is higher than a given set point, T_{bleed_delta}, bleed is started. When this temperature difference is lower than this given set point, bleed is stopped.

7.1.2. The heat pump model

To match the peak building loads of the hypothetical building, Climate Master HL Horizontal 072 water-to-air heat pump was selected. This water-to-air heat pump model is modeled in HVACSIM+ using four polynomial curve fit equations shown from Equations 7.1 to 7.4. It was assumed that the heat pump performance only changed with entering water temperatures. Curve fits describing capacity vs. entering water temperature and power consumption vs. entering water temperature, at a range of flow-rates, were derived from the catalogue data.

$$HP\_capacity = 22410.37 + 1122.66 * EWT - 3.0345 * EWT^2 \quad \text{Heating mode} \quad (7.1)$$

$$HP\_capacity = 97442.70 - 332.76 * EWT - 0.1491 * EWT^2 \quad \text{Cooling mode} \quad (7.2)$$

$$HP\_power = 6130.83 - 16.30 * EWT + 0.3305 * EWT^2 \quad \text{Heating mode} \quad (7.3)$$

$$HP\_power = 3198.09 + 39.03 * EWT + 0.0247 * EWT^2 \quad \text{Cooling mode} \quad (7.4)$$

Where *HP_capacity* is the heat pump capacity (But/hr);

HP_power is the power consumption of the heat pump (W);

EWT is the entering fluid temperature to the heat pump (ºF).

Inputs to this heat pump model include building loads, entering fluid temperatures (EWT), and fluid mass flow rate. The model computes the heat of rejection in cooling

model, heat of absorption in heating model, and the heat pump energy consumption. Outputs include exiting fluid temperature, energy consumptions.

7.1.3. The water pump model

The circulating water pump has a constant 65 % efficiency (Rafferty, 1998). Inputs to this mode include system pressure drop, fluid mass flow rate, and building loads. The model calculates power consumption of circulating water pump as follows.

$$w = \frac{\gamma Q H}{\eta} \tag{7.5}$$

Where: $\gamma = \rho g$

ρ is the water density (kg/m^3);

Q is the volume flow rate (m^3/s);

H is the total dynamic head (m);

η is the efficiency of the circulating water pump;

taken as 0.65 for this model (Rafferty ,1998);

w is the power consumption of the circulating water pump (W).

When the building load is zero, power consumption of water pump is zero too.

7.1.4. The vertical U-tube ground loop heat exchanger model

The vertical U-tube closed-loop ground heat exchanger model used in this study for comparison is that developed by Yavuzturk and Spitler (1999), which is an extension of the long-time step temperature response factor model of Eskilson (1987). It is based on dimensionless, time-dependent temperature response factors known as “g-functions”,

which are unique for various borehole field geometries. The model includes a hierarchical load aggregation algorithm that significantly reduces computation time. This component model configuration is shown in Figure 7-3. The initial size of single u-tube closed loop ground heat exchanger was chosen by GLHEPRO 3.0 (Spitler 2000).

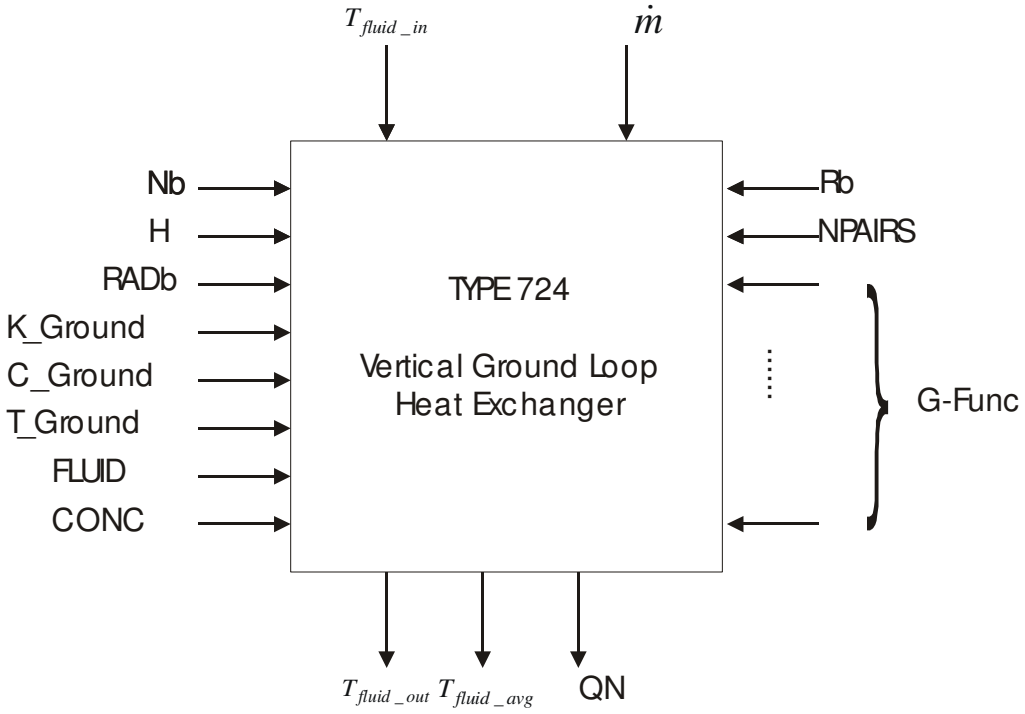

Figure 7-3 Component configuration of vertical ground loop heat exchanger

In Figure 7-3, inputs are shown at the top; parameters at the sides; and outputs at the bottom. The nomenclature may be summarized as follows:

Inputs:

T_{fluid_in} is the inlet fluid temperature (^{o}C);

$\dot{m}$ is the mass flow rate of fluid (kg/s).

Parameters:

C_Ground is the volumetric heat capacity of ground (J/m^3-K);

C_{fluid} is the specific heat capacity of fluid (J/(kg-K));

$g(\ )$ is the g-function (--);

H is the borehole length over which heat extraction takes place (m);

K_{Ground} is the thermal conductivity of the ground (W/m-K);

N_b is the number of boreholes (--);

$NPAIRS$ is the number of pairs of g-function data (--);

RAD_b is the borehole radius (m);

R_b is the borehole thermal resistance (K/(W/m));

T_{Ground} is the undisturbed ground temperature (^oC).

Outputs:

T_{fluid_out} is the outlet fluid temperature (^oC);

T_{fluid_avg} is the average fluid temperature (^oC);

QN is the normalized heat extraction rate for i^{th} hour (W/m).

7.1.4. Building description and loads calculation

A small building (the Meridian Technology Center Incubator) located in Stillwater, OK with Typical Meteorological Year (TMY) weather files in different locations was chosen for simulating the performance of ground heat exchangers. The building loads are determined using building energy simulation software (BLAST 1986). The annual building loads for Boston, MA are shown in Figure 4-21. This building was described in section 4.3.1.

This small office building has internal heat gain profiles like a typical office building. The peak heating and cooling loads are of 9 hours and 10 hours durations respectively. A typical 10 hours heat pulse can be seen in Figure 7-4.

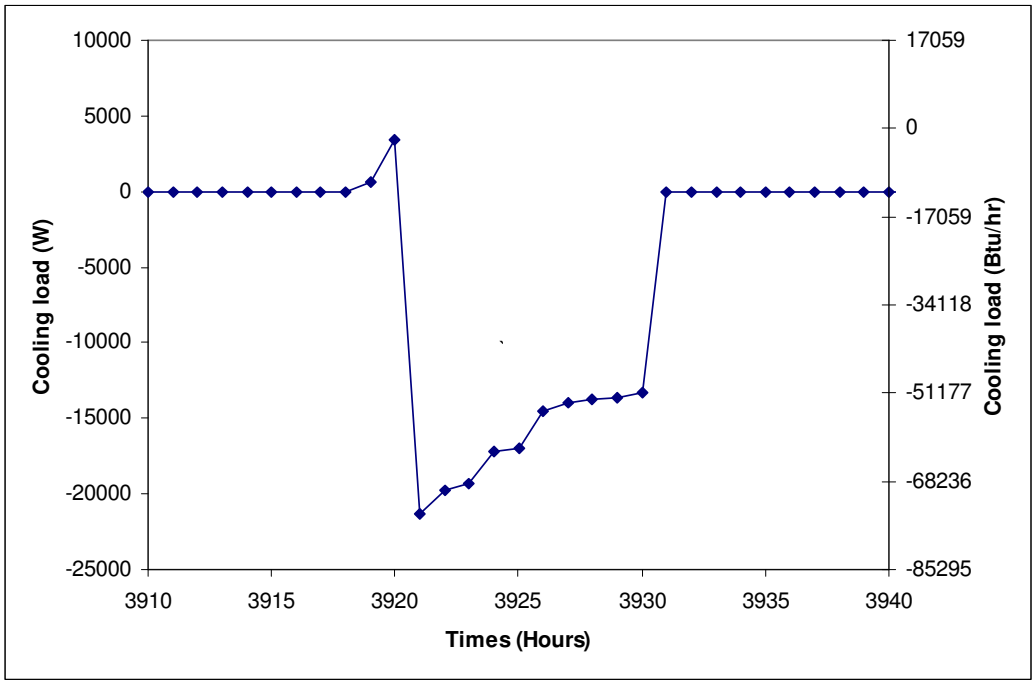

Figure 7-4 A peak of cooling load event in Boston, MA small office building

7.2. Simplified design procedure for standing column well system

There are many degrees of freedom to design standing column well system. In this section, to have a fair comparison between the different ground heat exchangers, a simplified design procedure is summarized in Figure 7-5.

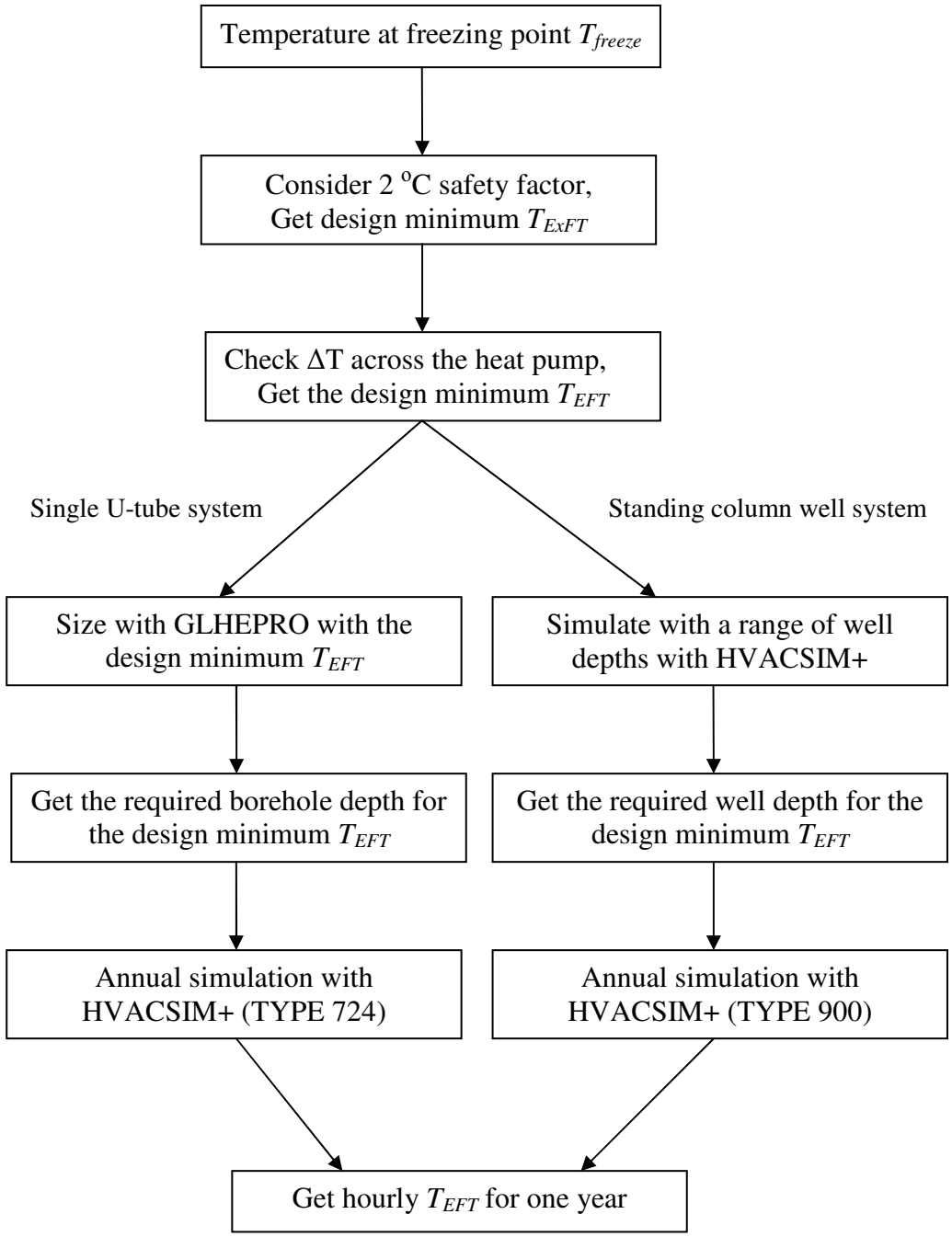

Figure 7-5 Flow chart for simplified design procedure

In Figure 7-5, the nomenclature is summarized as follows:

T_{freeze} is the fluid temperature at freezing point (°C [ºF)]);

T_{ExFT} is the exiting fluid temperature from the heat pump (i.e., the fluid

temperature entering the ground heat exchanger) (^{o}C [ºF)]);

T_{EFT} is the entering fluid temperature to the heat pump (i.e., the fluid temperature leaving the ground heat exchanger) (^{o}C [ºF)]);

ΔT is the fluid temperature change across the heat pump (^{o}C [ºF)]).

In this study, the following assumptions are used during the ground heat exchanger design procedure:

1). GLHEPRO (Spitler 2000) is used to size the vertical U-tube heat exchanger for a given building load profiles. The closed-loop system uses an antifreeze mixture of 12.9% propylene glycol by weight, which has -3.89 ºC (25 ºF) freezing point. It should be noticed that different concentrations of antifreeze will affect the sizing results, but this work has been chosen as a reasonable typical value. The freezing point for water in the standing column well system is 0 ºC (32 ºF).

2). The safety factor for the freezing point temperature is 2 ºC (35.6 ºF). And the fluid temperature change across the heat pump at the design load is 5 ºC (9 ºF).

3). The resulting design minimum entering fluid temperature to the heat pump, T_{EFT}, is 3.11 ºC (37.6 ºF) and 7 ºC (44.6 ºF) for the single vertical U-tube closed-loop system and the standing column well system respectively.

4). The vertical U-tube closed-loop ground heat exchanger model (TYPE 724) described in section 7.1.3 is applied in the HVACSIM+ environment. The size of U-tube closed-

loop ground heat exchanger and g-functions from GLHEPRO are used as input parameters for this model. After coupling with given building load, the fluid temperatures back to the heat pump are calculated with this model. The peak temperatures should be close to those from GLHEPRO.

5). The simplified one-dimensional numerical standing column well model (TYPE 900) developed in Chapter 6 is applied in the HVACSIM+ environment. Based on conversations with contractors and engineers (Orio 2001), in this study, a deadband bleed control with a 10 % bleed rate is used for bleed cases. In winter, when the water temperature leaving the well is lower than 8 ºC (46. 4 ºF), bleed is started. When the water temperature leaving the well is higher than 10.8 ºC (51.4 ºF), bleed is stopped. In summer, bleed is started when the water temperature leaving the well is higher than 29.2 ºC (84.5 ºF), and stopped when the water temperature leaving the well is lower than 26.4 ºC (79.5 ºF). After selecting local thermal and geological properties, building loads, and other borehole parameters, maximum and minimum water temperatures leaving the well (returning to the heat pump) are calculated with a guessed well depth for the standing column well system with bleed and without bleed.

6) The standing column well depth is adjusted in 1 meter increments to let the peak water temperature leaving the well approach the given design peak water temperature. If this difference is less than 0.05 ºC (0.09 ºF), this adjustment is stopped. The design goal in this simplified procedure is to find the minimum length that meets the design minimum

and maximum entering fluid temperatures to the heat pump (i.e., the fluid temperatures leaving the ground heat exchanger).

Using the above procedure, the final size of the standing column well system with bleed and without bleed can be calculated. Therefore, the hourly water temperatures leaving the well can be obtained from running TYPE 900 standing column well model in HVACSIM+ environments. The following sections will focus on the economic analysis based on these simulation results.

7.3. Economic analysis

It is economics that make standing column well systems practical and popular. A perfect economic analysis may not be possible considered the large discrepancy of loop drilling costs across the United States (Yavuzturk and Chiasson 2002). A simple economic analysis is performed to give some insight into the benefits of standing column well systems compared with single vertical U-tube closed-loop system.

The net present value is calculated for the initial cost and 20-year operating cost. The net present value is based on the following assumptions (Yavuzturk and Chiasson 2002).

1) The installation cost per meter of borehole for a single U-tube ground heat exchanger is assumed to be $19.69 per meter of borehole. This amount includes trenching and headering.
2) The installation cost per meter of borehole for standing column well is assumed to be $17.88 per meter of borehole.

3) The cost per meter of borehole is broken into drilling costs (including pipe installation, trenching, and headering), pipe costs (material only), and grouting costs (labor and materials). Table 7-1 lists unit installation cost breakdowns for single U-tube closed loop and standing column well systems. The higher drilling costs for the standing column well installation are attributed to the assumption that the upper part of the borehole is cased with steel.

Table 7-1 Installation costs for different ground heat exchanger system ($/m borehole)

Unit installation costs for ground heat exchanger system ($/m borehole)	Single U-tube closed-loop	Standing column well
Drilling, trenching, pipe handling & installation	$15.75	$17.23
Pipe materials	$1.97	$0.65
Grout materials and placement	$1.97	$-
Total Unit installation cost	$19.69	$17.88

4) The pumping energy consumption is determined based on a piping network design (Spitler et al. 2002). The efficiency of the circulating water pump is assumed to be 0.65 (Rafferty 1998).

5) A 6 % annual percentage interest rate is used for the present value analysis.

6) The cost of electricity is listed in Table 7-2 for different states.

Table 7-2 Electric utility monthly average cost per kilowatt-hour for commercial building in different states

(cents per kilowatt-hour)*

States	Jan.	Feb.	March	April	May	June	July	Aug.	Sep.	Oct.	Nov.	Dec.
MA	7.8	7.5	7.8	8.5	8.7	9.8	10.2	10.1	10.7	9.5	8.6	8.7
OR	5.0	5.0	5.1	5.2	5.2	5.1	5.1	5.1	5.2	5.2	5.2	5.1
PA	5.9	5.7	5.9	5.8	5.7	7.2	6.6	6.8	6.6	6.2	6.0	6.7
AL	6.4	6.4	7.0	7.0	6.5	6.5	7.5	7.5	7.6	7.5	7.15	7.25
NH	11.1	11.2	11.2	11.4	11.7	11.3	11.6	11.3	11.6	11.2	10.7	11.0

*data from http://www.eia.doe.gov/cneaf/electricity/page/at_a_glance/sales_tabs.html

7.4. Simulation results and discussions

In this section, simulation results for a real building using different ground heat exchanger systems (i.e., single vertical U-tube closed-loop system, standing column well system without bleed, and standing column well system with bleed) are described. First, the case in Boston, MA is discussed in detail. Then, the simulation results for other cities are presented and discussed.

Boston, MA

The ground heat exchanger design parameters used in this study, including the borehole thermal resistance values for each case, are summarized in Table 7-3. The ground conditions are assumed to be similar to that in the northeast of the U.S (Northeastern Appalachians Region). The simplified design procedure described in section 7.2 was used in here.

Table 7-3 Summary of ground heat exchanger design parameters for Boston, MA

Designer Parameter	**Single U-tube closed-loop**	**Standing column well (without bleed)**	**Standing column well (with 10% bleed)**
Geologic Conditions:			
Rock Type	Fractured igneous and metamorphic rock	Fractured igneous and metamorphic rock	Fractured igneous and metamorphic rock
Thermal Conductivity (W/m-K) (Btu/hr-ft-ºF)	3.0 (1.73)	3.5(Enhanced) (2.02)	3.5(Enhanced) (2.02)
Vol. Heat Capacity (J/m^3-ºC) (Btu/ft^3-ºF)	2,600,000 (38.78)	2,600,000 (38.78)	2,600,000 (38.78)
Undisturbed Earth Temperature (ºC) (ºF)	12.2 (53.96)	12.2 (53.96)	12.2 (53.96)
Water Table Depth (m) (ft)	5 (16.41)	5 (16.41)	5 (16.41)
Borehole:			
Diameter (m) (in)	0.11 (4.33)	0.1524 (6)	0.1524 (6)
Depth (m) (ft)	81.68 (267.99)	391 (1282.87)	263 (862.90)
Borehole Geometry	1 × 8	Not applicable	Not applicable
U-tube:			
Diameter inner (m) (in)	0.025 (1)	Not applicable	Not applicable
U-tube Shank Spacing (m) (in)	0.0367 (1.44)	Not applicable	Not applicable
Thermal Conductivity (W/m-K) (Btu/hr-ft-ºF)	0.3895 (0.225)	Not applicable	Not applicable
Grout			
Type	Standard Bentonite	Not applicable	Not applicable
Thermal Conductivity (W/m-K) (Btu/hr-ft-ºF)	0.7443 (0.433)	Not applicable	Not applicable
Borehole Thermal Resistance:			
$R_{borehole}$ (ºC/W/m) (ºF/(Btu/hr)/ft)	0.1398 (0.2419)	0.0011 (0.0019)	0.0011 (0.0019)

In Table 7-3, the borehole thermal resistance for single vertical U-tube closed-loop system is calculated from GLHEPRO, and the borehole thermal resistance for standing column well system is obtained from the methodology described in section 6.1.5.

The simulation results of the detailed system simulation are provided in Table 7-4. From GLHEPRO, the minimum and maximum fluid temperatures leaving the borehole (i.e., fluid temperature returning to the heat pump) for the vertical U-tube closed-loop system is calculated to be 3.23 ºC (37.81 ºF) and 30.16 ºC (86.28 ºF) respectively, which are quite closed to results (i.e., 3.43 ºC (38.17 ºF) 29.71 ºC (85.46 ºF) from HVACSIM+ simulation. The "Feet per ton" is a common figure of merit for GSHP systems. The total borehole length is divided by the nominal system capacity.

Table 7-4 Summary of ground heat exchanger simulation results for Boston weather file

Ground Heat Exchanger Type	**Borehole Geometry**	**Borehole Depth (m) [ft]**	**Required Total Borehole Length (m) [ft]**	**EFT_{max} (ºC) [ºF]**	**EFT_{min} (ºC) (ºF)**	**Feet per ton**
Single U-tube closed-loop	1 × 8	81.68 (267.99)	653.44 (2143.94)	29.71 (85.46)	3.43 (38.17)	121
Standing Column Well Without Bleed	1 × 1	391 (1282.87)	391 (1282.87)	22.82 (73.08)	7.00 (44.6)	72
Standing Column Well With 10 % Bleed (Deadband Control)	1 × 1	263 (862.90)	263 (862.90)	28.08 (82.54)	7.01 (44.6)	48

Figure 7-6 shows the required total borehole depths for different ground heat exchanger systems in Boston, MA. Compared with the single U-tube closed-loop system, the standing column well system without bleed and with bleed reduces the required depths by 40.1 % and 59.7 % respectively. The importance of the bleed is clear – the SCW system without bleed requires about 50 % greater well depth than the SCW system with bleed. Therefore, the standing column well system can significantly reduce the capital costs, such as drilling costs, compared to a closed-loop system.

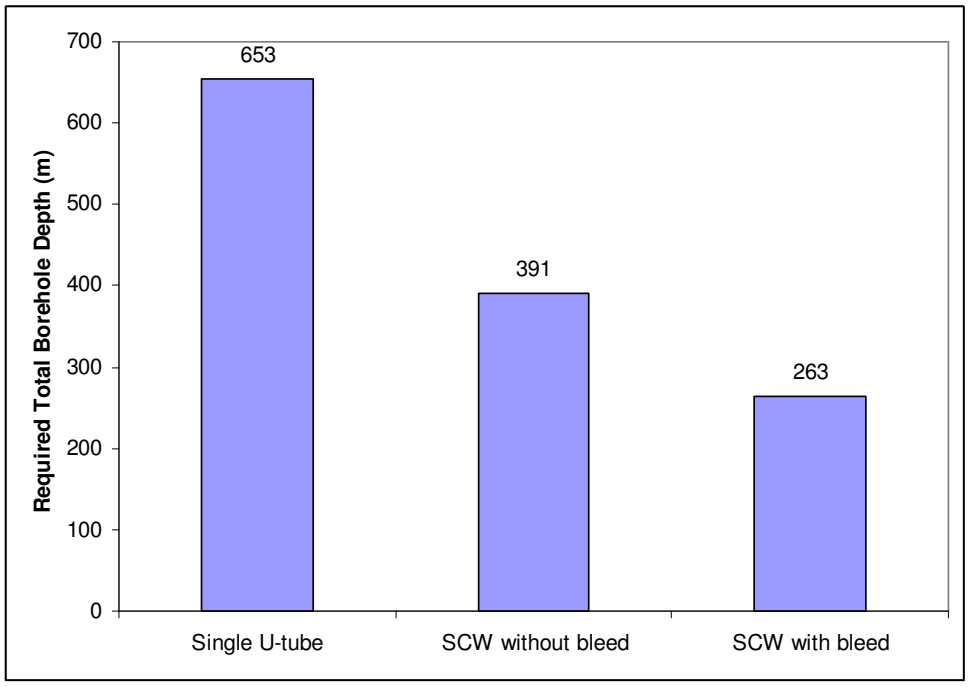

Figure 7-6 Required total borehole depth for different ground heat exchanger systems in Boston, MA

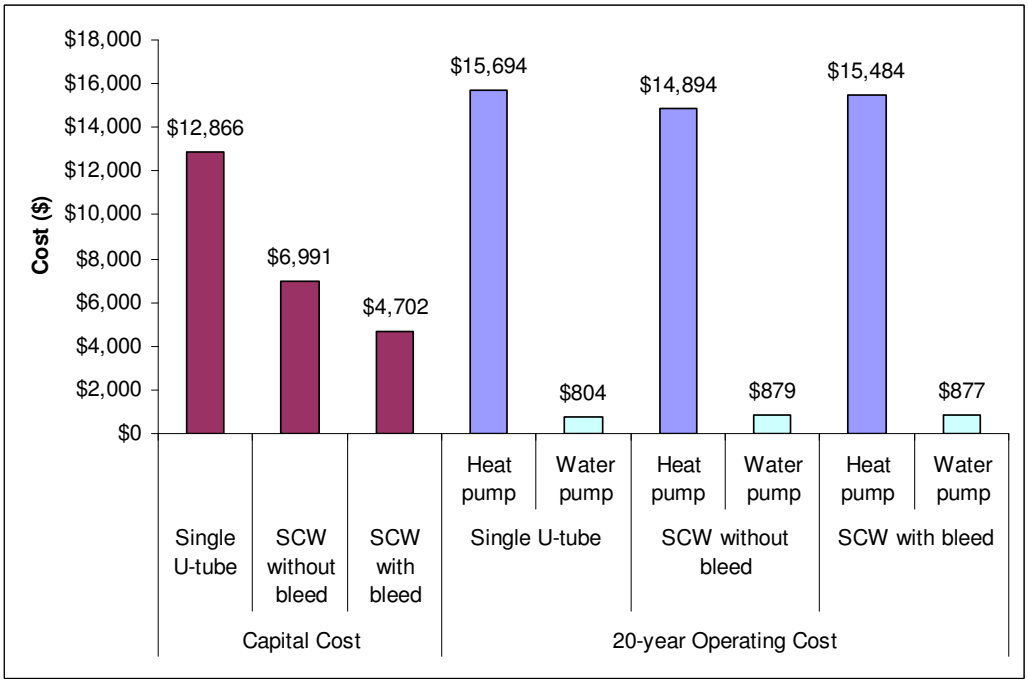

Figure 7-7 20-year life cycle cost (present value) in Boston, MA

Figure 7-7 shows 20-year life cycle cost analyses for different ground heat exchanger systems in Boston, MA. The results show that the operating costs are fairly similar. The capital costs are significantly different, though. This could be due to the different required borehole depth for these ground heat exchanger systems.

It should be noticed that the circulating water pump costs for the SCW system are greatly dependent on the water table depth. Based on the study in Chapter 5, when the water table is high (i.e., 5 meters [16 ft]), the circulating water pump cost difference between SCW systems with bleed and without bleed is very small, but if the water table is lower (i.e., 30 meters [98 ft]), circulating water pump costs for bleed cases with higher bleed rates are much higher than non-bleed cases.

The parametric study described in Chapter 5 shows that for constant and continuous bleed operation, when the water table is high, on the order of 5 meters (16 ft), the increased pump power when bleeding is not significant and the greatest efficiencies result when bleed rate is maximized. However, when the water table is low, on the order of 30 meters (98 ft), pump power requirements increase significantly when bleed is introduced. The benefits of higher rates of bleed (> 10 % in the study in Chapter 5) are then outweighed by the increased pumping costs.

However, when SCW system is in bleed control operation, no matter what the water table depth is, increased bleed rate (in the range from 0 to 20 %) will result in improved performance of the SCW system. Figure 7-8 shows annual energy costs for the SCW

system with deadband bleed control with different bleed rates and water table depths in Boston, MA. These costs are calculated with the simplified model. Table 7-5 lists the annual energy cost breakdowns for those cases. The results show that for the same water table depth, energy consumption from the water pump is almost same for cases with different bleed rates. The improved performance of SCW system comes from the improved heat pump efficiency, which is caused by the moderate water temperatures back to the heat pump due to bleed operation. The results also show the water table depth has some effects on the energy consumption of circulating water pump. The case with 30 meters (98 ft) water table depth required 15 % more electrical energy consumption for circulating water pump than the case with 5 meters (16 ft) water table depth. But the total energy consumption difference between the cases is less than 1 %. This is because the circulating water pump energy consumption only accounts for a small amount of the total energy consumption in these cases, and the bleed only runs about 7 % of the year.

This accounts for the difference in findings between Chapter 5 and this study. In Chapter 5, the pumping costs changed significantly with water table depth - in this case the bleed was running 8760 hours per year. With the deadband bleed control strategy, it is only running 610 hours or less per year.

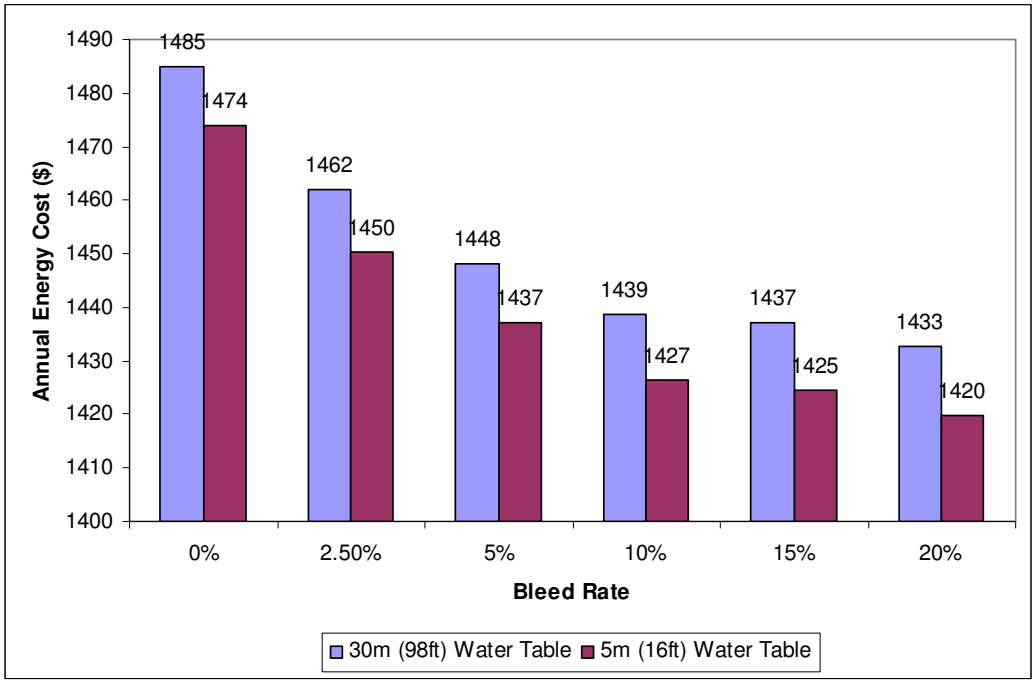

Figure 7-8 Annual energy cost for SCW systems for bleed control operation in 5-meter and 30-meter water table depths with different bleed rates in Boston, MA

Table 7-5 Annual energy cost breakdowns for SCW system deadband bleed control in Boston, MA

Water table depth =30 meters (98 ft)						
Bleed Rate	0%	2.50%	5%	10%	15%	20%
Annual Energy Cost($)	1485	1462	1449	1439	1437	1433
Annual Energy Cost from Heat Pump($)	1398	1374	1361	1351	1348	1344
Annual Energy Cost from Water Pump($)	87	88	88	88	89	89
Water table depth =5 meters (16 ft)						
Bleed Rate	0%	2.50%	5%	10%	15%	20%
Annual Energy Cost($)	1474	1450	1437	1427	1425	1420
Annual Energy Cost from Heat Pump($)	1398	1374	1361	1350	1349	1344
Annual Energy Cost from Water Pump($)	76	76	76	76	76	76

Other locations

The same office building was chosen for simulating the performance of the standing column well systems and single vertical U-tube closed-loop systems in four other locations. Those cities were chosen in geological regions where standing column well systems are currently installed (Spitler et al. 2002). Table 7-6 gives the far field temperature and annual building loads for different cities.

Table 7-6 Far field temperatures and building loads for different cities

	Concord NH	**Harrisburg PA**	**Boston MA**	**Portland OR**	**Birmingham AL**
Far field temperature* (ºC) (ºF)	8.3 (46.9)	11.1 (52.0)	12.2 (54.0)	12.8 (55.0)	15.6 (60.0)
Annual heating load (kW) (kBtu/hr)	33,329 (113,712)	19,526 (66,623)	22,218 (75,808)	10,422 35,560	5,273 (17,991)
Annual cooling load (kW) (kBtu/hr)	29,560 (100,859)	40,940 (139,687)	29,290 (99,937)	29,247 (99,791)	58,697 (200,274)
Ratio heating load/cooling load	1.13	0.48	0.76	0.36	0.09

* Well water temperatures, taken from GLHEPRO (Spitler 2000).

The simulation results from the detailed system simulation for the ground heat exchangers including single U-tube closed loop system and standing column well systems in different regions are provided from Table 7-7 through Table 7-11. The same procedures used for simulating and analysis the cases in Boston, MA were employed for these cities.

For cases in Concord, NH, the design minimum fluid temperature leaving the standing column well system is adjusted to be 5 ºC (41 ºF) rather than 7 ºC (44.6 ºF) by eliminating the safety factor. Because the heating load in Concord, NH is very large, even

the SCW depth is increased to be 1500 m (4921.5 ft), the original design minimum temperature could not be obtained.

Also, it should be noticed that the far field mean temperature listed in Table 7-6 is primarily for use in the design of U-tube closed-loop ground heat exchangers, whose depth usually is on the order of a hundred feet. Currently, the SCW1D model is still using those mean ground temperatures even for the standing column well with the depth on the order of a thousand feet, where the mean ground temperature is higher than the temperature listed in Table 7-6. This probably will oversize the standing column well system to some extent. In the future, this mean ground temperature should be adjusted based on the geothermal gradient and the actual depth of the borehole.

Table 7-8 Summary of ground heat exchanger simulation results for Harrisburg, PA

Harrisburg , PA	Single U-tube	Standing Column Well (Without bleeding)	Standing Column Well (With bleeding)
Ground Heat Exchanger System Summary			
Number of borehole	10	1	1
Borehole depth (m) (ft)	68.66 (225.27)	518 (1699.55)	351 (1151.63)
Total bore length required (m) (ft)	686.6 (2252.7)	518 (1699.55)	351 (1151.63)
Flow rate (m^3/s) (GPM)	0.001387 (22)	0.001387 (22	0.001387 (22
Maximum heat pump entering fluid temperature (ºC) (ºF)	30.52 (86.94)	21.97 (71.55)	26.66 (79.99)
Minimum heat pump entering fluid temperature (ºC) (ºF)	3.57 (38.42)	7.00 (44.60)	7.00 (44.60)
Ground Heat Exchanger System Capital Cost			
Total ground heat exchanger loop cost	$13,519	$9,262	$6,276
Ground Heat Exchanger System Operating Cost			
Heat pump plus circulating pump electrical power consumption - annual cost	$1,090	$1,083	$1,120
Heat pump plus circulating pump electrical power consumption - 20 year operating cost (present value)	$12,502	$12,422	$12,846
20-year Life Cycle Cost (present value)	$26,022	$21,684	$19,122
Feet per ton	137	104	69

Table 7-9 Summary of ground heat exchanger simulation results for Portland, OR

Portland, OR	Single U-tube	Standing Column Well (Without bleeding)	Standing Column Well (With bleeding)
Ground Heat Exchanger System Summary			
Number of borehole	8	1	1
Borehole depth (m) (ft)	84.85 (278.39)	237 (777.60)	151 (495.43)
Total bore length required (m) (ft)	678.78 (2783.9)	237 (777.60)	151 (495.43)
Flow rate (m^3/s) (GPM)	0.001387 (22)	0.001387 (22)	0.001387 (22)
Maximum heat pump entering fluid temperature (ºC) (ºF)	30.66 (87.19)	33.47 (92.25)	32.36 (90.25)
Minimum heat pump entering fluid temperature (ºC) (ºF)	7.38 (45.28)	7.01 (44.62)	6.94 (44.49)
Ground Heat Exchanger System Capital Cost			
Total ground heat exchanger loop cost	$13,365	$4,238	$3,933
Ground Heat Exchanger System Operating Cost			
Heat pump plus circulating pump electrical power consumption - annual cost	$613	$618	$644
Heat pump plus circulating pump electrical power consumption - 20 year operating cost (present value)	$7,035	$7,093	$7,382
20-year Life Cycle Cost (present value)	$20,400	$11,331	$10,082
Feet per ton	148	52	33

Table 7-10 Summary of ground heat exchanger simulation results for Concord, NH

Concord, NH	Single U-tube	Standing Column Well (Without bleeding)	Standing Column Well (With bleeding)
Ground Heat Exchanger System Summary			
Number of borehole	10	1	1
Borehole depth (m) (ft)	119.67 (392.64)	608 (1994.85)	447 (1466.6)
Total bore length required (m) (ft)	1196.7 (3926.4)	608 (1994.85)	447 (1466.6
Flow rate (m^3/s) (GPM)	0.001387 (22)	0.001387 (22)	0.001387 (22)
Maximum heat pump entering fluid temperature (ºC) (ºF)	16.32 (61.38)	17.25 (63.05)	20.54 (37.39)
Minimum heat pump entering fluid temperature (ºC) (ºF)	3.70 (38.66)	5.01* (41.02)	5.01* (41.02)
Ground Heat Exchanger System Capital Cost			
Total ground heat exchanger loop cost	$23,563	$10,871	$7,992
Ground Heat Exchanger System Operating Cost			
Heat pump plus circulating pump electrical power consumption – annual cost	$1,839	$1,843	$1,871
Heat pump plus circulating pump electrical power consumption – 20 year operating cost (present value)	$21,093	$21,139	$21,460
20-year Life Cycle Cost	$44,656	$32,010	$29,452
Feet per ton	164	83	60

Table 7-11 Summary of ground heat exchanger simulation results for Birmingham, AL

Birmingham, AL	Single U-tube	Standing Column Well (Without bleeding)	Standing Column Well (With bleeding)
Ground Heat Exchanger System Summary			
Number of borehole	10	1	1
Borehole depth (m) (ft)	88.71 (291.06)	431 (1414.11)	351 (1151.63)
Total bore length required (m) (ft)	887.1 (2910.6)	431 (1414.11)	351 (1151.63)
Flow rate (m^3/s) (GPM)	0.001387 (22)	0.001387 (22)	0.001387 (22)
Maximum heat pump entering fluid temperature (ºC) (ºF)	30.18 (86.32)	29.98 (85.96)	30.03 (86.05)
Minimum heat pump entering fluid temperature (ºC) (ºF)	12.57 (54.63)	13.28 (55.90)	12.74 (54.93)
Ground Heat Exchanger System Capital Cost			
Total ground heat exchanger loop cost	$17,467	$7,706	$6,276
Ground Heat Exchanger System Operating Cost			
Heat pump plus circulating pump electrical power consumption - annual cost	$1,352	$1,339	$1,363
Heat pump plus circulating pump electrical power consumption - 20 year operating cost (present value)	$15,507	$15,357	$15,638
20-year Life Cycle Cost (present value)	$32,974	$23,063	$21,914
Feet per ton	135	66	53

Table 7-12 Feet per ton for different ground heat exchangers

	Single U-tube	SCW without bleed	SCW with 10% deadbleed control
Concord, NH	164	83	60
Harrisburg, PA	137	104	69
Boston, MA	121	72	48
Portland, OR	148	52	33
Birmingham, AL	135	66	53
Average	141	75	53

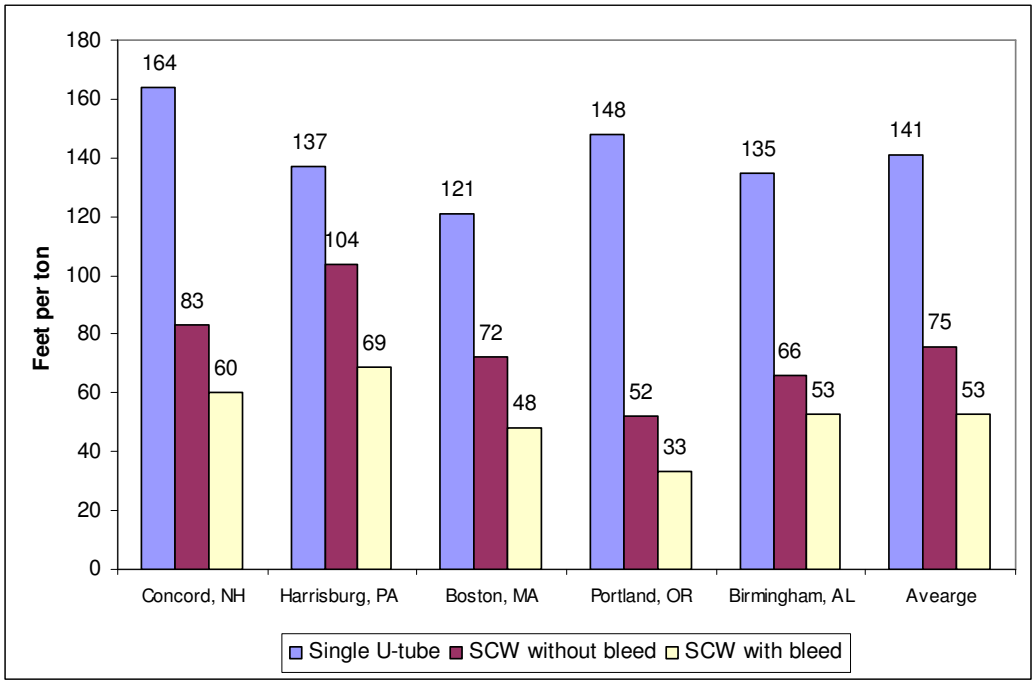

Figure 7-9 Feet per ton for different ground heat exchangers for small office building

Table 7-12 and Figure 7-9 summarize the calculated feet per ton for different ground heat exchangers for the small office building. The results show that on average, the standing column well system without bleed can reduce the required feet per ton by 46.8 %, and the system with bleed can reduce the feet per ton by 62.4 %. Likewise, total length requirements, as shown in Figure 7-10 are reduced in the same proportions.

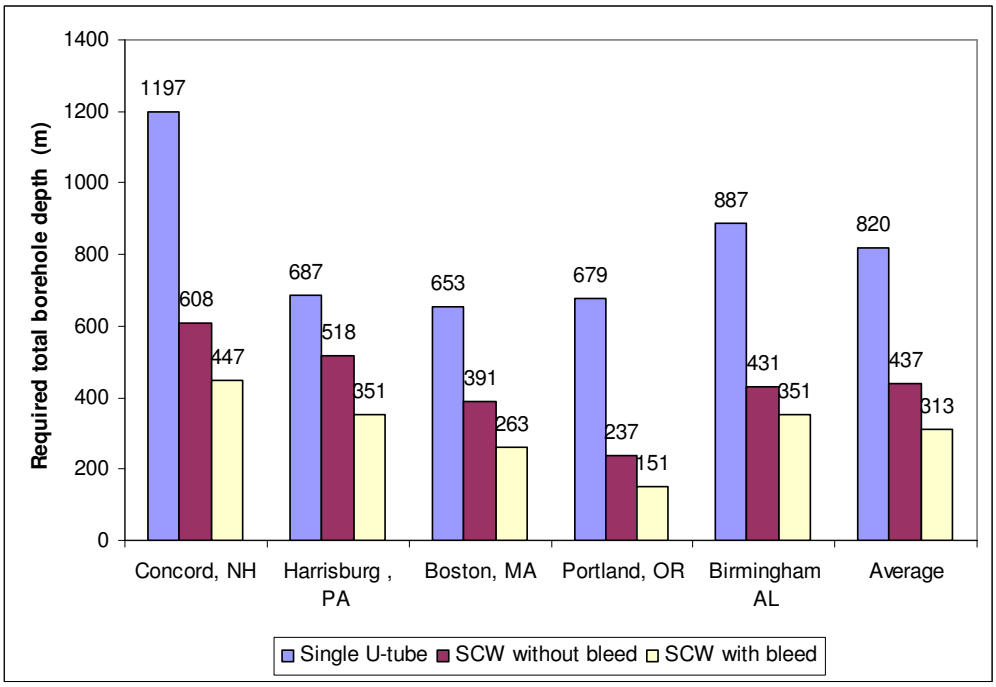

Figure 7-10 Required total borehole depth for different ground heat exchanger systems in different cities

Table 7-13 and Figure 7-11 give the comparison of the capital costs between standing column well systems and closed-loop systems. Compared with the single U-tube closed-loop system, the standing column well system without bleed and with bleed reduces capital costs by at least 31.5 % and 53.6 % (Harrisburg, PA) respectively.

Table 7-13 Comparisons of capital cost for different cites

Cities	Single U-tube	SCW without bleed		SCW with bleed	
	Capital Cost	Capital Cost		Capital Cost	
Concord, NH	$23,563	$10,871	53.86%	$7,992	66.08%
Harrisburg , PA	$13,529	$9,262	31.54%	$6,276	53.61%
Boston, MA	$12,866	$6,991	45.66%	$4,702	63.45%
Portland, OR	$13,365	$4,238	68.29%	$2,700	79.80%
Birmingham AL	$17,467	$7,706	55.88%	$6,276	64.07%

* Percentages are the cost reductions compared with single U-tube system.

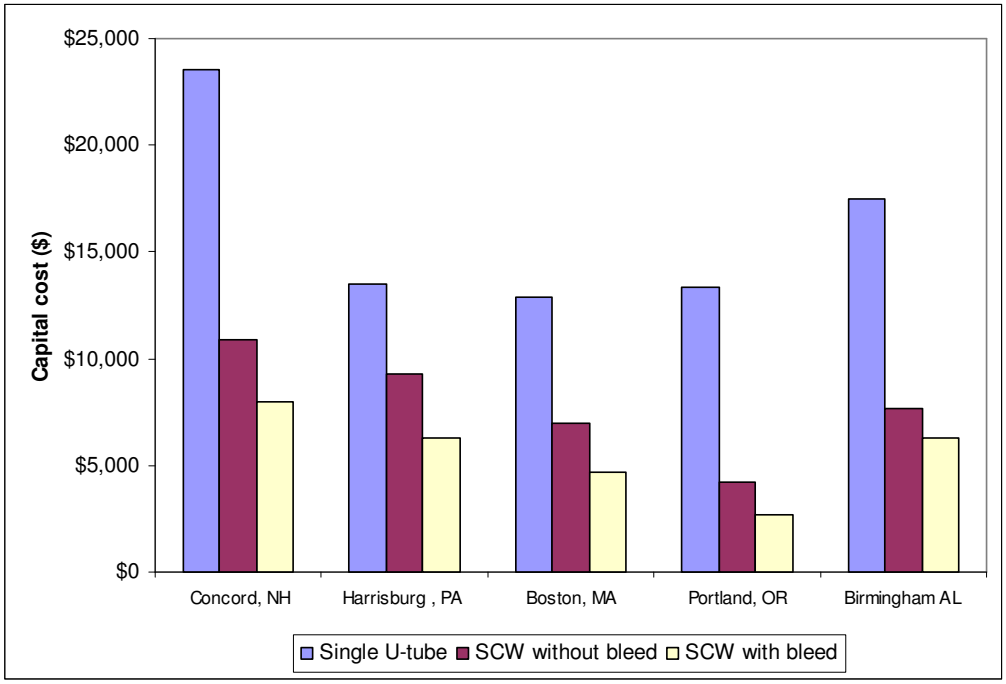

Figure 7-11 Capital cost for different ground heat exchanger systems in different cities

Table 7-14 and Figure 7-12 present the results for 20-year life cycle cost analysis for different ground heat exchanger systems in different cities. Compared with the single U-tube closed-loop system, the standing column well system without bleed and with bleed reduces 20-year life cycle cost by at least 16.7 % and 26.5 % (Harrisburg, PA) respectively. The operating costs of different systems for the same city are fairly similar,

but there is significant difference between the capital costs, which causes the great change in the total life cycle costs.

Table 7-14 20-year life cycle cost (present values) for different cites

Cities	Single U-tube	SCW without bleed		SCW with bleed	
Concord, NH	$44,656	$32,010	28.32%	$29,452	34.05%
Harrisburg , PA	$26,022	$21,684	16.67%	$19,122	26.51%
Boston, MA	$29,364	$22,767	22.47%	$21,063	28.27%
Portland, OR	$20,400	$11,331	44.46%	$10,082	50.58%
Birmingham AL	$32,974	$23,063	30.06%	$21,914	33.54%

* Percentages are the cost reductions compared with single U-tube system.

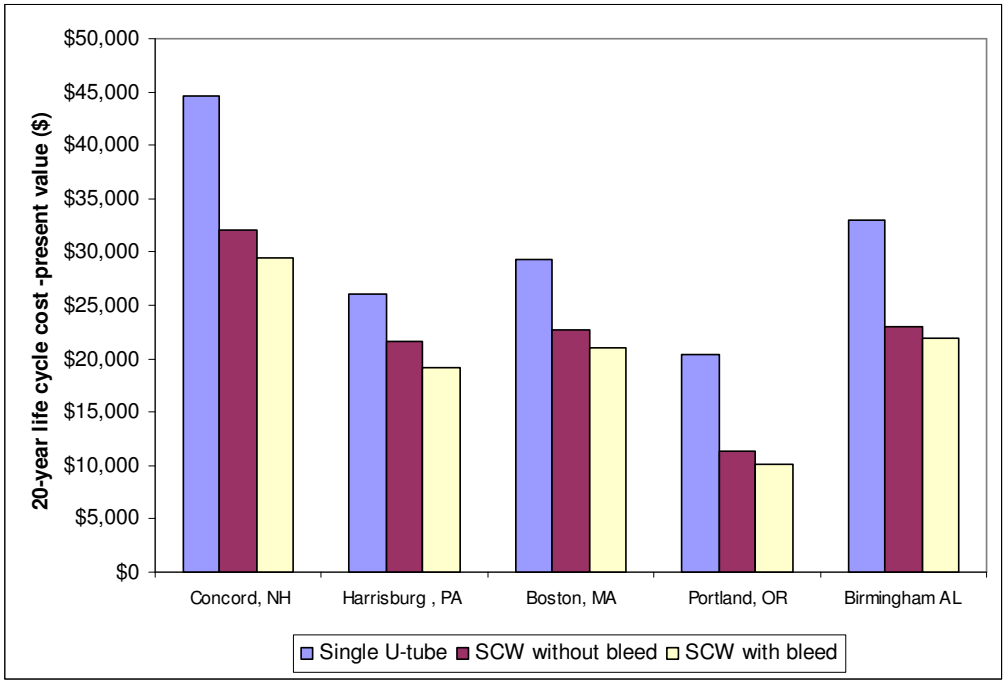

Figure 7-12 20-year cycle cost (present value) for different ground heat exchanger systems in different cities

8. CONCLUSIONS AND RECOMMENDATIONS

This chapter summarizes the conclusions that can be drawn from the previous chapters, and gives recommendations for potential future work. The following conclusions can be drawn from this work:

1. A detailed two-dimensional numerical model of a standing column well has been developed to calculate groundwater flow and heat transfer. This model has been validated against limited experimental data and employed in a parametric study of standing column well system performance. A base case design was developed with parameter values representative of common standing column well installation conditions. Calculations were made over a one-year operating period, where a single design parameter value is varied relative to the base case. This has enabled the effect and significance of each design parameter to be studied.
2. The parametric study has confirmed many of the standing column well performance characteristics found in practice. Better performance is possible where thermal and hydraulic conductivities are higher and the water table is higher. Indeed, these are the characteristics of the regions in which current installations are found. Regions where SCW systems are currently installed also have good quality groundwater and do not require isolation of the heat pump from the groundwater. This study has focused on thermal performance of SCW systems, but it is also important to note their reliance on groundwater quality. In

practice, the designer, for a given location, has no control over the thermal and hydraulic properties of the geological formation. However, the designer does have control over borehole parameters such as length, diameter, dip tube size and material, in addition to the system bleed rate and bleed control strategies. Of these parameters, the length and bleed have been shown to affect performance most significantly. The results of this study show that introduction of bleed flow can dramatically improve the performance of the SCW system. Significant improvements in performance were found with only moderate rates of bleed (5-15 % of system flow). However, in practice there may be a number of limitations on the amount of bleed that can be achieved, including local hrdaulic conditions, well pumping capacity and practical difficulties in disposing of the bleed water.

3. Annual energy consumption has been estimated for each case in the parametric study. Results show that the poorest energy performance occurs in cases with the least favorable thermal and hydraulic conductivities. The lowest energy costs are found in cases where continuous bleed is introduced and, consequently, more moderate fluid temperatures are achieved, and therefore, heat pump efficiency is improved. Where the water table is high, on the order of 5 meters, the increased pump power when bleeding is not significant and the greatest efficiencies result when bleed rate is maximized. However, when the water table is low, on the order of 30 meters, pump power requirements increase significantly when bleed is introduced. The benefits of higher rates of continuous bleed (> 10 % in this study) are then outweighed by the increased pumping costs.

4. Due to the computationally intensive nature of the calculations required for a detailed study of standing column well performance, it is unlikely that the detailed model developed in this work will be directly suitable for use in design tools. The governing partial differential equation is non-linear and, therefore, simplified analytical models are difficult to apply. However, a simplified one-dimensional numerical model that explicitly models the advection has been developed. This simplified model with "enhanced" thermal conductivities has been validated against the detailed two-dimensional numerical model and limited experimental data.
5. A parametric study for economic analysis based on the simplified model was performed. SCW systems allowed significant reductions in borehole depth. Compared with single vertical U-tube closed-loop systems, without bleed, borehole depth reductions between 24.6 % and 65.1 % are possible. With 10 % deadband bleed control, significant reductions in design borehole depth on the order of 48.9 % to 77.8 % are achieved. Because of the significant reduction of capital cost due to less required total borehole depth, the 20-year life cycle cost analysis shows cost savings in the standing column well system with bleed control over single vertical U-tube closed-loop system of at least 26.5 %.
6. This study shows that the average required design depth for standing column well systems for a particular building in a few selected climates without bleed is 75 feet per ton, and 53 feet per ton for standing column well systems with 10 % deadband bleed control. This compared to 141 feet per ton for U-tube closed-loop systems.

7. The study on the limiting case, where groundwater flows in an impermeable medium with a large fracture in it, shows that 2 ºC (3.6 ºF) safety factor might be prudent for designers of standing column well systems operating near the freezing point. In the reality, this safety factor will be smaller considering that the conservative analysis done for the limiting case.

Recommendations for future research include the following:

1. Integrate the simplified model into building simulation software, such as EnergyPlus. This will facilitate greater usage of the model by designers.
2. Extend the model to account for well-to-well interference in multiple standing column well systems.
3. Perform validation against a better experimental data set. Currently available data sets suffer from several significant limitations. An ideal experimental plan might include the following prior to commencement of system operation:
    - General information about aquifer characteristics.
    - Measurement of water table depth.
    - An *in situ* measurement of the thermal conductivity. (Austin, et al. 2000).
    - A well drawdown test to determine the hydraulic conductivity.

After commencement of system operation, the following measurements would need to be made continuously for several years on short time intervals, perhaps five minutes:

- Water temperatures entering and exiting the well.

- Flow rate to and from the well. (Two flow measurements are needed to keep track of bleed operation).

Additional measurements, which if made throughout the measurement period, would be useful, though not absolutely necessary include:

- Water level in the well.
- Temperatures inside the well at several locations and depths, e.g. dip tube inside, dip tube outside, etc.

4. Only one building type (small office building) was studied. Future work might extend parametric study of the life cycle cost and required design borehole depth to other building types, with different load profiles.
5. Future research might study combined heat and mass transfer for specific fracture geometries. This would more accurately model flow in the fractures, and be useful to more accurately determine the safety factor required.
6. Refinement of drilling and installation cost comparisons through case studies.
7. Only one bleed control strategy with one set of temperature set points was studied. It would be useful to investigate other bleed control strategies.

9. REFERENCES

Ashtiani, B.A., R.E. Volker, and D.A. Lockington, 1999. Numerical and experimental study of seepage in unconfined aquifers with a periodic boundary condition. *Journal of Hydrology*, 222: 165-184.

ASHRAE. 1999. *R&D studies applied to standing column well design* (1119-TRP). Atlanta: American Society of Heating, Refrigerating, and Air-Conditioning Engineers.

ASHRAE Handbook, *Fundamental Volume*, American Society of Heating , Refrigerating and Air-Conditioning Engineers, Inc., Atlanta, GA,2001.

Austin, W., C. Yavuzturk, and J.D. Spitler, 2000. Development of an in-situ system for measuring ground thermal properties. *ASHRAE Transactions,* 106(1): 365-379.

Bear, J. 1972. *Dynamics of Fluids in Porous Media*. New York: Dover Publications, Inc.

Bernier, M.A. 2001. Ground-coupled heat pump system simulation. *ASHRAE Transactions*, 107(1): 605-616.

Bhatii, M.S. and R.H. Shah, 1987. Turbulent and transition flow convective heat transfer in ducts. *Handbook of Single-Phase Convective Heat Transfer*. New York: John Wiley & Sons, Inc.

Bose, J.E., C. W. Ledbetter, and J. R. Partin, 1979. Experimental results of a low-cost solar-assisted heat pump system using earth coil and geo-thermal well storage. *The 4th Annual Heat Pump Technology Conference*, Stillwater, OK.

Bose, J.E., J. R. Partin, C. W. Ledbetter, and G.D. Cason, 1980. Earth coupled and solar assisted heat pump systems. *The 5th Annual Heat Pump Technology Conference*, Stillwater, OK.

Bose, J.E. 1988. *Closed-loop/Ground-source Heat Pump System Installation Guide*. Oklahoma State University, Stillwater, OK.

Braud, H., H. Klimkowki, and J. Oliver, 1983. Earth source heat exchanger for heat pumps. *Transactions of ASAE*, 26: 1818-1822.

Carslaw, H.S. and J.C. Jaeger, 1959. *Conduction of heat in solids*. Second Edition. Oxford: Clarendon Press.

Chen, C. and J.J. Jiao, 1999. Numerical simulation of pumping tests in multiplayer wells with non-Dacican flow in the well bore. *Groundwater*, 37(3): 465-474.

Chen, N.H. 1979. An explicit equation for friction factor on pipe. *Industrial and Engineering Chemistry Fundamentals*, 18: 296-297.

Chen, X, 1996. *Addition of Annual Building Energy Analysis Capacity to A Design Load Calculation Program*. Master Thesis, Oklahoma State University, Stillwater, OK.

Chevalier, S. and O. Banton, 1999. Modeling of heat transfer with random walk method, Part 1" Application to thermal energy storage in porous aquifers. *Journal of Hydrology*, 222: 129-139.

Chiasson, A. 1999. *Advances in Modeling of Ground-Source Heat Pump Systems.* Masters thesis, Oklahoma State University, Stillwater, OK.

Chiasson, A., S.J. Rees, and J.D. Spitler, 2000. A preliminary assessment of the effects of ground-water flow on closed-loop ground-source heat pump systems. *ASHRAE Transactions*, 106(1): 380-393.

Churchill, S.W. and H.S. Chu, 1975. Correction equations for laminar and turbulent free convection from a vertical plate. *International Journal of Heat and Mass Transfer*, 18: 1323-1329.

Claesson, J. and P. Eskilson, 1987. *Conductive Heat Extraction by a Deep Borehole.*

Analytical Studies. Departments of Mathematical Physics and Building Technology, Lund University, Box 118, SE-221 00 Lund, Sweden.

Claesson, J. and G. Hellström, 2000. Analytical studies of the influence of regional groundatwater flow on the performance of borehole heat exchangers. *The 8th International Conference on Thermal Energy Storage*. TERRASTOCK 2000, Stuttgart, Germany. pp. 105-115.

Clark, D.R. 1985. *HVACSIM+ Building Systems and Equipment Simulation Program Reference Manual.* NBSIR 84-2996. National Bureau of Standard, January, 1985.

Cooper Union Research Foundation, 1986. *A semi-closed loop ground-water heat pump*. Final report submitted to Consolidated Edison Company.

DenBraven, R.K. 2002. Regulations for open-loop ground-source heat pumps in the United States. *ASHRAE Transactions*, 108 (1): 962-967.

Deerman, J.D. and S.P. Kavanaugh, 1991. Simulation of vertical U-tube ground-coupled heat pump systems using cylindrical heat source solution. *ASHRAE Transactions* 97(1): 287-295.

Domenico, P.A., and F.W. Schwartz, 1990. *Physical and Chemical Hydrogeology*. New

York: John Wiley & Sons, Inc.

Driscoll, F.G. 1986. *Groundwater and Wells*. Second Edition. St. Paul MN: Johnson Filtration Systems, Inc.

Eskilson, P. 1987. *Thermal Analysis of Heat Extraction Boreholes*. Doctoral Thesis, University of Lund, Department of Mathematical Physics. Lund, Sweden.

Fetter, C.W. 1994. *Applied Hydrogeology*. Third Edition. New York: Macmillan.

Freeze, R.A. and J.A. Cherry, 1979. *Groundwater*. Englewood Cliffs, N J: Prentice-Hall, Inc.

Gehlin, S.E.A. 2002. *Thermal response test-method development and evaluation.* Ph.D dissertation, Luleå University of Technology, Luleå, Sweden.

Gnielinski, V. 1976. New equations for heat and mass transfer in turbulent flow pipes and ducts. *International Chemical Engineering*, 16: 359-367.

Greenkorn, R. 1983. *Flow phenomena in porous media*. New York: Marcel Dekker, inc.

Hall, S.H. and J.R. Raymond, 1992. Geohydrologic characterization for aquifer thermal

energy storage. *27th Intersociety Energy Conversion Engineering Conference Proceedings*, San Diego, pp. 101-107.

Hart, D.P. and R. Couvillion, 1986. *Earth Coupled Heat Transfer*. Dublin, OH: National Water Well Association.

Hellström, G., J. Bennet, and J. Claesson, 1986. *Heat Storage in the Ground: Aquifer Thermal Energy Storage-Single Well Model. Manual for Computer Code*. Department of Mathematical Physics, University of Lund, Box 118, SE-221 00 Lund, Sweden.

Hellström, G. and J. Bennet, 1986. *Heat Storage in the Ground: Aquifer Thermal Energy Storage-Double Well model. Manual for Computer Code*. Department of Mathematical Physics, University of Lund, Box 118, SE-221 00 Lund, Sweden.

Hellström, G. 1991. *Ground Heat Storage: Thermal Analyses of Duct Storage Systems-Theory.* Department of Mathematical Physics, University of Lund, Box 118, SE-221 00 Lund, Sweden.

Henderson, H. 2003. Personal communication.

Hopkirk R. J. and R. Burkart, 1990. Earth-coupled heat pumps: solving energy and

environmental challenges. *Proceedings of the 3rd International Energy Agency Heat Pump Conference*. Tokyo, Japan, pp. 411-421.

HYY, 2000. *Central Liquid State Cooling & Heating Source Environmental System Catalogue*. Beijing ever source science & technology development Co. LTD. Beijing, China.

Ingersoll, L. R. and H. J. Plass, 1948. Theory of the ground pipe heat source for the heat pump. *ASHVE Transaction*, 54: 339-348.

Ingersoll, L. R., F.T. Adler, H.J. Plass, and A.C. Ingersoll, 1951. Theory of earth heat exchangers for the heat pump. *ASHVE Transaction*, 57: 167-188.

Ingersoll, L.R., O.J. Zobel, and A.C. Ingersoll, 1954. *Heat Conduction with Engineering, Geological and Other Applications.* Madison, WI: The University of Wisconsin Press.

International Ground Source Heat Pump Association (IGSHPA). 1988. *Closed-loop/ground-source heat pump systems. Installation guide* (National Rural Electric Cooperative Association (NRECA) Research project 86-1). IGSHPA, Oklahoma State University, Stillwater, OK.

Johnson, C. 2003. Personal communication.

Kangas, M.T. 1996. Thermohydraulic analysis of ground as a heat source for heat pumps using vertical pipes. *Transactions of ASME: Journal of Energy Resources Technology*, 118: 300-305.

Kangas, M.T. and P.D. Lund, 1994. Modeling and simulation of aquifer storage energy systems. *Solar Energy*, 53(3): 237-247.

Kavanaugh, S.P. 1984. *Simulation and Experimental Verification of Vertical Ground-Coupled Heat Pump System*. Ph.D. dissertation, Oklahoma State University, Stillwater, OK.

Kavanaugh, S.P. and K. Rafferty, 1997. *Ground-source Heat Pumps: Design of Geothermal Systems for Commercial and Institutional Buildings*. American Society of Heating, Refrigeration and Air-conditioning Engineers, Inc., Atlanta, GA.

Marseille, T.J. and D.A. Wilke, 1992. Review of the aquifer seasonal energy storage building HVAC system at the Melville, New York, mid-island mail facility. *27th Intersociety Energy Conversion Engineering Conference Proceedings.* San Diego, CA, pp. 143-148.

Molson, J.M. and E.O. Frind, 1992. Thermal energy storage in an unconfined aquifer 2.Model development, validation, and application. *Water Resource Research*,

28(10): 2857-2867.

Midkiff, K.C., C.E. Brett, K. Balaji, and Y.K. Song, 1992. Long-term performance of an air-conditioning system based on seasonal aquifer chill energy storage. *27th Intersociety Energy Conversion Engineering Conference Proceedings*. San Diego, CA, pp. 49-54.

Mikler, V. 1993. *A Theoretical and Experimental Study of the "Energy Well" Performance*. Masters thesis, Pennsylvania State University, College Park, PA.

Norris, R.H. 1971. Some simple approximate heat transfer correlations for turbulent flow in ducts with rough faces. *Augmentation of Convective Heat and Mass transfer, ASME*. pp. 16-26.

Oliver, J., and H. Braud, 1981. Thermal exchange to earth with concentric well pipes. *Transactions of ASAE*. 24(4): 906-910.

Orio, C.D. 1988. Vertical earth coupling Kelvin line theory. *Technical Bulletin #43*. Water &Energy System Crop, Atkinson, NH.

Orio, C.D. 1994. Geothermal heat pumps and standing column wells. *Geothermal Resources Council Transactions,* 18: 375-379.

Orio, C.D. 1995. Design, use & example of standing column wells. *IGSPHA Technical Meeting*.

Orio, C.D. 1999. Geothermal heat pump applications industrial /commercial. *Energy Engineering*, 96(3): 58-66.

Orio, C.D. 2001. Personal communication.

Rafferty, K.D. 1998. Well-pumping issues in commercial groundwater heat pump system. *ASHRAE Transactions*, 104(1B): 927-931.

Rawlings, R.H.D. and J.R. Sykulski, 1999. Ground source heat pumps: a technology review. *Building Services Engineering Research and Technology*. 20(3): 119-129.

Rees, S.J. 2000. *An Introduction to the Finite Volume Method: Tutorial series*. Oklahoma State Univesity, Stillwater, OK.

Rees, S. J. 2001. Advances in modeling of standing column wells. *International Ground Source Heat Pump Association Technical Conference & Expo*, Stillwater, OK.

Sachs, H.M. and D.R. Dinse, 2000. Geology and the ground heat exchanger: What engineers need to know. *ASHRAE Transactions*, 106(2): 421-433.

Singhal, B.B.S. and R.P. Gupta. 1999. *Applied Hydrogeology of Fracture Rocks*. Kluwer Academic Publishers, Dordrecht, the Netherlands.

Spitler, J.D. 2000. GLHEPRO- A Design Tool for Commercial Building Ground Loop Heat Exchangers. *Proceedings of the Fourth International Heat Pumps in Cold Climates Conference*, Aylmer, Québec. August 17-18, 2000.

Spitler, J. D., S.J. Rees, Z. Deng, A. Chiasson, C.D. Orio, and C. Johnson, 2002. *ASHRAE 1119-RP: R & D Studies Applied to Standing Column Well Design.* Final Report. Oklahoma State University, Stillwater, OK.

Sun, J. 2004. Personal communication.

Tan, C. and E. Kush, 1986. Semi-closed loop standing column well groundwater source heat pump. *GHPC website* www.geoexchange.org R&D Project Profile No.3.

Techo, R., R.R. Tickner, and R.E. James, 1965. An accurate equation for the computation of the friction factor for smooth pipes from the Reynolds-number. *Journal of Applied Mechanics*, 32: 443.

Voss, C.I. 1984. *SUTRA: A finite element simulation model for saturated-unsaturated fluid-density dependent ground-water flow with energy transport or chemically reactive single species solute transport*. U. S. Geological Survey, Reston, VA.

Yavuzturk, C. 1999. *Modeling of Vertical Ground Loop Heat Exchangers for Ground Source Heat Pump System*. Ph.D. dissertation, Oklahoma State University, Stillwater, OK.

Yavuzturk, C. and A. D. Chiasson. 2002. Performance Analysis of U-Tube, Concentric Tube, and Standing Column Well Ground Heat Exchangers using a System Simulation Approach. *ASHRAE Transactions*. 108(1):925-938.

Yuill, G.K. and V. Mikler, 1995. Analysis of the effect of induced groundwater flow on heat transfer from a vertical open-hole concentric-tube thermal well. *ASHRAE Transactions*. 101(1): 173-185.

APPENDIX A

Numerical characteristics of the detailed model

The solution domain, grid size and time-step size are important for the numerical model. This section discusses numerical characteristics of the detailed two-dimensional finite volume model.

The same building loads and simulation procedure described in Chapter 4 for the detailed simulation of the base case are used in this study. The geometrical configuration of the SCW chosen for this study is listed in Table A-1.

Table A-1 Geometrical configuration of the borehole (Mikler 1993)

Parameter	**Depth**	**Diameter**
Units	**m (ft)**	**mm (in)**
Borehole	320 (1049.6)	152.4 (6)
Discharge pipe	2 (6.56)	33.4 (1.3)
Suction pipe	318 (1043)	101.6 (4)

The given SCW system (Mikler 1993) will be simulated by the detailed numerical model to find the integral mass flow rates along the lower half of the borehole and to find the minimum temperatures back to heat pump. The mass flow rate and temperature sensitivities with respect to the domain size and the grid size will be discussed, followed by a discussion of the time-step size.

Because the simulation time is rather large, first the head equation will be solved to get the integral mass flow rate along the lower half of the borehole. Then, only specific cases of interest will be chosen to do further sensitivity analysis of minimum temperatures back

to the heat pump. This means that both head and energy equations will be solved in the model. In the detailed model, the head equation solution is independent of the energy equation. However, the energy equation solution is largely dependent on the head equation.

Discussion of the selection of the simulation domain

First, the domain for the simulation should be chosen (see Figure A-1). During the calculations for selection of appropriate domain, the grid size (see Table A-2) is set to be fine for accuracy because the appropriate grid size is not available at this earlier stage. The computational speed is not taken into account at this time.

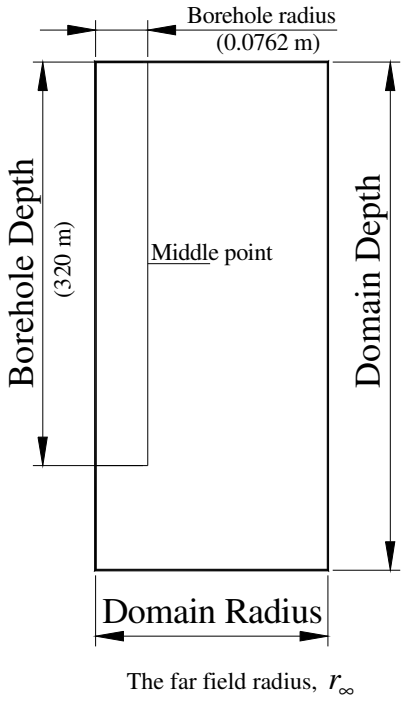

Figure A-1 The schematics of simulation domain

Table A-2 Grid size used in the selection of the domain

Depth (m)	Radius (m)	Grid size (Depth direction × R direction)
600	200	250×220
500	200	230×220
400	200	210×220
++380	200	210×220
360	200	190×220
340	200	190×220
380	30	210×50
380	60	210×80
380	90	210×110
380	++160	210×180
380	180	210×200
380	190	210×210
380	200	210×220
380	240	210×260
380	280	210×300
380	340	210×360

++ Final value for the domain size.

Different types of distribution functions (e.g., EQUAL, SINH, TANH, EXPONENTIAL, etc.) are used to define the variation of cell length in the spatial grid system. One grid generation input file is listed in Appendix B.

First, the head equation is solved to find the integral mass flow rate along the lower half of the borehole. At this stage, the domain radius (the far field radius, r_∞, in Figure A-1) is set to be 200 m. The far field radius, r_∞, is the physical distance from the borehole at which the ground temperature remains constant. The ground at a distance from the borehole greater than r_∞ is assumed to at the undisturbed ground temperature T_∞. The far field radius value depends on the length of the time (t) that the SCW system has been operating and on the ground's thermal diffusivity (α).

According to Hart and Couvillion (1986), a far field radius, r_∞, of $4\sqrt{\alpha \cdot t}$ should be sufficient for simulation of the problem. If the simulation is assumed to be an annual simulation, then r_∞ can be calculated to be 23.67 m. However, this approach does not consider the effect of groundwater movement. So, the domain should also be checked for groundwater flow.

Figure A –2 shows the sensitivity of the integral mass flow rate to the domain depth. Based on the sensitivity analysis results shown in Figure A-2, three more cases (i.e., depth 360m, 380m, 500m) were chosen to study the sensitivities of minimum water temperatures to the domain depth. For these three cases, both head and energy equations are solved in the detailed model. Figure A-3 shows the variations of the minimum water temperatures with the domain depth. Figure A-4 shows the variations of the water temperature back to the heat pump after one-year simulation (at the 8760^{th} hour) with the domain depth. The final domain depth size is chosen to be 380 m.

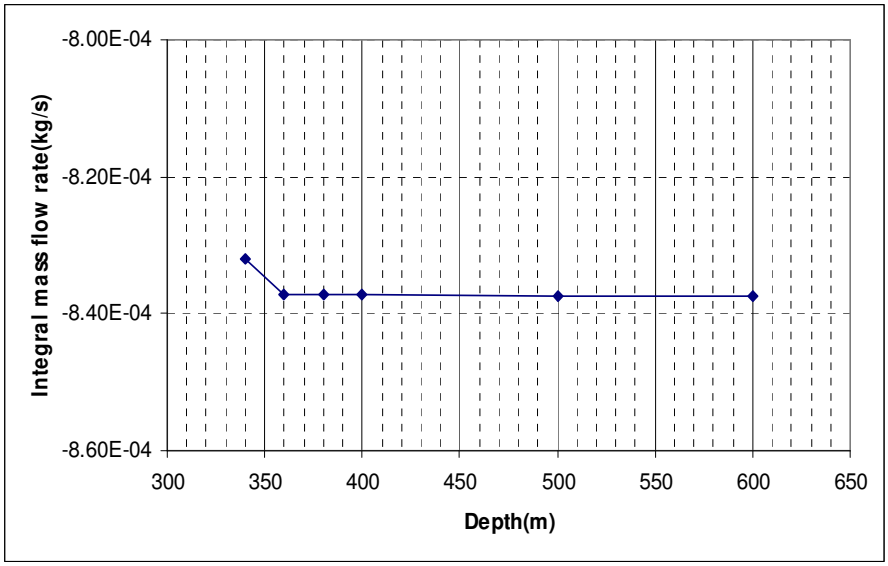

Figure A-2 Sensitivity of integral mass flow rate to the domain depth (Domain radius: 200m)

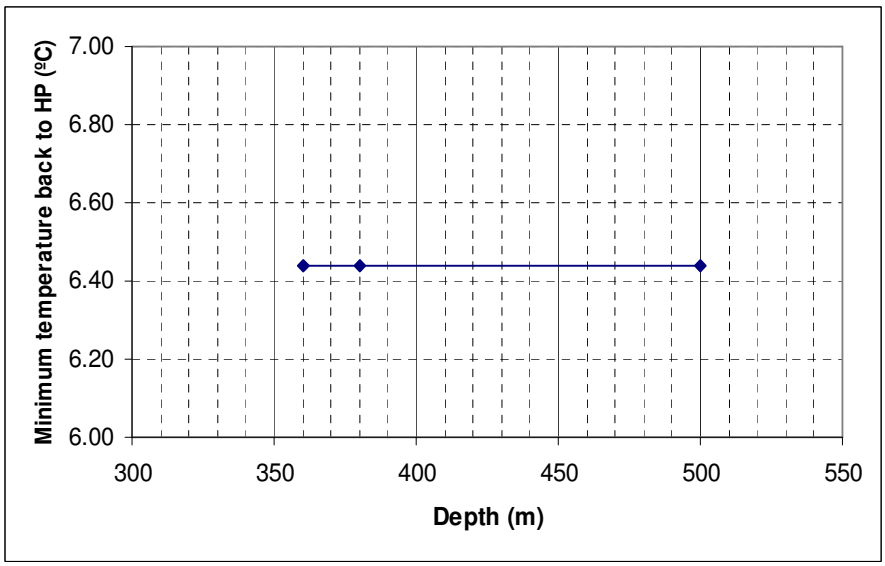

Figure A-3 Sensitivity of minimum temperature back to the heat pump to the domain depth (Domain radius: 200m)

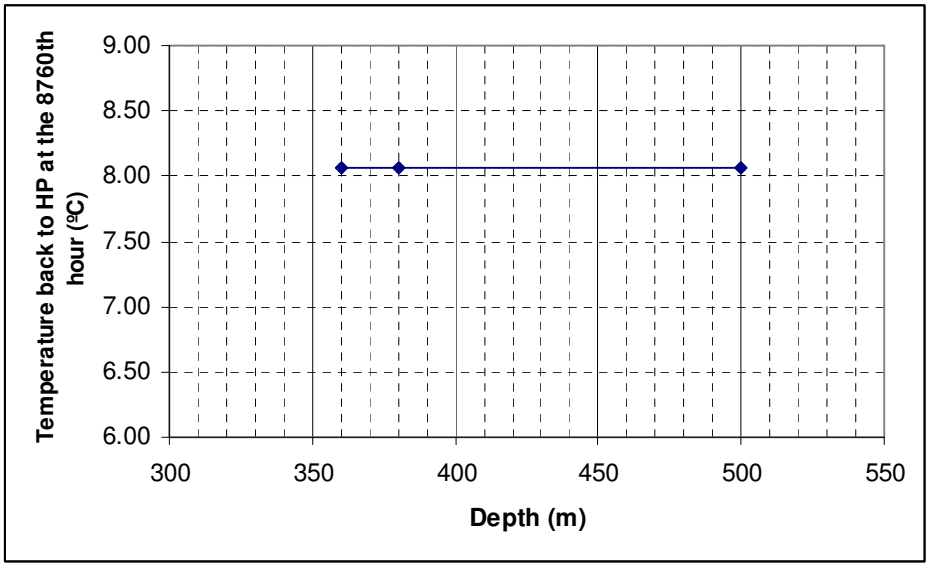

Figure A-4 Sensitivity of temperature back to the heat pump at the 8760th hour to the domain depth (Domain radius: 200m)

After the domain depth was chosen to be 380 m, a domain radius sensitivity analysis was performed. The sensitivity of the integral mass flow rate to the domain radius is shown in Figure A-5. Four more cases (i.e., radius 90m, 160 m, 180 m, 200 m) were chosen for studying the minimum water temperature sensitivities to the domain radius. Figure A-6 shows the variations of the minimum water temperatures with the domain radius. Figure A-7 shows the variations of the water temperature back to the heat pump after one-year simulation (at the 8760th hour) with the domain radius. The final domain radius size is chosen to be 180 m.

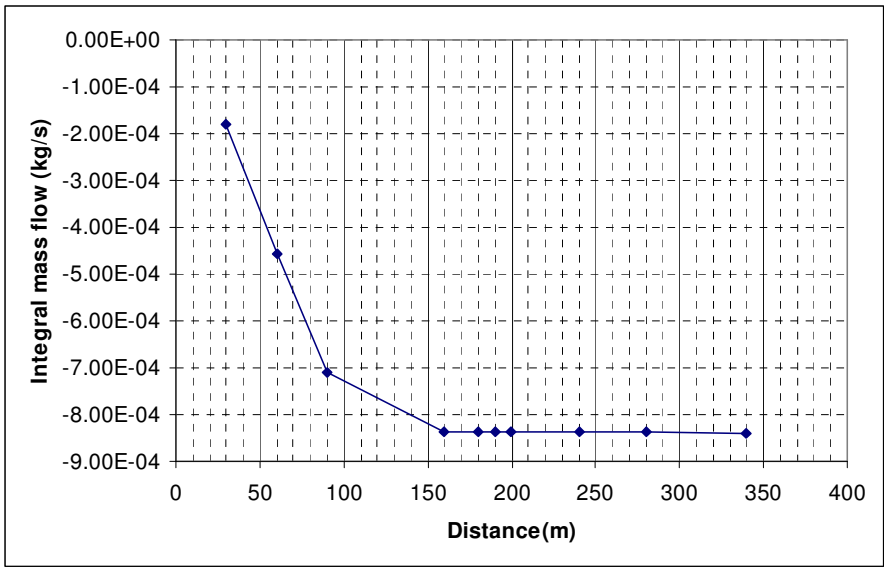

Figure A-5 Sensitivity of integral mass flow rate to the domain radius (Domain depth: 380m)

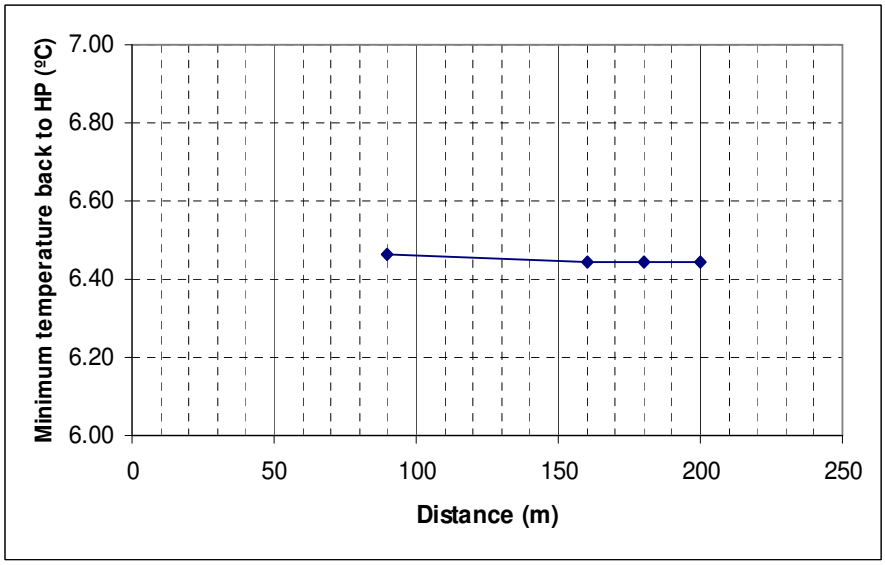

Figure A-6 Sensitivity of minimum temperature back to the heat pump to the domain radius (Domain depth: 380m)

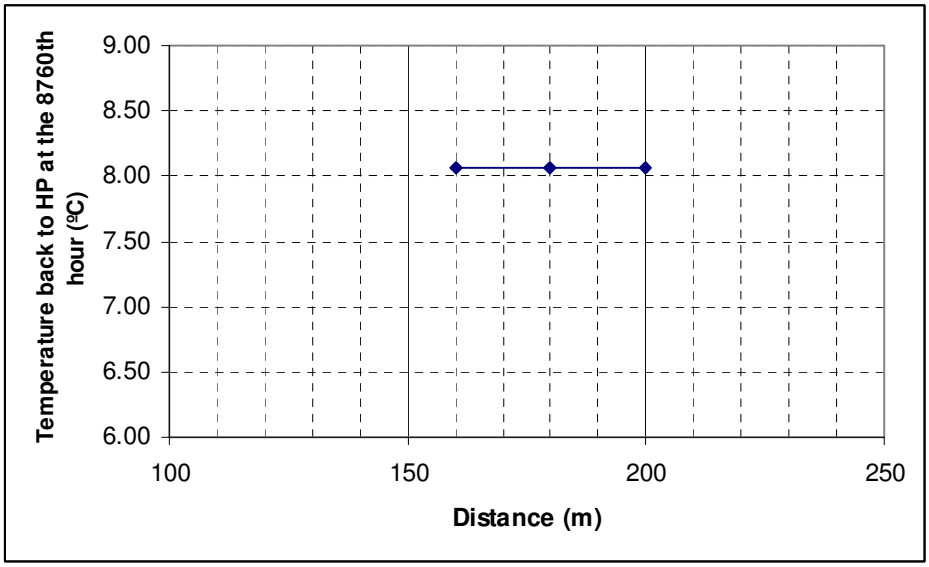

Figure A-7 Sensitivity of temperature back to the heat pump at the 8760th hour to the domain radius (Domain radius: 380 m)

Discussion of grid independence analysis

After the simulation domain (380m × 180m) was chosen, the grid independence analysis was performed. Figures A-8and A-9 show the sensitivities of simulation results (integral mass flow rate and minimum temperatures back to the heat pump) to the grid numbers in depth direction. At this stage, the radial direction grid number was set to be 200. The final value of the grid number in depth direction was chosen to be 160 as the best compromise between accuracy and computational speed.

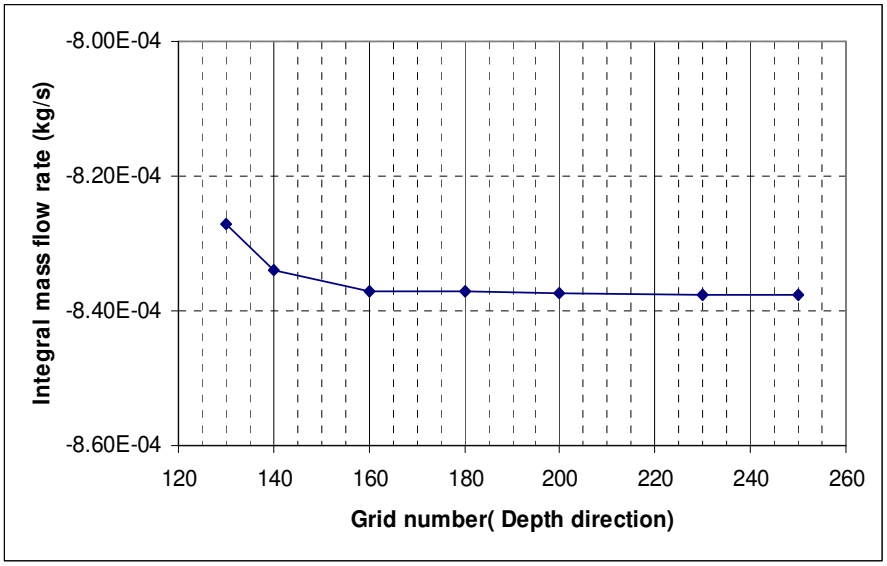

Figure A-8 Sensitivity of integral mass flow rate to grid number in depth direction (Grid number in R-direction: 200)

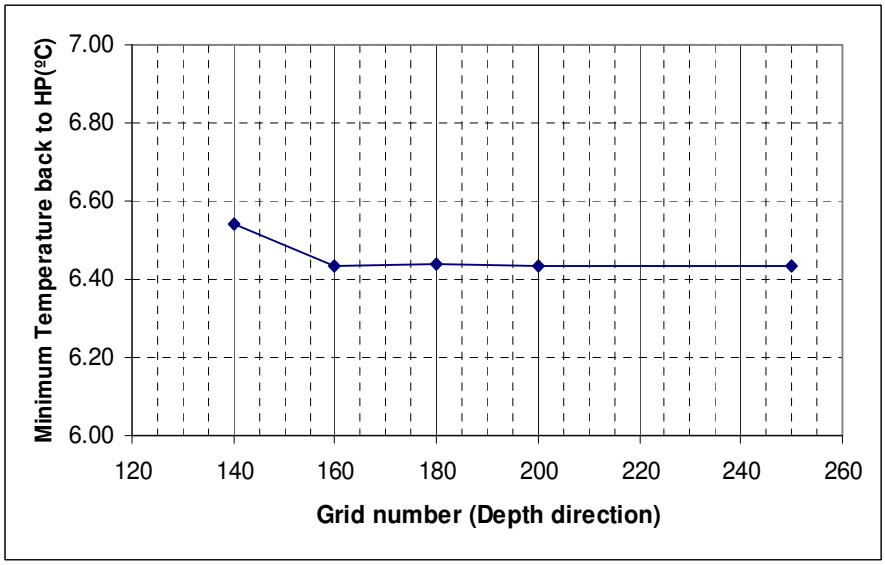

Figure A-9 Sensitivity of minimum temperatures back to the heat pump to the grid number in depth direction (Grid number in R-direction: 200)

After the depth direction grid number was decided to be 160, the grid independence analysis in radial direction was performed. Figures A-10 and A-11 show the variations of the simulation results (integral mass flow rate and minimum temperatures back to the heat pump) with the grid numbers in the radial direction. The final value of the grid number in the radial direction was chosen to be 70 as the best compromise between accuracy and computational speed.

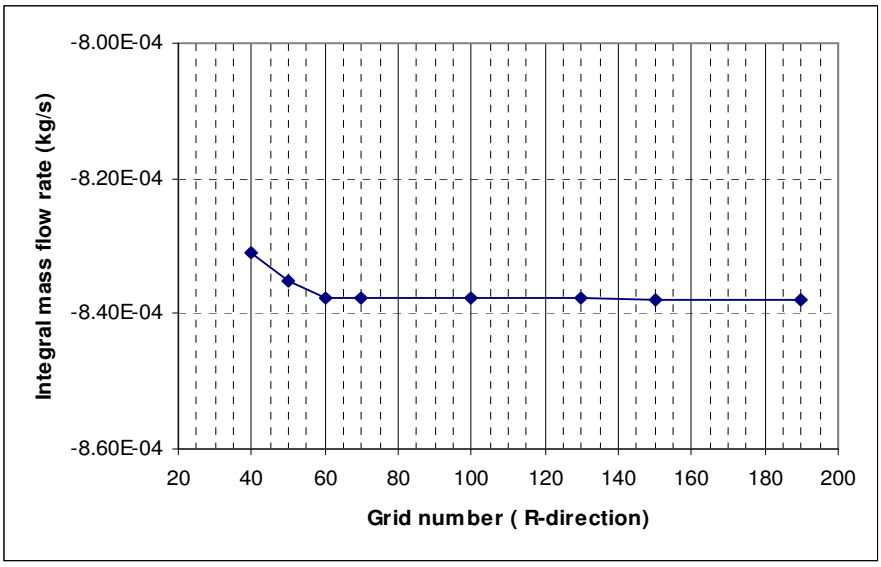

Figure A-10 Sensitivity of integral mass flow rate to grid number in radial direction (Grid number in depth direction: 160)

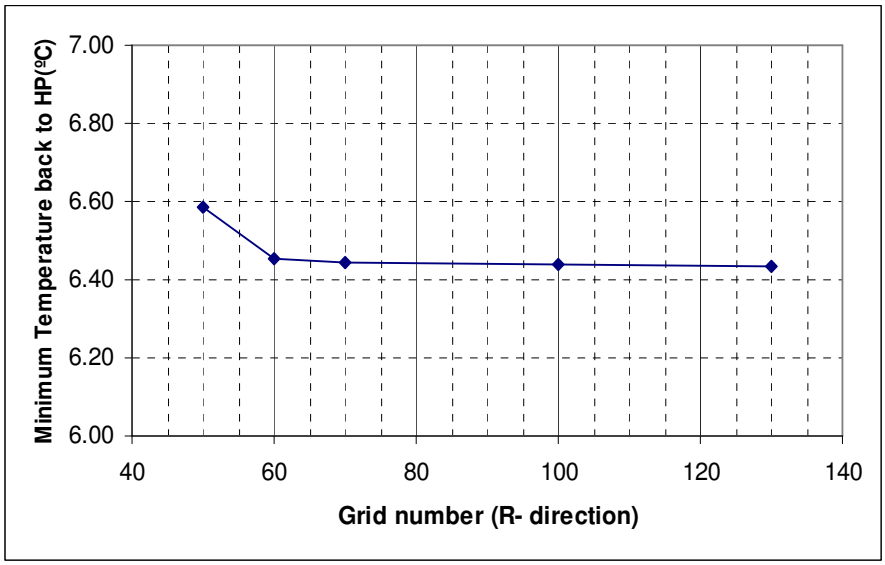

Figure A-11 Sensitivity of minimum temperatures back to the heat pump to the grid number in radial direction (Grid number in depth direction: 160)

A final grid size of 160×70 was chosen as the best compromise between accuracy and computational speed.

Discussion of time-step size

Time step size is important to the numerical calculation. In building simulation, hourly energy analysis is the focus. Due to the time consumption required for the whole year hourly simulation for the detailed numerical model, different time-step sizes have been used in the simulation (see Table A-3). Finally, time-step size was chosen to be 6 hours for the parametric study.

Table A-3 Simulation results for the base case in different time step sizes

	Time-step 6 hours	Time-step 5 hours	Time-step 2 hour	Time-step 1 hour
Maximum temperature back to the heat pump (ºC)	26.62	26.51	26.64	26.96
Minimum temperature back to the heat pump (ºC)	6.44	6.77	6.32	6.28
One year operation cost ($) (water table 5 m)	1482	1480	1484	1486
One year operation cost ($) (water table 30 m)	1503	1501	1504	1506

Fully implicit scheme is used in the detailed finite volume model. The discretized equation from this scheme can be said to be first-order accurate in time and second-order accurate in space. The fully implicit scheme is unconditionally numerical stable.

CFL (Courant, Friedrichs and Lewy) condition for hyperbolic equation

There are three different types of partial differential equation (PDE): elliptic, parabolic and hyperbolic.

$$au_{xx} + 2bu_{xy} + cu_{yy} + du_x + eu_y + fu = g \qquad \text{(A-1)}$$

If $b^2 - ac < 0$, then the PDE is elliptic;

If $b^2 - ac = 0$, then the PDE is parabolic;

If $b^2 - ac > 0$, then the PDE is hyperbolic.

For hyperbolic equations involving the transport of fluid properties such as typical advection-diffusion equation:

$$\frac{\partial T}{\partial t} + u\frac{\partial T}{\partial x} = k\frac{\partial^2 T}{\partial x^2} \qquad \text{(A-2)}$$

requires CFL condition for stability

$$|u|\Delta t \le \Delta x$$

Where Δt is time-step size;

Δx is grid size in a given direction;

u is velocity is in a given direction.

The CFL condition requires that the numerical domain of dependence of a finite difference scheme include the domain of dependence of the associated partial differential equations.

Flow outside the borehole

The governing energy equation (Equation (4.10)) for the flow outside the borehole is a hyperbolic partial differential equation. The groundwater velocity in both directions in the porous rock outside of the borehole is about 10^{-8} m/s or less. The CFL condition is satisfied even with 24-hour time-step size for the grid size used in the simulations.

Flow inside the borehole

The flow is turbulent pipe flow. Because there is more than 300 meters between the suction point and discharge point (base case), the flow is assumed to be in fully developed region. The average water velocity is calculated based on the mass balance. These average velocities are used in the correlations for heat transfer coefficients. The nodal network thermal model described in section 4.1.2.2 is used to handle the thermal

energy transport inside the borehole. The governing energy equation (Equation (4.16)) for the flow inside the borehole is an ordinary differential equation, where the CFL condition is not applicable. The fluid flow in the borehole is treated as quasi-steady. Results from a sensitivity study of time-step size in borehole model are shown in Figure A-12. The given SCW system (Mikler 1993) is modeled in this sensitivity study. This study shows that the time-step size effects are small.

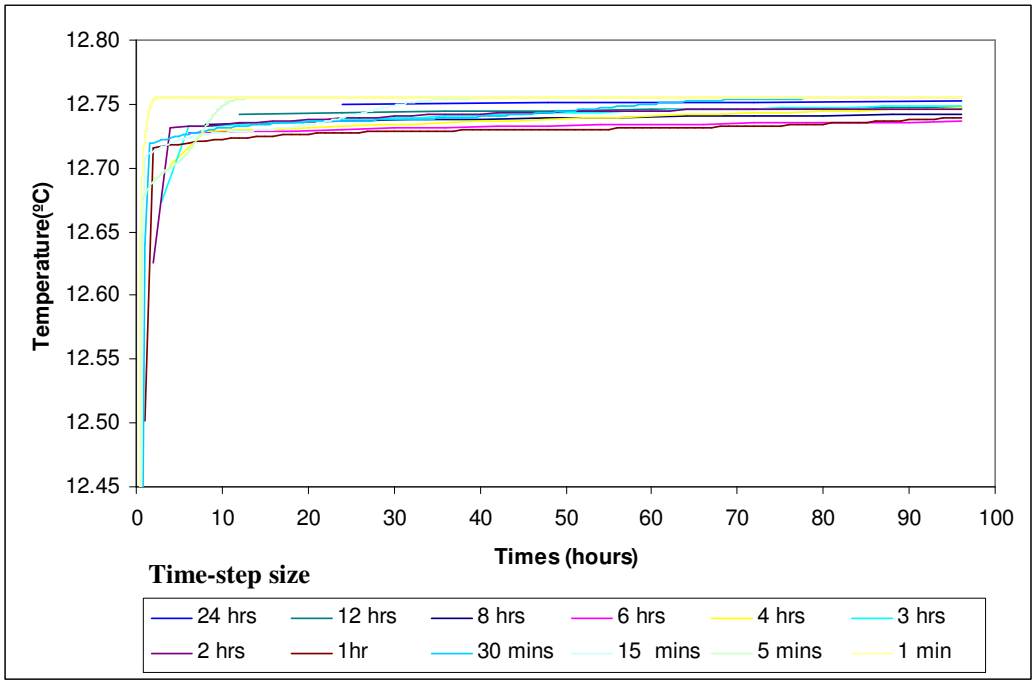

Figure A-12 Sensitivity of temperatures back to the heat pump to the time-step size

APPENDIX B

Grid generation input file

```
# Job Title

SCW Geometry
# No. of Blocks, No. of Edges
1,  26
# Block Edge Definitions
# No.Type,     x1,     y1,     x2,     y2,     Cells,    Distribution, Distribution Coef.
1,    LINE,    0.0,   380.0,  0.0762,   380.0,    4,         equal,        1.0
2,    LINE,  0.0762,   380.0,    1.5,   380.0,    20,        tanh,         1.619
3,    LINE,    1.5,   380.0,    15.0,   380.0,    20,        sinh,        -3.700
4,    LINE,    15.0,   380.0,    50.0,   380.0,    10,        sinh,        -1.679
5,    LINE,    50.0,   380.0,   180.0,   380.0,    16,        sinh,        -1.461
6,    LINE,   180.0,   380.0,   180.0,   378.0,    10         tanh,        -1.260
7,    LINE,   180.0,   378.0,   180.0,   376.0,    10         tanh,         1.260
8,    LINE,   180.0,   376.0,   180.0,   220.0,    45,        tanh,         2.387
9,    LINE,   180.0,   220.0,   180.0,    64.0,    45,        tanh,        -2.387
10,   LINE,   180.0,    64.0,   180.0,    62.0,    10,        tanh,        -1.260
11,   LINE,   180.0,    62.0,   180.0,    60.0,    10         tanh,         1.260
12,   LINE,   180.0,    60.0,   180.0,    40.0,    20,        tanh,         1.567
13,   LINE,   180.0,    40.0,   180.0,     0.0,    10,        tanh,         1.317
14,   LINE,   180.0,     0.0,    50.0,     0.0,    16         sinh,         1.461
15,   LINE,    50.0,     0.0,    15.0,     0.0,    10,        sinh,         1.679
16,   LINE,    15.0,     0.0,     1.5,     0.0,    20,        sinh,         3.700
17,   LINE,     1.5,     0.0,  0.0762,     0.0,    20,        tanh,        -1.619
18    LINE,  0.0762,     0.0,     0.0,     0.0,    4,         equal,        1.0
19,   LINE,     0.0,     0.0,     0.0,    40.0,    10,        tanh,        -1.317
20,   LINE,     0.0,    40.0,     0.0,    60.0,    20,        tanh,        -1.567
21,   LINE,     0.0,    60.0,     0.0,    62.0,    10,        tanh,        -1.260
22,   LINE,     0.0,    62.0,     0.0,    64.0,    10,        tanh,         1.260
23,   LINE,     0.0,    64.0,     0.0,   220.0,    45,        tanh,         2.387
24,   LINE,     0.0,   220.0,     0.0,   376.0,    45,        tanh,        -2.387
25,   LINE,     0.0,   376.0,     0.0,   378.0,    10,       tanh,        -1.260
26,   LINE,     0.0,   378.0,     0.0,   380.0,    10        tanh,         1.260
#Block Definitions - edges listed NESW clockwise order
START BLOCK,  TFI,  1
   N,              1
   N,              2
   N,              3
```

```
   N,          4
   N,          5
   E,          6
   E,          7
   E,          8
   E,          9
   E,          10
   E,          11
   E,          12
   E,          13
   S,          14
   S,          15
   S,          16
   S,          17
   S,          18
   W,          19
   W,          20
   W,          21
   W,          22
   W,          23
   W,          24
   W,          25
   W,          26
END BLOCK
```

APPENDIX C

Pre-processing of flow rate for the experimental validation in Haverhill library

Because experimental data for system flow rates for the standing column well system in Haverhill library, MA are not available, the following procedure is used to decide the system flow rates.

1. Least square method is used to find the following correlations based on the date from Climate master WE120 heat pump catalog:

   Winter:

$$HP\_power = 5.1222 + 0.012977 \times EWT - 0.00004019 \times EWT^2 \quad \text{(C-1)}$$

$$HP\_capacity = (36.7558 + 1.34808 \times EWT - 0.0025877 \times EWT^2)/3.412 \quad \text{(C-2)}$$

   Summer:

$$HP\_power = 3.0691 + 0.002439 \times EWT + 0.00043867 \times EWT^2 \quad \text{(C-3)}$$

$$HP\_capacity = (117.7476 + 0.11218 \times EWT + 0.0026446 \times EWT^2)/3.412 \quad \text{(C-4)}$$

$$COP = \frac{HP\_power}{HP\_capacity} \quad \text{(C-5)}$$

   Where *EWT* is entering water temperature of the source side of the heat pump (ºF);

   HP_power is the power consumption of one single heat pump (kW);

   HP_capacity is the load of one single heat pump (kW);

   COP is the coefficient of performance of the heat pump.

2. Number of heat pump (n)

$$n = \frac{total\ hourly\ power\ consumption\ of\ the\ SCW\ system}{HP\_power} \quad \text{(C-6)}$$

Total hourly power consumption of the SCW system is provided by CDH Energy Corp.

3. Source side heat transfer rate Q_{source}

Winter:

$$Q_{source} = n \times HP\_capacity \times \frac{COP - 1}{COP} \quad \text{(C-7)}$$

Summer:

$$Q_{source} = n \times HP\_capacity \times \frac{COP + 1}{COP} \quad \text{(C-8)}$$

Where Q_{source} is the source side heat transfer rate (i.e. heat transfer rate between SCW and the ground) (kW).

4. Flow rates of SCW system

$$Flowrate = \frac{Q_{source}}{C_p \Delta T} \quad \text{(C-9)}$$

Where *Flowrate* is the flow rate of SCW system (kg/s);

C_p is the specific heat of water (kJ/kg-K);

Q_{source} is the source side heat transfer rate (kW);

ΔT is the temperature difference across the well water side of the heat pump (ºC).

There is an adjustment on the number of heat pump in operation, which is calculated from Equation (C-6)

1. If temperature difference across the well side of the heat pump is less than 1 ºF, then the number of heat pump, n, is equal to 1.

There is another adjustment on the flow rate which calculated from Equation (C-9).

1. When the power consumption of the circulating pump is less than 0.1, the flow rate will be equal to 0 kg/s.

APPENDIX D

Calculation of short-circuiting heat flux by integral method

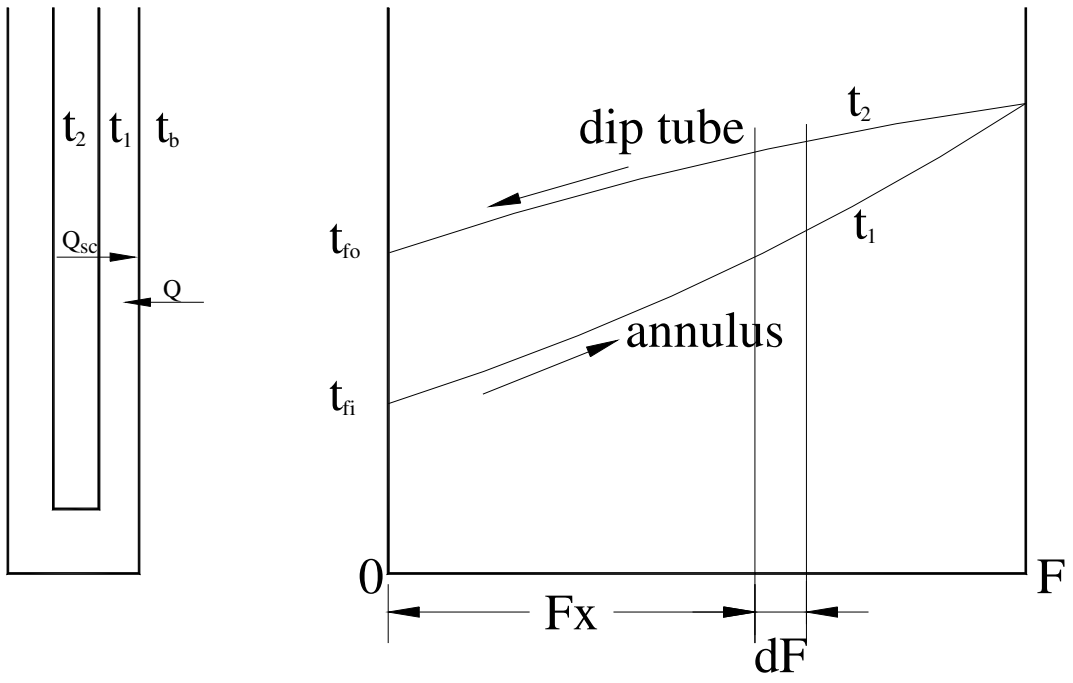

Figure D-1 Illustration of calculation of short-circuiting flux

The short-circuiting flux (driven by the temperature difference between water in the dip tub and the annulus) transferred through element of area *dF* (Figure D-1) can be written:

$$dQ_{sc} = U_x (t_2 - t_1)_x \, dF \tag{D-1}$$

Assume that ground load Q is evenly distributed along the borehole, and then the heat flux (driven by the temperature difference between water in the annulus and borehole wall) transferred through element of area *dF* (Figure D-1, corresponding to *dx* in the depth of the borehole) can be written:

$$dQ = \frac{Q}{2\pi r_b L} \cdot dF = \frac{Q}{2\pi r_b L} \cdot 2\pi r_b dx = \frac{Q}{L} dx \tag{D-2}$$

The total short-circuiting flux can be written after integrating Equation (D-1) from *0* to *F*

$$Q_{sc} = \int_0^F U_x (t_2 - t_1)_x dF = U \Delta t_m F \tag{D-3}$$

The mean temperature difference is defined as:

$$\Delta t_m = \frac{1}{F} \int_0^F \Delta t_x dF \tag{D-4}$$

At the location $F_{x,}$ the heat transferred through an element of area *dF* could be written for the water in the dip tube:

$$dt_2 = -\frac{dQ_{sc}}{M_2 C_2} \tag{D-5}$$

Similarity, at the location $F_{x,}$ the heat transferred through an element of area *dF* could be written for the water in the annulus:

$$dt_1 = \frac{d(Q_{sc} + Q)}{M_1 C_1} = \frac{dQ_{sc}}{M_1 C_1} + \frac{dQ}{M_1 C_1} \tag{D-6}$$

From Equation (5) and Equation (6), the following equation is obtained:

$$dt_2 - dt_1 = -dQ_{sc} (\frac{1}{M_1 C_1} + \frac{1}{M_2 C_2}) - \frac{dQ}{M_1 C_1} \tag{D-7}$$

Substituting Equations (D-1) and (D-2) into Equation (D-7):

$$d(t_2 - t_1)_x = -U(t_2 - t_1)_x \cdot dF \cdot (\frac{1}{M_1 C_1} + \frac{1}{M_2 C_2}) - \frac{Q}{L} \cdot dx \cdot \frac{1}{M_1 C_1} \tag{D-8a}$$

$$d(t_2 - t_1)_x = -U(t_2 - t_1)_x \cdot 2\pi r_{dip} \cdot dx \cdot (\frac{1}{M_1 C_1} + \frac{1}{M_2 C_2}) - \frac{Q}{L} \cdot dx \cdot \frac{1}{M_1 C_1} \tag{D-8b}$$

$$\frac{d(t_2 - t_1)_x}{(t_2 - t_1)_x + \dfrac{Q/L \cdot \dfrac{1}{M_1 C_1}}{U \cdot 2\pi r_{dip} \cdot (\dfrac{1}{M_1 C_1} + \dfrac{1}{M_2 C_2})}} = -U \cdot 2\pi r_{dip} \cdot (\frac{1}{M_1 C_1} + \frac{1}{M_2 C_2}) \cdot dx \qquad \text{(D-8c)}$$

The above differential equation now is integrated from *0* to *x* in the Figure 1,

given $x = 0, \Delta t_x = \Delta t' = t_{f0} - t_{fi}$:

$$\Delta t_x = (\Delta t' + \eta) \cdot e^{-U\varphi F_x} - \eta \qquad \text{(D-9)}$$

Where: $\eta = \dfrac{Q/L \cdot \dfrac{1}{M_1 C_1}}{U \cdot 2\pi r_{dip} \cdot (\dfrac{1}{M_1 C_1} + \dfrac{1}{M_2 C_2})}$ $\qquad\qquad$ $\varphi = \dfrac{1}{M_1 C1} + \dfrac{1}{M_2 C_2}$

Substituting Equation (D-9) into Equation (D-4):

$$\Delta t_m = \frac{1}{F}\int_0^F \Delta t_x dF = \frac{\Delta t' + \eta}{-UF\varphi}(e^{-U\varphi F} - 1) - \eta \qquad \text{(D-10)}$$

Substituting Equation (D-10) into Equation (D-3):

$$Q_{sc} = U\Delta t_m F = \frac{\Delta t' + \eta}{\varphi}(1 - e^{-U\varphi F}) - UF\eta \qquad \text{(D-11)}$$

Where U is the over all heat transfer coefficient between water in the dip tube and the annulus (W/m^2-K [Btu/hr-ft^2-ºF]);

F is the surface area of the dip tube (m^2 [ft^2]) $F = 2\pi r_{dip} L_{dip}$;

L is the depth of the borehole (m [ft]);

M_1 is the mass flow rate in the annulus (kg/s [lbm/sec]);

M_2 is the mass flow rate in the dip tube (kg/s [lbm/sec]);

C_1 is the specific heat of the fluid in the annulus (J/kg-K [Btu/lbm-ºF]);

C_2 is the specific heat of the fluid in the annulus (J/kg-K [Btu/lbm-ºF]);

Q_{sc} is short circuiting heat transfer rate (W [Btu/hr]);

Q is the ground load (W [Btu/hr]);

T_{fi} is the inlet fluid temperature (ºC [ºF]);

T_{fo} is the outlet fluid temperature (ºC [ºF]).

APPENDIX E

Correlation for enhanced thermal conductivity

The performance of even a non-bleed SCW system is improved by induced groundwater flow. In Chapter 6, the "enhanced" thermal conductivity is used to consider groundwater movements from pumping and buoyancy. This Appendix describes development of the correlation for this enhanced thermal conductivity.

The best enhancement factor for the individual non-bleed cases could be found using parameter estimation, comparing the simplified model results with the detailed model results. It may be possible to develop a correlation describing the relationship between the enhancement factor and some parameters such as hydraulic conductivity and thermal conductivity. Then, the enhanced thermal conductivity found with the correlation can be directly used in the simplified model.

Development of correlation

First, the best enhancement factor for individual non-bleed cases is found. Then, a correlation is developed to correlate the "enhanced" thermal conductivity factor with some parameters such as hydraulic conductivity, thermal conductivity and borehole depths in non-bleed cases. After considering some preliminary results, a first order approximation is made during the correlation. A first order correlation assumes that the "enhanced" thermal conductivity is mainly affected by the thermal conductivity and hydraulic conductivity of the surrounding rock in non-bleed cases. All other insignificant parameters will be ruled out. The validity of this assumption has been validated by applying this correlation into different cases with different building load, depths etc.

To get the correlation describing the relationship between the "enhanced" thermal conductivity factor and hydraulic conductivity, thermal conductivity, there are *39* × 3 cases where three parameters (i.e., hydraulic conductivity, thermal conductivity, build load type) variation are varied. These variations are shown in Figure E-1.

Also, Table E-1 lists the values of hydraulic conductivity and thermal conductivity used in these simulations.

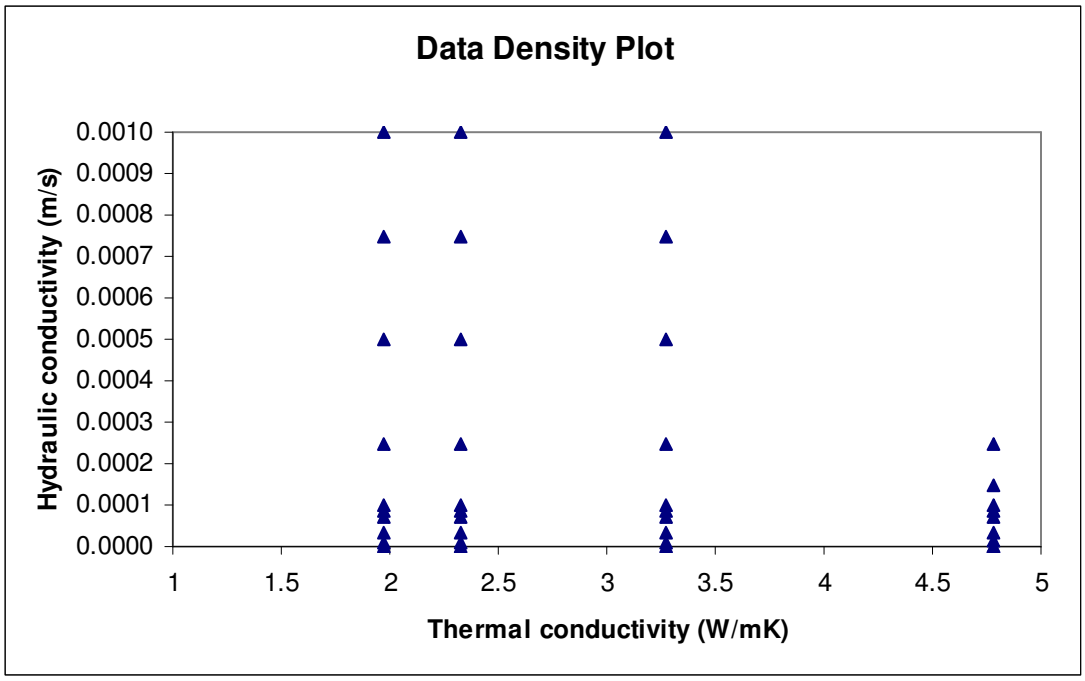

Figure E-1 Data density plot (totally 39 × 3 cases: three different type building loads)

Table E-1 Enhancement factor for different cases

From office building load in Boston			From "in-situ" load		From "sine" load	
Thermal conductivity k=1.97 W/m-K						
Hydraulic conductivity	Enhanced thermal conductivity	Enhanced factor	Enhanced thermal conductivity	Enhanced factor	Enhanced thermal conductivity	Enhanced factor
0	1.97	1	1.97	1	1.97	1
1.00E-05	2.20	1.12	2.31	1.17	2.29	1.16
3.50E-05	2.32	1.18	2.33	1.18	2.3	1.17
7.00E-05	2.41	1.22	2.36	1.20	2.31	1.17
8.50E-05	2.43	1.23	2.41	1.22	2.38	1.21
1.00E-04	2.45	1.24	2.44	1.24	2.46	1.25
2.50E-04	2.63	1.34	2.64	1.34	2.63	1.34
5.00E-04	2.92	1.48	3.06	1.55	3.01	1.53
7.50E-04	3.45	1.75	3.45	1.75	3.38	1.72
1.00E-03	3.89	1.97	3.93	1.99	3.86	1.96
Thermal conductivity k=2.33 W/m-K						
Hydraulic conductivity	Enhanced thermal conductivity	Enhanced factor	Enhanced thermal conductivity	Enhanced factor	Enhanced thermal conductivity	Enhanced factor
0	2.33	1	2.33	1	2.33	1
1.00E-05	2.63	1.13	2.71	1.16	2.61	1.12
3.50E-05	2.75	1.18	2.74	1.18	2.62	1.12
7.00E-05	2.78	1.19	2.77	1.19	2.65	1.14
8.50E-05	2.83	1.21	2.78	1.19	2.71	1.16
1.00E-04	2.85	1.22	2.85	1.22	2.78	1.19
2.50E-04	3.05	1.31	2.93	1.26	2.87	1.23
5.00E-04	3.15	1.35	3.35	1.44	3.28	1.41
7.50E-04	3.52	1.51	3.81	1.64	3.65	1.57
1.00E-03	3.98	1.71	4.5	1.93	4.3	1.85
Thermal conductivity k=3.27 W/m-K						
Hydraulic conductivity	Enhanced thermal conductivity	Enhanced factor	Enhanced thermal conductivity	Enhanced factor	Enhanced thermal conductivity	Enhanced factor
0	3.27	1	3.27	1	3.27	1
1.00E-05	3.63	1.11	3.68	1.13	3.57	1.09
3.50E-05	3.64	1.11	3.72	1.14	3.59	1.10
7.00E-05	3.65	1.12	3.76	1.15	3.62	1.11
8.50E-05	3.65	1.12	3.78	1.16	3.63	1.11
1.00E-04	3.67	1.12	3.88	1.19	3.71	1.13
2.50E-04	3.72	1.14	4.01	1.23	3.92	1.20
5.00E-04	4.03	1.23	4.23	1.29	4.15	1.27
7.50E-04	4.51	1.38	4.82	1.47	4.59	1.40
1.00E-03	4.85	1.48	4.95	1.51	4.83	1.48
Thermal conductivity k=4.78 W/m-K						
Hydraulic conductivity	Enhanced thermal conductivity	Enhanced factor	Enhanced thermal conductivity	Enhanced factor	Enhanced thermal conductivity	Enhanced factor
0	4.78	1	4.78	1.00	4.78	1
1.50E-06	4.84	1.01	5.16	1.08	5.01	1.05
1.50E-05	4.85	1.01	5.2	1.09	5.02	1.05
3.50E-05	4.87	1.02	5.28	1.10	5.05	1.06
7.00E-05	4.9	1.03	5.31	1.11	5.09	1.06
8.50E-05	4.92	1.03	5.35	1.12	5.12	1.07
1.00E-04	4.95	1.04	5.46	1.14	5.22	1.09
1.50E-04	4.96	1.04	5.54	1.16	5.32	1.11
2.50E-04	4.96	1.04	5.61	1.17	5.38	1.13

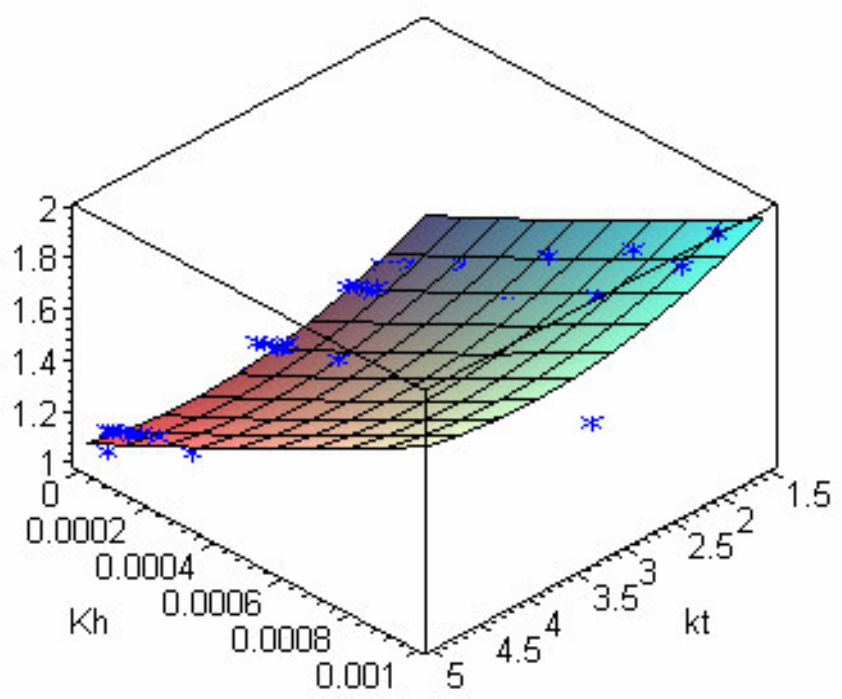

Figure E-2 Three-dimensional relationship among the enhanced factor, hydraulic conductivity and effective thermal conductivity

The data listed in Table E-1 show that the effect from the different building loads profiles on the enhancement factor is small. Based on the data (from the "*in-situ*" load) listed in the above Table E-1, the least square method is used to find a correlation describing the relationships among the "enhanced" thermal conductivity, hydraulic conductivity and effective thermal conductivity. Figure E-2 shows this three–dimensional relation. Also, the data used in this regressing are indicated in this figure. The correlation is given as:

$$F = 0.0413 \times k^2 - 0.3226 \times k + 51779.7923 \times Kh^2 + 635.209 \times Kh + 1.6551 \quad \text{(E-1)}$$

Where F is the enhanced thermal conductivity factor;

k is the effective thermal conductivity(W/m-K);

Kh is the hydraulic conductivity (m/s).

VITA

Zheng Deng

Candidate for the Degree of

Doctor of Philosophy

Thesis: MODELING OF STANDING COLUMN WELLS IN GROUND SOURCE HEAT PUMP SYSTEMS

Major Field: Mechanical Engineering

Biographical:

Education: Received Bachelor of Science Degree in Thermal Engineering from Shenyang Architectural and Civil Engineering Institute, Shenyang, P. R. China, in July, 1996. Received Master of Science Degree in Thermal Engineering from Tongji University, Shanghai, P. R. China, in January, 2000. Completed the requirements for Doctor of Philosophy with a major in Mechanical Engineering from Oklahoma State University, Stillwater, Oklahoma in December 2004.

Experience: Employed as Research Assistant at the School of Mechanical & Aerospace Engineering, Oklahoma State University, Stillwater, Oklahoma from August 2000 to present. Employed as Mechanical Engineer at Gebrüder TROX GmbH, Shanghai, China from January, 1999 to July, 2000.

Professional Memberships: Phi Kappa Phi Honor Society, American Society of Heating, Refrigerating and Air-Conditioning Engineers (ASHRAE), American Society of Mechanical Engineers (ASME), International Building Performance Simulation Association (IBPSA).